Integrated Optical Components for Optical Fibre Sensors

A thesis submitted to the Faculty of Engineering in the University of Glasgow for the degree of Doctor of Philosophy by:

Julian Paul Gregory Bristow

October 1985

Acknowledgements

I should like to thank Professor J.Lamb for the use of the facilities in the Department of Electronics and Electrical Engineering, and for encouragement during the project.

Professor P.J.R. Laybourn is to be thanked for his supervision and helpful discussions.

Mr K.Piecowiak receives thanks for crystal polishing, and Mr G.Boyle and Mr R.Harkins for preparation of masks. Mrs L.Hobbs is thanked for assistance and encouragement during use of the clean room facilities in the department. The assistance of Mr R.Hutchins is acknowledged, as is the help of all the technical and workshop staff in the department.

Miss A.Mackinnon and the computer staff are to be thanked for assistance with computer software.

My colleagues are also thanked for support and encouragement, in particular Mr C.Macgregor for helpful discussions on metal clad waveguides, and Mr A.C.G.Nutt for the fabrication of ion-milled grooves used in the coupling experiments.

The Science and Engineering Research Council is acknowledged for provision of computing facilities and other financial support.

Barr and Stroud Ltd are to be thanked for support of the CASE award and for provision of lithium niobate. Dr N. Macfadyen deseves special thanks for allowing use of the clean room facilities at Barr and Stroud Ltd.

Finally Dr M.Maccauley, Dr D.Winning and Dr H.Davie are to be thanked for the provision of the word-processing facility used to prepare the thesis.

Table of Contents

Summary

The signal processing requirements of optical fibre sensors have been examined and a range of integrated optical processing systems on lithium niobate substrates considered. Requirements on the constituent components of the system have been analysed. It was found that mode filters with extinction ratios of 60dB were required for Mach-Zender interferometers and for short-term gyroscopes, with the figure increasing to 90dB for inertial single-pass systems. Couplers were required to be stable and have as low an insertion loss as possible. A need for a new processing scheme for single fibre polarimetric sensors was identified.

The phenomenon of surface plasma wave TM attenuation resonance was examined, and the properties of the various surface waves which could propagate along the surface of a thin metal film examined. These considerations were used to design metal clad stripe waveguide polarisers using silicon monoxide/aluminium claddings. Extinction ratios of up to 80±13dB with excess losses of 2±3dB were measured for an individual device, and methods for the measurement of such high ratios examined. These results were shown to be better than any reported in the literature. Extrapolation of such results to yield extinction ratios normalised with respect to length has been shown to be invalid. Attempts at excitation of the short-range surface plasmon using waveguide geometries have been unsuccesful to date, but are shown to offer greatly enhanced extinction ratios or shorter devices. Other applications of a variety of surface plasma waves have been considered.

The design of waveguide polarisers using proton exchanged sections was considered and a novel geometry proposed. Due to fundamental limits of the devices and experimental considerations it was not possible to produce polarisers with sufficiently high extinction ratio and low excess loss.

A device to enable efficient coupling between single-mode optical fibres and integrated stripe guides was designed and developed. The device used ion-milled grooves in lithium niobate to locate the fibres. A loss of 2.6dB was determined for the device with a projected loss of 1.8dB for the same device using index matching fluid. The device would be suitable for mass

production, but further work is necessary to reduce the losses to acceptable limits.

The use of field overlap calculations to evaluate coupling losses due to waveguide dissimilarties has been investigated. The method has been shown to be suitable for the optimisation of the waveguide parameters but is not generally accurate. An experimental system to evaluate the integrals has been demonstrated and the results obtained validated. The method has been shown to be a useful tool for design of integrated optical/fibre optical systems. Other applications of the recorded data have been considered, but further work is necessary before refractive index distributions may succesfully be reconstructed from the field profiles. The use of the data in optimising the design of electro-optic guided wave modulators is proposed.

A novel detection and signal processing scheme has been proposed for the single fibre polarimetric sensor. The system operates in a closed loop configuration and uses different optical frequencies in the two eigenmodes. The system requires two orthogonal polarisers and a frequency shifter operating on one mode. The requirements on integrated optical components for an implementation of such a system have been analysed. Frequency shifters have been reported in the literature with sufficiently high performance, and TE-polarisers have been demonstrated in this thesis with the requisite performance. Edge polishing has been shown to be an unsuitable technique for the fabrication of TM-like mode filters, but a novel geometry using ion milling to produce a vertical wall in the crystal has been demonstrated. The extiction ratio was measured to be 17 ± 3dB while the associated excess loss was 7 ± 3dB. Although these values preclude the inclusion of the device in the proposed system, they are important as they enable the TM-like modes to be selected. It is shown that the devices would be useful for other systems incorporating phase modulators on Z-cut $LiNbO_3$. Other implementations, including all-fibre versions, of the proposed system have been considered, but are unlikely to offer comparable dynamic range.

A number of suggestions have been offered for work based on the contents of this thesis.

Chapter 1 The Appication of Integrated Optical Devices and Systems to Optical Fibre Sensors

1.1. Introduction.

Optical fibre sensors have been under investigation for approximately 10 years, and have now reached the stage of commercial availability, with several companies now marketing a range of simple sensor types (ref 1). Much commercial development is taking place to realise the potentially high sensitivity of these sensors (ref 2).

Although there are many types of optical fibre sensor, they all offer significant advantages in some aspect of their performance over their conventional counterparts (ref 3). Among their potential advantages are high sensitivity compared to their conventional counterparts, immunity to electromagnetic interference, and the ability to detect the quantity to be measured remotely (ref 4). The range of physical properties so far measured includes temperature (ref 5,6,7,8), acoustic pressure (ref 9,10), rotation rate (ref 11,12,13,14,15), displacement (ref 17), chemical composition (ref 19), rate of flow of liquids, strain (ref 20,21), magnetic field (ref 22,23), electric field (ref 24), voltage and current (ref 25,26). The sensors have even found applications in clinical monitoring (ref 27)

The sensors may be divided into two broad categories; those in which the parameter to be measured affects the light externally to the fibre (the fibre then simply serving to transfer the light to the sensing region) , and those in which the transduction takes place internally. Both offer the great advantage over normal optical sensors that the sensing region may be remote from the detecting region, the distance being limited by the attenuation of the fibre , the sensitivity of the detection equipment used, and the sensitivity of the non-sensing leads to external perturbations. However, the most sensitive devices generally rely on internal transduction.

Excellent reviews of optical fibre sensors are given in references (refs 1,2,3,4,9,10,11). For the purposes of this discussion it will be necessary to re-examine some of the

reported sensor types.

1.2 Multimode sensors

From the point of view of alignment of components and simplicity of construction, combined with low cost, sensors fabricated from multimode optical fibres (ref 28) appear attractive. Within this category there are two broad subdivisions, distinguishing those systems in which the light is affected externally to the fibres from those in which it takes place internally.

1.2.1 External modulation

Multimode optical fibres may be used to modify previously demonstrated optical sensors, confering upon them the added benefits of simple alignment and remote sensing. Within this category lie simple intensity modulation schemes, including balanced detection schemes (ref 29). Another example is the all-fibre Michelson interferometer shown in figure 1.

Alignment of a bulk optical interferometer is a time-consuming process, the fibre arrangement offering considerable advantages. If, instead of merely reflecting the light in the appropriate arm, one miror is moved at a certain velocity, as shown in figure 1, a Doppler shift of the beam by a frequency related to the velocity will result. Each speckle in the far-field interference pattern (ref 30) will then contain information on the out-of-plane vibration. Bristow (ref 30), and Ueha (ref 18) have used the technique to detect displacements as small as 0.1um at 0.6328 micron wavelength. However, alignment of mirrors with respect to the fibre end-face presents experimental difficulties.

1.3 Internal modulation- the Fibredyne system

Perhaps the simplest fibre sensor system is the "fibredyne" system (ref 31). A single length of multimode fibre is used as the sensing element, coherent light being input so as to excite all the modes of the fibre. Each mode will then suffer a differing phase delay according to the transit time for the fibre, the relative delay being greater for a step rather than for a gradient index fibre . The resultant far-field speckle pattern is then determined by the spatial and temporal variations between the modes (ref 32). If some external influence is allowed to affect the propagation constants of the modes to differing

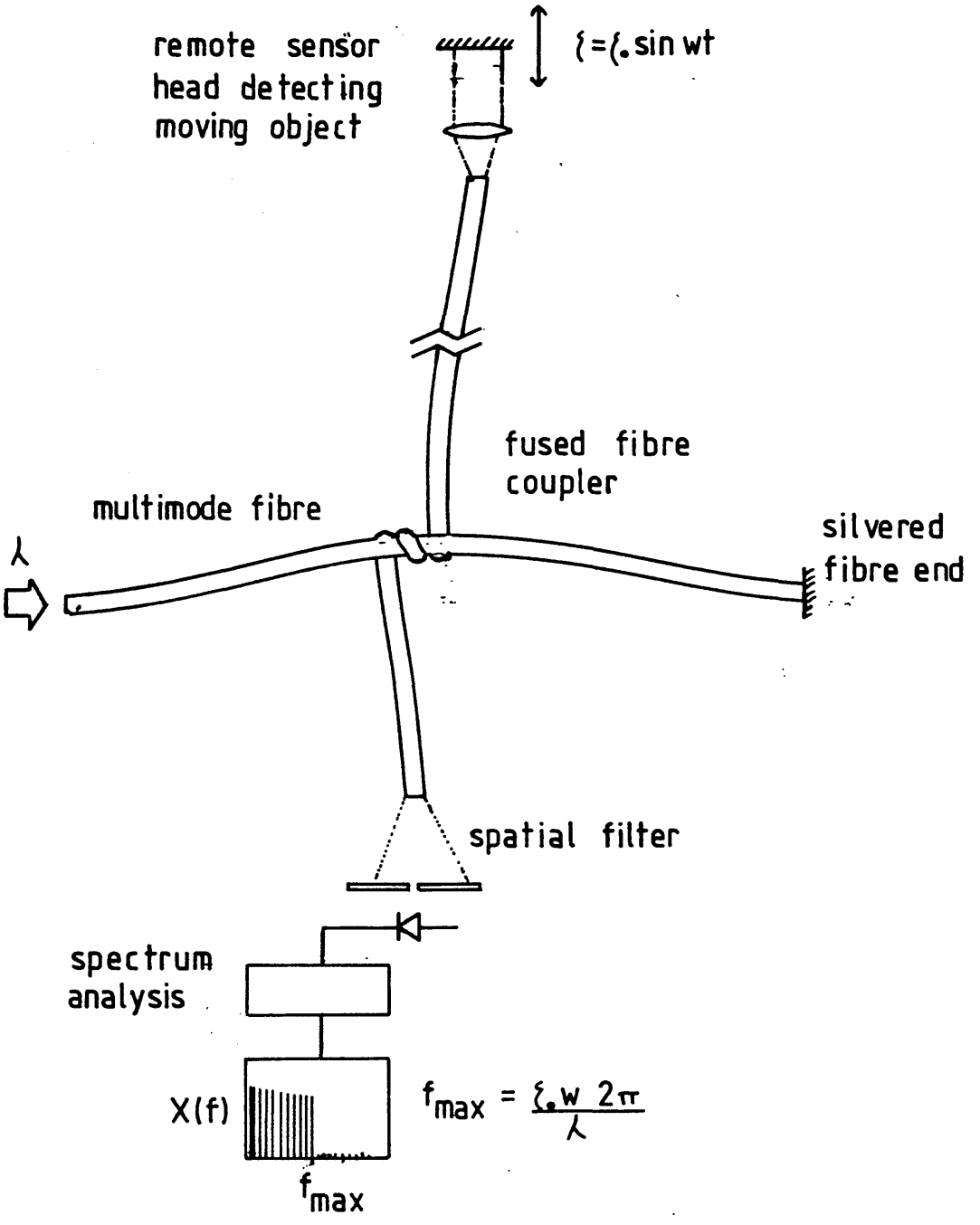

FIG 1 A SIMPLE MULTIMODE OPTICAL FIBRE IMPLEMENTATION OF A MICHELSON INTERFEROMETER USING EXTERNAL MODULATION. TO MEASURE AMPLITUDE OF VIBRATION OF A REMOTE OBJECT

extents, the spatial distribution of the speckle pattern will be altered. Since the total power will to a first order be unchanged, it is necessary to select a small area, generally one speckle, to obtain the desired information concerning the influence. Although the output is a nonlinear function of the influence, and rather worse, non-linear in a non predictable way by virtue of the Rayleigh phasor distribution, the system is inherently simple. Although the sensitivity is lower than that of the best single-mode devices, no restriction of the selected modes is imposed. Coherent (ie heterodyne or homodyne) detection techniques may be used to eliminate problems associated with signal fading (ref 31)

1.4 Single Mode Sensors

The greatest sensitivity is in general offered by the use of single-mode fibres, and the majority of reported sensors have used such fibres.

1.4.1 The Mach-Zehnder configuration

A widely reported technique is the Mach-Zehnder sensing configuration. Such systems have been used to measure temperature, pressure, magnetic field (with some modification) and a wide range of other parameters with high sensitivity. The standard experimental arrangement is shown in figure 2. A coherent input beam is divided, ideally equally, between two fibres by either a bulk or guided wave optical beamsplitter. The light then propagates through both arms, one of which is exposed to some external influence which shall be referred to as **X**. If the phase delays of the two beams are (neglecting temporal variations) $e^{i\phi_1}$ and $e^{i\phi_2}$ then the resulting intensity , upon recombination, if powers P_0 are launched into each beam is:

$$P = P_0 \left(1 + \cos(\phi_1 - \phi_2)\right) \qquad 1.1$$

If the reference arm is totally isolated fron the influence (a situation difficult to realise in practice) then for a change in influence ΔX one may write:

$$\Delta\phi_1 = \left[nk_0 \frac{dL}{dX} + Lk_0 \frac{dn}{dX} \right] \Delta X \qquad 1.2$$

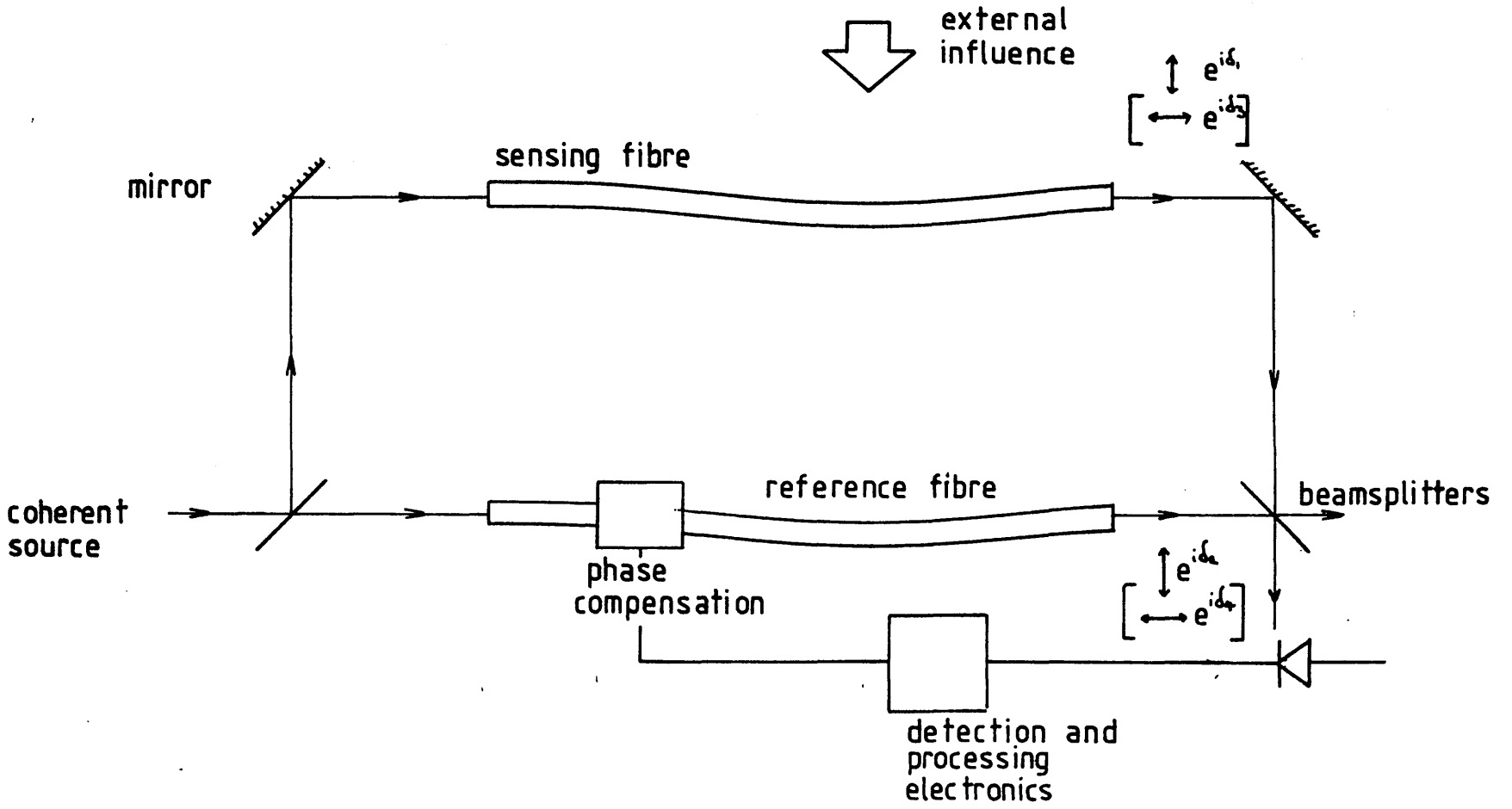

FIG 2 SCHEMATIC DIAGRAM ILLUSTRATING A FIBRE OPTIC IMPLEMENTION OF A MACH-ZEHNDER INTERFEROMETER. PHASE DELAYS $e^{i\delta_1}$ and $e^{i\delta_2}$ ARE ASSOCIATED WITH MODES ALIGNED WITH ONE FIBRE BIREFRINGENT AXIS, $e^{i\delta_3}$ and $e^{i\delta_4}$ WITH THE OTHER.

where the first term is generally larger (ref 22). k_0 represents the free-space wavevector, n the mode-index of the fibre (ref 34) and L the length of the sensing region. It is seen that for maximum sensitivity, the angle $(\delta_1-\delta_2)$ must be maintained at $\pi/2$-the quadrature condition. Any variation in this bias would appear as noise in the output, thus active phase compensation may be beneficially employed (ref 33).

Sensors based on the Mach-Zehnder principle with unmodified fibres are extremely sensitive to most influences. For example, using 10m of single mode fibre, the shot-noise limit of sensitivity corresponds to an acoustic sensitivity of 20dB below the threshold of hearing at 1kHz (ref 10), and in a simple magnetic field sensor relying on magnetostriction of nickel, magnetic fields of 10^{-12} gauss (ref 22). The sensitivity of the arangement gives rise to problems in discriminating between the different influences which may affect the fibre.

3.1.1 Polarisation effects in Mach-Zehnder based Sensors

In general, the fibres used in the fabrication of optical fibre sensors have some birefringence, either intrinsically or by virtue of their geometrical arrangement (ref 35,36). For a typical fibre sensor with length 1m the difference in phases of the two orthogonal modes may be some tens of radians. If the power is allowed to fluctuate between the now non-degenerate orthogonal modes indiscriminantly, the sensitivity of the sensor will be reduced. It will therefore be necessary to select only one of the eigenmodes of both the sensor and reference arms. The mode-filter will then form an essential part of the ancillary optics associated with this sensor, whether utilising bulk-optics, fibre optics or integrated optics. At this point it should be pointed out that such a filter is often referred to as a "polariser" in the literature, a misnomer as the two eigenmodes do not necessarily correspond to linear polarisations (ref 37). With this in mind, the state of polarisation in a general birefringent fibre may be represented as the resultant of two linear orthogonal polarisations: however the representation is not unique, the use of, for example, left- and right-handed circular polarisations being equally valid (ref 38,41).

To determine the performance requirement on the polariser,

we consider the Mach-Zehnder configuration shown in figure 2. The two arms are both birefringent with phase terms δ_1 and δ_3 in the sensing arm, and phase terms δ_2 and δ_4 in the reference arm. If the electric field amplitudes in each mode are E_1 etc, and the powers launched into each fibre are P_0, then the fields parallel and normal to mode 1 are, respectively:

$$E_{par} = E_1 e^{i\delta_1} + E_2 e^{i\delta_2}$$

$$E_{perp} = E_3 e^{i\delta_3} + E_4 e^{i\delta_4} \qquad 1.3$$

If the magnitudes of the electric field are now made equal in the othogonal modes, normalising with respect to P_0 the total power launched into each fibre:

$$\begin{aligned} I &= I_{par} + I_{perp} \\ &= \left(\frac{P_0}{2}\right)\left(2 + \cos(\delta_1 - \delta_2) + \cos(\delta_3 - \delta_4)\right) \end{aligned} \qquad 1.4$$

From which the rate of change of intensity with external influence X is:

$$\begin{aligned} \frac{dI}{dX} &= \left(-\frac{P_0}{2}\right)\left[\sin(\delta_1 - \delta_2)\frac{d\delta_1}{dX} + \sin(\delta_3 - \delta_4)\frac{d\delta_3}{dX}\right] \\ &= \left(-\frac{P_0}{2}\right)\left[\sin(\delta_1 - \delta_2)\left(n_1 k\frac{dL}{dX} + Lk\frac{dn_1}{dX}\right)\right. \\ &\quad \left. + \sin(\delta_3 - \delta_4)\left(n_3 k\frac{dL}{dX} + Lk\frac{dn_3}{dX}\right)\right] \end{aligned} \qquad 1.5$$

If now the quadrature condition is applied to both sets of modes simultaneously the rate of change of intensity is:

$$\frac{dI}{dX} = \left(\frac{P_0}{2}\right)\left[(n_1 + n_3)k\frac{dL}{dX} + Lk\frac{d(n_1 + n_3)}{dX}\right] \qquad 1.6$$

Although this improves upon the non-birefringent case by a factor of approximately two, the simultaneous quadrature condition would be hard to achieve. The analysis has also assumed that the power and relative phases of the two modes remain constant, conditions difficult to maintain in practice. If the quadrature condition were applied to one mode only, an erroneous result would be obtained

If the powers in modes 1 of the two fibres are both P_0-a, and in the orthogonal modes are a, then the resultant intensity is:

$$I = P_0 + (P_0 - a)\cos(\delta_1 - \delta_2) + a\cos(\delta_3 - \delta_4) \quad 1.7$$

and

$$\frac{dI}{da} = \cos(\delta_1 - \delta_2) - \cos(\delta_3 - \delta_4) \quad 1.8$$

Since the desired modal outputs will be maintained in quadrature, $(d_1 - d_2) = \pi/2$

$$\frac{dI}{da} = 1 - \cos(\delta_3 - \delta_4) \quad 1.9$$

Expressed as a fractional change of intensity this becomes:

$$\frac{dI}{I} = \frac{1 - \cos(\delta_3 - \delta_4)}{2P_0}\, da \quad 1.10$$

Since we may expect to detect at best a change in intensity of one part in 10^6 with interferometric arrangements (ref 39), and choosing the "worst" case of the numerator, we find in that the power in the uncontrolled mode must be less than 10^{-6} of the total power, or that an extinction ratio of 60dB is required.The extinction ratio defines the ratio of the power in the desired mode to that in the unwanted mode.

The above treatment has neglected any coupling between the modes that may result from any anisotropic perturbation (ref 35,40). There are in reality many sources of such perturbations such as acoustic fields and mechanical vibration. Since the

acoustic sensitivity of this sensor is 20dB below the threshold of hearing for a 1m length of fibre (ref 10), the fibre used would ideally maintain constant powers in the two orthogonal modes. This necessitates the use of high birefringence fibre (ref 35). However, as pointed out by Payne (ref 77), it is still necessary to use input and output polarisers. This may be understood since a randomly fluctuating direction of linear input will give rise to a varying apparent phase of the output signal. For random coupling along the fibre, a certain fraction of launched power will appear in the orthogonal mode, with an unrelated phase delay. Thus minimisation of the error will be obtained by use of linear polarisers at the input and output ports of the sensor. A variety of polarisation rotation and transformation schemes have been proposed and developed (ref 42) which enable arbitrary polarisation transformations to be performed. These devices are important since for applications such as coherent transmission systems it may be important to maximise the power in one mode, the small phase changes used in sensor systems no longer being important here.

1.5 The Fibre Gyroscope

By far the largest volume of published material has concerned the optical fibre gyroscope. This consists of a coil of single mode optical fibre and some associated processing optics, the latter being either bulk or guided wave. The sensor is expected to measure rotation with high sensitivity, exceeding that of more conventional mechanical gyroscopes. Optical fibres also confer the added benefit of low cost. The sensor is most easily understood by considering the modification of the Mach-Zehnder configuration shown in figure 3. The arrangement may be extended to form an optical fibre gyroscope as shown by removing the second beamsplitter and joining the two arms together. The operational principles of the resulting gyroscope have been well descibed by Culshaw (ref 11) and Chow (ref 46), however for the ensuing discussion a brief resume will be given.

If the coil of fibre is rotated, one beam (propagating clockwise in the example) spends longer in the coil than the other beam. Thus the intensity of the recombined beams (initially at a maximum) will vary. We assume that the light passes only

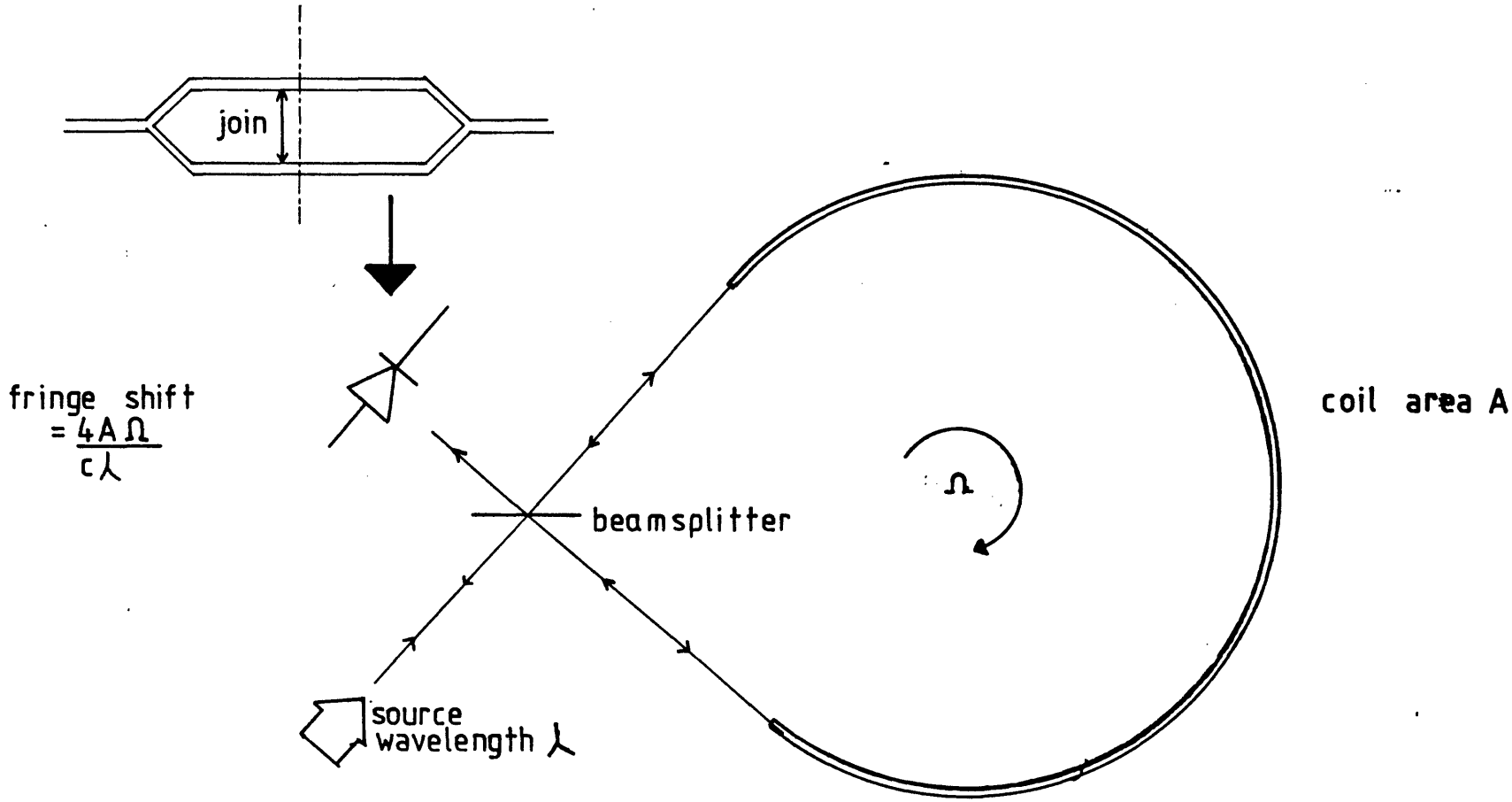

FIG 3 ILLUSTRATING THE MODIFICATION OF THE BASIC MACH-ZEHNDER CONFIGURATION TO FORM AN OPTICAL FIBRE GYROSCOPE. NOTE THAT THIS ARRANGEMENT DOES NOT ENSURE RECIPROCAL OPERATION.

once through the fibre coil, although other operational regimes are possible (ref 47,48). For an angular rate Ω the expression for the fringe shift Δz resulting from the non-reciprocal Sagnac phase shift $\Delta\varphi$, named after its discoverer (ref 94) may be derived as described by Post (ref 49)

$$\Delta z = \frac{4A\Omega}{c\lambda} \qquad 1.11$$

Or;

$$\Delta\varphi = \frac{4A\Omega}{c\lambda} \cdot 2\pi \qquad 1.12$$

Where c is the speed of light in free space, λ the wavelength in vacuum, A the effective area of the coil (ref 11). In practice many turns are used with a radius of between 5 and 10cm and a total fibre length of 1km. An perfectly constructed device would be reciprocal to all parameters except for rotation and magnetic field, the latter inducing a non-reciprocal polarisation rotation via the Faraday effect. To fabricate a device exhibiting a high degree of reciprocity it is necessary to use the "minimum configuration" system illustrated in figure 4. To ensure that the two beams "see" an equal number of reflections and transmissions, two beamsplitters must be used. Also, since the propagation constants of the fibre for the two orthogonal modes may differ, a polariser or mode filter is needed (ref 11). In addition, the alignments of the fibre with respect to the optical components (whether guided or bulk devices) must be the same for both fibre ends. In other words, a common mode must be defined at the input and output ports.

The output of the system may be monitored by use of a photodiode. Unfortunately this simple detection scheme has several major problems. Firstly, the sensor may be required to operate with high dynamic range, detecting rotation rates of between 0.01^0/hr and 400^0/sec. Due to the periodic nature of the output, ambiguity would arise. Secondly the sensitivity of the device is at a minimum for low rotation rates. Thus an increasing complexity of processing systems is needed to realise the potentially high sensitivity, and the intrinsic simplicity of the

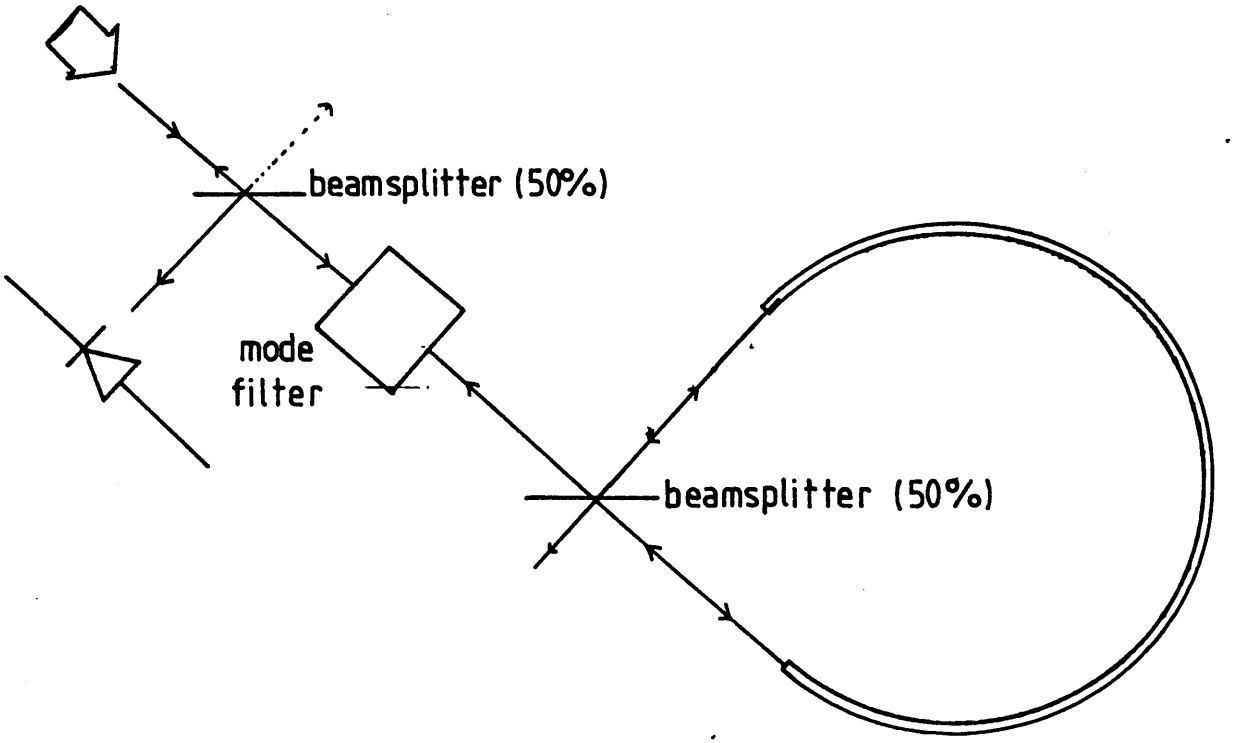

FIG 4 ILLUSTRATING THE MINIMUM CONFIGURATION NEEDED FOR THE OPTICAL FIBRE GYROSCOPE TO ENSURE RECIPROCAL OPERATION.

device is lost.

The sensitivity problem, but not the restricted dynamic range, may be overcome by use of a $\pi/2$ phase bias (ref 11). Unfortunately any noise in the bias gives rise to noise in the apparent rotation rate. Alternating bias (phase modulation) may be used to produce an output at the modulating frequency (in prctical cases this will be sinusoidal) of magnitude $A_0 \sin\phi(2J_1(\phi_m))$ where ϕ_m is the maximum induced phase change and ϕ the Sagnac phase shift (ref 11). Unfortunately, the dynamic range is still a problem, but may be overcome by use of a range of phase-nulling techniques in closed loop configurations. If a suitable, small frequency difference could be introduced between the two beams the Sagnac phase difference could be nulled. Knowledge of the applied frequency shift would then yield inormation on the rotation rate. This detection scheme has the advantage of an essentially digital output, but the dynamic range of the system will be dependent upon the device used to change the frequency. Cahill and Udd (ref 50) have shown that the required frequency shift is:

$$\Delta\nu = \frac{2\Omega R}{\lambda n} \qquad 1.13$$

Where n is the effective index of the fibre coil. It is seen that this result is independent of the length of the fibre coil. For a typical practical device, the frequency shift is given by $Df=10^5\Omega$ where Ω is the rotation rate of the gyroscope in radians/second. Thus for the dynamic range previously quoted, a frequency difference of 1.4Mhz would be required. Here integrated optical frequency shifters have great potential (ref 51), frequency shifts of up to 400MHz having been reported.

For phase nulling techniques, the light source must have a large coherence length. Any light backscattered from the fibre within the coil may then add coherently with the unscattered light to corrupt the signal. Dispersion effects (ref 53) will give rise to a temperature dependent error term. Despite these difficulties, the closed loop approach has yielded high sensitivities . A large zero drift of $6^0/hr/^0C$ results from the use of only one modulator. Barlow et al (ref 53) have shown that

a second modulator is necessary to achieve the higher zero-point stability required in tactical applications.

The most impressive result to date was a noise floor equivalent to a rotation rate of 0.1^0/hr, albeit with an integration time of 30 seconds (ref 56). Bulk optical components were used.

Using a system with phase modulation, Bohm et.al (ref 55) were able to demonstrate a sensor with linearity to less than 1% for rotation rates between 300 and 200,000 degrees/hour. For an integration time of 1 second a noise equivalent error rate of 0.11^0/hr was reported. A somewhat poorer figure was obtained with digital data processing, however the system coped with the high dynamic range.

Kim (ref 57) has used a sinusoidal phase modulation in a closed-loop all-fibre configuration. The method relies on the differing phase delays imposed on the counterpropagating beams due to the asymmetric mounting of the PZT modulator with respect to the geometric centre of the fibre.

1.5.1 Applications to other sensors

It will be seen that the processing systems suitable for the optical fibre gyroscope may be applied to other optical fibre sensors, where the same requirements of high sensitivity and dynamic range apply. For example, heterodyne detection schemes may also be used with Mach-Zehnder configurations. The absence of any need for reciprocity relaxes the requirements on the optical components. Techniques developed for use with the sensors described may also be of benefit for coherent detection in long-haul optical fibre communication systems (ref 58).

1.5.2 Practical implementation of processing schemes

In the preceding discussion, no choice of implementation was mentioned. It would be possible to use either bulk optical or guided wave systems. The former require complex alignment of sensitive parts, are costly, and would be adversely affected by mechanical perturbations.

While the sensing coil itself is by definition an optical fibre, guided wave implementations of the processing scheme may use either integrated optical or optical fibre components. Both have in fact been used with varying degrees of success (ref 60).

All fibre systems (ref 59) have no interfaces to cause alignment problems or reflections. In-line fibre polarisers have been demonstrated with sufficiently high performance (ref 61), and alignment problems are eliminated. However, fibre couplers (such as fused biconical taper couplers (ref 62)) would not lend themselves easily to mass production, as may eventually be required. In addition, PZT modulators, generally used to implement the frequency shift in an all-fibre phase-nulling gyroscope, have limited dynamic range (ref 63), this modified modulator giving frequency shifts up to some tens of MHz.

Integrated optical implementations would lend themselves to mass production, but suffer from the increased complexity of fibre-waveguide interfaces. To date, poor performances have been obtained with integrated optical processing schemes (84). The signal processing requirements will now be investigated in the context of previously demonstrated integrated optical components.

Refering to the closed loop configuration shown in figure 5 a variety of components may be identified

Sources

It would appear that due to the interferometric nature of the sensor, light sources with high coherence lengths would be required. However, the corrupting effect of Rayleigh backscattered light from the fibre (a mechanism which also provides depolarisation) is worsened by coherent sources (ref 64). In addition, the optical Kerr effect leads to a bias indistinguishable from the Sagnac phase shift should the beamsplitter splitting ratio not be exactly 50% (ref 65). The effect may be reduced (but not eliminated) by the use of broadband sources (ref 65). Since light sources have not been incorporated into lithium niobate processing systems to date (ref 34), and the other required components have not been demonstrated on semiconductor substrates, a separate source will be required. Superluminescent diodes and multi-longitudinal mode lasers (ref 66) are ideal candidates. Semiconductor lasers are generally adversely affected by reflections from optical interfaces in their immediate vicinity (ref 67), thus an optical isolator (ref 68) or non-planar interface is required. Choice of wavelength

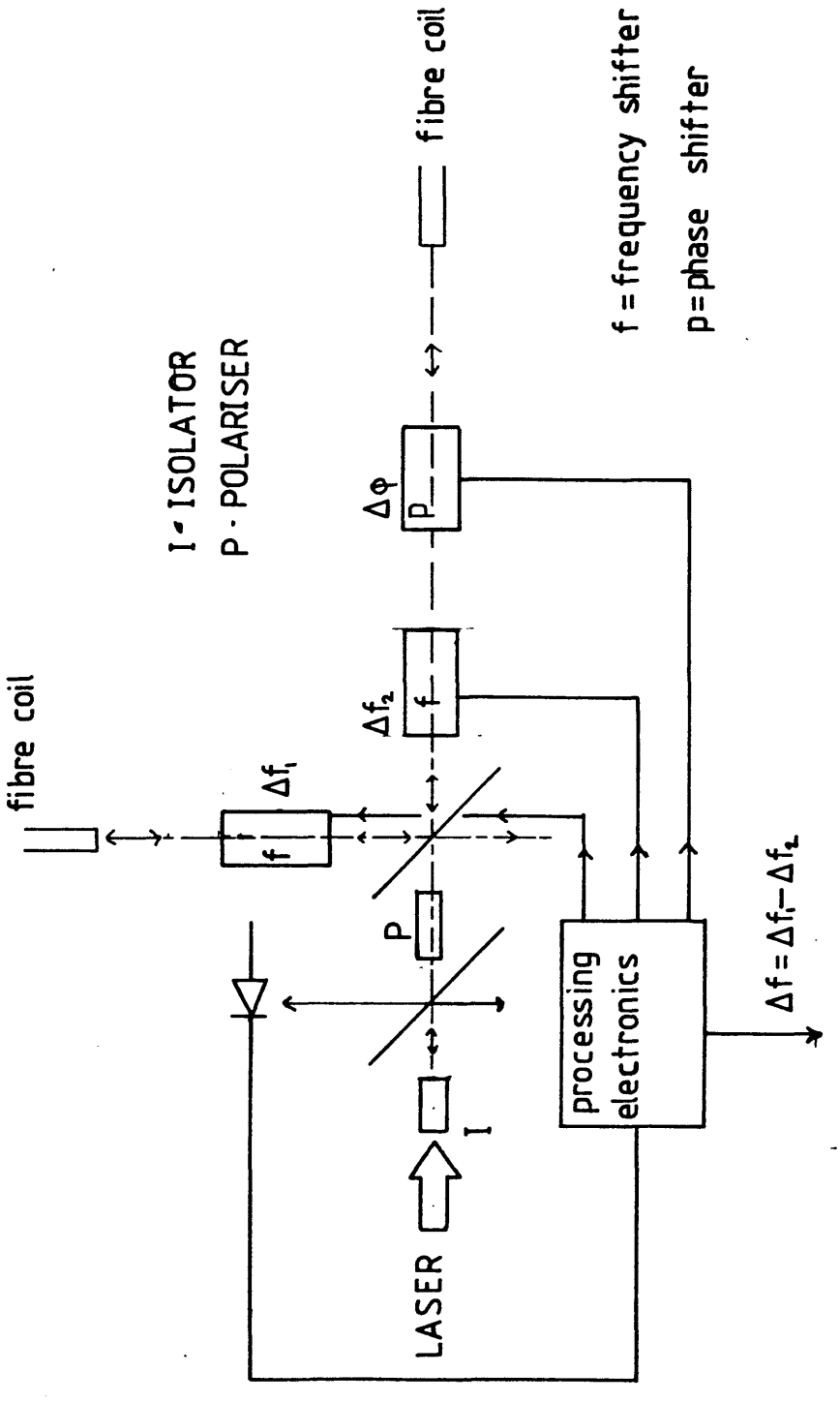

FIG 5 SCHEMATIC DIAGRAM OF CLOSED LOOP PHASE NULLING FIBRE OPTIC GYROSCOPE.

will be important as the sensitivity of the gyroscope depends upon this parameter. In addition,for integrated optical applications the photorefractive effect has an adverse effect on the long term stability of components fabricated on lithium niobate by indiffusion of titanium for sufficiently high photon energies (ref 69,70).

Beamsplitters.

The two beamsplitters may be implemented by either y-junctions (ref 71) or directional couplers (ref 72). It is known that the splitting ratio should be as close to 3dB (ie. a 50/50 split) as possible (ref 64). The fabricational tolerances would thus preclude the selection of the directional coupler approach unless tuning electrodes were to be employed (ref 72). Y-junctions are more easily made with repeatable, even splitting ratios. However the devices are in reality four-port couplers with the substrate serving as the fourth port as shown in figure 6 (ref 59). Light radiated into this fourth port may subsequently couple into another waveguide with an adverse effect on the sensitivity as reported by Papuchon et al. Modified geometries may alleviate the problem. Electrical tuning may also benefit Y-junctions (ref 73)

Mode filters

As discussed in references 74,75,76 it is necessary that both counter-propagating modes have the same polarisation mode. This implies that both fibre and integrated optical mode filters must support one spatial mode, which corresponds exactly to one mode of the fibre. Until recently, such devices were lacking. Ideally, the power launched into the one mode would remain within that mode. However, defects in the fibre, and external influences with the appropriate periodicity will serve to couple power between the two modes. Since these have different propagation constants, if only by virtue of the coiling of the fibre, corrupted outputs will result. For a rotation of polarisation in a fibre mounted between two perfect polarisers, complete fading may result (ref 74). Thus the fibre would ideally maintain the polarisation state. Such specialised fibres are the subject of current research by other workers (ref 77) However, for the class of polarisation holding fibres which rely on stress induced

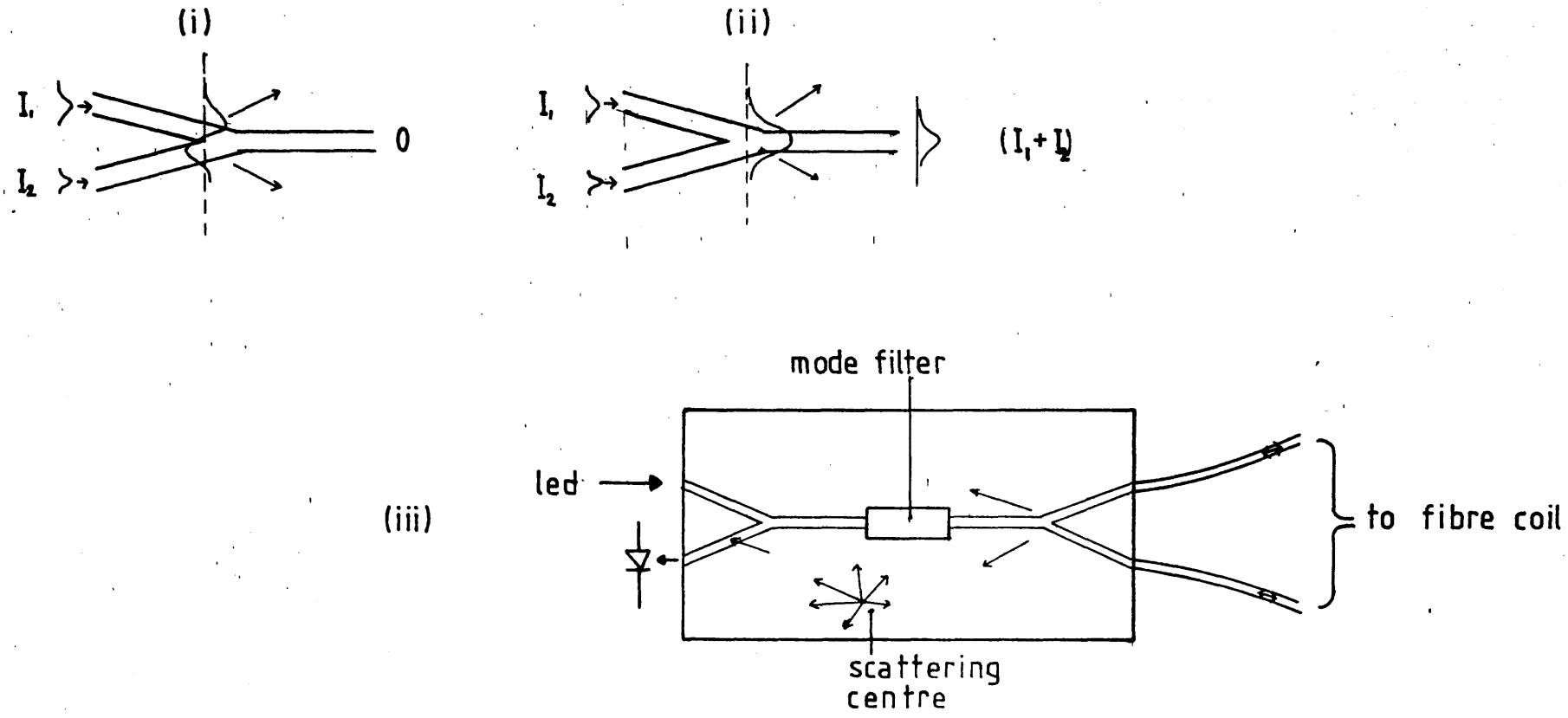

FIG 6 ILLUSTRATING THE RADIATION FROM Y-JUNCTION COMBINERS (i)SYMMETRIC CASE (ii)ANTISYMMETRIC CASE AND (iii)ITS EFFECT ON THE DETECTED SIGNAL FROM A DOUBLE Y-JUNCTION INTEGRATED OPTICAL IMPLEMENTATION OF A FIBRE GYRO PROCESSOR.

birefringence (ref 78) it is believed that there is an ultimate limit of approximately 50dB to the maintained extinction ratio (ref 79). A full discussion of currently available mode selection techniques will be presented in a later section. It can be shown that for a single-pass gyroscope, an extinction ratio of at least 60dB is required for even modest system performance (ref 80). Figures of 90dB are required for tactical applications (ref 15), however, Burns et al (ref 15) have used partially coherent sources with polarisation holding fibre to achieve low drift, requiring a figure of only 50dB.

For a fibre gyroscope, one would ideally pass all the power in one mode, while eliminating cross-scattering together with the power in the orthogonal mode. If this condition is not met, bias errors will result (ref 81), unless the product of the two off-diagonal elements of the Jones matrix (ref 82) describing the complete system is equal to the second element of the leading diagonal (ref 81)

Phase modulation and frequency translation

Integrated optical phase modulators have been reported with low drive power requirements for devices fabricated in titanium indiffused lithium niobate using both proton exchange (ref 83) and titanium indiffusion waveguide fabrication techniques. For a full discussion, the reader is referred to ref 43. Bandwidths of up to 10Ghz have been reported. Frequency translators have also been demonstrated using the above components in a "serrodyne" arrangement (ref 83), yielding shifts of up to 4MHz, limited by electrical considerations. In this publication it is also seen that signals are present at frequencies other than that of the main lobe. In particular, signals are still present at the unshifted (source) frequency. This will lead at best to non-linearities if the effect does not vary with time, and at worst errors in detected rotation rate if it does. The effect was attributed to guiding in out-diffused layers (ref 83), a phenomenon which limits the performance of many other integrated optical components unless properly suppressed.

Couplers

Since the signal processing optics are separate from the fibre sensing coil in this implementation, some method of

coupling the power between the two guides is required. A variety of methods have been reported, ranging from simple mechanical butt-joints to externally defined alignment grooves. A novel coupler fabricated in the course of this work will be described in chapter 6. A coupler to be used in this application should be mechanically stable, insensitive to temperature, and allow stable, efficient power transfer.

1.5.3 Conclusion

While individual components suitable for the fabrication of an integrated optical processing scheme for an optical fibre gyroscope have been demonstrated, their performance is either too poor, or has not been sufficiently thoroughly investigated to enable their integration. More work is necessary to improve the rather poor performance of these systems, currently -1000 times poorer than bulk optical versions with all electronic processing. (ref 84)

1.6 The Single Fibre Polarimetric Sensor

The Mach-Zehnder sensor described in section 2 is capable of extremely sensitive measurement of temperature, pressure, and if a magnetostrictive coating such as a suitable metallic glass (ref 23) is used on the sensing arm, magnetic field. As it is often difficult to isolate these parameters, the high cross-sensitivity (ie. sensitivity to parameters other than that to be detected) of the devices is a problem. In addition, with simple intensity detection systems the phase change becomes ambiguous for phases greater than $\pi/2$ (ref 85). While more complicated fringe-counting methods could be used, the inherent simplicity of the sensor is lost. Thus the dynamic range of the basic Mach-Zehnder configuration is low.

The Michelson configuration (ref 86) offers some geometric advantages over the Mach Zehnder for applications where the reference arm needs to be separate from the sensing arm, and offers a doubling in sensitivity per unit length. However, the arrangement suffers from essentially the same limitations as the Mach-Zehnder.

A variety of methods of overcoming this problem have been reported, using for example a source-frequency modulated system analogous to certain radar techniques (ref 87) which has a

theoretical dynamic range of 10^8 with a greatly reduced sensitivity to displacement of 0.1μm using currently available sources and detectors.

Another possible arrangement is the single-fibre polarimetric sensor (ref 88), also referred to in the literature as a "polarimeter", which offers improved cross-sensitivity and dynamic range compared to the Mach-Zehnder at the expense of lower sensitivity. Fibre birefringence led to adverse effects on the sensitivity of the Mach-Zehnder: here the birefringence of the fibres is employed beneficially. The configuration is shown in figure 7. A single, birefringent fibre is exposed to the parameter to be measured. As the two mode indices will be affected in different ways, the relative phase delay of the two orthogonal components will depend on the parameter. This interferometric arrangement is similar to the Fibredyne system, but gives a predictable output and a higher sensitivity. However, the two orthogonal eigenmodes cannot, by definition, interfere, so the detection scheme must incorporate some form of polarisation rotator. In bulk optical detection schemes, this function is accomplished with a Wollaston prism (ref 88). Alternatively, at the expense of a reduction in received power, a linear polariser may be used with its axis at 45^0 to the fibre birefringent axis. The scheme has been modified to extend even further the dynamic range using a combined polarimetric and Michelson interferometer (ref 91) In chapter 7 a novel detection scheme will be proposed making use of integrated optical components-this will be shown to have both high sensitivity and dynamic range.

For a system using an unmodified fibre, the temperature sensitivity is far superior to the pressure sensitivity (ref 88). In addition, arrangements have been proposed whereby the non-sensing leads may be made immune to the external parameter (ref 91). Coatings may be applied to significantly enhace the pressure sensitivity while negating the relative phase change due to temperature.

The sensitivity of such a sensor to the generalised external influence **X** will now be developed. With reference to figure 7, fields E_0 are incident in the two modes of the fibre. Phase

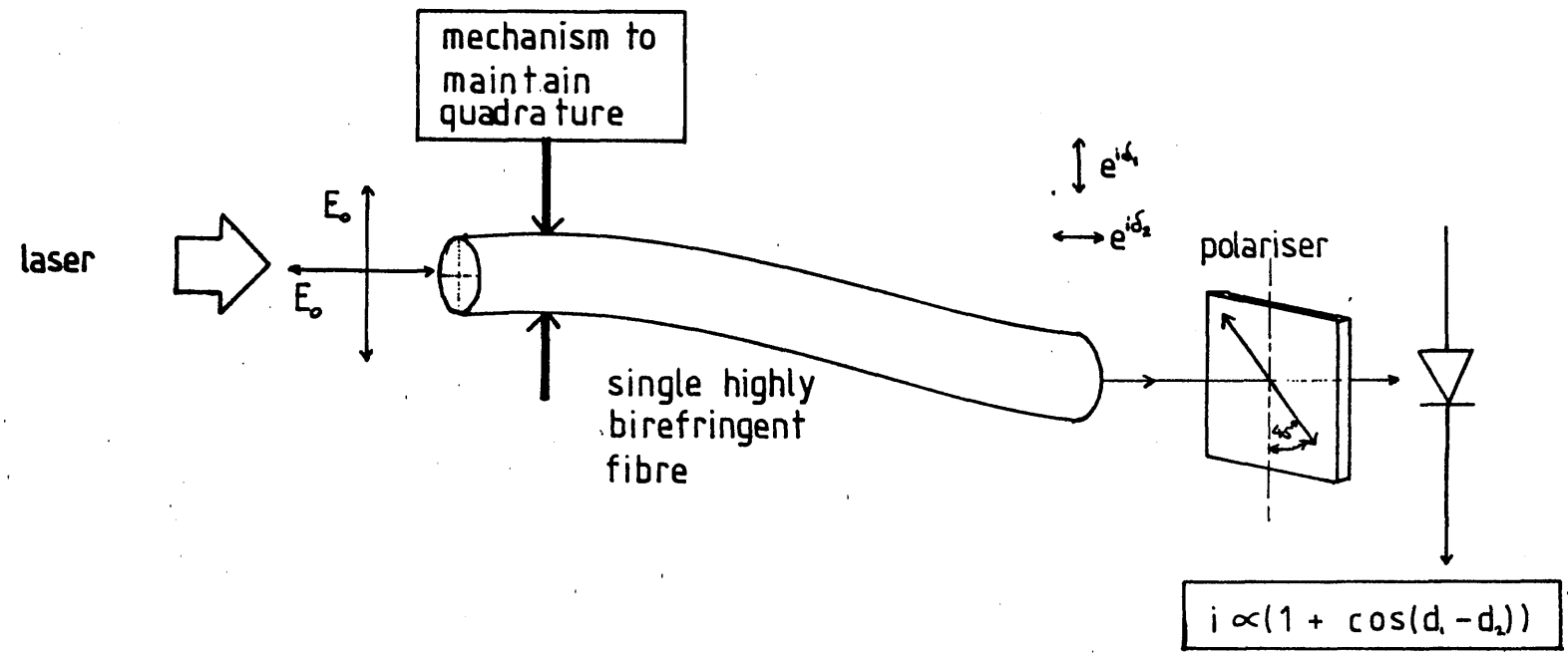

FIG 7 ILLUSTRATING THE SINGLE FIBRE POLARIMETRIC SENSOR (POLARIMETER)

delays $\delta_1=n_1kl$ and $\delta_2=n_2kl$ are associated with each mode. A similar treatment to that given for the Mach-Zehnder configuration yiels for the intensity transmitted by a polariser with its axis at 45^0 to the birefringent axes,

$$\frac{dI}{dx} = \frac{E_0^2}{4}\left[\sin(n_1-n_2)\left(k(n_1-n_2)\frac{\partial L}{\partial x} + kl\frac{\partial n_1}{\partial x} - kl\frac{\partial n_2}{\partial x}\right)\right] \qquad 1.14$$

Applying the quadrature condition replaces $\sin(n_1-n_2)lk$ by unity, and we see that the rate of change of intensity depends on the change of birefringence with external influence, rather than the absolute value of the indices. Replacing (n_1-n_2) by B, the birefringence, yields:

$$\frac{dI}{dx} = \frac{E_0^2}{4}\left(kB\frac{\partial L}{\partial x} + kl\frac{\partial B}{\partial x}\right) \qquad 1.15$$

The relative importance of the two terms in parentheses will depend on the application of the sensor. The sensitivity is reduced by a factor of approximately B/n compared to the Mach-Zehnderconfiguration. Although the dynamic range of the system is improved compared to the Mach-Zehnderconfiguration, the signal still becomes ambiguous for a certain value of external parameter. In addition, the sensitivity depends on the relative power in the two modes and on the source intensity: this may be shown as follows:

Suppose a fraction f of the incident field is launched into one mode, and a fraction (1-f) launched into the other, then the intensity transmitted by a polariser with its axis at θ to the first mode is:

$$I \propto E_0^2 f^2 \cos^2\theta + E_0^2 \sin^2\theta + E_0^2 f(1-f)\sin 2\theta \cos Bkl \qquad 1.16$$

The variation in output intensity with splitting fraction f is therefore:

$$\frac{dI}{df} = 2fE_0^2\cos^2\theta + E_0^2(1-2f)\sin 2\theta \cos Bkl \qquad 1.17$$

which with the quadrature condition becomes:

$$\frac{dI}{df} = 2f E_0^2 \cos^2\theta \qquad 1.18$$

which will be zero if f=0 or $\theta = \pi/2$. If these conditions are not met, then since we may detect a minimum intensity change of one part in 10^6 (ref 39), we require

$$2f\cos^2\theta < 10^{-6} \qquad 1.19$$

Considering now the effect of source intensity changes, we find:

$$\frac{dI}{dE_0} = E_0\left(2\sin^2\theta - 2f^2\cos^2\theta + 2f(1-f)\sin 2\theta \cos Bkl\right) \qquad 1.20$$

which will again be zero for $f=\sin^2\theta=1/2$, but will otherwise be finite. The effect of both these parameters on the sensitivity of the device is given by:

$$\frac{d}{df}\left(\frac{dI}{dx}\right) = (1-2f)E_0^2 \sin 2\theta \left(kL\frac{\partial B}{\partial x} + Bk\frac{\partial L}{\partial x}\right)\sin BkL$$

$$\frac{d}{dE_0}\left(\frac{dI}{dx}\right) = -2E_0 f(1-f)\sin 2\theta\left(kL\frac{\partial B}{\partial x} + Bk\frac{\partial L}{\partial x}\right)\sin BkL \qquad 1.21$$

It is seen that the sensitivity is affected by **variation** of alignment of both input and output polarisers.

A variety of schemes have been proposed to overcome the problems of dynamic range. Kersey (ref 91) reports two methods, both utilising the dependence of the relative phase delay of the two orthogonal modes on source frequency. A complex series of electronic processing operations are performed on the resultant output, when the input source frequency is switched between two well-defined frequencies. Using this technique, a minimum detectable strain of 0.003μm could be calculated from the measured signal to noise ratio. The method requires either a well-defined fibre length for a fixed source frequency difference, or a variable difference for an arbitrary fibre

length.

Alternatively, pseudo-heterodyne techniques may be used, again with the result of converting the D.C. phase to phase modulation of a carrier. In this case the source frequency is ramped, a technique also reported for Mach-Zehnder sensor geometries.

In the polarimetric sensor, it is also necessary to maintain at the input constant relative powers in each mode, also with constant input phase. This requires stable coupling between substrate and fibre for an integrated optical implementation, both in terms of mechanical alignment and polarisation stability.

1.7 Choice of fibre

As discussed earlier, the need for polarisers, or mode filters, arises from the ambiguity in output from a fibre sensor with birefringent sensing or reference arms in the presence of external influences.. The need for these devices is removed if a fibre could be produced wherein the two modes are degenerate, or a single polarisation fibre is used. To date, all fibres produced have some birefringence by virtue of their fabrication, a situation generally worsened by their geometrical arrangement (ref 36). The lowest value reported for the birefringence is approximately 10^{-7}. In any case, external influences such as mechanical deformation and coiling the fibre introduce birefringence (ref 40,35). By introducing a sufficiently high fibre birefringence and with suitable core geometries, it is possible to make one mode leaky while the other remains guided (ref 92,93). Single polarisation fibre is, as yet, not of sufficiently high performance. "Zing" fibre, available commercially from York Technology, has a loss of 5dB/km for the "guided" mode and 50dB/km for the leaky, orthogonal mode (Ref 96). There is in fact an intrinsic limit to the polarisation holding ablility of real birefringent fibres. As described by Brinkmeyer (ref 79), the birefringence induces into the fibre some anisotropy. Thus the radiation re-emitted from scattering centers within the fibre by Rayleigh scattering may not have the same state or degree of polarisation as the incident wave. This situation is not present in an ideal fibre with degenerate eigenmodes using isotropic cores and cladding.

A more economic solution for interferometric sensors would be offered by the use of high-birefringence fibre with high-extinction ratio polarisers at input and output ports. The performance of such a system is expected to be correspondingly poorer, but may still be acceptable for some applications (ref 97). For the optical fibre gyroscope, the act of coiling the fibre may be used to enhance the birefringence of the fibre and hence its polarisation holding ability.

For polarimetric sensors, improvements in sensitivity are likely to result from efforts to increase the birefringence.

1.8 Conclusion

A variety of optical fibre sensors and processing schemes have been investigated. Their requirements in terms of signal processing have been discussed. Integrated optical implementations are possible, but devices and systems reported to date have been of insufficiently high performance to offer significant advantages over their bulk optical counterparts when incorporated in systems.

Systems suitable for processing signals from optical fibre gyroscopes may also be used to process those from other optical fibre sensors, with relaxed requirements on their performance. Requirements for components for integrated optical implementations are:

(i) Beamsplitters with good isolation (100dB) from the substrate, ideally 50% splitting ratio, and stable reciprocal operation.

(ii) Polarisers must be fabricated to select one eigenmode of a single mode fibre with an extinction ratio of **at least** 60dB

(iii) couplers to transfer power between integrated optical substrate and optical fibre are required, with repeatable, efficient coupling. Mechanical stability is again essential.

(iiii) phase modulators are required: stability and repeatable operation are essential. In addition, the action of the phase modulator should not alter the optical field profile in the waveguide (a phenomenon inevitable due to the electrooptic effect).

(iv) Frequency shifters should have a high dynamic range (up to 4MHz at least), have repeatable operation, and ideally be linear.

Sidebands should be well suppressed, and their relative intensity not vary with time.

References

1.1 McMahon,D.H, Nelson,A.R, Spillman,W.B, "Fiber-Optic Transducers", I.E.E.E. Spectrum, December 1981

1.2 Dandridge,A, Tveten,A.B, Miles,R.O, Giallorenzi,T.G, "Fiber Optic Interferometric Sensor Development at N.R.L.", 1st International Conference on Optical Fibre Sensors, London, 1983

1.3 Zilber,J "Fibreoptic Sensor Market Technology", Optical Fibre Sensors, Stuttgart, 1984

1.4 Quick,W.H, James,K.A, Coker,J.E, "Fibre Optics Sensing Techniques", 1st International Conference on Optical Fibre Sensors, London, 1983

1.5 Gottleib,M, Brandt,G.B, "Measurement of Temperature with Optical Fibres", Fibre Optic Communications, Chicago, 1979

1.6 Dakin,J.P, Kahn,D.A, "A Novel Fibre Optic Temperature Probe", Optical and Quantum Electronics, Vol 9 (letter), 1977

1.7 Mitsuhashi,Y, Ishihara,S "Fiber Optic Polarisation Interferometer for Temperature Sensing Using a Polarisation Rotating Coupler", Optical Fibre Sensors, Stuttgart,1984

1.8 Salour,M.M, Schoner,G, Kull,M, Bectel,J.H, "Semiconductor Platelet Fibre Optic Temperature Sensor", Electronics Letters, Vol 21, No 4 pp135-136, 1985

1.9 Culshaw,B, Fiddy,M.A, Hall,T.J,Kingsley,S.A, "Fibre Optic Acoustic Sensors", IPC Science and Technology Press.

1.10 Bucaro,J.A, Lagakos,N, Cole,J.H, Giallorenzi,T.G, "Fibre

Optic Acoustic Transduction",Physical Acoustics Vol xvi, Academic Press, 1982.

1.11 Culshaw,B, Giles,I.P, "Fibre Optic Gyroscopes", Journal of Physics E:Scientific Instruments, Vol 16 pp5-14, 1983

1.12 Meyer,R.E, Ezekeil,S, Stowe,D.W, Tekippe,V.J, "Passive Fibre Optic Ring Resonator for Rotation Sensing", Optics Letters,Vol 8, no.12,pp644-646, 1983

1.13 Vali,V, Shorthill,R.W, "Fiber Ring Interferometer", Applied Optics, Vol 15 No 5, pp1099-1102, 1976

1.14 Udd,E, Cahill,R.F, "Fibre Optic Gyroscope Development", 7th Topical Meeting on Integrated and Guided Wave Optics, Kissimee, Florida, April 1984

1.15 Burns,W.K, Moeller,R.P, Villaruel,C.A, Abebe,M, "Fibre Optic Gyroscope with Polarisation Holding Fibre",Optics Letters, Vol 8, No 10, pp540-542

1.16 Imai,M, Ohashi,T, Ohtsuka,Y, "High Sensitive All Fiber Michelson Interferometer by use of Differential Output Configuration", Optics Communications, Vol 39, No 1,2 pp7-10 1981

1.17 Cookson,R.A, Bandyopadhyay,P, "Mechanical Vibration Measurements using a Fibre Optic Laser Doppler Probe", Optics and Laser Technology, pp33-36, February 1978

1.18 Ueha,S, Shibata,N, Tsujiuchi,J, "Flexible Coherent Probe for Vibration Measurements", Optics Communications, Vol 23,No 3, pp407-409, 1977

1.19 Giuliani,J,F, Wohltjen,H, Jarvis,N.L, "Reversible Optical Waveguide Sensor for Ammonia Vapors", Optics Letters Vol 8 No 1, pp54-56, 1983

1.20 Culshaw,B, Davies,D.E.N, Kingsley,S.A, "Fibre Optic Strain,

Pressure and Temperature Sensors", 4th European Conference on Optical Communications, Genoa, Italy, 1978

1.21 Butter,C.D, Hocker,G.B, "Fiber Optics Strain Guage", Applied Optics, Vol 17,No 18, pp2867-2869, 1978

1.22 Yariv,A, Windsor,H.V, "Proposal for Detection of Magnetic Fields through Magnetostrictive Perturbation of Optical Fibres", Optics Letters, Vol 5, No 3,pp87-89, 1980

1.23 Jones,R,E, Wlson,J.P, Pitt,G.D, Pratt,R.H, Foulds,K.W.H, Batchelder,D.N, "Detection Techniques for Measurement of DC Magnetic Fields using Optical Fibre Sensors", 1st International Conference on Optical Fibre Sensors, London, 1983

1.24 Shibata,K "A Fibre Optic /electric Field Sensor using the Electrooptic Effect of $Bi_4Ge_3O_{12}$, 1st International Conference on Optical Fibre Sensors, London, 1983

1.25 Rogers,A.J, "Optical Measurement of Current and Voltage on Power Systems", Electric Power Applications, Vol 2,No 4, pp120-124, 1979

1.26 Rashleigh,S.C, Ulrich,R, "Magneto Optic Current Sensing with Birefringent Fibers", Applied Physics Letters, Vol 34, No 11, pp768-770, 1979

1.27 Wald,A, Post,K, Ransohoff,J, Hass,W, Epstein,F, "A New Technique for Monitoring Epidural Intracranial Pressure", Medical Instrumentation, Vol 11, No 6, pp352-355, 1977

1.28 Culshaw,B, "Optical Fibre Transducers", The Radio and Electronic Engineer, Vol 52, No 6, pp283-290, 1983

1.29 Culshaw,B, Foley,J, Giles,I.P, "A Balancing Technique for Optical Fibre Intensity Modulated Transducers", Optical Fibre Sensors, Stuttgart, 1984

1.30 Bristow,J.P.G, Final Year Undergraduate Project, Department of Physics, University of Southampton, 1982

1.31 Culshaw,B, Davies,D.E.N, Kingsley,S.A, "Multimode Optical Fibre Sensors", Advances in Ceramics, Vol 2, Physics of Fibre Optics, American Ceramic Society, 1981

1.32 Hioki,R, Suzuki,T, "Coherent Light Transmitted Through Optical Fibers", Japanese Journal of Applied Physics, Vol 4, p817, 1965

1.33 Yoshino,T, Nara,M, "Accurate Fiber Optic Sensors using Differential Heterodyne Method", Optical Fibre Sensors, Stuttgart, 1984

1.34 Maclaughlin, A, Ph.D thesis ,University of Glasgow, 1981

1.35 Rashleigh,S.C, "Origins and Control of Polarisation Effects in Single Mode Fibers", Journal of Lightwave Technology, Vol lt-1, No 2, pp312-331, 1983

1.36 Ross,J.N, "The Rotation of the Polarisation in Low Birefringence Monomode Optical Fibres due to Geometric Effects", Optical and Quantum Electronics, Vol 16, pp455-461, 1984

1.37 Yeh,C, Marshadi,F, "On Weakly Guiding Single Mode Optical Waveguides", Journal of Lightwave Technology, Vol LT-3, No 1, pp199-205, 1985

1.38 Jerrard,H.G, "Transmission of Light through Birefringent and Optically Active Media: the Poincare Sphere", Journal of the Optical Socity of America, Vol 44, No 8, 1954

1.39 Jackson,D.A, Dandridge,A, Sheem,S.K, "Measurement of Small Phase Shifts using a Single Mode Optical Fibre Interferometer", Optics Letters, Vol 5, No 4, pp139-141, 1980

1.40 Kaminow,I.P, "Polarisation in Optical Fibres", I.E.E.E.

Journal of Quantum Electronics, Vol QE-17, No 1, pp15-22, 1981

1.41 Schurcliff,W.A, "Polarised Light", Oxford,1962

1.42 Alferness,R.C, "Electrooptic Guided Wave Device for General Polarisation Transformations", I.E.E.E. Journal of Quantum Electronics, Vol QE-17, No 6, pp965-969, 1981

1.43 Alferness,R.C, Buhl,L.L, Korotky,S.K, "Ti:$LiNbO_3$ Guided-Wave Devices for Long Wavelength Telecommunications", 7^{th} Topical Meeting on Integrated and Guided Wave Optics, Kissimee, Florida, April 1984

1.44 Alferness,R.C, Buhl,L.L, "Waveguide Electro Optic Polarisation Transformer", Appied Physics Letters, Vol 38, No 9, pp655-657, 1981

1.45 Culshaw, Fibre Optic Gyroscopes, Jornal of Physics E: Scientific Instruments, Vol 16, pp5-14, 1983

1.46 Chow,W.W, Gea-Banacloche,J, Pedrotti,L.M, "The Ring Laser Gyro", Reviews of Modern Physics, Vol 57 No 1, January 1985

1.47 Ohtsuka,Y, "Analysis of a Fiber-Optic Passive Loop Resonator Gyroscope: Dependence on Resonator Parameters and Light-Source Coherence", Journal of Lightwave Technology, Vol LT-3, No 2 pp378-384, 1985

1.48 Fisher,B, Sternklar,S, "New Optical Gyroscope based on the Ring Passive Phase Conjugator", Applied Physics Letters, Vol 47, No 1, pp1-3, 1985

1.49 Post, E.J. "Sagnac Effect", Reviews of Modern Physics, Vol 39, No 2, pp475-493, 1967

1.50 Cahill,R.R, Udd,E, "Phase Nulling Fiber Optic Laser Gyro", Optics Letters, Vol 4, No 3, pp93-95, 1979

1.51 Stallard,W.A, Daymond-John,B.E, Booth,R.C, "$LiNbO_3$ Optical Frequency Translators for Coherent Optical Fibre Systems", 4th European Conference on Integrated Optics, Berlin 1984

1.52 Richmond, K.R, "Coherent Systems Make Gains", Electronics and Power, May 1985

1.53 Barlow,A.J, Dye,M.S, Traynor,B.T, "Dispersion Induced Non-Reciprocal Effects in Phase Nulling Fibre Gyroscopes", 1st International Conference on Optical Fibre Sensors, London 1983

1.54 Ourmazd,A, Birch,R.D, Varnham,M.P, Payne,D.N, Tarbox,E.J, "Enhancement of Birefringence in Polarisation Maintaining Fibres by Thermal Annealing", Electronics Letters, Vol 19, No 4, pp143-144, 1983

1.55 Bohm,K, Marten,P, Staudigel,C, Weitel,E, "Fiber Optic Gyro with Digital Data Processing", Optical Fibre Sensors, Stuttgart, 1984

1.56 Davis,J.L, Ezekiel,S, "Closed Loop Low Noise Fibre Optic Rotation Sensor", Optics Letters, Vol 6, No 10, pp505-507, 1981

1.57 Kim,B.Y, Shaw,H.J, "Phase Modulation Approach to Closed Loop Fibre Optic Gyroscope and Scale Factor Stabilisation"

1.58 Okoshi,T, "Recent Progress in Heterodyne/Coherent Optical Fiber Communications", Journal of Lightwave Technology, Vol LT-2, No 4, pp341-346, 1984

1.59 Lefevre,H.C, Arditty,H.J, Graindorge,Ph, "Compact All-Fibre Gyroscope Brassboard", ECOC 84

1.60 Bone,M.C, Parker, J.W, "An Integrated Optic Fibre Gyroscope: Performance and Limitations", 1st International Conference on Optical Fibre Sensors, London 1983

1.61 Varnham,M.P, De Fornel,F, Payne,D.N, Ragdale,C.M,

Barlow,A.J, Tarbox,E.J, "Comparison Between Coil and Taper Fibre Polarisers", Optical Fibre Sensors, Stuttgart, 1984

1.62 Slonecker,M, ITT Electro Optics Product Division, Confidential Publication, 1979

1.63 Risk,W.P, Youngquist,R.C, Kino,G.S, Shaw,H.J, "Acousto Optic Birefringent Fiber Frequency Shifters", 7th Topical Meeting on Integrated and Guided Wave Optics, Kissimee, Florida, April, 1984

1.64 Takada,K, "Calculation of Rayleigh Backscattering in Fiber Optic Gyroscopes", Journal of the Optical Society of America, Vol 2, No 2, pp872-877, 1985

1.65 Frigo,N.J, Taylor,H.F, Goldberg,L, Rashleigh,S.C, "Optical Kerr Effect in Fiber Gyroscopes: Effects of Nonmonochromatic Sources", Optics Letters, Vol 8, No 2, pp119-121, 1983

1.66 Kirkby,R.A, "Semiconductor Lasers Sources for Optical Communication", The Radio and Electronic Engineer, Vol 51, No 7, pp362-376, July/August 1981

1.67 Hirota,O, Suematsu,Y, "Noise Properties of Injection Lasers Due to Reflected Waves", I.E.E.E. Journal of Quantum Electronics, Vol QE-15, No 3, 1979

1.68 Mitsunaga,K, Masuda,M, Koyama,J, "Optical Waveguide Isolator in Ti:Diffused $LiNbO_3$", Optics Communications, Vol 27, No 3, pp361-364, 1978

1.69 Becker,R.A, "Characterisation of Instability in Ti:indiffused $LiNbO_3$ Modulators Due to Photorefractive and Non-Optical Sources", 7th Topical Meeting on Integrated and Guided Wave Optics, Kissimee, Florida, April 1984

1.70 Bulmer,C.H, Burns, W.K, Hiser,S.C, "Ti:$LiNbO_3$ Linear Interferometric Modulators and Photorefractive Effects", ibid

1.71 Cullen,T.J, Ph.D. Thesis, University of Glasgow, 1985

1.72 Alferness,R.C, Buhl,L.L, Korotky,S.K, Divino,M.D, "Ti:$LiNbO_3$ Guided Wave Devices for Long Wavelength Telecommunications", 7^{th} Topical Meeting on Integrated and Guided Wave Optics, Kissimee, Florida, April 1984

1.73 Sasaki,H, Anderson,I, "Theoretical and Experimental Studies on Acitve Y-Junctions in Optical Waveguides", I.E.E.E. Journal of Quantum Electronics, Vol QE-14, No 11, pp883-892, 1978

1.74 Pavlath,G.A, Shaw,H.J, "Birefringence and Polarisation Effects in Fiber Gyroscopes", Appied Optics, Vol 21, No 10, pp1752-1757, 1982

1.75 Ulrich,R, Johnson,M, "Fiber-ring Interferometer; Polarisation Analysis", Optics Letters, Vol 4, No 5, pp152-154, 1979

1.76 Mears,R.J, Varnham,M.P, Payne,D,N, Barlow,A.J, "Polarisation Control in Resonant Ring Fibre Gyroscopes", Optical Fibre Sensors, Stuttgart, 1984

1.77 Payne,D "Fibres for Sensors", ibid

1.78 Marrone,M.J, "Polarisation Holding in Long Length Polarising Fibres", Electronics Letters, Vol 21, No 6, pp244-245,1985

1.79 Brinkmeyer,E, Eickhoff,W, "Ultimate Limit of Polarisation Holding in Single Mode Fibres", Electronics Letters, Vol 19, No 23, pp996-997, 1983

1.80 Kintner,E.C, "Polarisation Control in Optical Fibre Gyroscopes", Optics Letters, Vol 6, No 3, pp154-156, 1981

1.81 Jones,E, "Analysis of Noise and Bias in the Fibre Optic Gyro", 1^{st} International Conference on Optical Fibre Sensors, London, 1983

1.82 Feymat,A.L, "Jones Matrix Representation of Optical Instruments: 1 Beamsplitters", Applied Optics, Vol 10, No 11, pp2499-2503, 1971

1.83 Wong,K.K, De La Rue,R.M, "Electro Optic Waveguide Frequency Translation in $LiNbO_3$ by Proton Exchange", Optics Letters, Vol 7, No11, pp546-548, 1982

1.84 Bulmer,C.H, Moeller,R.P, "Fiber Gyroscope with Nonreciprocally Operated Fiber Coupled $LiNbO_3$ Phase Shifter", Optics Letters, Vol 6, No 11, pp572-574, 1981

1.85 Al-Chalabi,S.A, Culshaw,B, Davies,D.E.N, "Partially Coherent Sources in Interferometric Sensors", 1st International Conference on Optical Fibre Sensors, London, 1983

1.86 Martinelli,M, Barberis,A, "Interferometric Michelson-type Optical Fiber Sensor; comparison between phase modulation and frequency modulation detection", Journal of the Optical Society of America, Vol 2, No 4, pp603-609, 1985

1.87 Giles,I.P, Uttam,D, Culshaw,B, Davies,D.E.N, "Coherent Optical Fibre Sensors with Modulated Laser Sources", Electronics Letters, Vol 19, No 1, pp14-15, 1983

1.88 Eickhoff,W, "Temperature Sensing by Mode-Mode Interference in Birefringent Optical Fibres", Optics Letters, Vol 6, No 4, pp204-206, 1981

1.89 Rashleigh,S.C. "Polarimetric Sensors: Exploiting the Axial Stress in High Birefringence Fibers", 1st International Conference on Optical Fibre Sensors, London, 1983

1.90 Kikuchi,Y, Yamauchi,R, Akiyama,M, Fukada,O, Inada,K, "Polarimetric Strain and Pressure Sensors Using Temperature-Independent Polarisation Maintaining Optical Fibre", Optical Fibre Sensors, Stuttgart, 1984

1.91 Kersey,A.D, Corke,M, Jackson,D.A, "Linearised Remote Sensing Using a Monomode Fibre Polarimetric Sensor", ibid

1.92 Snyder,A.W, Ruhl,F, "New Single Mode Single Polarisation Fibre", Electronics Letters, Vol 19, No 5, pp185-188, 1983

1.93 Varnham,M.P, Payne,D.N, Birch,R.D, Tarbox,E.J, "Single Polarisation Operation of Highly Birefringent Bow-Tie Optical Fibres", Electronics Letters, Vol 19, No 7, pp267-247, 1983

1.94 Hecht,E, Zajac,A, "Optics", Addison Wesley, 1979

1.95 Corke,M, Jones,J.C.C, Kersey,A.D, Jackson,D.A, "Combined Michelson and Polarimetric Fiber Optic Interferometric Sensor", Electronic Letters, Vol 21, No 4, pp148-149, 1985

1.96 York Technology, Sales literature

1.97 Harmer,A.L, "Optical Fibre Sensor Markets", 1st International Conference on Optical Fibre Sensors, London, 1984

Chapter 2 Integrated Optical Mode Filters Using Hybrid Titanium Indifused/ Proton Exchanged Waveguides in Lithium Niobate

2.1 Introduction

A recent development within the field of integrated optics based on lithium niobate has been the use of proton exchanged wavegides (ref 1,2,3). The process consists essentially of exposing a selected area of the lithium niobate to a carboxylic acid at an elevated temperature. For example, immersion in pure benzoic acid at 210^0C for several minutes is known to produce slab waveguides with single mode properties.

The waveguides are characterised by a large increase in refractive index compared to more traditional titanium indiffusion techniques. In addition, the process operates on the extraordinary refractive index only, the ordinary refractive index being lowered (ref 4). It is seen that the method enables mode selective waveguides to be fabricated, the transmitted mode depending on the particular orientation of the crystal. For example, Z-cut $LiNbO_3$ would, after proton exchange waveguide fabrication, yield preferential transmission of TM-like modes.

The majority of reported work on the technique has concerned slab geometries. While such guides do indeed posess the required mode-selective properties, they would be of little use for interfacing with optical fibres where stripe geometries are required (ref 5,6). The high resulting relative refractive index difference would require narrow geometries for efficient power transfer to single mode optical fibres. In addition, many integrated optical devices have been demonstrated using titanium indiffused waveguides. Thus a hybrid geometry is called for whereby some components are fabricated using titanium indiffused waveguides, while the polarising, or mode selective function is performed by a proton exchanged waveguide. The use of two different waveguide fabrication methods on the same substrate gives rise to two major problems.

(i) Alignment between the two waveguide sections will be critical

(ii) more complex fabrication procedures will be required.

Proton exchanged waveguides fabricated under certain conditions (ref 7,8,9) are known to change their properties with time,

however recent developments with annealing (ref 10) and dilute-melt fabrication techniques (ref 11) go some way to rectifying the situaution.

2.2 Design of hybrid H^+/Ti $LiNbO_3$ polarisers

Various different configurations are possible for the polarisers. They may be divided into two broad categories

(i) those in which the proton exchanged section is used to modify an existing titanium indiffused guide, and

(ii) those in which the proton exchanged guide completes an otherwise discontinuous titanium indiffused waveguide.

As an example of the former category, a polariser first reported by Papuchon is illustrated in figure 1a. Two "blocks" of proton exchanged substrate border a continuous titanium indiffused waveguide. By suitable choice of gap between the two sections, the evanescent wave associated with the titanium indiffused guide (ref 12) may extend into the proton exchanged section. This will give rise to leaky wave proagation (ref 5) if the refractive index of the external sections is lower than that of the substrate, and confinement otherwise. Thus a polariser may be produced. Papuchon (ref 13) has reported an extinction ratio of 30dB for the device, with an excess loss of 1dB. The polariser may be optimised by design based on the model of figure 2, wherein light in the central, titanium indiffused waveguide is allowed to couple to the neighbouring waveguides representing the proton exchanged sections. Coupling will only take place for those modes with the major electric field component aligned along the crystal extraordinary axis. The proton exchanged sections fabricated in this geometry will support many modes.

Alternatively, an existing titanium indiffused waveguide may be modified to endow it with mode-selective properties by superposing proton exchanged sections. Figure 3, reproduced from ref 13, illustrates the refractive increases and decreases induced by both titanium indiffusion and proton exchange techniques. It will be seen that for the extraordinary polarisation, the net effect of superposing the guides is to increase the index above that of the substrate, while for the ordinary polarisation the opposite is true. Thus mode selection is again possible, but the effect will not be as pronounced as in

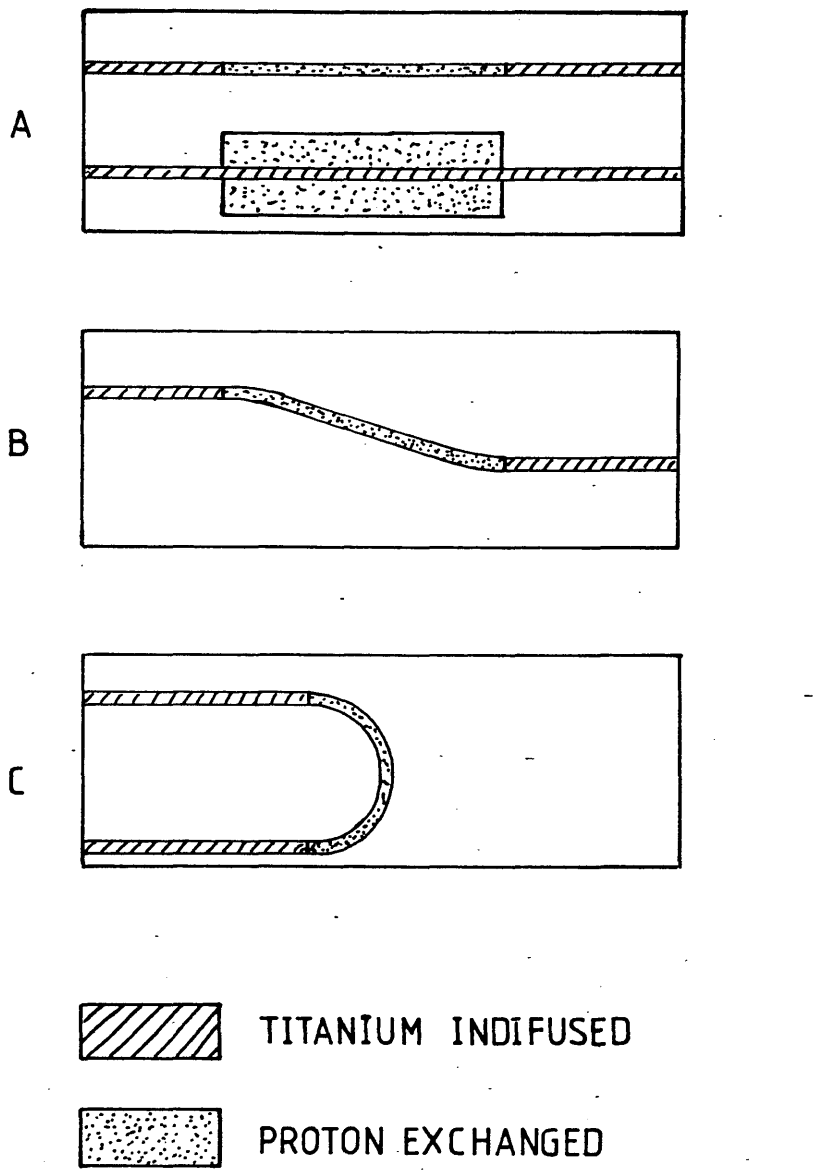

FIG 1 VARIOUS CONFIGURATIONS OF HYBRID Ti/H^+ WAVEGUIDE POLARISERS: (A) INTERNAL AND EXTERNAL MODIFICATION OF STRAIGHT GUIDES (B)MODIFICATION TO REDUCE RE-COUPLING OF SCATTERED LIGHT (C)COMPACT U-SHAPED DEVICE.

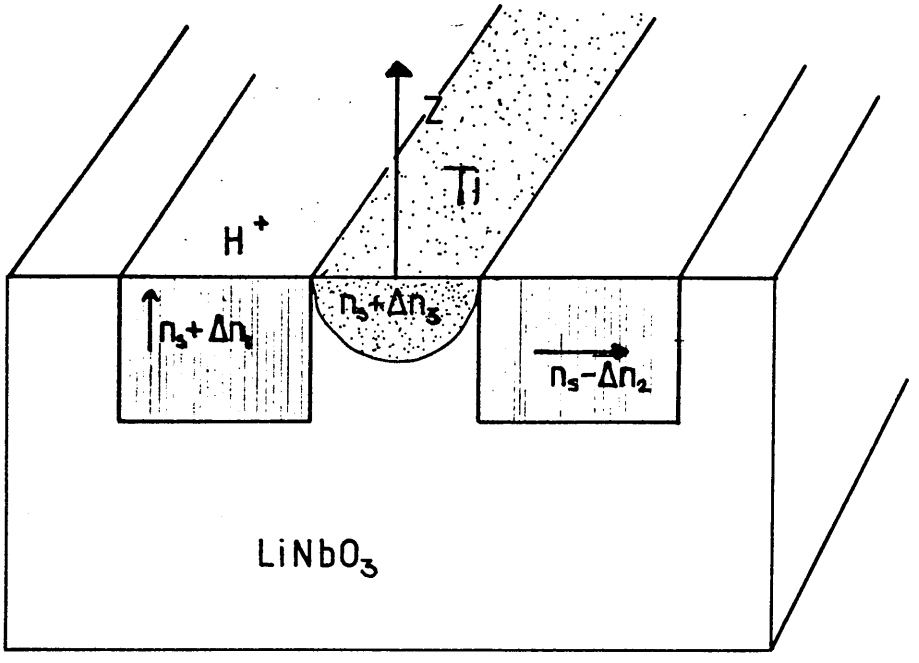

FIG 2 ILLUSTRATING PROTON EXCHANGED POLARISATION MODIFICATION OF TITANIUM INDIFFUSED WAVEGUIDES.

	PROTON EXCHANGE	TITANIUM INDIFFUSION
EXTRAORDINARY INDEX	+0·12	+0.005
ORDINARY INDEX	+0.1	+0·005

FIG 3 INCREASES OR DECREASES OF REFRACTIVE INDICES OF LITHIUM NIOBATE DUE TO WAVE-GUIDE FABRICATION TECHNIQUES

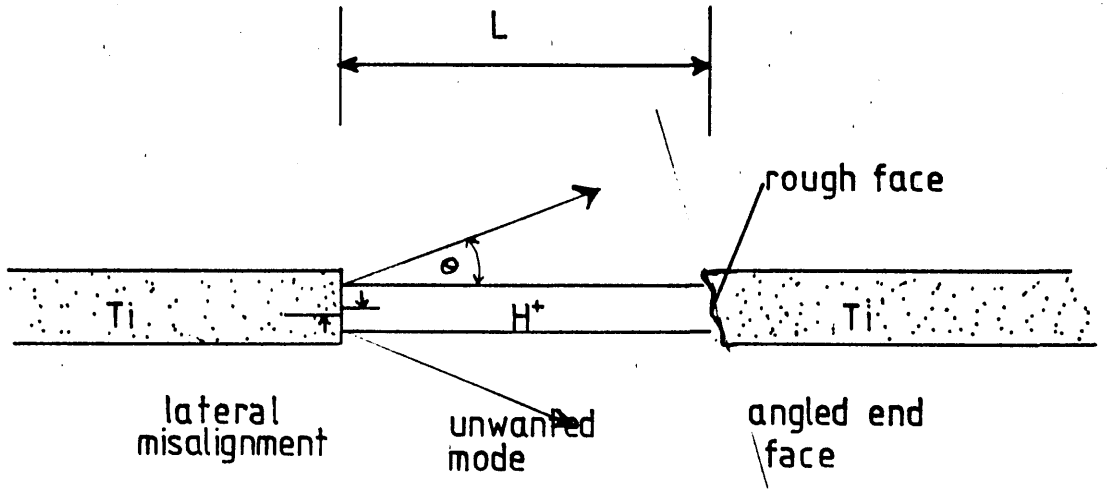

FIG 6 ILLUSTRATING THE DESIGN AND POSSIBLE DEFECTS IN A STRAIGHT HYBRID PROTON EXCHANGE / TITANIUM IN-DIFFUSED WAVEGUIDE POLARISERS.

the previous example. The resulting waveguide is referred to by the acronym "TIPE" (Titanium Indiffused Proton Exchange).

Within the second category a variety of geometries are again possible: some are illustrated in figure 1. To consider the effect on device performance of various fabricational considerations we refer to figure 4. Light, initially of arbitrary degree and state of polarisation propagates along the unmodified titanium indiffused waveguide. Upon reaching the interface with the proton exchanged section, a certain fraction will be reflected, and the remainder excite the modes of the second waveguide (proton exchanged section). According to the length, numerical aperture (ref 14) and width of the various waveguide sections, a significant fraction of the light corresponding to the ordinary polarisation will diverge, while that aligned along the extraordinary axis will remain guided. The guided energy then impinges on a further boundary, this being with a conventional titanium indiffused waveguide. According to their relative alignments, either or both of the orthogonal waveguide modes will be excited. Ideally, only one mode of the titanium indiffused guide will carry any energy, however a variety of corrupting influences will exist to re-distribute the energy:

(i) Due to the waveguide discontinuity, a given fraction of the energy incident upon each interface will be reflected. This may be calculated using the following equation. For incident and reflected fields E one may write (ref 15):

$$E_y^i + a_r E_y^r + \int_{-\infty}^{\infty} q_r(\rho) E_y^t(\rho)\, d\rho = C_t E_y^t + \int_{-\infty}^{\infty} p_t(\rho) E_y^t(\rho)\, d\rho \qquad 2.1$$

The terms represent from left to right: the incident guided field, the reflected guided field, the reflected radiated field, the transmitted guided field, and the transmitted radiated field. Thus, depending on the relative magnitude of the various coefficients, incident guided waves may be reflected or give rise to transmitted radiation. The equation cannot however be solved for the general case, approximations being necessary (ref 15).

(ii) The modes of the individual sections, while being orthogonal within themselves, will not necessarily be mutually orthogonal.

This may give rise to polarisation conversion with a concommittant adverse effect on device performance

(iii) non-perpendicular waveguide boundaries and rough waveguide edges will give rise to loss (ref 16) and polarisation conversion (ref 17)

(iv) Scattering centres within the crystal will give rise to increased loss (ref 18) and polarisation coupling due to the anisotropic nature of the Rayleigh scattering.

(v) Non-coincidence of waveguide axes will give rise to increased loss and possibly polarisation conversion.

It is a feature of all the hybrid polarisers so far described that the unwanted mode is merely diverted and not absorbed. Thus scattering centres within the crystal may re-couple the light into the guide. In addition, the divergence of the unwanted mode may be such as to enable a significant fraction of the mode to be captured by the second guide.

To avoid these problems, the geometry illustrated in figure 1c is proposed, whereby the proton exchanged section consists of a U-shape. Thus the direction of propagation of the guided mode is altered by 180^{o} while the light initially in the unwanted mode continues undeviated in the substrate. Figure 5 illustrates the various mechanisms which may reduce the extinction ratio and increase the excess loss of the device. Rayleigh backscattering will contribute to the former: the magnitude will depend on the fabrication conditions.

2.3 Performance of Hybrid Proton Exchanged/ Titanium Indiffused Polarisers on $LiNbO_3$ reported in literature

Papuchon (ref 13) has reported an extinction ratio of 30dB and an excess loss of 1dB/cm (with unspecified experimental error) using the device illustrated in figure 1a.

Findlaky and Chen (ref 19) have investigated devices using two separate 1mm sections of proton exchanged guide in a discontinuous titanium indiffused guide, obtaining an extinction ratio of 33dB with excess loss of 4.2dB. Subsequent annealing at 300^{o}c for 2 hours in air reduced the excess loss to 0.8dB while leaving the extinction ratio esentially unchanged. However, the authors did not specify the masking conditions used for the annealing: as will be shown in section 2.5.3, this has a profound

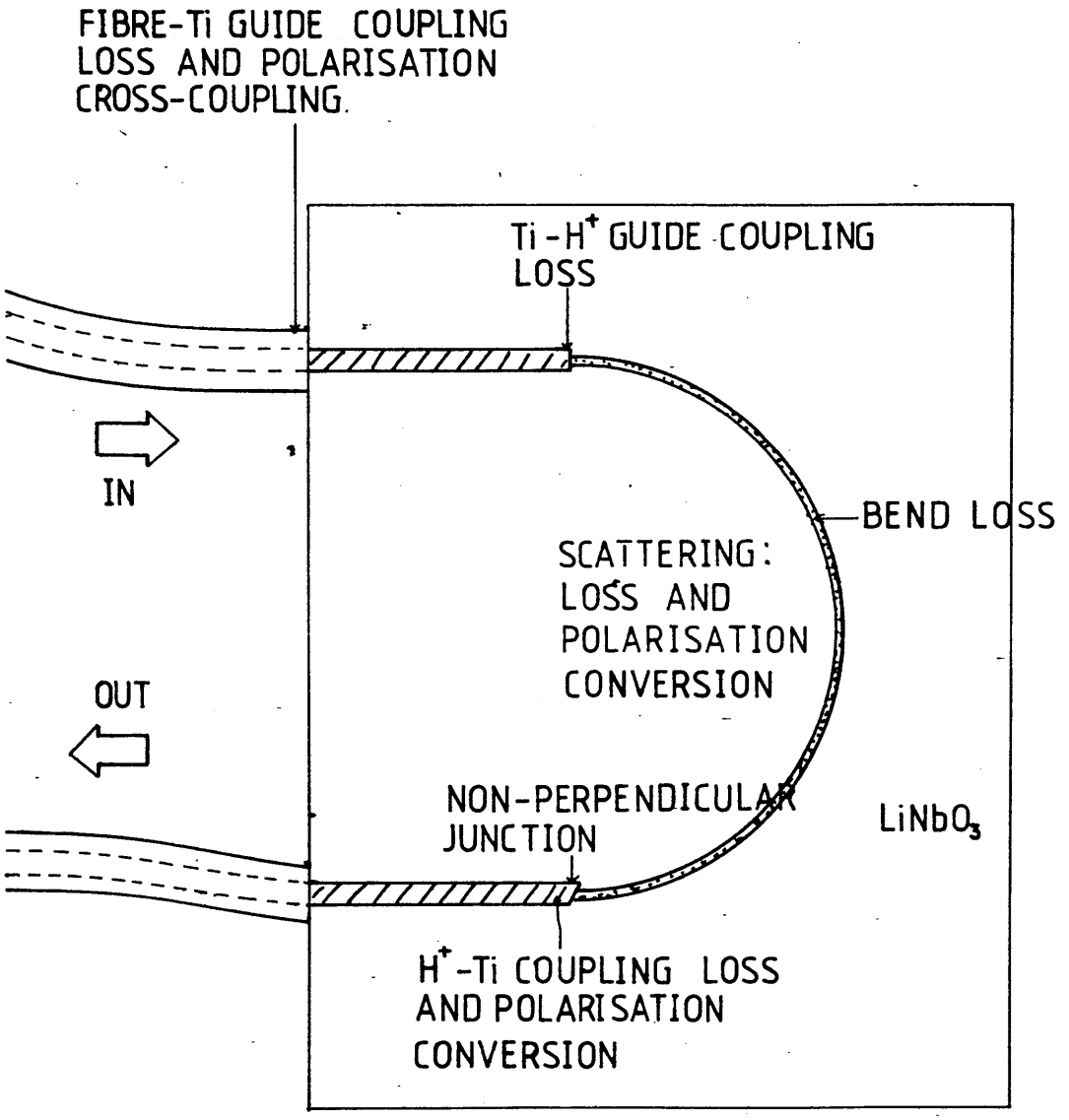

FIG 5 U-SHAPED POLARISER SELECTING A MODE IN AN OPTICAL FIBRE, ILLUSTRATING POSSIBLE LOSS AND POLARISATION NOISE MECHANISMS (KEY AS FIG 1).

effect on device performance.

2.4 Optimisation of Hybrid Polarisers

It is seen from reference to equation 2.1 that the waveguide geometries of the two sections will affect the extinction ratio and excess loss of both the straight and the U-shaped devives via both the effective index and the optical field distribution. To investigate the variation in extinction ratio and excess loss with waveguide width and length of proton exchanged section a series of polarisers was fabricated according to figure 6. Modelling of the devices is difficult. The beam propagation method (ref 20), which would be ideally suited to the description of the proton exchanged sections in isolation is a two-dimensional technique. Furthermore, it cannot cope with abrupt changes in refractive index along the propagation direction.

A crude estimate of the effect on the extinction ratio of length of proton exchanged section for the straight devices may be obtained from the model illustrated in figure 6. We assume that the mode corresponding to the ordinary polarisation is not guided in the proton exchanged section, and that $\Delta n_o=0$. The field emerging from the titanium indiffused guide is represented as diverging from a point source at an angle defined by the numerical aperture of the system. Simple ray optics shows that this maximum angle θ_s is given by:

$$\frac{(n_g-n_c)^{1/2}}{n_s} = \sin\theta_s \qquad 2.2$$

Substitution of typical values for the ordinary polarisation yields $\theta = 3.8^0$. The model then gives for the extinction ratio,

$$E \simeq 20\log_{10}\left(\frac{d}{2L\theta}\right) \qquad 2.3$$

Using a guide width of 5 microns, assuming step indices, and a length of exchanged region of 1mm, we obtain an extinction ratio of approximately 60dB.

From our simple model, we expect the extinction ratio to increase with length of proton exchanged section, while the excess loss should vary little. Provided the proton exchanged

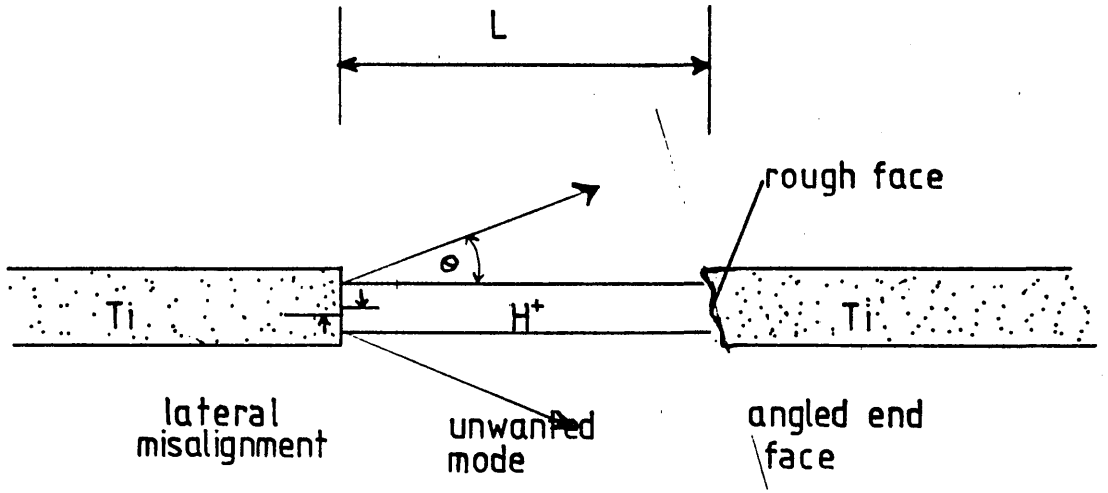

FIG 6 ILLUSTRATING THE DESIGN AND POSSIBLE DEFECTS IN A STRAIGHT HYBRID PROTON EXCHANGE / TITANIUM IN-DIFFUSED WAVEGUIDE POLARISERS.

section supported only a single mode, we would also expect the excess loss to be a minimum for some well defined width of titanium indiffused guide, all other fabricational parameters remaining constant. In addition we would expect the excess loss to be increased by using a three-stage waveguide transition as illustrated in figure 7. While such an arrangement is not desirable, it will be difficult to avoid overlapping of the two waveguide sections in practice.

2.5 Experimental

2.5.1 Sample preparation and waveguide definition

Before the photolithographic process may proceed, all traces of dust and grease must be removed from the substrate to be used. Failure to do so will result in discontinuities in the final waveguide and poor adhesion of masking layers.

The lithium niobate as supplied by the manufacturers was in the form of 1mm thick wafers, approximately 2" in diameter. The material was supplied by Barr and Stroud Ltd and was specified to be of optical quality. However, difficulties with quality control of some batches of Z-cut material led to wafers being purchased from Crystal Technology Co, California. Since small samples were required, to avoid waste the wafer was cut into smaller sections, these being approximately 2cm x 1cm. The cutting was performed with a circular diamond saw, lubricated with **Syton**. At this stage, some samples (usually Z-cut) were observed to acquire cracks at approximately 45^0 to the cut. Such samples were discarded. During the cutting process, the sample was mounted on a glass support, wax being used to fix the two. The wax must be removed, in addition to any dust which may accumulate on the sample.

Cleaning proceeded by immersing the samples in concentrated sulphuric acid. Hydrogen peroxide was added from a dropper with its end held under the surface of the acid. By adding the peroxide gradually, the temperature increase associated with the process could be controlled to reduce the risk of thermal shock. Having added 20% by volume of the hydrogen peroxide, the mixture was allowed to cool. The sample was then transferred to **Analar** acetone in a plastic beaker using metal tweezers and agitated

TM	+0·005	+0·105	+0·1	+0·105	+0·005
TE	+0·005	-0·995	-0·1	-0·995	+0·005

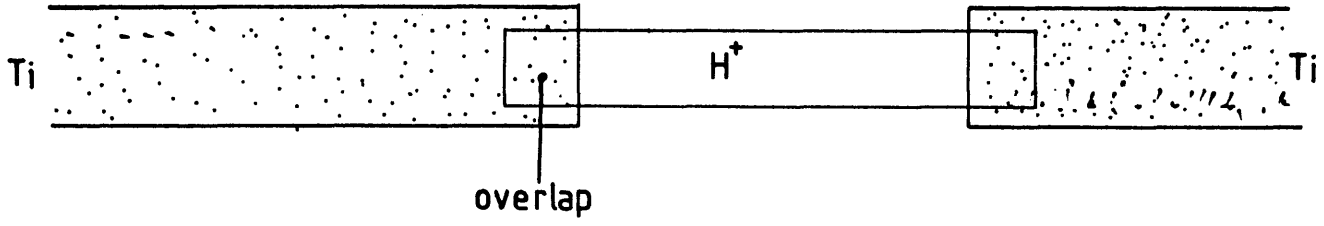

FIG 7 ILLUSTRATING THE INCREASE IN EXCESS LOSS OF HYBRID POLARISER ARISING FROM OVERLAPPING OF WAVEGUIDE SECTIONS FIGURES SHOWN ARE REFRACTIVE INCREASES ABOVE SUBSTRATE.

ultrasonically for 5 minutes. The sample was then transferred to a plastic beaker of **Analar** methanol with plastic tweezers and the agitation repeated. The lithium niobate was transferred to a clean plastic beaker with fresh acetone and agitated, followed by a further 5 minutes in methanol. At no time was the sample allowed either to dry (to avoid electrostatic attraction of dust particles) or to come into contact with water, where charged particles (ref 21) in the water may be attracted to the cleaned crystal surface. If more than one sample was to be prepared at the same time, the same procedure was used, except that individual beakers were used to avoid the generation of particles of lithium niobate by abrasion. The sample was then transferred directly from the methanol to a spinner in a class 100 clean cabinet, where rotation at 2,000 rpm for 20 seconds removed the remaining methanol. Photoresist (Shipley AZ1350J) was dropped using a syringe with a 0.2μm filter to give a thick coating of the liquid. Spinning with the same parameters followed.

The masks to be used were subjected to the same cleaning treatment, except in the case of ferric oxide (transparent) masks: this coating is dissolved by the acid:peroxide mixture. The first stage was then replaced with scrubbing with detergent (**Decon 90**) and a plastic sponge.

Transferring the coated samples in a closed petri dish to a hotplate avoided contamination with dust particles. Drying for 10 minutes on the hot-plate preceded curing at 70^0C. Standard contact printing and development procedures were used to define the waveguides.

2.5.2 Titanium Indiffused Waveguide Fabrication

Electron beam evaporation of a 500Å film of Titanium was followed by standard lift-off processes. The completed samples were then diffused in an atmosphere of flowing wet argon (2l/min through water at 70^0C) for 9 1/2 hours, including a linear increase in temperature from room conditions for one hour, to 1000^0C. The samples were allowed to cool down in flowing wet oxygen for one hour, after which no special environment was used. These diffusion conditions are known to suppress outdiffusion of Li_2O (ref 22,23) while the diffusion time was known to give a minimum in the in=plane scattering loss of y-cut samples at the

temperature used. The controller and thermocouples used ensured repeatability of the temperature from batch to batch of $\pm 1^0$C. Following cleaning, the sample was then ready for the fabrication of the proton exchanged sections.

To ensure a sufficient range of waveguide widths and lengths of exchanged section, a mask was used which had 3 sets of waveguides, within each set the guide width varying from 2 to 10 microns in 1 micron steps. The same mask was used for both titanium indiffused guides and proton exchanged sections to ensure accurate alignment for each waveguide. The mask had been modified during the definition of the titanium indiffused sections by the addition of **Rubylith** strips, tapering in width, normal to the waveguides on the mask. The strips tapered from 0.5mm to 2mm over a 2cm length, thus enabling a range of gaps in the titanium indiffused section to be defined. The strips were mounted on the non-contacting side of the ferric oxide mask. The strips were then removed for the fabrication of the proton exchanged sections and a complementary set of **Rubylith** strips used to cover the remainder of the mask. The dimensions of the latter were such as to allow 0.5mm overlap of the two sections at either end.

2.5.3 Fabrication of Proton Exchanged Waveguide Sections

Fabrication of the proton exchanged sections followed standard practice (ref 3). The cleaned samples were coated with approximately 1μm of aluminium, this being deposited with a conventional thermal evaporator at 1.0×10^{-5} mm Hg pressure. Preparation of the photoresist proceded as previously described. The exposure was performed using a mask aligner-this also allowed fine control over the alignment of the mask with respect to the sample. The titanium indiffused waveguides were faintly visible with a slightly de-focussed viewing microscope due to a slight raising of the surface of the aluminium in the region of the guide with respect to the remainder of the substrate. This is due to a corresponding "bump" on the surface of the titanium indiffused lithium niobate (ref 23). Following exposure and development, the exposed aluminium was etched in standard aluminium etch to reveal the substrate in the desired areas. Removal of the remaining photresist in acetone preceded the $Li\text{-}H^+$

exchange.

The proton exchange was accomplished by immersion of the samples in molten pure benzoic acid at 210^{0}C for 30 minutes. The U shaped polarisers were all made using the same mask: however, a range of different diffusion times were used, varying from 30 minutes to 8 hours. The former were expected from data concerning slab guides to be single-mode at 1.3 microns, while the latter should be strongly multimode. Following cooling, the samples were cleaned and polished in the normal way for end-fire excitation and subsequent testing. At this stage the photographs shown in figure 9 and 10 were taken. These show excellent lateral alignment between the two waveguide sections, but rather poor end-face quality. The corners are seen to be poorly defined with lens-like structures resulting.

Some devices were later annealed. This process involves raising the temperature of the substrate for prolonged periods to allow the H^+ ions to re-distribute within the lattice. The effect on the surface index is minimal, while the initially abrupt index change at the boundary with the bulk sample becomes progressively more rounded with annealing time, to leave a complementary error function profile (ref 10). The number of modes supported by such a guide will be greater than for a non-annealed guide. Two situations are possible for the annealing: the aluminium mask may be removed, in which case the diffusion takes place laterally as well as vertically. Alternatively, leaving the layer in position prevents significant lateral diffusion due to the conductivity of the aluminium (ref 33). The devices to be annealed were heated to between 250^o and 300^{o}C for between 10 minutes and 1 hour in a flowing wet oxygen atmosphere. A comparison of the fabricational steps involved in the fabrication of proton exchanged and titanium indiffused waveguides is presented in figure 8.

2.6 Testing of Integrated Optical Polarisers

Having fabricated integrated optical polarisers (of whatever type) it is important to devise an accurate method of testing them. Three parameters will be of interest, namely:

(a) the extinction ratio, ie. the differential attenuation of the two modes,

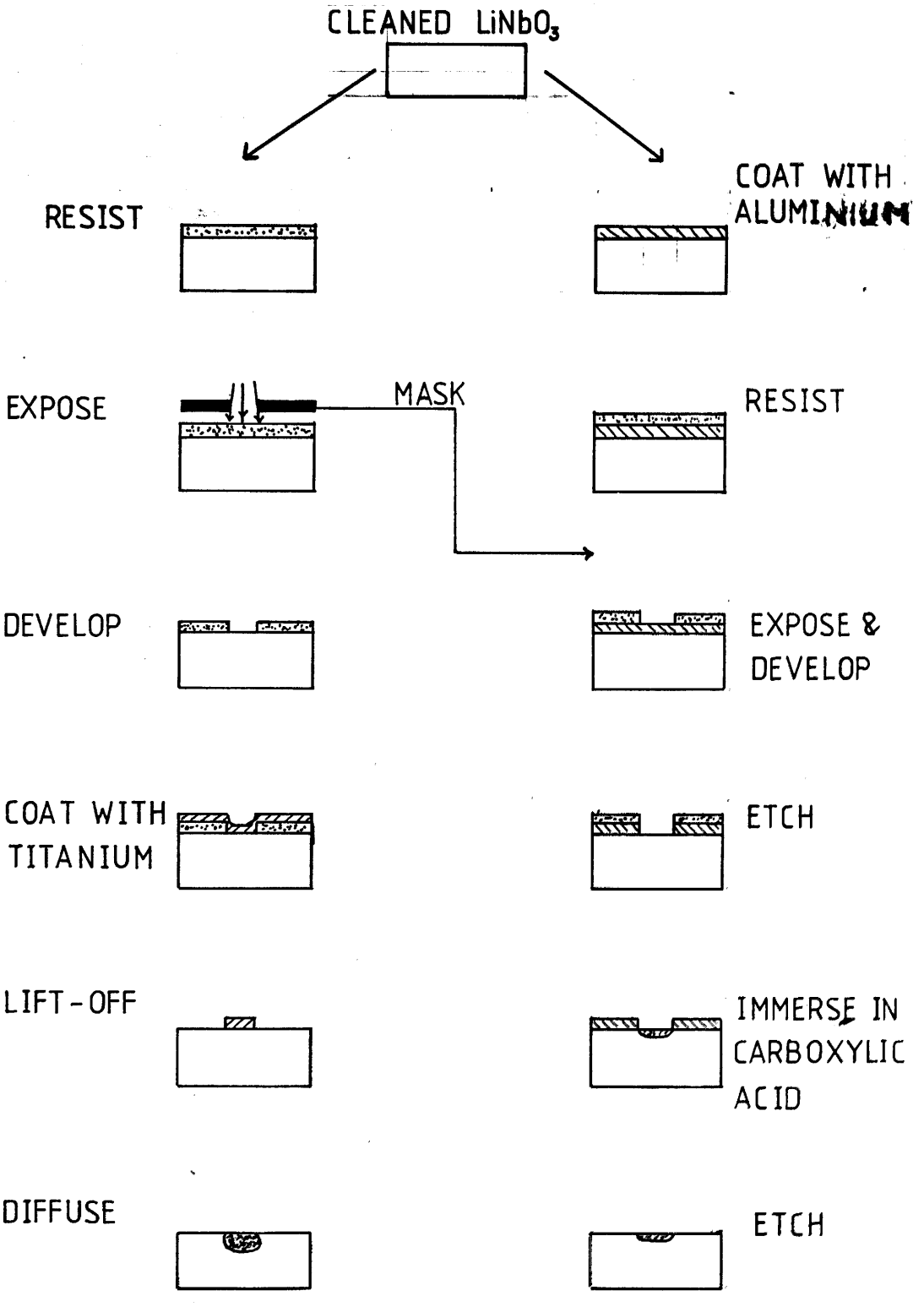

FIG 8 FABRICATION OF (a) TITANIUM INDIFFUSED AND b PROTON EXCHANGED WAVEGUIDES IN LITHIUM NIOBATE

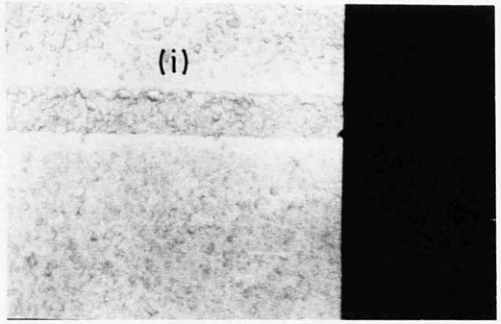

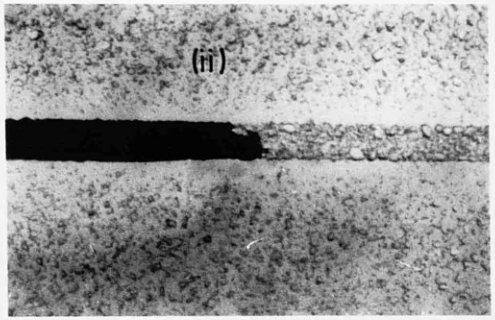

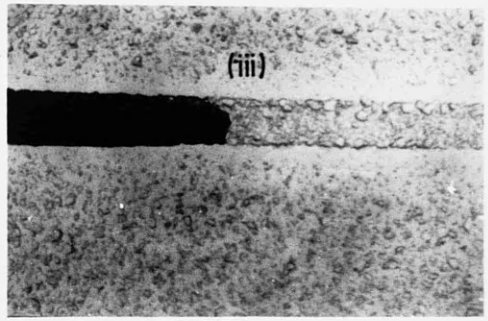

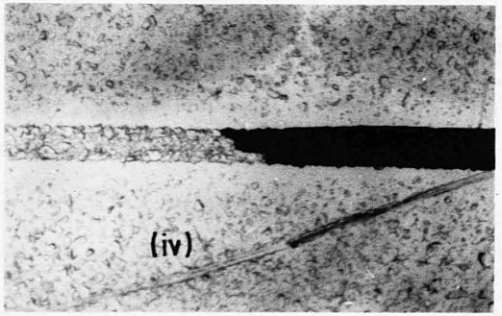

FIG 9 (i) POOR VISIBILITY OF TITANIUM INDIFFUSED $LiNbO_3$ WAVEGUIDE (BEFORE COATING WITH PHOTO-RESIST (ii), (iii), AND (iv) LENS-LIKE STRUCTURES AND END-FACE DEFECTS OF ALUMINIUM MASK

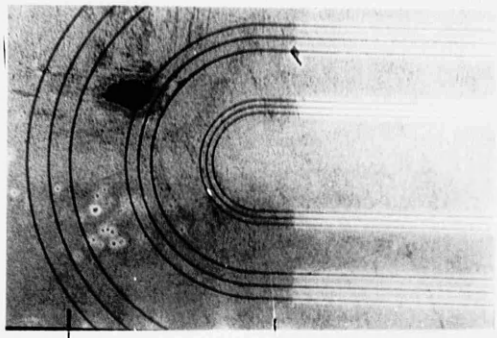

(i)

Al

(ii)

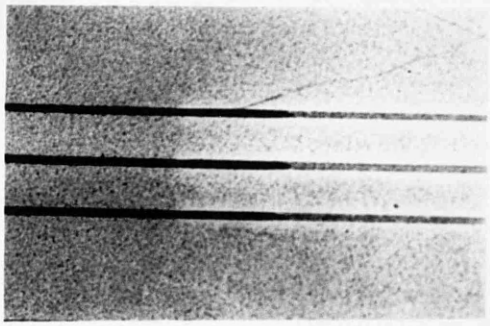

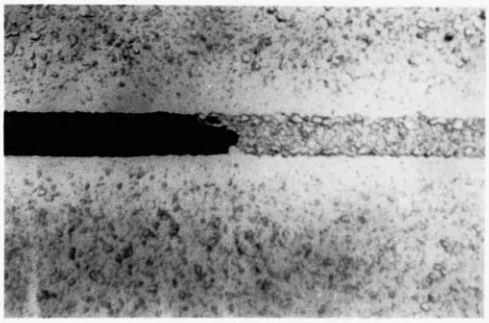

(iii)

FIG 10 (i)THE MASKING LAYER OF ALUMINIUM USED IN THE FABRICATION OF THE PROTON EXCHANGED SECTIONS OF THE U-SHAPED POLARISERS (ii) EXCELLENT LATERAL ALIGNMENT BETWEEN THE TWO WAVEGUIDE SECTIONS. AND (iii) LENS-LIKE STRUCTURE AT ROUGH MASK EDGE

(b) the insertion loss of the device,
(c) the excess loss of the device, i.e. the additional loss of the polarising section above the loss of a conventional waveguide.

2.6.1 Testing procedures

Considering the polariser in isolation, the simplest method of testing is to use linearly polarised light, this being defined by bulk optical polarisers. Testing methods then include:
(i) using unpolarised input, and examining the intensities in the two orthogonal output polarisations
(ii) Using linearly polarised inputs and examining the output in the parallel and orthogonal polarisations (this is equivalent to determining the Jones, and therefore the Stokes parameters of the device (ref 24)
(iii) using linearly polarised inputs, and merely recording the output from the waveguide with either input polarisation.
(iv) using optical fibres to define input and output paths: the power in the two fibre orthogonal modes may then be detected using a fibre version of method (i),(ii), or (iii).

The insertion loss or excess loss may be determined in the free-space excitation cases (i),(ii), and (iii) by comparing the transmitted intensities for the device with the loss of the testing system when the device is removed. Similarly, in method (iv) the fibre may be broken and the intensity initially incident on the device detected.

In the context of defining polarisation modes of optical fibre sensors, method (iv) would appear to be the most valid. However, in order to select one of the fibre modes for analysis, it will still be necessary to use a bulk optical linear polariser between fibre output face and detector. Thus the possible advantages of the method may be lost. Throughout the experiments, method (ii) was used wherever possible, as this afforded a complete description of the device performance.

2.6.2 Accuracy of measuring technique

High performance bulk optical polarisers relying on total internal reflection have an intrinsic extinction ratio of about 60dB. Thus for an unpolarised laser source, any measurements of device extinction ratio of approximately this figure, or greater,

must be regarded with caution. However, the lasers used in these experiments at 0.6328 and 1.15 micron wavelength were themselves linearly polarised, the bulk polariser aligned along the same axis merely providing improved extinction of the unwanted mode.

2.6.3 Comparison of methods (i),(ii), and (iii)

It is important to ascertain whether methods (i),(ii), and (iii) are equivalent. The comparison is essential as a variety of different methods are used in the literature.

The effect of an optical device or system on the state of polarisation of the light passing through it may be desribed by the Jones matrix for the system (ref 24,25). The description may be extended to describe orthogonal waveguide modes instead of plane polarised light. For input field amplitudes E_x and E_y, the output field amplitudes E'_x and E'_y are given by:

$$\begin{pmatrix} E'_x \\ E'_y \end{pmatrix} = \begin{pmatrix} J_{11} & J_{12} \\ J_{21} & J_{22} \end{pmatrix} \begin{pmatrix} E_x \\ E_y \end{pmatrix} \qquad 2.4$$

The total emergent power P will be given by:

$$P = |E'_x|^2 + |E'_y|^2 \qquad 2.5$$

The elements J_{11} and J_{22} give the transmitted fields in the two orthogonal modes, while the off-diagonal elements represent the cross-scattering into the unwanted modes. In general for a polariser, we will attempt to make J_{11} as close to unity as possible, while making all other elements zero. It is to be noted that the formalism does not describe the degree of polarisation: for this it would be necessary to use the Stokes formalism and to make rather more complicated measurements (ref 24). Jones (ref 26) has shown that for a polariser to be used with an optical fibre gyroscope, if the off-diagonal elements are non-zero, then their product must be equal to the second element on the leading diagonal. Since this includes phase terms, the condition will be difficult to achieve in practice.

According to the experimental arrangement used, a variety

of different combinations of Jones matrix elements will be determined. The extinction ratio, as defined by the ratio of the powers in the two modes requires unpolarised inputs, and analysis of the power present in the two orthogonal output modes. This may be found if all four elements of the matrix are known Thus comparing the outputs of the two modes in method (i) yields an extinction ratio based on the ratio:

$$\left(\frac{J_{11} + J_{12}}{J_{22} + J_{21}} \right)^2 \qquad 2.6$$

(the true value). On the other hand, the four parameters determined from method (ii) may be used to determine the same ratio. If however method (iii) is used, comparing the two intensities yields the ratio :

$$\left(\frac{J_{11} + J_{21}}{J_{22} + J_{12}} \right)^2 \qquad 2.7$$

If this were erroneously assumed to be the true value, the fractional error introduced may be shown to be:

$$\frac{(J_{11}+J_{12})^2(J_{12}+J_{22})^2 - (J_{11}+J_{21})^2(J_{21}+J_{22})^2}{(J_{12}+J_{22})^2(J_{11}+J_{12})^2} \qquad 2.8$$

It is seen that this error will be zero if the off-diagonal elements are both zero.

2.6.4 Summary

To obtain a strictly accurate measurement of the extinction ratio of a device, it is necessary to use either method (i) or (ii). If method (iii) is used, error will be introduced, unless there is no cross-scattering within the device. Jones matrices have been seen to afford a useful description of the effect of a device. However, no information on the polarisation mechanism may be obtained, and the degree of polarisation is not found.

While the above procedure decribes the performance of the polariser with respect to linear polarisation of input and output light, this may not give a complete indication of the performance when connected to an optical fibre. This is due to the approximate description of the optical fields as linearly polarised modes breaking down due to the weakly-guiding

approximation being violated (ref 27).

2.6.5 The validity of scaled measurements

In many theories and experimental results describing polarising waveguides using selective attenuation of one mode, the extinction ratio is expressed in dB/cm, or some other length-dependent figure. When measuring the performance of integrated optical polarisers it may be necessary to compare the performance of devices of differing lengths. It is therefore important to determine whether, for example, doubling the length of a device, will double the insertion loss and extinction ratio. Two mechanisms will generally operate with the result that the postulate will not be true. These are (i) the effect of reflections from edges, and (ii) the cross-scattering of light (ref 28) between the two modes within the waveguides.

2.6.6 Corruption due to cross-scattering

It is well known that scattering of light in an anisotropic material is also anisotropic (ref 29). This mechanism is repsonsible for an ultimate limit in the polarisation maintaining ability of a birefringent optical fibre (ref 29). In the following analysis it will be shown that scaling of measurements is invalid if (a) scattering is present, and further (b) this scattering is anisotropic in nature. The model is shown in figure 11. A waveguide of length **L** has a length dx of scattering waveguide at a distance x from the input face. If all scattered light is still guided by the fibre (the validity of this assumption depending on the numerical aperture of the particular waveguide), and the loss rate due to scattering is K, with a fraction R of the scattered light being scattered into the "wrong" polarisation, the a fraction KRdx of the incident light is converted into the orthogonal polarisation. This is illustrated in figure 11. If the input field amplitudes are E_a and E_b then the emergent field amplitude in polarisation a is:

$$E_a' = E_a e^{-A\alpha}(1-KR\,d\alpha)e^{-A(1-\alpha)} + E_b e^{-B\alpha} KR\,d\alpha\, e^{-A(1-\alpha)} \qquad 2.9$$

and in polarisation b:

$$E_b' = E_b e^{-B\alpha}(1-KR\,d\alpha)e^{-B(1-\alpha)} + E_a e^{-A\alpha} KR\,d\alpha\, e^{-B(1-\alpha)} \qquad 2.10$$

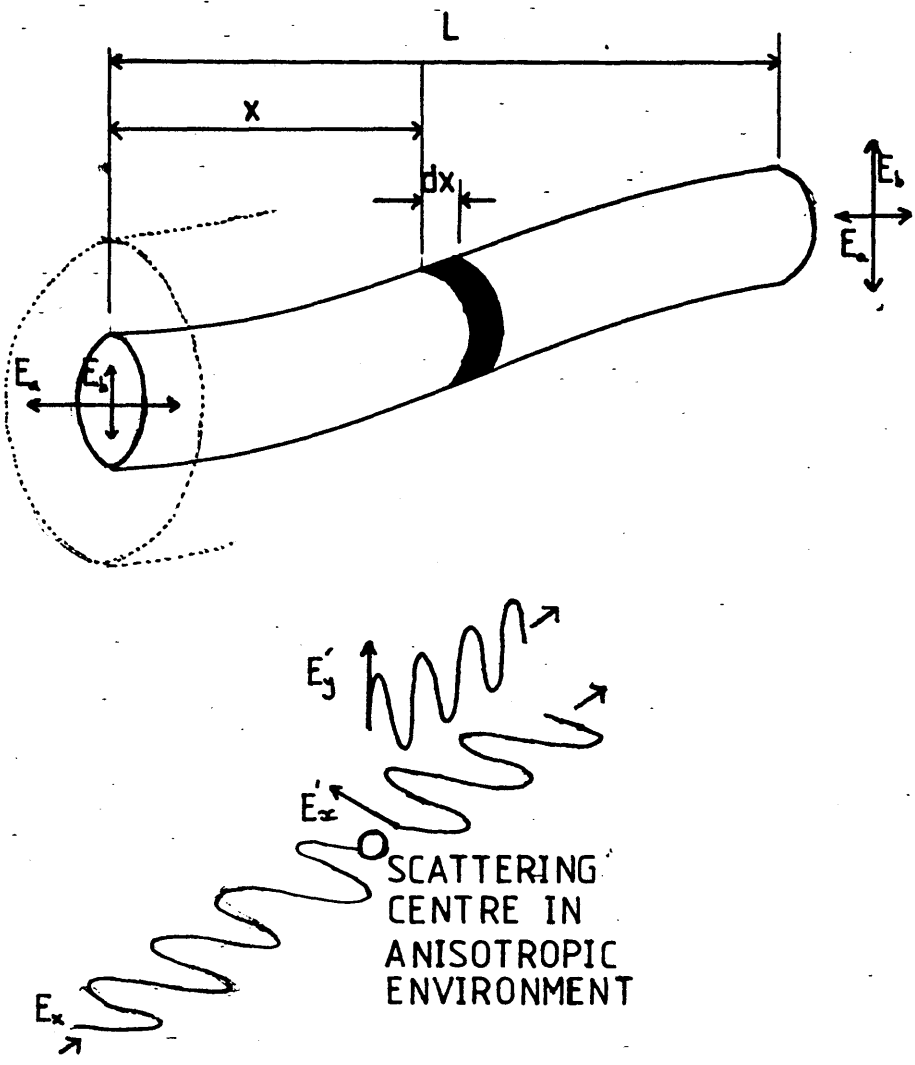

FIG 11 THE MODEL USED TO CALCULATE THE ELEMENTS OF THE JONES MATRIX DESCRIBING A WAVEGUIDE WITH DIFFERENTIAL MODAL ATTENUATION. AND ANISOTROPIC RAYLEIGH SCATTERING.

Integrating over the entire length and considering excitation and analysis with linear polarisers to determine the elements of the Jones matrix for the device, we obtain:

$$\bar{J}_{11} = e^{-AL} - KR\,e^{-AL}$$

$$\bar{J}_{21} = \frac{\left(e^{-AL} + e^{-BL}\right)}{B-A}$$

$$\bar{J}_{12} = \frac{\left(e^{-BL} + e^{-AL}\right)}{A-B}$$

$$\bar{J}_{22} = e^{-BL} - KR\,e^{-BL} \qquad 2.11$$

Thus the extinction ratio which in the case of no cross-scattering would be of the form:

constant x (A-B)l

is now given by:

$$20\log_{10}\frac{e^{-AL}(1-KR) + \dfrac{\left(e^{-BL} + e^{-AL}\right)}{A-B}}{e^{-BL}(1-KR) + \dfrac{\left(e^{-AL} + e^{-BL}\right)}{B-A}} \qquad 2.12$$

and is no longer proportional to length. Therefore, if there is Rayleigh scattering in the waveguide core, the scattered light from which is captured by the core, and the process is anisotropic, the measured extinction ratio may not be scaled to yield a normalised result. The error which would be introduced from such a process will depend on the capture fraction (ref 29), the anisotropy of the scattering, and the loss-rate due to scattering in the waveguide. The cross-scattered light which would then have corrupted the measurement may not be apparent, as some light scattered into the low-loss mode may be re-coupled back to the high-loss mode, and consequently suffer a lower total attenuation than if it had continued unscattered in the high-loss mode.

The effect of end-face reflections may be investigated as

follows. Light travelling in the waveguide, when incident upon the waveguide end-face will be reflected according to the Fresnel formulae (ref 14). The reflection coefficient will depend upon the particular mode, the effect of this being included by replacing the refractive indices with effective indices, these either being determined experimentally (ref 21) or theoretically with an appropriate waveguide analysis. Using the data of Rauber (ref 30) for 1.3μm wavelength in z-cut lithium niobate and effective indices for the multilayer structure to be described in chapter 4, the power reflection coefficients become:

$$R_{te}=0.1437 \qquad 2.13$$

$$R_{tm}=0.1340 \qquad 2.14$$

Referring to figure 11, if the attenuation rate for TE like modes is A and for the orthogonal modes B, then the field emerging in the TE polarisation is

$$E_{TE} = E_a e^{-AL}(1-r_{TE}) + E_a r_{TE}^2 e^{-3AL} e^{-2ink_0L}(1-r_{TE}) \qquad 2.15$$

plus higher terms in r^4, r^6 etc which will be too small to be significant. If the field amplitudes are equal in the two modes, then the extinction ratio is obtained from the ratio of the powers in the two modes, ie

$$E_x = 20\log_{10}\left[\frac{e^{-AL}(1-r_{TE}) + r_{TE}^2 e^{-3AL} e^{-2ink_0L}(1-r_{TE})}{e^{-BL}(1-r_{TM}) + r_{TM}^2 e^{-3BL} e^{-2ink_0L}(1-r_{TM})}\right] \qquad 2.16$$

Since the attenuation of mode B (the lossy mode) is large, allowing the phase terms to assume values of ± 1 gives the range of extinction ratios to be:

$$E_x = 20\log_{10}\left[\frac{e^{-AL} \times 0.62 \pm 0.09 e^{-3AL}}{e^{-BL} \times 0.633}\right] \qquad 2.17$$

Substitution of reasonable values for the two attenuation rates

shows that the fractional error induced by ignoring edge effects is at worst 4%- a small figure.

2.6.7 Experimental arrangement

The experimental arrangement is illustrated in figure 12, with figures 13 and 14 showing a typical experiment in progress. The output from the appropriate laser is incident upon a bulk optical polariser. This was an air-spaced calcite device supplied by **Optics for Research**, using the Archard-Taylor modification of the Glan-Foucault design, and had an intrinsic extinction ratio of 60dB (ref 31). Light is then focussed via a x40 microscope objective (not provided with antireflection coatings optimised for any particular wavelength) onto the input face of the waveguide under investigation. In order to be able to define the orthogonal polarisation, a half-wave plate optimised for the particular wavelength being used could be inserted between the linear polariser and the objective. This was aligned with its axis at 45^{o} to the axis of the polariser to rotate the plane of polarisation by 90^{o} (ref 25). Thus linearly polarised light with the electric field vector either parallel or perpendicular to the optical bench could be defined.

A corresponding objective at the output of the waveguide focussed the near field pattern onto the infra-red sensitive vidicon tube of a Hamamtsu camera. A Glan-Foucault polariser could be inserted between the objective and and the camera in order to be able to analyse the two orthogonal output polarisations. Thus movement of the sample on its mount enabled the transmitted power to be optimised using the camera as a visual aid. Although the information displayed on the screen could be stored for later use in constructing plots of optical intensity, due to the time taken for this process the recording capability was not used to determine the device performance.

It is important to ensure that fluctuations in laser output do not corrupt the measurement of the extinction ratio and insertion loss. A **Photodyne** double headed power meter (model 22XL) was therefore used to compare the intensities of light transmitted through the analysing system and a fraction of the initial light travelling unimpeded. The arrangement is

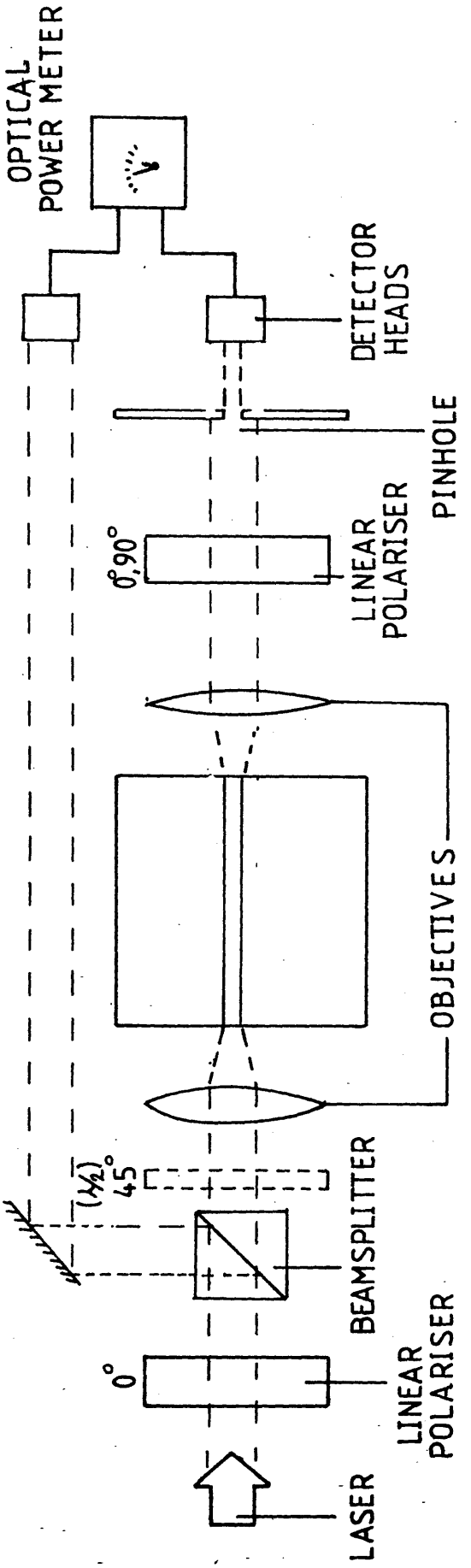

FIGURE 12 EXPERIMENTAL ARRANGEMENT FOR DETERMINATION OF PERFORMANCE OF INTEGRATED OPTICAL POLARISERS (ANGLES INDICATE ORIENTATION OF COMPONENTS WITH RESPECT TO FIRST POLARISER)

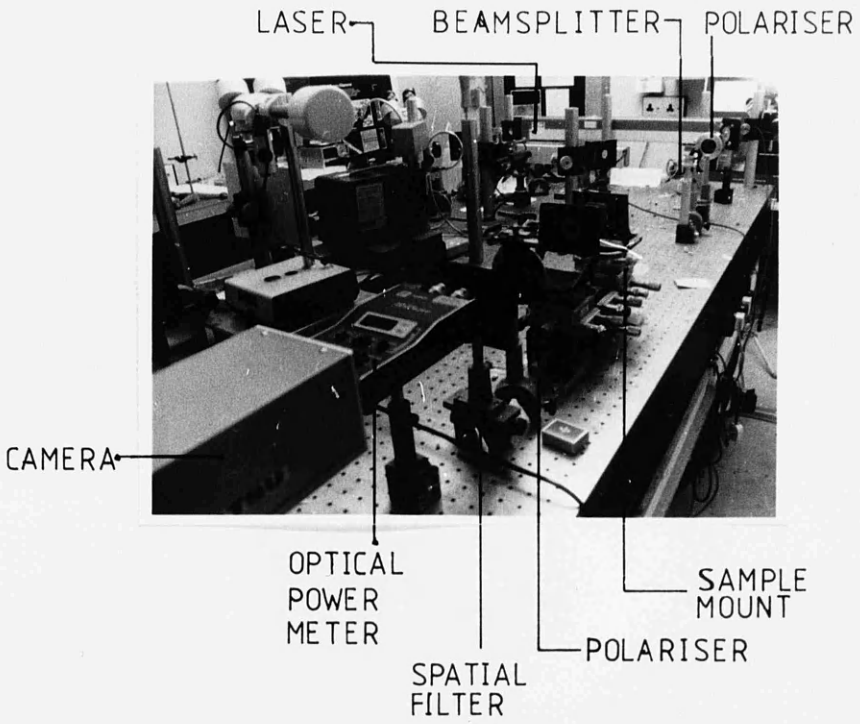

FIG 13 EXPERIMENTAL ARRANGEMENT USED FOR DETERMINATION OF EXTINCTION RATIO AND EXCESS LOSS OF INTEGRATED OPTICAL POLARISERS

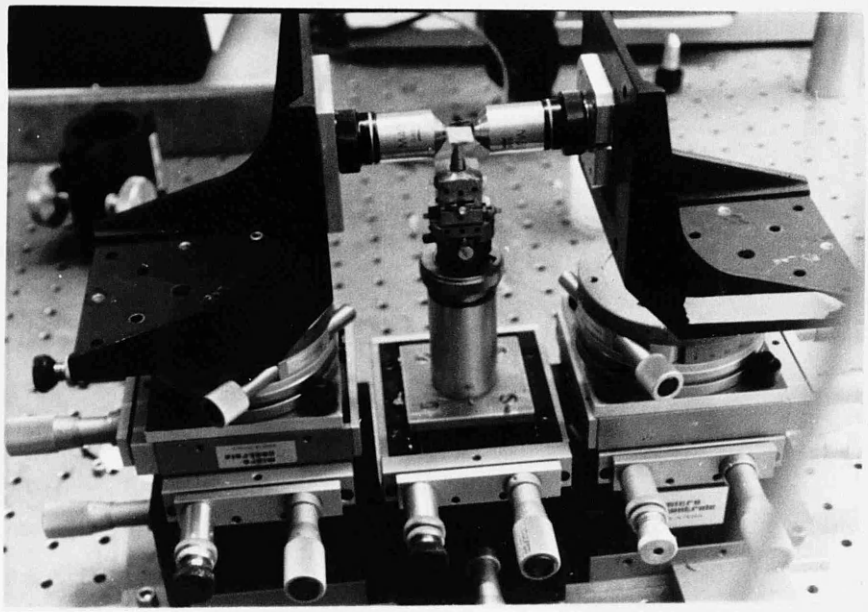

FIG 14 EXPERIMENTAL ARRANGEMENT FOR DETERMINATION OF POLARISER PERFORMANCE USING END-FIRE EXCITATION: SAMPLE MOUNT

illustrated in figure 12. The beamsplitter should be inserted between the polariser and the input objective, otherwise fluctuations in the polarisation of an unpolarised laser would corrupt the measurements. The situation is analogous to the selection of one spatial mode of a laser: although the total power in all modes may be constant, fluctuations in the partition of the power give rise to fluctuations in the intensity of the single mode selected. This is known as partition noise.

To obtain the extinction ratio, the transmitted intensities with the input and output polarisations both normal to and parallel to the crystal surface are recorded. The intensity is in each case monitored visually using the Hamamatsu camera system prior to taking the measurement. The cross-coupled power may be recorded in a similar way. The insertion loss may be determined by removing the integrated optical device from its mount, bringing the two objectives close together, and recording the transmitted power. Similarly, the excess loss may be found by recording the transmitted power when the polarising waveguide is replaced by a non-selective guide.

Throughout these experiments, care should be taken to eliminate stray light from the measuring instrument to avoid corrupting the measurements.

2.6.8 Summary

A method for testing integrated optical mode filters using linearly polarised input and output polarisations has been described. A range of different measurements may be taken using the system and used to find the extinction ratio and the insertion loss. If appreciable cross-scattering is present, the results must be treated with care, especially if they are to be compared with values published in the literature.

In general, it is **not** correct to normalise the extinction ratio and insertion loss to give a length-dependent figure.

2.7 Results of measurements on hybrid Ti/ H^+ polarisers.

For each of the polarisers fabricated, the extinction ratio and excess loss were determined. The former were measured using method (ii), ie using linear polarisers at input and output ports,

while the latter were found by comparing the loss measurements for the TM-like modes with those for an unmodified titanium indiffused guide. This was fabricated using the same conditions as were used for the Ti: indiffused sections of the hybrid device, although in a different process. The devices were tested at 1.15 μm wavelength, the source being a polarised Helium-Neon laser. Alignment of the end-fire arrangement was aided by imaging the near field profile via a x40 objective into the vidicon tube of a **Hamamatsu** camera with associated electronics.

2.8 Experimental Observations

Excitation of the waveguides followed standard procedures for end-fire coupling. However, some small differences were noted compared with excitation of the unmodified guides.

For conventional guides, an optimum alignment between the focussed beam and the substrate exists. Disturbance of the alignment from this position decreases the transmitted power. For the straight proton exchanged hybrid polarisers however, several local minima were noted as the substrate was moved horizontally or vertically. For example, in the case of a 6μm wide guide approximately 5 local maxima were seen. In no case did the transmitted power compare well with that of the unmodified guide, and with excitation of the unwanted mode the mode profile was clearly visible, albeit with adjustment of the gain of the camera system.

For the U-shaped devices a modification of the experimental apparatus is required. Due to the small separation of input and output ports, it was not possible to use launching objectives to couple in and out of the device. However, with the modification shown in figure 15 it was possible to use optical fibres to perform these functions.

2.9 Qualitative Results

The extinction ratios measured for the straight polarisers were in general poor. Few devices exceeded 20dB, while the excess loss was always high, generally above 10dB and in some cases as high as 20dB. No correlation appeared to exist between extinction ratio and either waveguide width or length of proton exchanged section, the measured values appearing to be random, but repeatable. Annealing under the conditions given in section 2.5.3

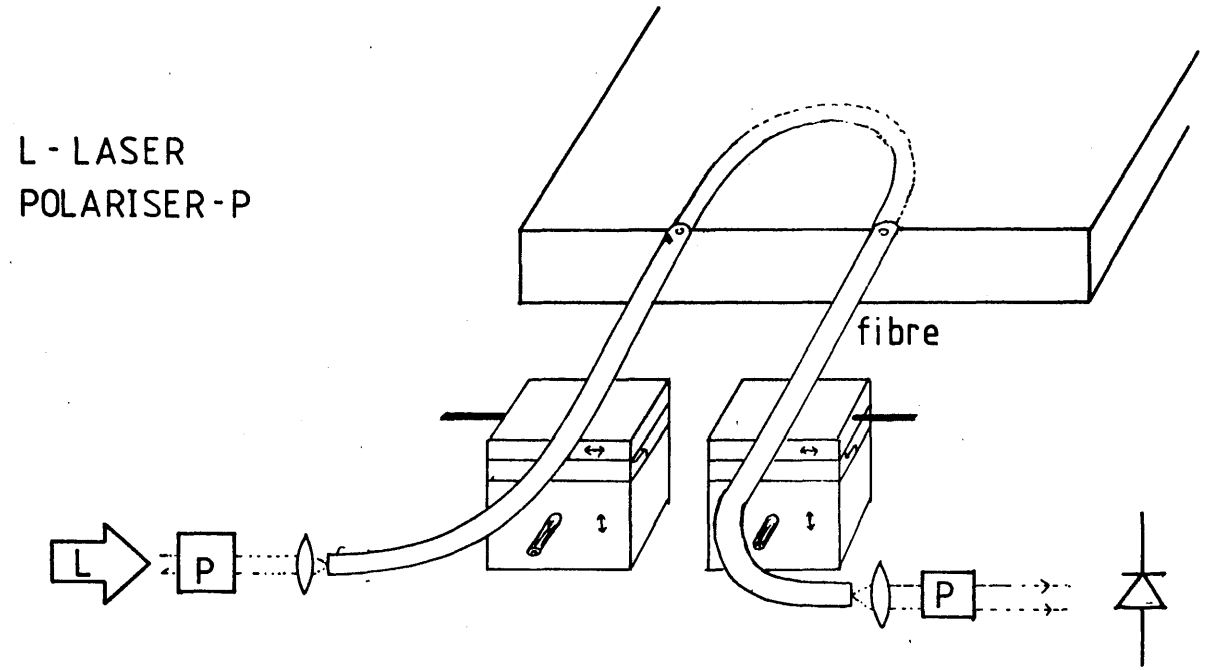

FIG 15 EXPERIMENTAL ARRANGEMENT FOR DETERMINATION OF EXTINCTION RATIO OF U-SHAPED POLARISERS

yielded little improvement in excess loss, and a reduction, rather than the predicted increase in extinction ratio.

The U-shaped devices were less succesful: although considerable effort was invested in an attempt to excite the waveguides, no output power could be detected. Using the fibre excitation rig illustrated in figure 15 no returned light could be observed from the device, no matter what bend radius was selected or what exchange time was used. Illumination with visible Helium Neon Laser light revealed pronounced radiation from the titanium indiffused- proton exchanged waveguide boundary. Annealed devices showed no improvement. The substrate was observed to be brilliantly illuminated, indicating that a large amount of energy was transferred to the substrate rather than to the waveguide.

2.10 Quantitative Results

Although few trends were observed, selected data taken from the guides are shown. Typical variations in extinction ratio with waveguide width are shown in figure 16: the coresponding excess loss is also shown. These results correspond to a device with a gap length of 1mm. No obvious variation of extinction ratio with either waveguide width or with length of proton exchanged section were observed. Figure 17 shows a spuriously high result for the extiction ratio at one guide width: although the value is high, this was not repeatable for other waveguides fabricated under the same conditions. In addition, the associated excess loss was 10 ± 3dB.

2.11 Discussion

The high insertion loss for the straight polarisers is believed to result from several causes. The radiation observed from the end of the titanium guide suggests this as a dominant loss mechanism. It appeared to be symmetrical about the waveguide axis, and could be caused by either the lens-like structures shown in figs 9 and 10, the rough end of the titanium indiffused waveguide, or the spatial mismatch of the optical fields (ref 32). However, annealing would certainly alter the latter (ref 10), the conditions used being known to have a drastic effect on the waveguide properties.

This also explains the poor results for the U-shaped

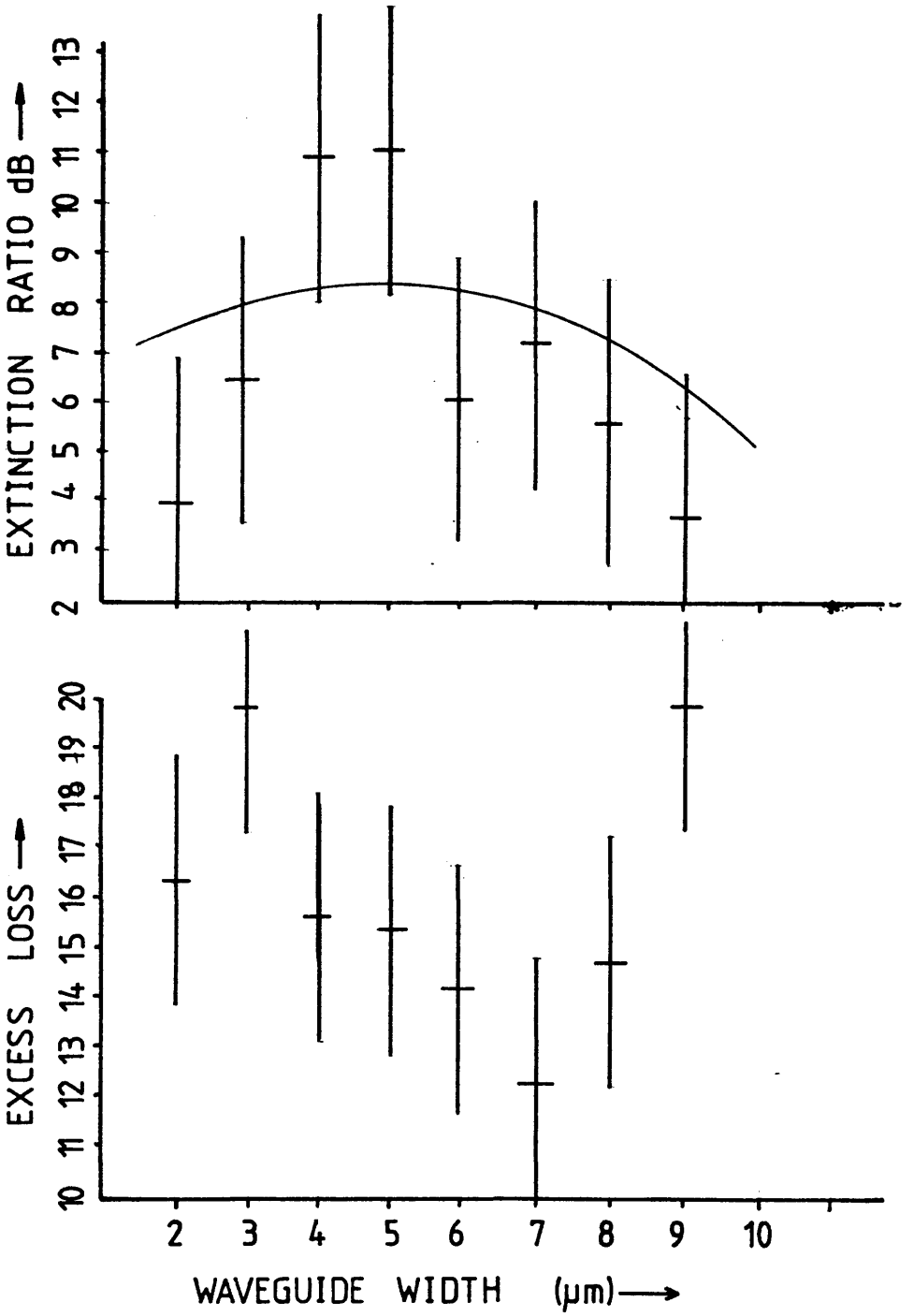

FIG 16 VARIATION OF EXTINCTION RATIO AND EXCESS LOSS WITH WAVEGUIDE WIDTH FOR HYBRID PROTON EXCHANGE / TITANIUM INDIFFUSED $LiNbO_3$ POLARISERS. LENGTH OF PROTON EXCHANGED SECTION = 1.5mm

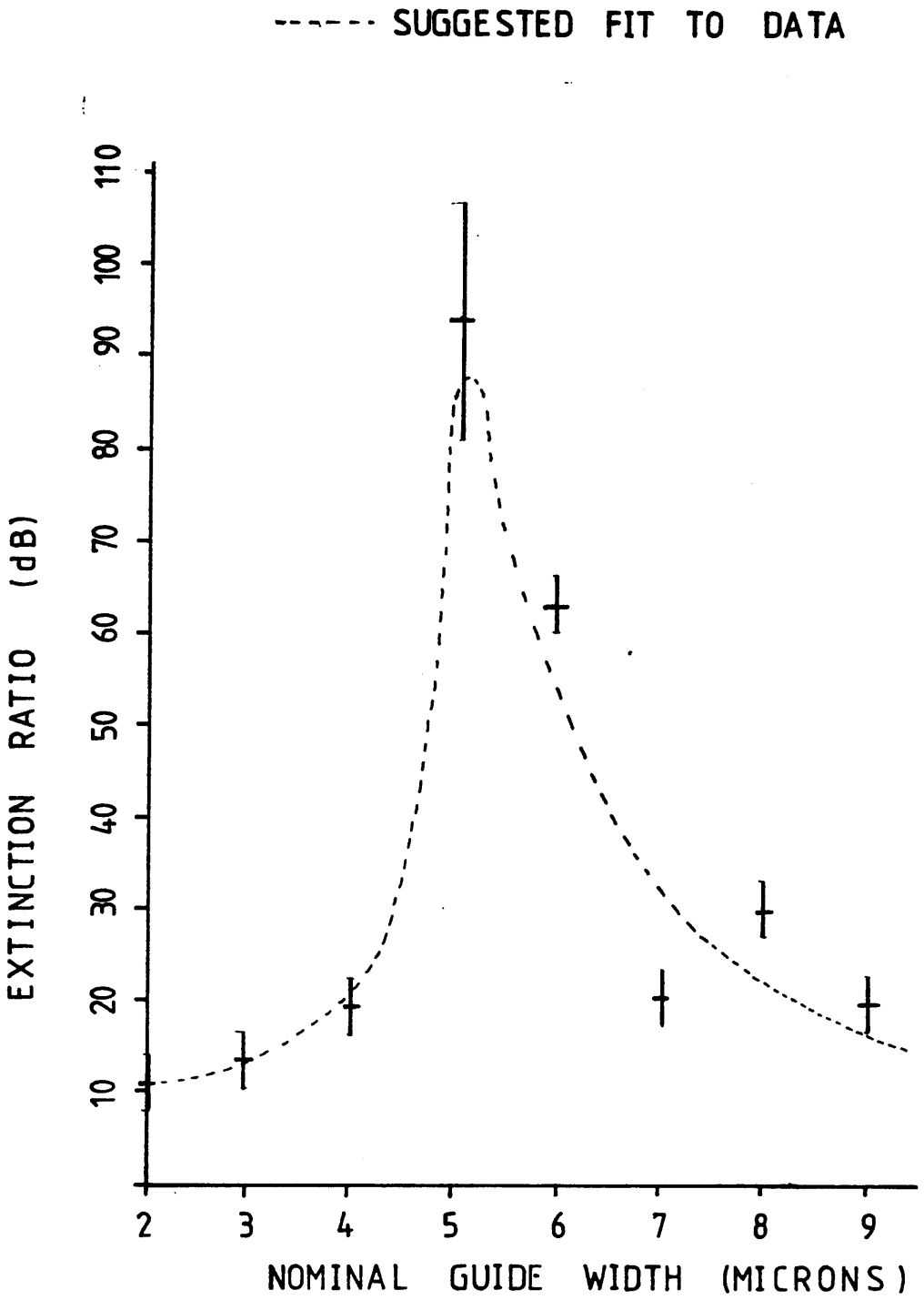

FIG 17 MEASURED EXTINCTION RATIO VS. NOMINAL WAVEGUIDE WIDTH FOR PROTON EXCHANGED / Ti INDIFFUSED $LiNbO_3$. DEVICE (a)

devices, where the same poor end-face quality was observed and a large amount of forward-scattered radiation seen.

The poor extinction ratio in all cases is believed to result from the multimode nature of the proton exchanged waveguide. Evidence for this is provided by the succession of local maxima observed when moving the substrate relative to the focussed beam. Annealing, while offering the possibility of improved mode-matching in the single-mode case, would here merely increase the number of modes supported.

The rough end of the titanium indiffused waveguide is believed to result from poorly defined corners at the photolithographic stage, and also from the lift-off process. Little work on this appears to have been reported in the literature: the vast majority of Ti:$LiNbO_3$ waveguides are subsequently polished for end-fire or fibre coupling.

The results obtained here compare well with those of Findlaky for the extinction ratio, while the excess loss is significantly poorer. It is believed that Findlaky left the aluminium masking layer in place during the exchange process and thus obtained superior lateral confinement with associated reduction in excess loss. It is suggested that future work be undertaken to investigate the effect.

It is also suggested that devices be made using a narrow (say lum) width of proton exchanged section. This would necessitate two separate masks being made: preserving alignment between a large number of guides would then be difficult. Further work is necessary to investigate the variation of extinction ratio and excess loss with fabrication conditions.

References

2.1 Jackel,J.L, Rice,C.E, Veselka,J.J, "Proton Exchange for High Index Waveguides in $LiNbO_3$", Post deadline paper, Meeting on Integrated and Guided Wave Optics, Asilomar, 1981

2.2 Spillman,W.B, Sanford,N.A, Soref,R.A, "Optical Waveguides in

$LiTaO_3$ Formed by Proton Exchange", Optics Letters, Vol 8, No 9, 497-498, 1983

2.3 Clark,D.F, Nutt,A.C.G, Wong,K.K, Laybourn,P.J.R, De La Rue, R.M, "Characterisation of Proton Exchange Slab Optical Waveguides in Z-cut $LiNbO_3$", Journal of Applied Physics, Vol 54, No 11, 1983 pp6218-6220

2.4 Nutt,A.C.G, "Experimental Observations of Light Propagating in Proton Exchanged Lithium Niobate Waveguides", Journal of Optical Communications, Vol 6, No 1, 1985 pp8-9

2.5 Riviere,L, Yi-Yan,A, Carru,H, "Properties of Single-Mode Optical Planar Waveguides with Gaussian Index Profile", Journal of Lightwave Technology, Vol LT-3, No 2, 1985, pp368-377

2.6 Ramer,O.G, Nelson,C, Mohr,C, "Experimental Integrated Optic Circuit Losses and Fiber Pigtailing of Chips", I.E.E.E. Journal of Quantum Electronics, Vol QE-17, No 6, 1981 pp970-974

2.7 Rottschalk,M, Rasch,A, Karthe,W, "Teperature Dependence of the Exrtraordinary Refractive Index in Proton Exchanged Lithium Niobate Waveguides", Journal of Optical Communications, Vol 6, No 1, pp10-13, 1985

2.8 Yi-Yan,A, "Index Instabilities in Proton Exchanged Lithium Niobate", Applied Physics Letters, Vol 42, No 8, 1983 pp633-635

2.9 Jackel,J, Rice,C.E, "Short and Long Term Stability in Proton Exchanged Lithium Niobate Waveguides", S.P.I.E, Vol 460, "Processing of Guided Wave Optoelectronic Materials", 1984.

2.10 De Micheli,M, Botineau,J, Neveu,S, Sibillot,P, Ostrowsky,D.B, Papuchon,M, "Independent Control of Index and Profiles in Proton Exchanged Lithium Niobate Guides", Optics Letters, Vol 8, No 2, 1983 pp114-115

2.11 Wong,K.K, Parsons,N.J, Olderoyd,A.R, O'Donnel,A.C, "High

Quality Optical Waveguides in $LiNbO_3$ by Dilute Melt Proton Exchange", IOOC/ECOC Integrated Optical Waveguide Fabrication, Venice, Italy, October 1985

2.12 Kogelnik,H, "Theory of Dielectric Waveguides", in Tamir, Integrated Optics

2.13 Papuchon,M, Vatoux,S, "Integrated Optical Polariser on $LiNbO_3$:Ti Channel Waveguides Using Proton Exchange", Electronics Letters, Vol 19, No 16, 1983 pp612-613

2.14 Born,M, Wolf,E, "Principles of Optics", Pergamon, 1959

2.15 Marcuse,D, "Radiation Losses of Tapered Dielectric Slab Waveguides", Bell System Technical Journal, 1970, pp273-291

2.16 Marcuse,D, "Radiation Losses of Dielectric Waveguides in Terms of the Power Spectrum of the Wall Distortion Function", Bell System Technical Journal, Vol 48, 1969, pp3233-3242

2.17 Danko,J.J, Haavisto,J.R. "Modal Conversion in a Gradient Index Channel Waveguide Due to Boundary Perturbations", Journal of Lightwave Technology, Vol LT-3, No 1, pp176-183, 1985

2.18 Armensise,M,N, Canali,C, DeSario,M, Franzosi,P, Singh,J, Hutchins,R.H, DeLa Rue,R.M, "Dependence of Inplane Scattering Levels in Ti:$LiNbO_3$ Optical Waveguides on Diffusion Time", I.E.E. Proceedings, Vol 131, Part H, 1984 pp295-298

2.19 Findlaky,T, Chen,B, "Single Mode Transmission Selective Integrated Optical Polarisers in $LiNbO_3$, Electronics Letters, Vol 20, No3, pp128-129, 1984

2.20 Cullen,T.C, Ph.D Thesis, University of Glasgow 1982

2.21 Maclaughlin,A Ph.D, University of Glasgow, 1981

2.22 Rasch,A, Rottschalk,M, Karthe,W, "Suppression of

Outdiffusion in Ti:$LiNbO_3$", Journal of Optical Communications, Vol 6, No 1, pp14-17, 1985

2.23 Griffiths,G.J, Esdaile,R.J, "Analysis of Titanium Diffused Planar Optical Waveguides in Lithium Niobate", I.E.E. Journal of Quantum Electronics, Vol QE-20, No 2, 1984, pp149-159

2.24 Scurcliff,W.A, "Polarised Light", Oxford, 1962

2.25 Hecht,E, Zajac,A, "Optics", Addison Wesley, 1979

2.26 Jones,E, "Analysis of Noise and Bias in the Fibre Optic Gyroscope", 1st International Conference on Optical Fibre Sensors, London, 1983

2.27 Gloge,D, "Weakly Guiding Fibres", Applied Optics Vol 10, pp2252-2258, 1971

2.28 Dakin,J.P, Gambling,W.A, "Theory of Scattering from the Core of a Multimode Optical Fibre", Optics Communications, Vol 10, No 2, 1974, pp195-199

2.29 Brinkmeyer,E, Eickhoff,W, "Ultimate Limit of Polarisation holding in Single-Mode Fibres", Electronics Letters, Vol 19, No 23, 1983 pp996-997

2.30 Rauber, "Chemistry and Physics of Lithium Niobate" in Current Topics in Materials Science, F.Kaldis editor, 1978

2.31 Optics For Research, Commercial Literature

2.32 Bristow,J.P.G, Nutt,A.C.G, McDonach,A, Laybourn P.J.R "Locating and Coupling Fibres to Integrated Stripe Waveguides", I.E.E. Proceedings J-Optoelectronics, October 1985

2.33 Nutt,A.C.G, University of Glasgow. Private Communication

Chapter 3 The Theory of 4 Layer Slab Waveguides with Complex Refractive Indices and Isotropic Waveguide Core and Cladding.

3.1 Introduction

In order to be able to design efficient integrated optical devices of any type, it is important to have a theoretical model on which to base decisions regarding fabrication conditions.

In many integrated optical modulators (ref 1,2) electrodes are used to induce refractive index changes via the electro-optic effect (ref 3). To avoid high losses, dielectric buffer layers are used to separate the electrodes from the substrate (ref 2).

Metal claddings have recently been used with dielectric buffer layers to fabricate fibre optic and integrated optical polarisers (ref 4,5,6). The selective attenuation properties of such devices have been shown to depend critically on the dielectric and metal properties.

A theoretical model of integrated optical waveguides coated with dielectric and metal layers would therefore be useful, to optimise the devices to achieve the high mode-selective losses needed for polarisers and the low losses needed for modulator systems.

Figure 1 shows a typical arrangement for a phase modulator using Z-cut lithium niobate. Marcuse (ref 7) has presented a theoretical study of such a device, optimising the theoretical efficiency from a knowledge of the optical and electrical fields and their interaction. Unfortunately it is impossible to analyse the optical fields in such a system without making approximations.

3.2 Exact and Approximate Analytical Methods

Slab waveguides, with layers of either dielectrics or metals may yield exact solutions (ref 8) although not necessarily in closed form (ref 9).

For an isotropic dielectric rod of circular cross section immersed in an isotropic medium exact solutions are obtainable- this is of course the problem to be solved in describing a step-index optical fibre.

For more complicated geometries, approximate solutions are necessary, their accuracy being dependent upon the particular

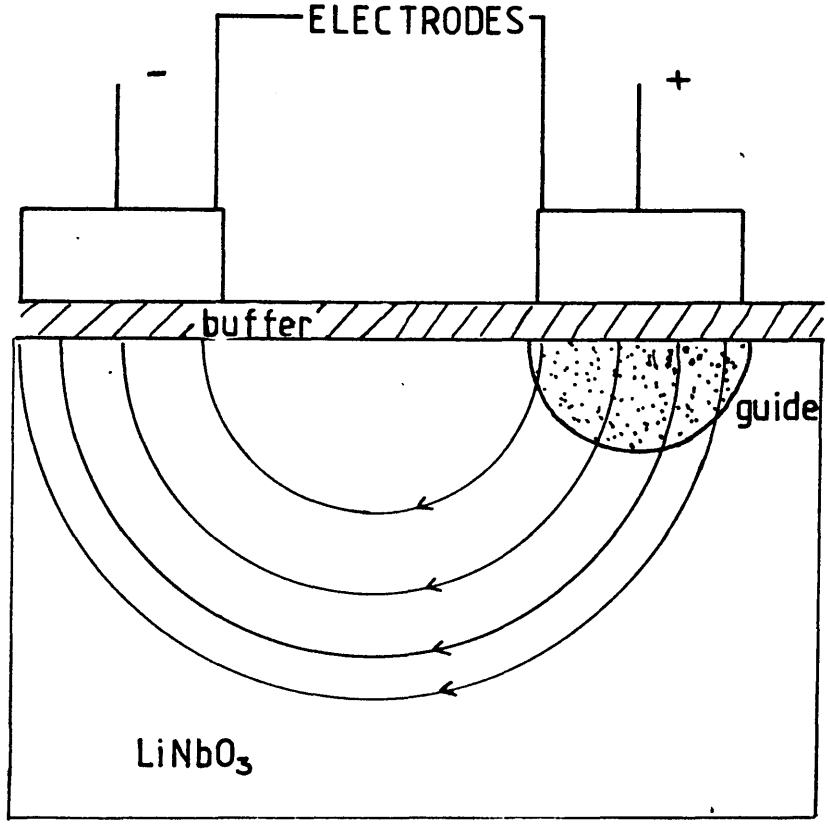

FIG 1 TYPICAL ARRANGEMENT FOR PHASE MODULATOR ON $LiNbO_3$ ILLUSTRATING USE OF DIELECTRIC BUFFER LAYERS.

application.

For a square waveguide in an isotropic medium approximate solutions may be used with success, generally provided that the mode under consideration is far from cut-off (ref 10). Such methods rely on the optical field being well confined to the waveguide core (ref 10). Unfortunately the method may yield incorrect results when applied to metal-clad devices (ref 11) An exact analytical solution for the propagation constant, which will in general be complex, is not possible (ref 12). Reviews of approximate methods of waveguide analysis are given by Yeh et al. (refs 12). Exact solutions have been reported for fibres with circular, homogeneous cores by Snitzer (ref 13). An analysis of an elliptical fibre was presented by Yeh (ref 14) in 1962. Goell (ref 16) reported a technique using a circular harmonic computer analysis, a technique which works well when the guide geometry exhibits small deviations from circularity. Marcatili has described an approximate analysis of rectangular homogeneous dielectric waveguides, a technique suitable for rectangular guides which have the optical field well confined to the core. A review of methods of dealing with radially inhomogeneous fibres has been given by Yeh (ref 15).

In many waveguide problems found in integrated optics these methods may not be used due to complicated refractive index distributions and profiles (ref 17). In addition, the optical field may not be well confined to the core. This is the case for metal-clad polarisers using surface plasma wave attenuation resonance (ref 18). In order to deal with a general waveguide, it is necessary to resort to finite element techniques, which place high demands on computer time and memory space (ref 12)

3.3 Model to be studied

Considerable insight into mode selective absorption mechanisms may be gained from considering a "slab" waveguide. This will serve two purposes. Firstly, the interaction of the various modes with the metal and dielectric layers will be understood, and secondly the results from the simplified model may be used to give approximate design parameters for the fabrication of real devices.

Due to the contradictory nature of many papers in the field,

it will be necessary to present a brief summary of reported investigations of multilayer slab and stripe guides.

3.4 Analytical techniques reported by other authors

The problem of a step-index 4 layer system with isotropic layers has been studied by Polky and Mitchel (ref 19). They found that introduction of a dielectric buffer layer between the metal and the waveguide serves both to increase the attenuation for TM modes and to reduce it for TE modes. However, they obtained solutions for only one mode- described by them as the TM_0 mode. Rashleigh (ref 20) later showed that the authors had neglected the effect of the surface plasma wave (SPW) which may be supported at the metal-buffer boundary (and indeed at any dielectric-metal boundary). This may couple to various modes of the un-clad guide with differing strengths, thus the TM attenuation depends on the mode order. Indeed, some modes show no coupling to the SPW whatsoever. Rashleigh points out that Polky and Mitchel were in fact studying the TM_1 mode and that the TM_0 mode shows no attenuation peak under his conditions. The nomenclature used here for the modes is such that the TM_n mode is that of the directly loaded guide (i.e. with no buffer). Solution of the appropriate transcendental equation has enabled Rashleigh to study the problem using metals with both positive and negative real parts of their permittivity (ref 20,9).

The slab guide with step refractive indices was also studied by Reisinger (ref 21)

Findlaky and Chen (ref 22) studied both slab and stripe diffused guides with exponential refractive index profiles in the diffused region from a theoretical standpoint. They describe the effect on both the effective index and attenuation of various modes for differing metal and dielectric overlays. They found a peak in attenuation for all modes (TE and TM) at a finite diffusion depth, and that the attenuation decreases with increasing mode order, the opposite of the behaviour observed for step index guides. They also draw the important conclusion that the effective index is insensitive to variations in the metal thickness when the latter is more than a small fraction of a free-space wavelength.

Oliner and Peng (ref 23) subsequently pointed out that

certain aspects of Findlakys' analysis were incorrect. In particular, they neglected the effect of the surface-plasmon mode, which will be the subject of a later section. For the planar case this did not affect the accuracy of reported results. However, for the stripe geometry, the previous authors' results were rendered incorrect. In reality, all TM modes are leaky.

Nosu and Hamasaki (ref 24) have studied the influence of the longitudinal plasma wave (LPW) on the propagation characteristices of a 3-layer system. They conclude that below the plasma wavelength, its effect may be neglected for all TM modes except the lowest order TM_0-this being the surface plasma wave. For the latter, both the phase and attenuation constant are considerably overestimated should the LPW not be taken into account.

Yamamoto et al (ref 48) have investigated the 4-layer slab system, taking into account the SPW. Resonance phenomena are observed for all TM modes above the fundamental, ie the attenuation is a maximum at some finite buffer thickness, decreasing with alteration of this parameter. They also report a continuous transformation in the modes, such that mode TM_0 of the guide with a thick buffer layer becomes TM_1 of the guide with direct metal coating. They also describe approximate methods for determining the position and attenuation of the absorption peak.

According to a simple theory of the dielectric properties of metals, the permittivity e and the conductivity σ for intraband absorption are given by (ref 11):

$$\frac{\varepsilon}{\varepsilon_0} = 1 - \frac{\omega_p^2}{\omega^2 + \gamma^2} \qquad 3.1$$

$$\sigma = \frac{\gamma \omega_p^2}{\omega^2 + \gamma^2} \qquad 3.2$$

where $\omega^2_p = n_e q^2/\varepsilon_0 m$, n_e is the free electron density, m_e the free electron density, γ an effective angular collision frequency. w_p represents the bulk plasma angular frequency. Since the plasma frequencies of metals are in general small (ref 11) the real part of the permittivity is predicted to be negative, a situation found in many real metals. Aluminium, silver, and gold fall into the this category.

However the conductivities are calculated, we may describe both a complex permittivity ε' and a complex refractive index N' where

$$n' = n + ik = \varepsilon'^{1/2} \qquad 3.3$$

$$\varepsilon' = \varepsilon_1 + i\varepsilon_2 \qquad 3.4$$

$$\varepsilon_1 = n^2 - k^2 \qquad 3.5$$

$$\varepsilon_2 = 2nk \qquad 3.6$$

or alternatively,

$$2n^2 = \varepsilon_1 + (\varepsilon_1^2 + \varepsilon_2^2)^{1/2} \qquad 3.7$$

$$2k^2 = -\varepsilon_2 + (\varepsilon_1^2 + \varepsilon_2^2)^{1/2} \qquad 3.8$$

The real and imaginary parts of the complex permittivity are not independent, being related by the Kramers-Kronig relations (ref 25). A metal clad waveguide with linearly varying refractive index difference was investigated by Garmire (ref 26). Masuda and Koyama (ref 30) describe the effect of a buffer layer of silicon dioxide of various thicknesses on the modes of a slab guide using a linearly varying refractive index in the core region to approximate the real titanium indiffused waveguide profile (ref 17). They conclude that all modes of the unclad guide exhibit a peak in the curve of absorption vs. buffer thickness, and that the magnitude of the absorption is independent of the mode number. This contrasts with the step index profile used by Rashleigh. Masuda and Koyama considered only TM modes.

In order to gain as much useful information as possible from the calculations, we shall use the model shown in figure 2. The substrate and waveguide will assume isotropically the appropriate refractive indices of lithium niobate, any crystal cut being allowed, with values for the optical constants taken from experimental data in the literature. A similar process will be used for the metals. The values of the constants for the buffer

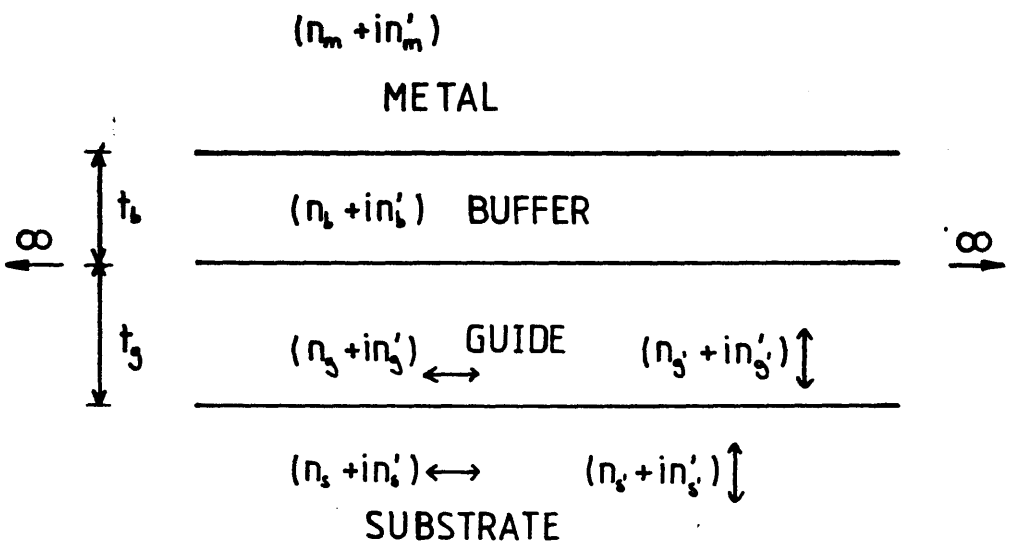

FIG 2 -THE MODEL USED FOR THE 4 LAYER SLAB WAVEGUIDE CALCULATIONS.

layer will be allowed to vary to investigate their effect on polarisation: the optimum values thus obtained will be compared with available materials at a later stage.

3.5 Method

The method adopted will be to solve the transcendental equation for the 4 layer system for both TE and TM modes, (being a planar system, the modes are pure TE or TM). Parameters of interest for both modes will be:

(i) the effective index, or, its equivalent, the propagation constant. In general, they will be a complex.

(ii) the attenuation, related to the imaginary part of the refractive index

(iii) the optical field distribution within the waveguide.

The variation of all three with differing metals and optical property of buffer layer will be investigated. The dispersion equation for the system is given by the following equation, this being reproduced directly from ref **20**

$$k_{x3}t_3 = \tan^{-1}\left[\frac{K_{31}\frac{jk_{x1}}{k_{x3}} - K_{32}\frac{k_{x2}}{k_{x3}}\tan k_{x2}t_2}{1 + K_{34}\frac{jk_{x4}}{k_{x3}}}\right] + \tan^{-1} K_{34}\frac{jk_{x4}}{k_{x3}} + n\pi \qquad 3.9$$

where $K_{ij} = 1$ (TE) 3.10

$= \frac{\varepsilon_i}{\varepsilon_j}$ (TM) 3.11

$$k_{xi}^2 = k_i^2 - k_z^2 \qquad 3.12$$

$$k_i^2 = \varepsilon_i k_0^2 = n_i^2 k_0^2 \qquad 3.13$$

For generality, any of the permittivities e_i may be complex. Approximations are possible in given regimes- for example, Wright (ref 6) has formulated an expression for the attenuation of TM modes for thick buffer layers.

It is also known that the boundary between a metal and a dielectric supports a surface plasma wave, this being TM polarised (ref 31), with dispersion relation given by:

$$\frac{\varepsilon_2}{\varepsilon_1} = \frac{-jk_{x2}}{jk_{x1}} \qquad 3.14$$

3.6 Surface plasma waves

Surface plasma waves are members of the set of surface polaritons: theses are waves which exist at ths boundary between two media (ref 33,37). Surface plasma waves (SPWs) may be divided into several categories. Radiative SPWs can be excited directly with electromagnetic waves and, as pointed out by Otto (ref 31), are involved in phenomena such as plasma-resonance absorption. Non-radiative SPWs on the other hand cannot be excited by radiation travelling in a dielectric when this is bounded by a metal with a smooth interface. To understand this, we refer to figure 3. A metal of complex permittivity E' is adjacent to a dielectric with permittivity η', which in practice is likely to be real. The dispersion relation is given by equation 3.14, or from ref 31:

$$\frac{\varepsilon'(\omega)}{\left(k^2 - \varepsilon'\frac{\omega^2}{c^2}\right)^{1/2}} = \frac{\eta'(\omega)}{\left(k^2 - \eta\frac{\omega^2}{c^2}\right)^{1/2}} \qquad 3.15$$

This class of SPW consists entirely of evanescent waves, and therefore does not emit light. It can be shown (ref 31) that for these solutions of the wave equation to be physically meaningful the following condition must be met:

$$\left(k^2 - \varepsilon'\frac{\omega^2}{c^2}\right)^{1/2} > 0 \quad \text{and} \quad \varepsilon_1 < 0$$

Thus the phase velocity

$$V_{ph} = \frac{\omega}{k} < \frac{c}{\eta'^{1/2}}$$

The phase velocity of the wave excited at the boundary between the two media is

$$\frac{c}{\eta'^{1/2}\sin\theta}$$

which will always be greater than the velocity of the SPW for a propagating wave. In other words, coupling of radiation from the dielectric to the SPW is not possible for physical solutions of the wave equation.

If however a dielectric layer with refractive index n_b less

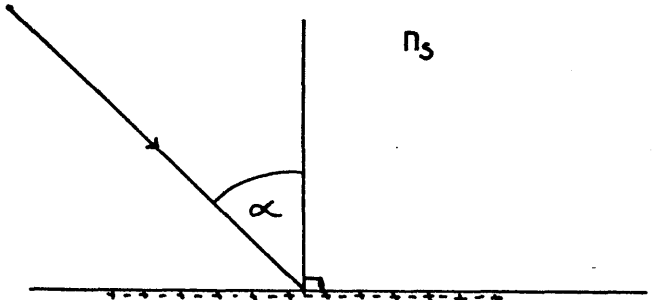

phase velocity of induced charges $V_{ph} = C/n_s \sin\alpha$

$V_{ph} < C/n_s$

$\therefore$ SPW NOT EXCITED

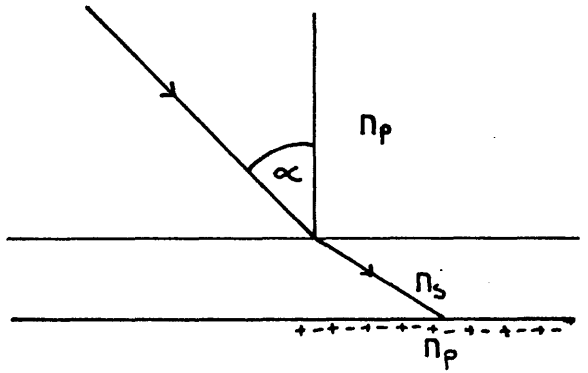

PHASE VELOCITY OF SURFACE CHARGES $V_{ph} = C/n_p \sin\alpha$

$\therefore$ SPW MAY BE EXCITED

FIG 3 ILLUSTRATING THE USE OF MULTILAYER STRUCTURES IN EXCITATION OF ω_L SURFACE PLASMA WAVES

than that of the bulk dielectric is introduced at the boundary, and its refractive index is n_b, then the phase velocity at the boundary will be:

$$\frac{c}{n_s \sin\theta} = \frac{c}{n_b \sin\theta'}$$

The SPW at the boundary has phase velocity c/n_b, and a wave may not be excited. The exact angle required for coupling will thus depend on the properties of the dielectric and the metal. In a multilayer waveguide, the effective index will be determined by the various constituent layers: in general only one effective index will give rise to coupling with the SPW. Otto (ref 34,35) has used the technique with a prism coupling arrangement to demonstrate experimentally the phenomenon. It is noted that the bulk metal may be replaced with a film approximately 1000Å thick with no modification of the theory.

If however the thickness of the metal film is reduced below a critical thickness, a variety of effects will be seen. Otto (ref 34,35) observed resonance in the absorption characteristics of waves excited at the boundaries of a silver film mounted between two identical dielectrics. He observed w_+ resonances with low attenuation corresponding to anti-symmetric charge distribution, while the w_- had high attenuation and symmetric charge distribution. Modified Fresnel formulae were used to model the phenomenon. Otto then refers to the wave excited at the bulk metal/dielectric boundary as the w_1 wave. Otto also points out that the waves may be excited without a low-index buffer layer if a rough surface is used (ref 31). Other workers have confirmed the phenomenon by observing light radiated from SPWs on aluminium films (ref 36)

Other authors (ref 38) have referred to the two modes as the long-range and short-range surface plasmon. The long range SPW is of considerable interest for non-linear work due to the large field enhancement associated with the effect (ref 38,39,40,41,42,43). Craig et al (ref 42) have observed experimentally the long range surface plasmon, detecting a range 63 times greater than that for the w_1 wave.

A range of methods are available for the excitation of SPWs with real sources. Those most commonly found are referred to by

than that of the bulk dielectric is introduced at the boundary, and its refractive index is n_b, then the phase velocity at the boundary will be:

$$\frac{c}{n_6 \sin\theta} = \frac{c}{n_b \sin\theta'}$$

The SPW at the boundary has phase velocity c/n_b, and a wave may not be excited. The exact angle required for coupling will thus depend on the properties of the dielectric and the metal. In a multilayer waveguide, the effective index will be determined by the various constituent layers: in general only one effective index will give rise to coupling with the SPW. Otto (ref 34,35) has used the technique with a prism coupling arrangement to demonstrate experimentally the phenomenon. It is noted that the bulk metal may be replaced with a film approximately 1000Å thick with no modification of the theory.

If however the thickness of the metal film is reduced below a critical thickness, a variety of effects will be seen. Otto (ref 34,35) observed resonance in the absorption characteristics of waves excited at the boundaries of a silver film mounted between two identical dielectrics. He observed w_+ resonances with low attenuation corresponding to anti-symmetric charge distribution, while the w_- had high attenuation and symmetric charge distribution. Modified Fresnel formulae were used to model the phenomenon. Otto then refers to the wave excited at the bulk metal/dielectric boundary as the w_1 wave. Otto also points out that the waves may be excited without a low-index buffer layer if a rough surface is used (ref 31). Other workers have confirmed the phenomenon by observing light radiated from SPWs on aluminium films (ref 36)

Other authors (ref 38) have referred to the two modes as the long-range and short-range surface plasmon. The long range SPW is of considerable interest for non-linear work due to the large field enhancement associated with the effect (ref 38,39,40,41,42,43). Craig et al (ref 42) have oserved experimentally the long range surface plasmon, detecting a range 63 times greater than that for the w_1 wave.

A range of methods are available for the excitation of SPWs with real sources. Those most commonly found are referred to by

Sarid (ref 38) as the Otto, Kretschmann and modified Kretschmann (or Sarid) geometries: all three are illustrated in fig 4

Many uses have been put forward for the SPWs (ref 46,47), including non-linear optics, chemical sensing, solar energy (ref 44)& for polarisers (ref 45).

3.7 Implementation

The computer analysis was to be performed on the GEC4090 computer at the Rutherford Appleton Laboratories, this being accessed by a telephone line, and, in turn, the GEC4180 at Glasgow. As some errors had been reported with the more versatile Fortran 4 language, the algorithm was written in Fortran 77. A flow chart of the computation is shown in figure 5, describing the method used to obtain one mode of the guide.

3.7.1 Basic algorithm

Using the "NAG" package available on the GEC computer, efficient iterative methods are available to solve N transcendental equations in N variables. We may regard the real and imaginary parts of equation 3.9 as two independent real equations, which may then be solved. The parameter to be returned is the complex propagation constant, the real part describing the phase of light propagating through the guide, the imaginary part describing the attenuation. The first section of the program defines the values of the optical constants to be used. The user may select any given crystal cut of lithium niobate, and either aluminium, silver, or gold, two different sets of data being available for the latter. Step indices are assumed for the waveguide core and substrate. The refractive index of the substrate is determined via interpolative routines for a given wavelength in a subroutine. High accuracy of the interpolant at extremes of data is ensured by the use of cubic spline interpolants (ref 49), NAG routine E01BAF defining the interpolant, with E02BBF interpolating the data for a given wavelength. The index is assumed to be real. The user may select a default refractive index difference between core and cladding of 5×10^{-3}, (assumed to be the same for both ordinary and extraordinary polarisations) or input a different value. Having selected the metal to be used, the refractive index (complex) is interpolated using another cubic spline interpolant. Where the

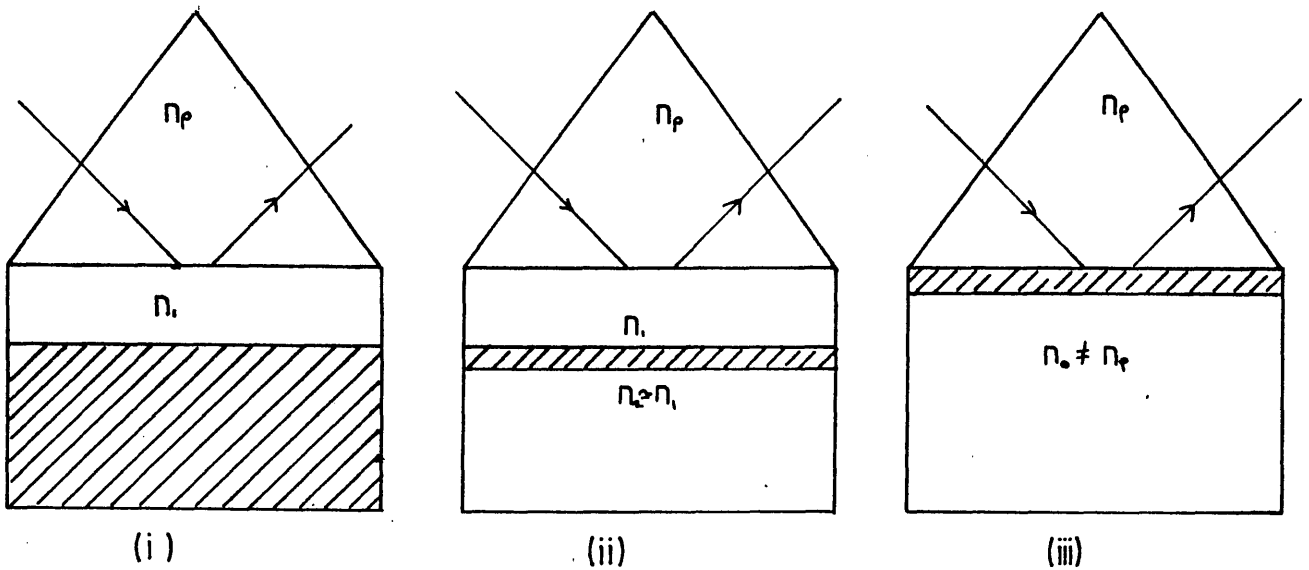

FIG 4 OTTO (i), SARID (ii), KRETSCHMANN (iii) GEOMETRIES FOR EXCITATION SURFACE PLASMA WAVE AT BOUNDARY BETWEEN DIELECTRIC AND METAL (AFTER SARID)

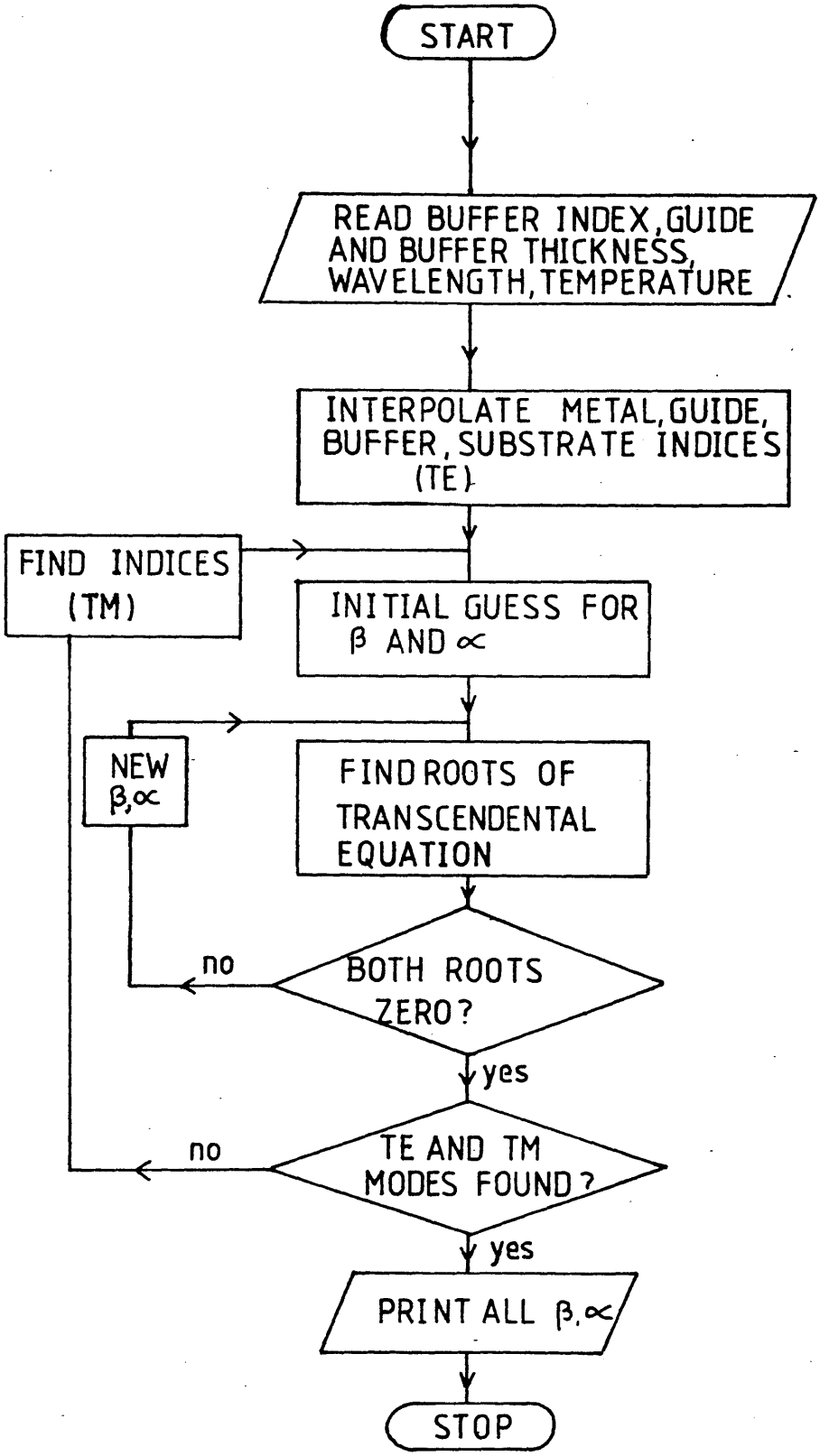

FIG 5 FLOW CHART FOR PROGRAM TO FIND EFFECTIVE INDEX AND ATTENUATION OF MODES OF MULTILAYER ANISOTROPIC WAVEGUIDES VIA COMPLEX TRANSCENDENTAL EQUATION

calculation requires the permittivity, it is evaluated using equations 3.5 and 3.6. Other parameters to be selected are the mode (TE or TM), thickness of the core and buffer layers, and the refractive index of the latter. Complex refractive indices are also permitted for the buffer layer.

Having initialised the various parameters, an initial guess for both the attenuation and effective index are input. If both guesses are sufficiently close to a root to allow convergence, and the NAG routine C05NBF to find the solutions, the resulting values of the propagation constant and attenuation are output. The equations to be solved are specified in an external function (ref 49). The routine allows up to 400 non-convergent iterations before reporting an error, in which case the initial guess for either the attenuation or propagation constant, or both, must be re-selected and the process repeated.

Due to the periodic nature of the tangent function, the mode number may not be input directly. Thus to obtain solutions for all modes guided by the system, a range of initial guesses must be used. The entire process must be repeated for the orthogonal set of modes (TM or TE). Individual runs of the program take a few seconds: however considerable time would be spent in choosing suitable starting values for all modes, thus a more efficient solution is sought.

3.7.2 Automatic solution

The program used to investigate the 4-layer system was the program "HUNTER", this being based on a modification of the above program. Three important differences are noted:

(i) Having decided which crystal cut was to be used, it was possible to re-initialise the optical constants for both guide and substrate. Thus both TE and TM modes could be obtained from one "run" of the program

(ii) A range of initial guesses were used in an automatic procedure, with those for the propagation constant ranging from $5x10^{-3}$ below that of the core, to $5x10^{-3}$ above that of the substrate. To use initial values ranging only between the core and substrate would be sufficient for thick buffer layers, however as this parameter is reduced, the roots may lie outside these limits. Approximately 150 initial guesses are used, the

resultant roots only being printed out if they differ from a previous solution by a specified amount. Thus for a given waveguide system all TE and TM modes may be found, the program then taking approximately 5 minutes to run.

(iii) Since it will generally be desired to investigate the variation of attenuation and effective index with buffer layer thickness, the entire (modified) program was automatically run for a pre-determined range of buffer thicknesses.

In summary, the user defines the guide thickness, buffer index, metal and crystal to be used, and wavelength. The program then returns, for a number of buffer thicknesses, the effective indices and attenuations for each guided TE and TM mode. The program in this final version takes approximately one hour to run for each waveguide system.

3.7.3 Optical constants of dielectric and metals

The data for lithium niobate were taken from Rauber (ref 50). Approximately 30 values for both the ordinary and extraordinary indices were available in the wavelength range 0.4 to 3.0 microns. While this range exceeded that likely to be encountered in practice, the increased range lent increased accuracy to the interpolant used (ref 49)

A wider choice of data are available for the optical constants of metals. Weaver et al (ref 25) have reviewed the published literature for many metals. We will consider metals which are easily evaporated under laboratory conditions and which have negative real parts of their permittivity in the wavelength region of interest. Aluminium, gold and silver fall into this category. Unfortunately, the reported data for many metals differ widely for both real and imaginary parts: for a comprehensive bibliograhy the reader is referred to ref 25. In particular, the optical properties vary with the quality of the surface: strain, oxide layers and crystallinity all contribute to corrupt their measurement. Weaver has selected the data which were collected under the closest conditions to ideal.

3.7.4 Determination of attenuation and effective indices of SPWs

It was also desired to investigate the surface plasma waves supported at the boundary between a dielectric and a metal. The program "PLAS" evaluates these quantities for a given real metal

(using the same data as for the program "HUNTER"). A range of permittivities of dielectric between 1 and 100 was automatically used and a large number of initial estimates for the two quantities used. Iterative methods, as described in previous sections, may then be used to evaluate the root of equation 3.14. The program was not efficient due to the large number of initial guesses needed for the automatic solution. The output from the program was in a form suitable for automatic plotting of the relevant graphs using the program "PLASPLOT". Production of a complete graph took approximately three hours.

3.8 Results

The data from the program are output in numerical form: subject to satisfactory inspection, they may then be presented in graphical form using the program "MULTPLOT" which allows the data from up to 8 modes to be presented on the same graph.

As 5 different sets of data relating to the metals are available with this implementation of the program, with three different crystal cuts and an infinity of choices for guide thickness, buffer index and wavelength, a large amount of data were generated. In the sections to follow, the general trends associated with each phenomenon will be presented in graphical form. Numerical values of the features of interest will be extracted and presented in tabular form.

A summary of all results is given in table 3: here the buffer thickness corresponding to maximum TM attenuation is presented, together with the corresponding TM and TE attenuations.

3.8.1 Variation of attenuation with buffer thickness

Figure 6 shows for several TM modes the variation in attenuation and effective index with thickness of the buffer layer. The system used for this graph used waveguide and substrate indices corresponding to those of lithium niobate, with buffer index of 2.0 and aluminium cladding. The guide thickness was 4.0 microns. The description of the modes follows Masuda (ref 30). The attenuation of TM modes varies so strongly with this parameter that a double logarithmic scale is needed to present the data.

For a sufficiently thick buffer layer, the loss for both TE

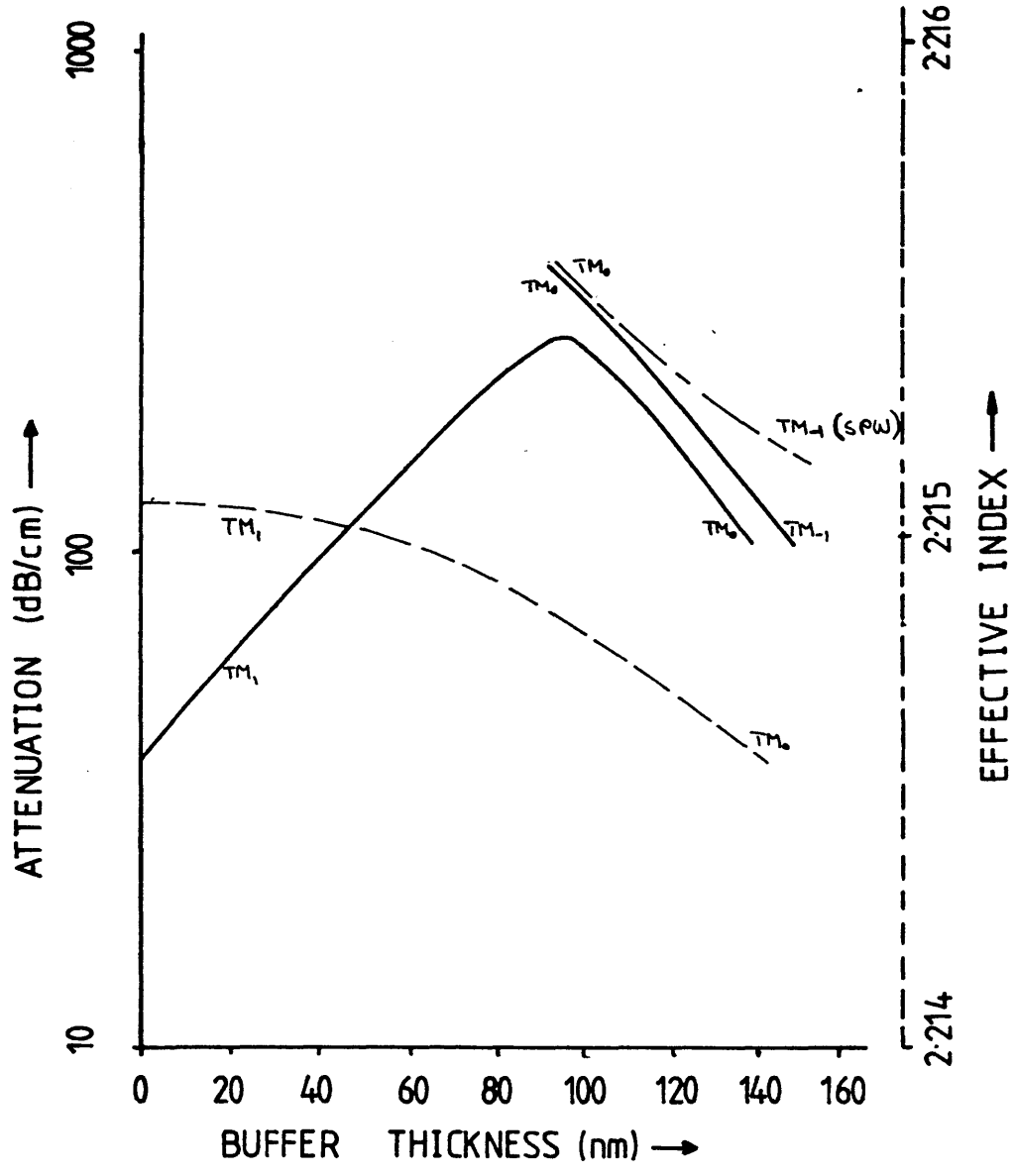

FIG 6a ILLUSTRATING $TM_n \rightarrow TM_{n+1}$ MODE TRANSITION AT ATTENUATION PEAK. USING Z-CUT $LiNbO_3$ INDICES. BUFFER INDEX = 2·0, ALUMINIUM

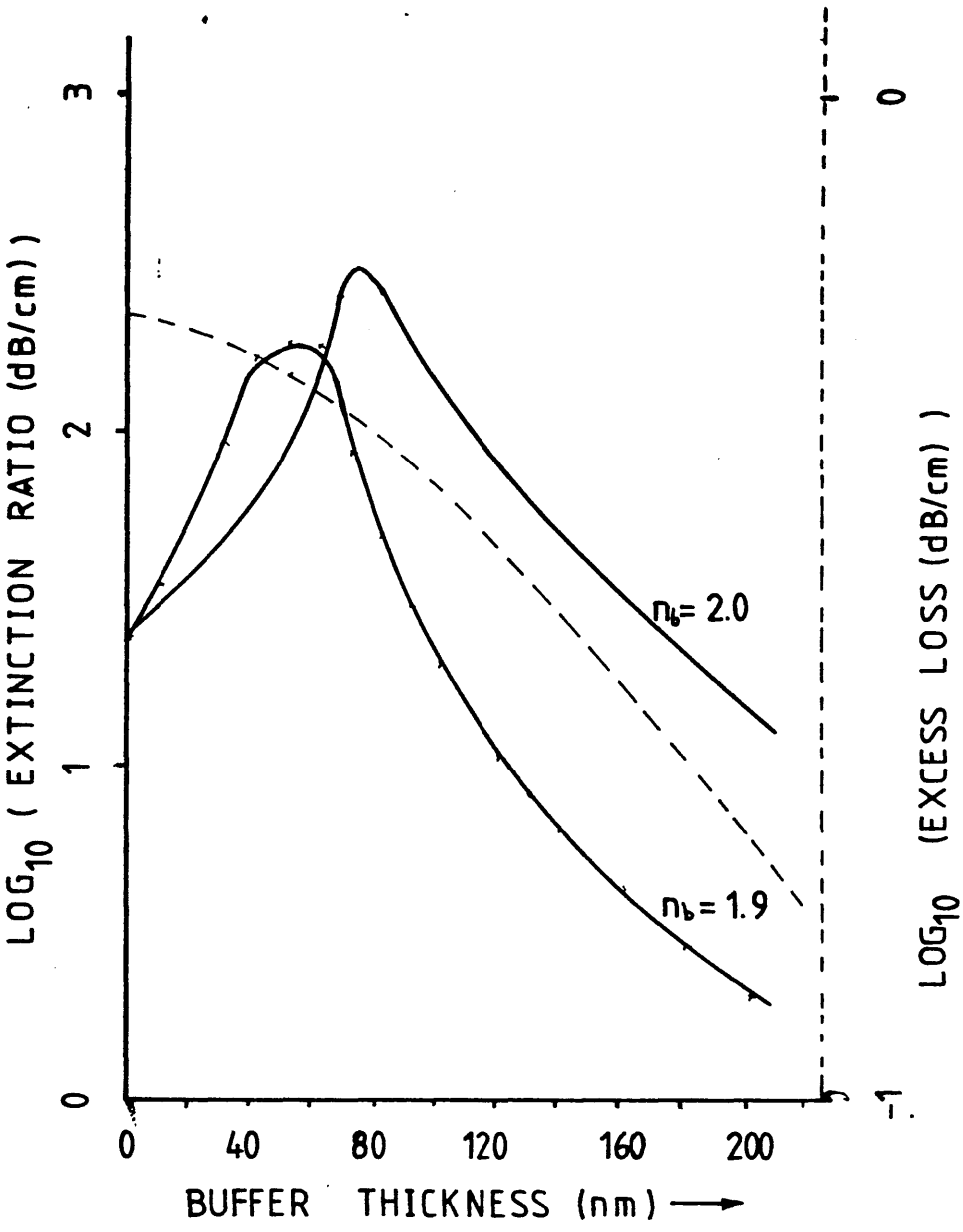

FIG 6 EXTINCTION RATIO VS. BUFFER LAYER THICKNESS FOR 4-LAYER SLAB MODEL WITH ALUMINIUM CLADDING. FOR BUFFER INDICES OF 1.9 AND 2.0 EXCESS LOSS (TE MODE) ALSO SHOWN FOR BUFFER INDEX OF 2.0 WAVELENGTH= 1.15 MICRONS

and TM modes is small (say 0.1dB/cm). (Note- this represents loss due to absorption-scattering is neglected in the model). As the thickness is reduced, the TE loss increases monotonically to a maximum value, this always being for zero buffer thickness, or for the metal being in contact with the waveguide. The TM modes however are more complex in their behaviour. One mode, TM_0 increases in loss with decreasing buffer thickness. This mode is the Surface Plasma Wave (SPW). All other TM modes show a peak in the absorption of the wave, the attenuation being smaller for zero buffer thickness than at the peak.

The effective index is seen to change in a simple manner for TE modes while the TM modes show an abrupt change in the vicinity of the absorption peak. With decreasing buffer thickness, the effective index increases first gradually and then abrubtly. At a well defined thickness, the mode continues with a much reduced index, which increases firstly abruptly and then more gradually. It is seen that the modes interchange at this critical thickness, the TM_{n-1} mode of the guide with thick buffer layer becoming the TM_n mode of the same guide with zero buffer thickness. The TM_0 mode of the directly coated guide coresponds to the TM_{-1} or SPW of the guide with thick buffer.

Two conclusions may immediately be drawn: for a phase modulator, thick buffer layers are necessary to avoid undue loss (although this action may result in reduced efficiency), while for a mode filter, a well defined, reduced, thickness is required.

3.8.2 Effect of Variation of Buffer Index

Figure 7 illustrates the variation in attenuation with buffer thickness for several buffer indices. Figure 8 illustrates the same data but with the horizontal scale altered to show more clearly the resonance phenomenon. Figures 9 and 10 show the effective indices associated with TE and TM modes in the region of the mode transitions. It is seen that with reducing buffer index, the thickness corresponding to maximum absorption for TM modes becomes smaller, while the magnitude of the absorption also decreases. TE modes show a reduction in attenuation with reducing buffer index.

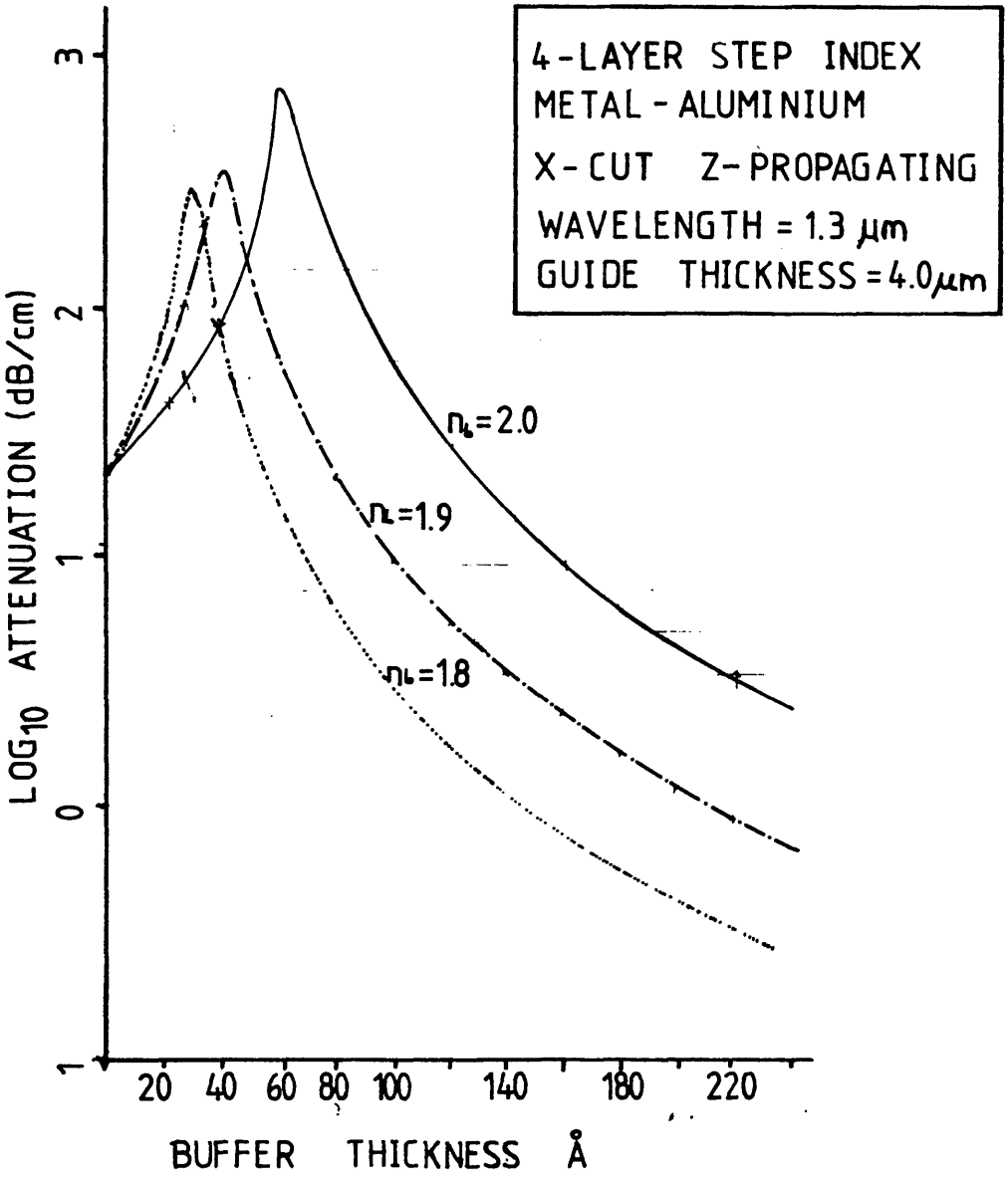

FIG 7 VARIATION OF ATTENUATION OF TM MODES WITH BUFFER THICKNESS FOR THREE BUFFER INDICES.

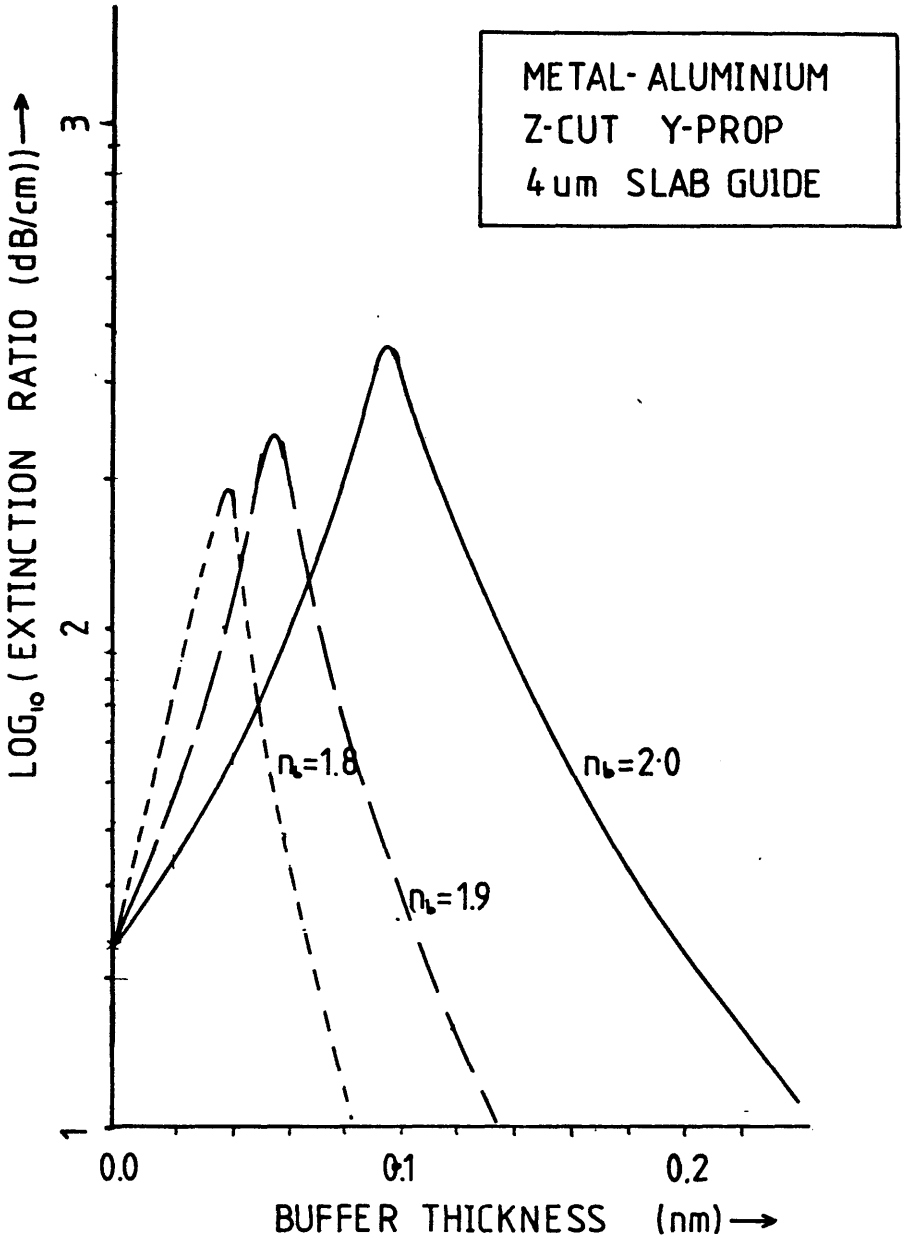

FIG 8 TM ATTENUATION VS. BUFFER THICKNESS FOR 4-LAYER SLAB SYSTEM WITH THREE DIFFERENT BUFFER INDICES

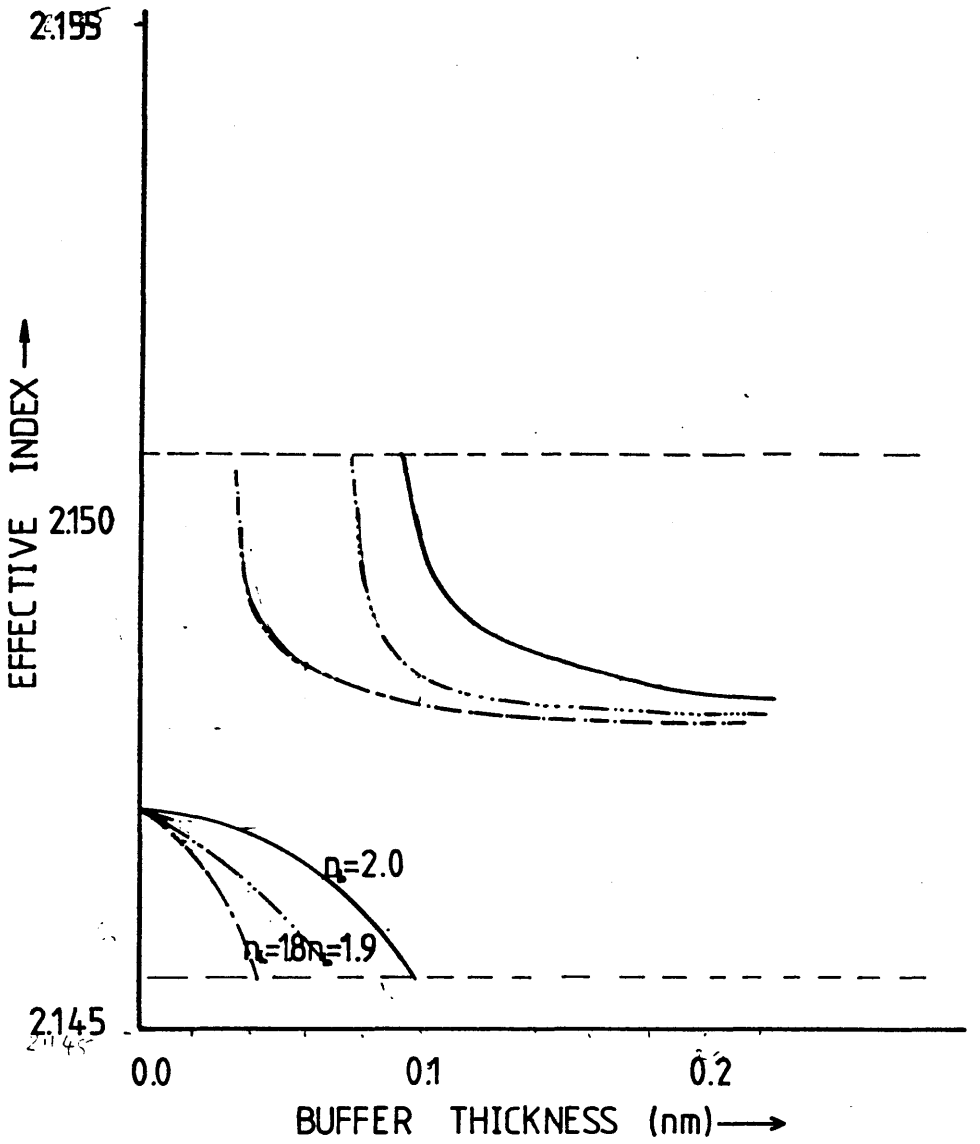

FIG 9 EFFECTIVE INDEX VS. BUFFER THICKNESS FOR 4-LAYER SLAB SYSTEM- TM MODES SHOWN FOR THREE DIFFERENT BUFFER INDICES

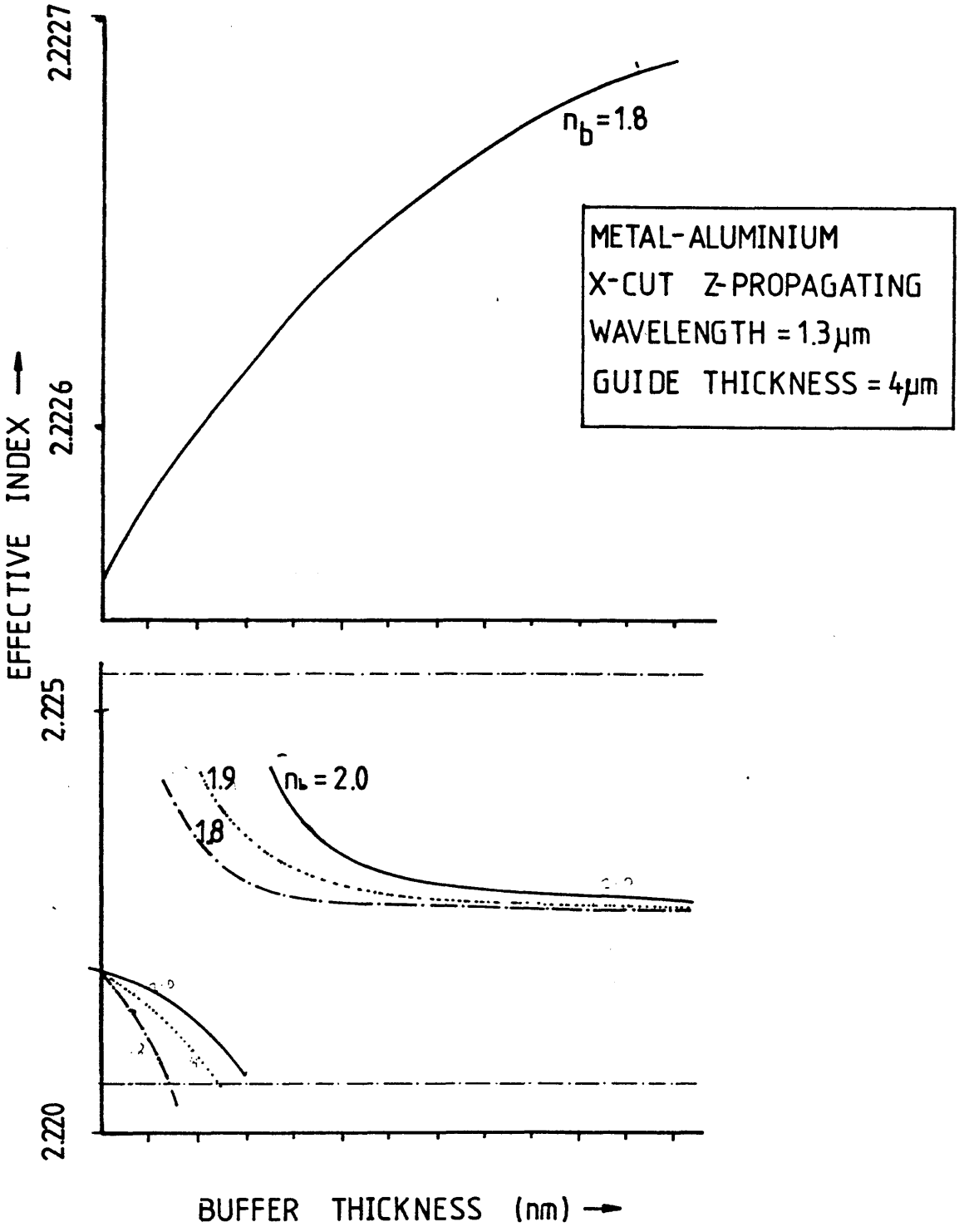

FIG 10 EFFECTIVE INDEX VS. BUFFER THICKNESS FOR TE AND TM MODES OF THE 4-LAYER SLAB SYSTEM.

3.8.3 Effect of Variation of Wavelength

No simple variation of attenuation with wavelength is seen: this results from the complex varition of the refractive indices of the metals and the lithium niobate in the wavelength region of interest.

Table 1 shows the variation in TM attenuation with wavelength for the 4-layer system with aluminium cladding and a buffer index of 1.9 on Z-cut Y-propagating lithium niobate. It is seen that the TE losses are approximately proportional to the TM losses, being a maximum at 0.7 microns. With increasing wavelength the TM attenuation decreases, until the attenuation at 1.4μm is one-tenth of that at 0.7 microns. This suggests the use of the systems in wavelength demultiplexers.

3.8.4 Variation of Attenuation of SPW with Permittivity of Dielectric

Fig 11 shows the variation of attenuation and effective index of surface plasma waves at a metal-dielectric boundary. The metal used was aluminium, and the wavelength 0.633 microns. It is seen that for increasing permittivity the attenuation also increases, generally with an increase in effective index. The properties of the SPW are seen to vary strongly with properties of both the metal and the dielectric.

3.9 Discussion

The need for a theoretical model describing the effects of metal overlays on integrated optical waveguides has been explained. The problem has been shown to be insoluble. Approximations taking into account the lateral confinement of the light have been shown to be unsuitable. Slab models, yielding exact solutions have been used with step indices to investigate the behaviour of the various modes present.

Although step indices were assumed, the values of the refractive indices used were based on those determined experimentally for real waveguides, with the exception of the buffer layer. This was allowed to assume arbitrary values in order to investigate the effect on the attenuations of the various modes.

For a suitable range of buffer indices, the TM modes show a resonance in their attenuation. This occurs at a thickness of

Table 1 Attenuation for TE and TM modes of 4-layer slab guide.
Buffer index = 1.9, metal- aluminium, Crystal- Z-cut Y-prop.

Wavelength (Microns)	Optimium Buffer Thickness (nm) (nearest 20)	TM attenuation (dB/cm)	Corresponding TE_0 mode Attenuation (dB/cm)
0.6	40	953	1.43
0.7	40	1544	2.09
0.8	40	3316	1.27
0.9	60	342	1.02
1.0	60	474	0.65
1.1	60	304	0.54
1.2	60	250	0.50
1.3	60	211	0.47
1.4	60	186	0.44

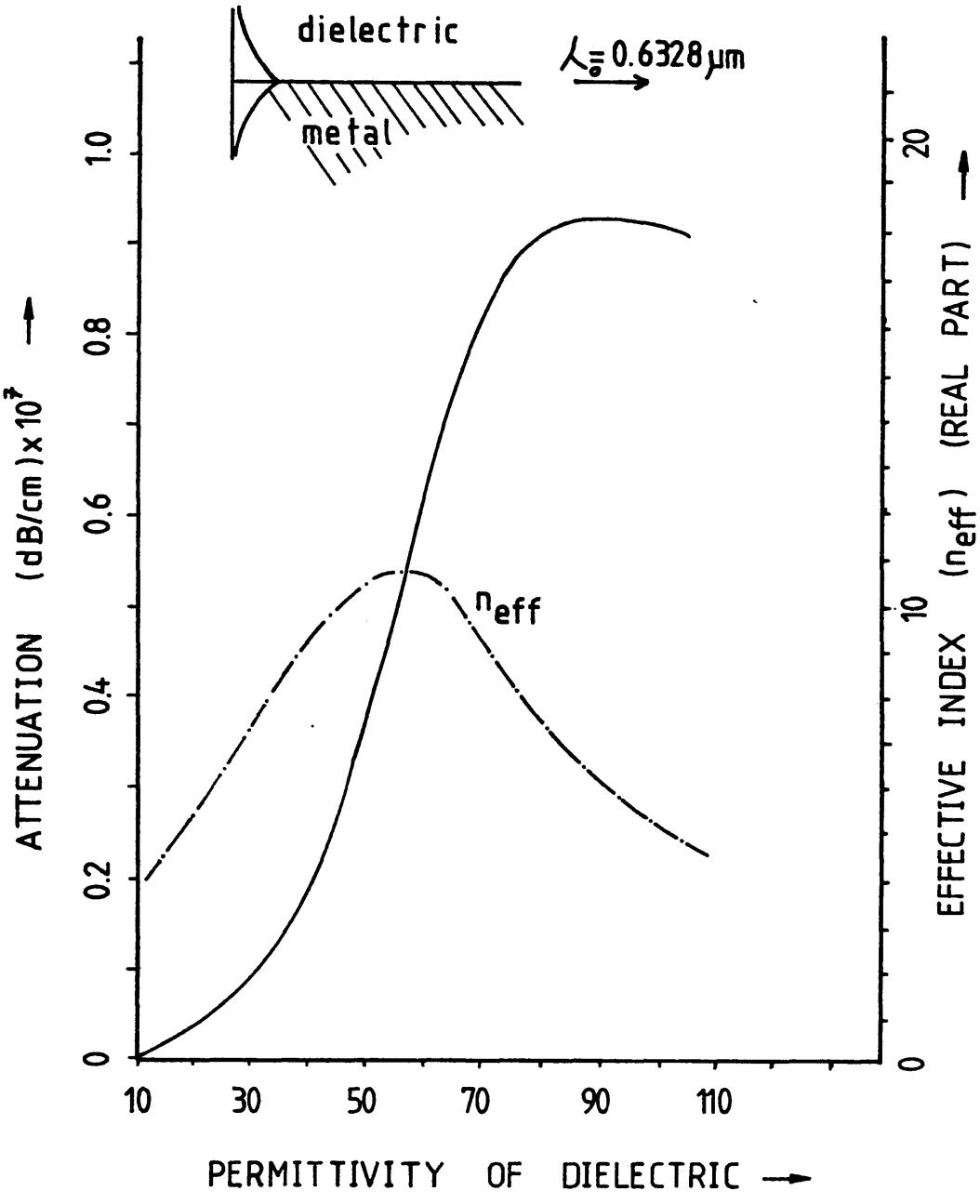

FIG 11 EFFECTIVE INDEX AND ATTENUATION OF SURFACE PLASMA WAVE SUPPORTED AT INTERFACE OF ALUMINIUM AND DIELECTRIC VS. PERMITTIVITY OF DIELECTRIC AT 0.6328μm WAVELENGTH.

buffer layer which depends on the metal indices, wavelength and other dimensional and physical parameters. The magnitude of the attenuation is high-up to 500dB/cm. The TE modes do not show this resonance, their attenuation decreasing monotonically with increasing buffer layer thickness.

For a sufficiently high buffer thickness, TM and TE attenuations may be reduced below 1dB/cm. The required thickness reduces with decreasing buffer index, but should be above 0.2um for an index of 2.0 for the system studied here if significant differential attenuations are to be avoided. These results are therefore important for the design of integtrated optical modulators.

In order to design integrated optical mode filters, careful control over buffer layer parameters is essential. A maximum in TM mode attenuation for all modes (although generally only the TM_0 mode of the unclad guide will be of interest) is observed at a finite buffer thickness. The extinction ratio is given to approximately 0.1% accuracy by the TM_0 attenuation. The 1/e width of the resonance is small, and the manufacturing tolerances on the buffer thickness will be strict as the device length will be minimised to reduce parasitic TE loss.

The effect of variation in guide thickness with all other parameters remaining constant is illustrated for one particular system in table 2. In this case it is seen that increasing the guide thickness results in a reduction of the attenuation for both modes. Detailed consideration of this will be given in chapter 7.

Some general conclusions concerning the choice of metal to be used for the construction of polarisers may be drawn from the data in table 3. For all of the wavelength and buffer index combinations studied here, aluminium yields the highest extinction ratio. Where gold is to be used, thicker buffer layers must in general be used than with aluminium or silver. In some cases, no attenuation resonance peak is observed for gold clad systems. Thus its use in the manufacture of polarisers is not recommended. The low losses for both modes of the gold-clad system suggest its use for electrodes to be used with phase modulators and other devices requiring close proximity of metal

Table 2 Attenuation for TE and TM modes, wavelength- 1.3um, metal-aluminium, Crystal- X-cut Y-prop, Buffer index-1.9, buffer thickness- 40nm

Guide Thickness (microns)	TM Attenuation (dB/cm)	TE atenuation (dB/cm)
3.2	388	.686
3.4	377	.654
3.6	367	.615
3.8	357	.573
4.0	348	.532
4.2	340	.491

Table 3 summary of results from 4 layer slab model with 4um guide thickness, all attenuations in dB/cm. Guide thickness 4.0um in each case, refractive index difference =0.005 (TE and TM). All optimum buffer thicknesses rounded to nearest 20nm

(i) Wavelength=1.3 microns Metal-Aluminium (Weavers Data) Buffer index=2.0

System	Optimum Buffer Thickness (nm)	TM attenuation	TE attenuation
Z-cut Y-prop	100	336	.42
X-cut Z prop	80	263	.46
X-cut Z-prop	80	137	.49

(ii) Wavelength=1.3 microns Metal-Gold (1) Buffer index=2.0

System	Optimum Buffer Thickness (nm)	TM attenuation	TE attenuation
Z-Cut Y-Prop	>18		
X-Cut Y-Prop	120	76	.1
X-Cut Z-Prop	120	76	.09

(iii)Wavelength=1.3 microns Metal-Silver (Weavers Data) Buffer index=2.0

System	Optimum Buffer Thickness (nm)	TM Attenuation	TE attenuation
Z-cut Y-prop	160	165	.13
X-cut Z prop	100	160	.18
X-cut Y-Prop	100	160	.20

(iv)Wavelength=1.3 microns Metal Gold (Weaver) Buffer index=2.0

System	Optimum Buffer Thickness (nm)	TM Attenuation	TE attenuation
X-Cut Y-Prop	120	79	.1
X-Cut Z-Prop	120	79	.09

Note Gold (1) refers to data taken from International Critical Tables

(v) Wavelength=1.15 microns, metal Aluminium, buffer index=2.0

System	Optimum Buffer Thickness (nm)	TM Attenuation	TE attenuation
Z-cut Y prop	100	246	.44
X-Cut Y-Prop	60	253	.59
X-Cut Z-Prop	60	253	.55

(vi) Wavelength=1.15 microns, metal Gold (1), buffer index=2.0

System	Optimum buffer Thickness (nm)	TM attenuation	TE attenuation
Z-Cut Y-Prop	80	116	.11
X-Cut Y-Prop	40	38	.13
X-Cut Z-Prop	60	66	.12

(vii)Wavelength=1.15 microns, metal Silver (Weavers Data), buffer index=2.0

System	Optimum Buffer Thickness (nm)	TM attenuation	TE attenuation
Z-cut Y-prop	160	117	.11
X-Cut Y-Prop	100	200	.2
X-Cut Z-Prop	100	200	.1

(viii)Wavelength=1.15 microns, metal Gold (Weavers Data), buffer index=2.0

System	Optimum Buffer	TM attenuation	TE attenuation
Z-cut Y-prop	>180		
X-Cut Y-Prop	120	117	.09
X-cut Z-Prop	120	117	.08

(ix) Wavelength=1.06um Metal Aluminium, Buffer index=2.0

System	Optimum Buffer Thickness (nm)	TM attenuation	TE attenuation
Z-cut Y-prop	100	420	.46
X-cut Y-prop	60	362	.66
X-cut Z-prop	60	362	.60

(x) Wavelength=1.06um, metal Gold (1), buffer index=2.0

System	Optimum Buffer Thickness (nm)	TM Attenuation	TE Attenuation
Z-cut Y-prop		NO PEAK OBSERVED	
X-Cut Y-Prop		NO PEAK OBSERVED	
X-Cut Z-Prop		NO PEAK OBSERVED	

(xi) Wavelength=1.06um, metal Silver (Weavers Data), buffer index=2.0

System	Optimum Buffer Thickness (nm)	TM Attenuation	TE Attenuation
Z-cut Y-prop	80	20.25	.19
X-Cut Y-Prop	100	267	.2
X-Cut Z-Prop	100	267	.17

(xii) Wavelength=1.06um, metal Gold (Weavers Data), buffer index=2.0

System	Optimum Buffer Thickness (nm)	TM Attenuation	TE Attenuation
Z-cut Y-prop	>180		
X-Cut Z-Prop	120	192	.07

(xiii) Wavelength=1.3 microns, metal Aluminium, Buffer index=1.9

System	Optimum Buffer Thickness (nm)	TM Attenuation	TE Attenuation
X-Cut Y-Prop	40	348	.53
X-Cut Z-Prop	40	348	.51
Z-Cut Y-Prop	60	212	.47

(xiv) Wavelength=1.3 microns, Metal Gold (1), Buffer Index=1.9

System	Optimum Buffer Thickness (nm)	TM Attenuation	TE Attenuation
X-Cut Z-Prop	60	35	.12
X-Cut Y-Prop	80	38	.12
Z-Cut Y-Prop	100	63	.09

(xv) Wavelength=1.3 microns, Metal-Silver (Weavers Data), Buffer index=1.9

System	Optimum Buffer Thickness (nm)	TM Attenuation	TE Attenuation
Z-Cut Y-Prop	80	174	.18
X-Cut Z-Prop	60	174	.20
X-Cut Y-Prop	60	174	.22

(xvi) Wavelength=1.3 microns, Metal-Gold (Weavers Data), Buffer Index=1.9

System	Optimum Buffer Thickness (nm)	TM Attenuation	TE Attenuation
X-Cut Y-Prop	80	40	.12
Z-Cut Y-Prop	80	7.4	.25

(xvii) Wavelength=1.15 microns, Metal-Aluminium, Buffer Index=1.9

System	Optimum Buffer Thickness (nm)	TM Attenuation	TE Attenuation
X-Cut Y-Prop	40	509	.6
X-Cut Z-Prop	40	509	.58

(xviii) Wavelength=1.15 microns, Metal-Gold (1), Buffer Index=1.9

System	Optimum Buffer Thickness (nm)	TM Attenuation	TE Attenuation
X-Cut Y-Prop	60	8.9	.12
X-Cut Z-Prop	40	52	.13
Z-Cut Y-Prop	40	44	.13

(xix) Wavelength=1.15 microns, Metal-Silver (Weavers Data), Buffer index=1.9

System	Optimum Buffer Thickness (nm)	TM Attenuation	TE Attenuation
X-Cut Y-Prop	60	222	.22
X-Cut Z-Prop	60	222	.20
Z-Cut Y-Prop	80	225	.18

(xx) Wavelength=1.15 microns, Metal-Gold (Weavers Data), Buffer Index=1.9

System	Optimum Buffer Thickness (nm)	TM Attenuation	TE Attenuation
X-Cut Y-Prop	80	45	.10
X-Cut Z-Prop	80	45	.09
Z-Cut Y-Prop	100	89	.08

(xxi) Wavelength=1.55 microns Metal-Aluminium,Buffer Index=2.0

System	Optimum Buffer Thickness (nm)	TM Attenuation	TE Attenuation
X-Cut Y-Prop	60	289	.45
X-Cut Z-Prop	60	289	.44
Z-Cut Y-Prop	100	238	.39

(xxii) Wavelength=1.55 microns, Metal-Gold (1), Buffer Index=2.0

System	Optimum Buffer Thickness (nm)	TM Attenuation	TE Attenuation
X-Cut Y-Prop	NO PEAK OBSERVED		
X-Cut Z-Prop	NO PEAK OBSERVED		
Z-Cut Y-Prop	NO PEAK OBSERVED		

(xxiii) Wavelength=1.55 microns, Metal-Silver (Weavers Data), Buffer index=2.0

System	Optimum Buffer Thickness (nm)	TM Attenuation	TE Attenuation
Z-Cut Y-Prop	160	130	.15
x-Cut Z-Prop	100	130	.19
X-Cut Y-Prop	100	130	.20

(xxiv) Wavelength=1.55 microns, Metal-Gold (Weavers Data), Buffer Index=2.0

System	Optimum Buffer Thickness (nm)	TM Attenuation	TE Attenuation
X-Cut Y-Prop	NO PEAK OBSERVED		
X-Cut Z-Prop	NO PEAK OBSERVED		
Z-CUT Y-Prop	>200nm		

and waveguide.

Data for the real and imaginary parts of the refractive index of aluminium, silver and gold are presented in figures 12, 13, 14, and 15. It is seen that for gold, the two data sets differ widely. This provides an indication of the widely varying data available for refractive indices of metals as discussed in reference 25. Of the three, aluminium is by far the most reliable: for other metals quantitative results based on the models presented here should be treated with caution.

The model predicts that low-loss mode filters may be made by gradual tapers of buffer layers. However, the more complex problem of an abrupt transition between the clad and unclad sections has not been considered. The TE_0 loss is likely to be higher than in the previous case

Finally, it is to be noted that the extinction ratios presented here are for an idealised system: real systems, or other dissimilar models will vary greatly in their performances and the analysis presented here should accordingly be repeated.

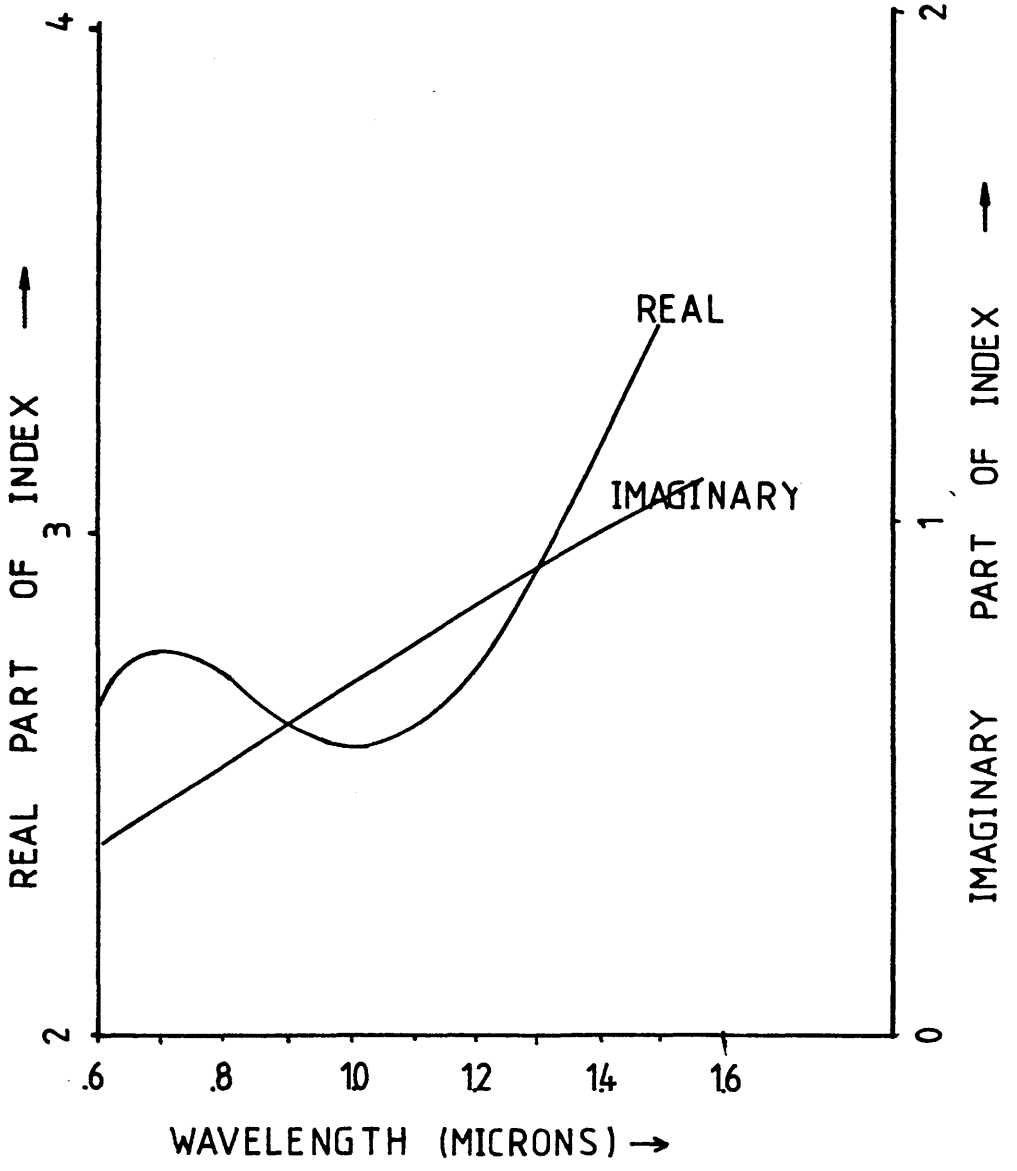

FIG 12 INTERPOLANTS USED TO EVALUATE REAL AND IMAGINARY PARTS OF REFRACTIVE INDEX OF SILVER. DATA TAKEN FROM WEAVER

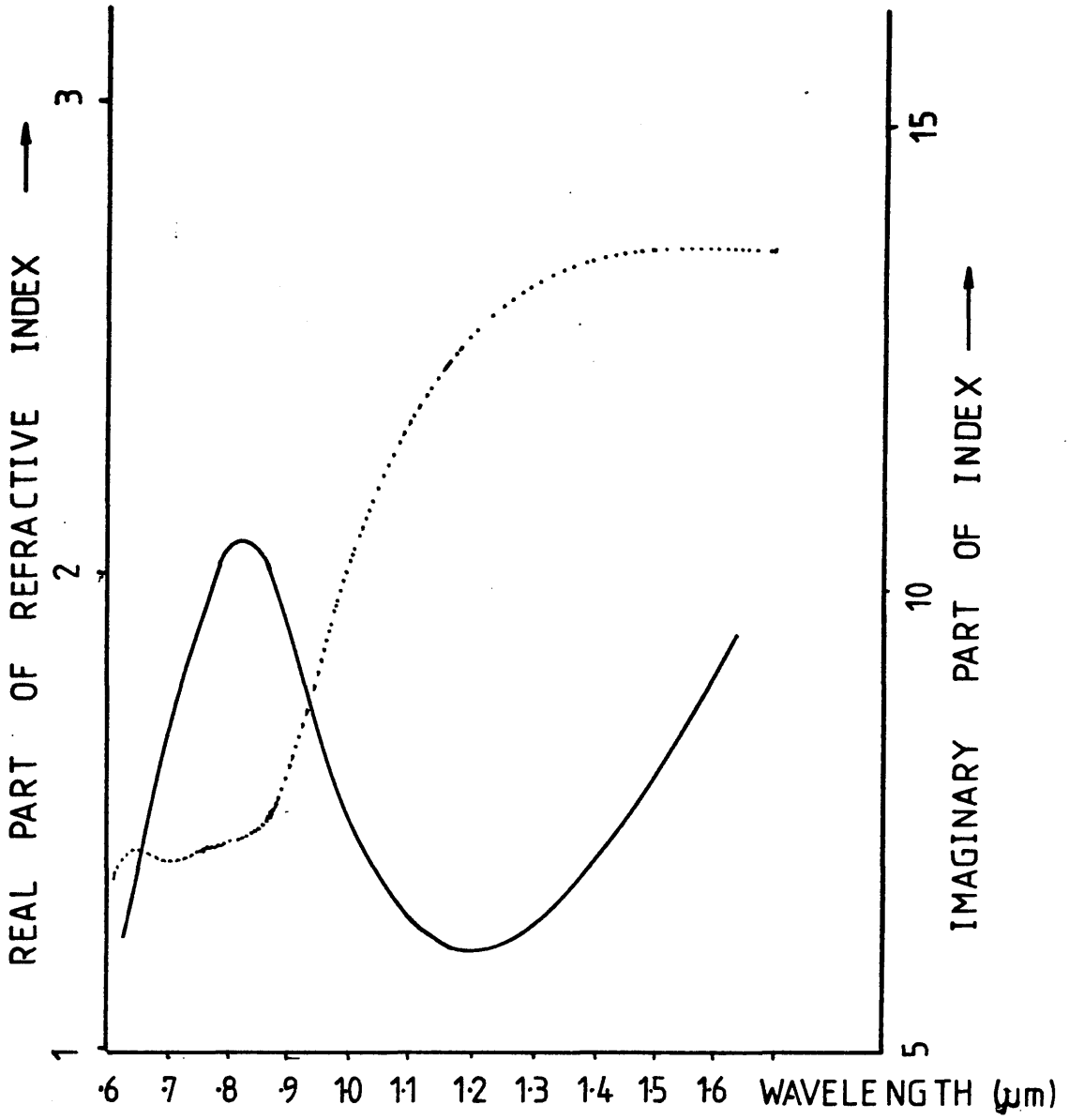

FIG 13 INTERPOLANTS USED FOR REAL AND IMAGINARY PARTS OF REFRACTIVE INDEX OF ALUMINIUM. DATA TAKEN FROM AMERICAN INSTITUTE OF PHYSICS HANDBOOK

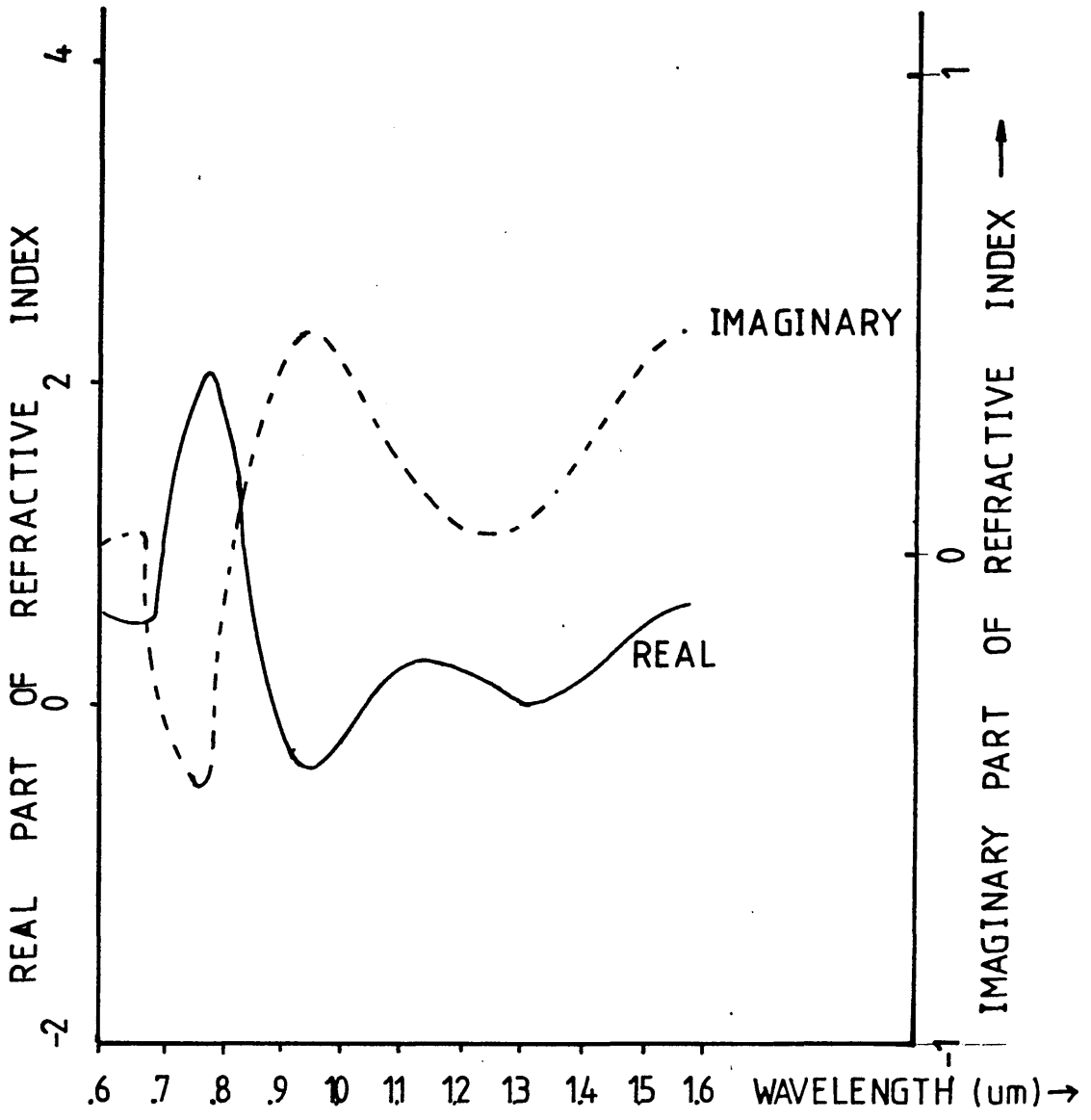

FIG 14 INTERPOLANTS USED FOR REAL AND IMAGINARY PARTS OF REFRACTIVE INDEX OF GOLD. BASED ON DATA FROM INTERNATIONAL CRITICAL TABLES

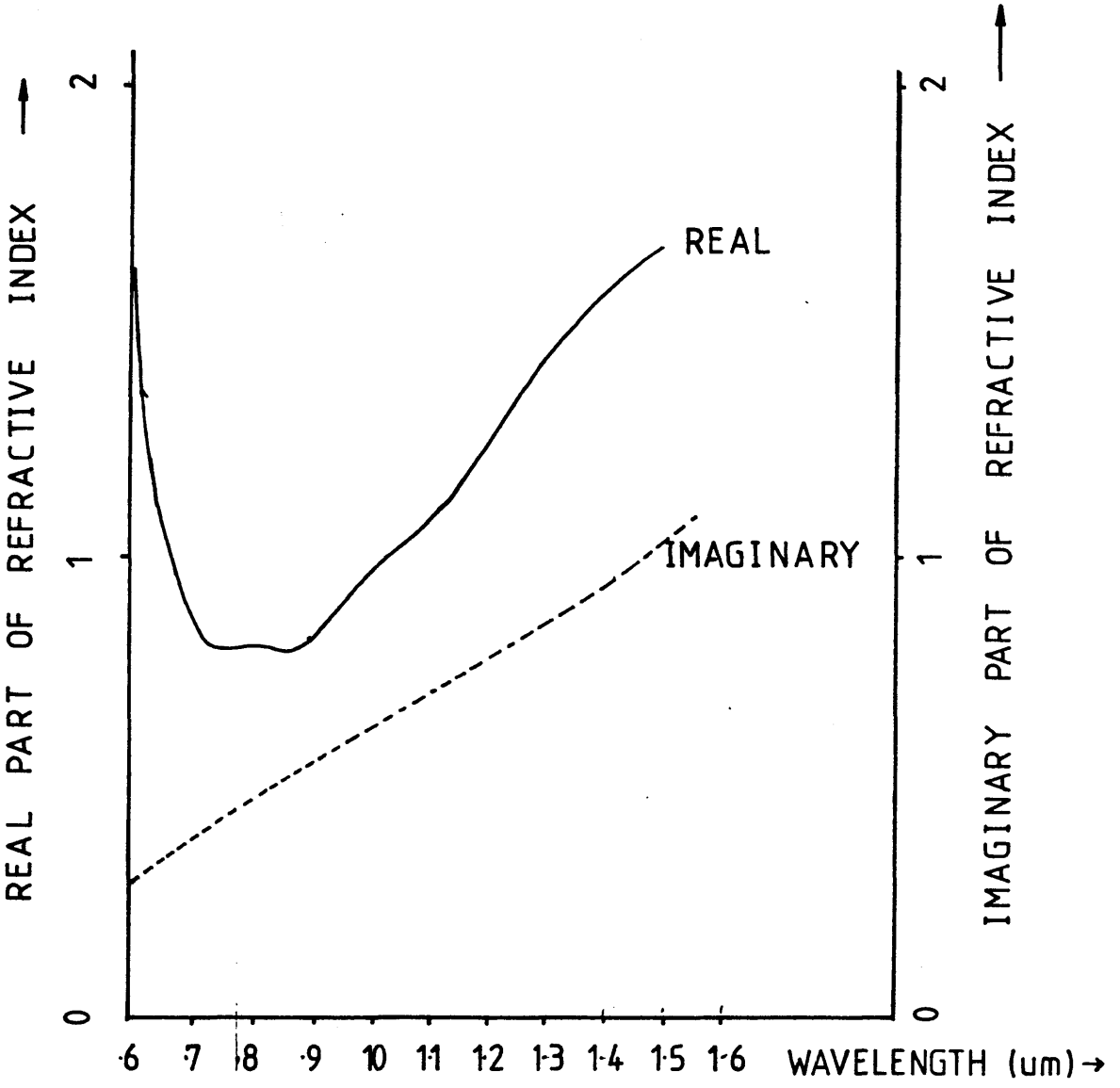

FIG 15 INTERPOLANTS USED FOR REAL AND IMAGINARY PARTS OF REFRACTIVE INDEX OF GOLD. DATA TAKEN FROM WEAVER.

References

3.1 Alferness,R.C, Buhl,L.L, Korotky,S.K, "Ti:$LiNbO_3$ Guided Wave Devices for Long-Wavelength Telecommunications", Florida

3.2 Alferness,R.C, "Guided Wave Devices for Optical Communication", I.E.E.E. Journal of Quantum Electronics, Vol QE-17, No 6, 1981 pp946-959

3.3 Hecht,E, Zajac,J "Optics", Addison Wesley, 1979

3.4 Bristow,J.P.G, Nutt,A.C.G, Laybourn,P.J.R, "Novel Integrated Optical Polarisers using Surface Plasma Waves and Ion Milled Grooves in Lithium Niobate", Electronics Letters, Vol 20, No 25/26, 1984 pp1047-1048

3.5 Bristow,J.P.G, "Integrated Optical Polarisers", Invited Paper, U.R.S.I. Colloquium, Royal Society, 12th July 1985

3.6 Wright,S, DeOliviera,A.D, Wilson,M.G.F, "Optical Waveguide Polariser with Synchronous Absorbtion", Electronics Letters, Vol 15, No 17, 1979 pp510-512

3.7 Marcuse,D, "Optimal Electrode Design for Integrated Optics Modulators", I.E.E.E. Journal of Quantum Electronics, Vol 18, No 3, pp393, 1982

3.8 Kogelnik, "Theory of Dielectric Waveguides", in Tamir, Integrated Optics Publisher/Date

3.9 Rashleigh,S.C, "Positive Permittivity Metal Cladding: its Effect on the Modes of Dielectric Optical Waveguides", Applied Optics, Vol 15, No 11, 1976 pp2804-2811a

3.10 Marcatili,E, Bell System Technical Journal, 1969 pp2072-2102

3.11 Takano,T, Hamasaki,J, "Propagating Modes of a Metal-Clad-Dielectric-Slab Waveguide for Integrated Optics", I.E.E.E.

Journal of Quantum Electronics, Vol QE-8, No 2, 1972, pp206-212

3.12 Yeh,C, Ha,K, Dong,S.B, Brown,W.P, "Single Mode Optical Waveguides", Applied Optics, Vol 18, No 10, 1979 pp1490-1504

3.13 Snitzer,E, "Cylindrical Dielectric Waveguide Modes", Journal of the Optical Society of America, Vol 51, pp491, 1961

3.14 Yeh,C, "Elliptical Dielectric Waveguides", Journal of Applied Physics, Vol 33, pp3235, 1962

3.15 Yeh,C, Lindgren,G, "Computing the Propagation Characteristics of Radially Stratified Fibres-An Efficient Method", Applied Optics, Vol 16, pp483, 1977

3.16 Goell,J.E. "A Circular Harmonic Computer Analysis of Rectangular Dielectric Waveguides", Bell System Technical Journal, Sept 1969 pp2133-2160

3.17 Riviere,L, Yi-Yan,A, Carru,H, "Properties of Single-Mode Optical Planar Waveguides with Gaussian Index Profile", Jornal of Lightwave Technology, Vol LT-3, No 2, 1985 pp368-377

3.18 Thyagarajan,K, Borbin,Y, Enard,A, Vatoux,S, Papuchon,M, "Experimental Demonstration of TM Mode Attenuation Resonance in Planar Metal-Clad Optical Waveguides", Optics Letters, Vol 10, No 6, 1985 pp288-290

3.19 Polky,J.N, Mitchell,G.L, "Metal-Clad Planar Dielectric Waveguide for Integrated Optics", Journal of the Optical Society of America, Vol 64, No 3, 1974 pp274-279

3.20 Rashleigh,S.C, "Four Layer Metal-Clad Thin Film Optical Waveguides",Optical and Quantum Electronics, 1976, pp49-60

3.21 Reisinger,A, "Characteristics of Optical Guided Modes in Lossy Waveguides", Applied Optics, Vol 12, No 5, 1973 pp1015-1025

Journal of Quantum Electronics, Vol QE-8, No 2, 1972, pp206-212

3.12 Yeh,C, Ha,K, Dong,S.B, Brown,W.P, "Single Mode Optical Waveguides", Applied Optics, Vol 18, No 10, 1979 pp1490-1504

3.13 Snitzer,E, "Cylindrical Dielectric Waveguide Modes", Journal of the Optical Society of America, Vol 51, pp491, 1961

3.14 Yeh,C, "Elliptical Dielectric Waveguides", Journal of Applied Physics, Vol 33, pp3235, 1962

3.15 Yeh,C, Lindgren,G, "Computing the Propagation Characteristics of Radially Stratified Fibres-An Efficient Method", Applied Optics, Vol 16, pp483, 1977

3.16 Goell,J.E. "A Circular Harmonic Computer Analysis of Rectangular Dielectric Waveguides", Bell System Technical Journal, Sept 1969 pp2133-2160

3.17 Riviere,L, Yi-Yan,A, Carru,H, "Properties of Single-Mode Optical Planar Waveguides with Gaussian Index Profile", Jornal of Lightwave Technology, Vol LT-3, No 2, 1985 pp368-377

3.18 Thyagarajan,K, Borbin,Y, Enard,A, Vatoux,S, Papuchon,M, "Experimental Demonstration of TM Mode Attenuation Resonance in Planar Metal-Clad Optical Waveguides", Optics Letters, Vol 10, No 6, 1985 pp288-290

3.19 Polky,J.N, Mitchell,G.L, "Metal-Clad Planar Dielectric Waveguide for Integrated Optics", Journal of the Optical Society of America, Vol 64, No 3, 1974 pp274-279

3.20 Rashleigh,S.C, "Four Layer Metal-Clad Thin Film Optical Waveguides",Optical and Quantum Electronics, 1976, pp49-60

3.21 Reisinger,A, "Characteristics of Optical Guided Modes in Lossy Waveguides", Applied Optics, Vol 12, No 5, 1973 pp1015-1025

3.22 Findlaky,T, Chen,C.L, "Diffused Optical Waveguides with Exponential Profile: Effects of Metal-Clad and Dielectric Overlay", Applied Optics, Vol 17, No 3, 1978 pp469-474

3.23 Oliner,A.A, Peng,S.T, "Effects of Metal Overlays on 3-D Optical Waveguides", Applied Optics, Vol 17, No 18, 1978 pp2866-2867

3.24 Nosu,K, Hamasaki,J, "The Influence of the Longitudinal Plasma Wave on the Propagation Characteristices of a Metal-Clad-Dielectric Slab Waveguide", I.E.E.E. Journal of Quantum Electronics, Vol QE-12, No 12, 1976 pp745-748

3.25 Weaver,J.H, Krafka,C, Lynch,D.W, Koch,E.E, "Optical Properties of Metals", Physics Data, Nr 18-12, Fach-Informations Zentrum, ISSN 0344-8401, 1981

3.26 Garmire,E.M, "Propagation Losses in Metal-Film-Substrate Optical Waveguides", I.E.E.E. Journal of Quantum Electronics, Vol QE-8, No 10, 1972 pp763-766

3.27 Suematsu Y et al. "Fundamental Transverse Electric Field (TE_0) Mode Selection for Thin Film Assymmetric Light Guides", Applied Physics Letters, Vol21, No6, sept 1972 pp291-293

3.28 Burke,J.J, "Propagation Constants of Resonant Waves on Homogeneous Isotropic Slab Waveguides", Applied Optics,Vol9,Noll,Nov 1970 pp2444-2452

3.29 Masuda, M "Propagation Losses of Guided Modes in an Opical Graded Index Slab Waveguide with Metal Cladding", I.E.E.E. Transactiuons on Microwave Theory and Technique, Vol MTT-25 No9 Sept 1977 pp773-776

3.30 Masuda, M, Koyasma,J, "Effects of a buffer Layer on TM modes in a Metal-Clad Optical Waveguide using Ti-diffused $LiNbO_3$ C-Plate", Applied Optics, Vol 16, No 11, pp2994-3000, 1977

3.31 Otto, A "Excitation of Nonradiative Surface Plasma Waves in Silver by the Method of Frustrated Total Reflection", Zeitschrift fur Physik, Vol 216, pp398-410, 1968

3.32 Barlow,H.M, Karbowiak,A.E, "An Incestigation of the Characteristics of Cylindrical Surface Waves", Proceedings of the Institution of Electrical Engineers, Vol 100, Part III, No 68, 1953, pp321-347 (including comments and reply)

3.33 Stern,E.A, Ferrel,R.A, "Surface Plasma Oscillations of a Degenerate Electron Gas", Physical Review, Vol 120, No 1 pp130-136, 1960

3.34 Otto, A, "Excitation by Light of w_+ and w_- Surface Plasma Waves in Thin Metal Layers", Zeitschrift fur Physik, Vol 219, pp227-223, 1969

3.35 Otto,A "Streustrahlung von Silber durch Anregung von Oberflachenplasmaschwingungen", Zeitschrift fur Physik, Vol 224, pp65-73, 1969 (In German)

3.36 Burker,U, Steinmann,W, "Strahlung von Oberflachenplasmonen in Aluminium", Zeitscrift fur Physik, Vol 224, pp179-189, 1969

3.37 Stegeman,G.I, Burke,J.J, Hall,D.G., "Surface Polaritonlike Waves Guided by Thin Lossy Metal Films", Optics Letters, Vol 8, No 7, 1983 pp383-385

3.38 Sarid,D, "Long-Range Surface Plasma Waves on Very Thin Metal Films", Physical Review Letters, Vol 47, No 26, pp1927-1934, 1981

3.39 Sarid,D, Deck,R.T, Craig,A.E, Hickernell,R.K, Jameson,R.S, Fasano,J.J, "Optical Field Enhancement by Long-Range Surface Plasma Waves", Applied Optics, Vol 21, No 22, pp3993-3995, 1982

3.40 Deck,R.T, Sarid,D, "Enhancement of Second-Harmonic Generation by Coupling to Long Range Surface Plasmons", Jornal of the Optical Society of America, Vol 72, No 12, pp1613-1617

3.41 Sarid,D, Deck,R.T, Fasano,J.J, "Enhanced Nonlinearity of the Propagation Constant of a Long-Range Surface Plasma Wave", Journal of the Optical Society of America, Vol 72, No 10, pp1345-1347, 1982

4.42 Craig,A.E, Olson,G.A, Sarid,D, "Experimental Observation of the Long-Range Surface-Plasmon Polariton", Optics Letters, Vol 8, No 7, pp380-382, 1983

4.43 Quail,J.C, Rako,J.G, Simon,H.J, "Long Range Surface Plasmon Modes in Silver and Aluminium Films", Optics Letters, Vol 8, No 7, 1983 pp377-379

3.44 Anderson,L.M, "Harnessing Surface Plasmons for Solar Energy Conversion", Integrated Optics III, Arlington, Virginia, April 5-6, 1983, SPIE Vol 408

3.45 Zavada,J.M, Fasano,J.J, "Strong Absorption of Light by Multilayer Dielectric-Metal Structures", ibid.

3.46 Sarid,D, "Enhanced Magnetic Interaction of Surface-Magnetoplasmon Polaritons", I.E.E.E Journal of Quantum Electronics, Vol QE-20, No 8, 1984 pp943-948

3.47 Seymour,R.J, Stegeman,G.I, "Use of Overcoated Surface Plasmon Components in the Far Infrared and Submillimeter", Integrated Optics III, Arlington, Virginia, April 5-6, 1983

3.48 Yamamoto,Y, Kamiya,T, Yanai,H, "Characteristics of Optical Guided Modes in Multilayer Metal-Clad Planar Optical Guide with Low-Index Buffer Layer", I.E.E.E. Journal of Quantum Electronics, Vol QE-11, No 9, 1975 pp729-736

3.49 NAG Library Document, S.E.R.C. Rutherford Appleton Laboratory

3.50 Rauber,A, "Chemistry and Physics of Lithium Niobate", Curent

Topics in Materials Science, F.Kaldis ed, 1978

Chapter 4 Practical TE polarisers using dielectric/metal overlay layers

4.1 Introduction

As was discussed in chapter 1, certain integrated optical implementations of processing systems for optical fibre sensors require the fabrication of high extinction ratio polarisers, or mode filters, a figure of 60dB for a device being regarded as acceptable for most applications.

In chapter 3 the theory of TE mode selection in slab waveguides with "step" indices was discussed. From this study, the phenomenon of surface plasma wave attenuation resonance in such a system may be understood. While the extinction ratios of devices fabricated according to such a model would be high, with low insertion losses for the TE mode, it would not be possible to construct the device using titanium indiffusion in lithium niobate owing to the resultant graded index profile of the slab guide (ref 1). In addition, slab guides are not suitable for efficient interfacing with optical fibres. Thus stripe guides (ref 1) must be used, and either the TE-like or TM-like mode selected.

Several workers (refs. 1,2,3,4,5,6,7,8,9) have used dielectric/metal coatings on both optical fibres and integrated optical waveguides, demonstrating TM mode attenuation resonance in both cases. In ref 8 the phenomenon was demonstrated using tapered buffer layers on lithium niobate and a drop of mercury as the metal. This would obviously not be acceptable in practical situations. Bristow (ref 3) reported a a device fabricated to transmit TE modes, yielding an extinction ratio of 22 ± 3 dB per cm with an excess loss of 2.5 ± 3dB/cm. Cytroky (ref 5) reported high theoretical extinction ratios using a slab model, and demonstrated practical slab guides with ratios of up to 40.4dB. The device consisted of Ti:$LiNbO_3$ waveguides with dielectric (n=1.7, material unstated)/ gold overlays. For stripe guides

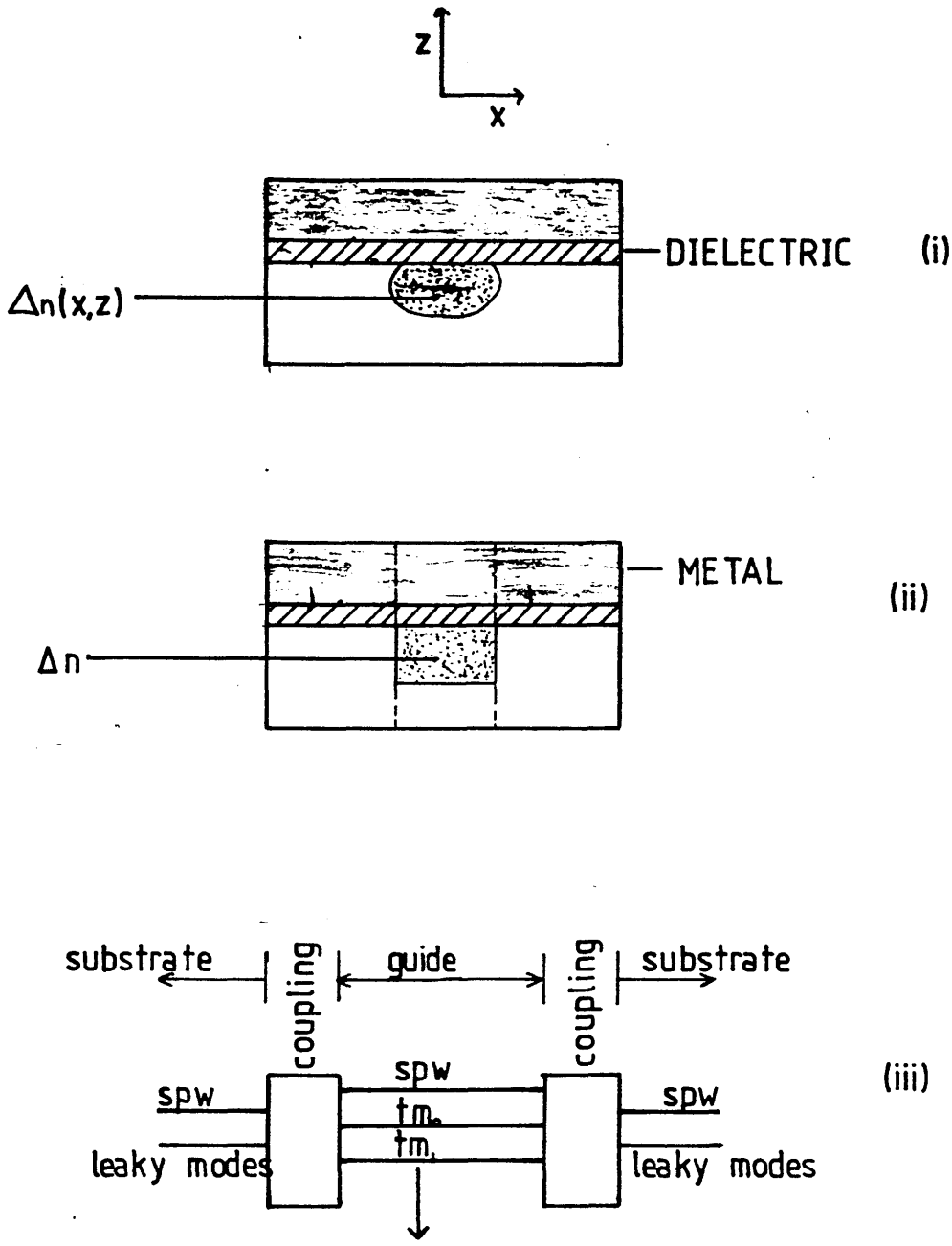

FIG 1 (i) DIELECTRIC/METAL OVERLAY STRIPE WAVE-GUIDE POLARISERS (ii) MODEL OF SYSTEM USED FOR EQUIVALENT REFRACTIVE INDEX METHOD OF CALCULATION OF WAVEGUIDE PROPERTIES. (iii) ILLUSTRATING COUPLING BETWEEN MODES OF THE THREE DISCRETE SECTIONS.

(width unspecified) the maximum value reported was 23dB, measured using end-fire excitation. Neither experimental error nor values for the insertion loss of the TE-like modes were quoted. Subsequent private communication revealed that excess loss values for slab were 0.5±0.5dB for gold claddings, the figure increasing to 5.5±0.5dB for silver claddings, also claiming that comparable measurements were determined for the stripe case. The same author reported an intrinsic de-polarisation of the unclad guides of 13-25dB per 15mm of guide using 70-100nm Ti diffused for 5 hours (conditions unspecified)

Eberhart and Bulow (ref 9) reported an extinction ratio of 100dB for a device using a planar geometry, although the latter was a scaled measurement, the value obtained presumably being only 10dB for the 1mm device fabricated. As was shown in chapter 2 such extrapolation is not necessarily valid. In addition, since the extinction ratio is a sensitive function of buffer thickness, problems of uniformities of coatings provide an experimental objection to such extrapolations.

Hosaka (ref 7) has investigated experimentally the variation in extinction ratio with cladding thickness of an optical fibre anisotropically etched to leave a flat face some distance from the core, this being coated with aluminium. The effect of this is to set up a 4 layer system with the waveguide core displaced from the metal layer by a low index buffer.

4.2 Theory

In order to design a polariser of optimal performance, it would be helpful to have a theoretical model of the device. A schematic diagram of the polariser to be designed is shown in figure 1. The buffer layer and metal overlay are deposited on a previously fabricated titanium indiffused waveguide. The aim of this procedure is to couple the guided TM modes of the unclad waveguide to the lossy surface plasma wave which may be excited at the dielectric-metal boundary, while disturbing the TE modes as little as possible. This prediction is based on the results of

the slab model of chapter 3.

Modifications to the slab model would be required to model this device. Factors to be taken into account include:

(i) The confinement of light in two, rather than one, dimensions

(ii) The graded index of the waveguide resulting from the titanium indiffusion, rather than a step index.

(iii) Possible absorption in dielectrics fabricated under real conditions.

(iv) Variation of metal index with deposition conditions

(v) Possible outdiffused layers of Li_2O on the crystal surface (ref 10)

(vi) Surface roughness at waveguide edges, and at the buffer-waveguide boundary.

(vii) The resultant non-linearly polarised waveguide modes

(viii) Power dependent effects, due either to non-linearities or to photorefractive effects. Consideration of (i) shows that ALL TM modes are expected to couple with the SPW and hence exhibit attenuation peaks. A simple argument explaining this phenemenon was proposed by Oliner and Peng (ref 11) . It is known that the SPW may propagate for all buffer thicknesses: variation of other waveguide parameters will only serve to vary the strength of the coupling of the various modes to the SPW. The system, shown in fig 1.(ii) may be modelled by the equivalent refractive index approach provided only one mode propagates in each section. However, the junction between the two sections will serve to couple any mode on one side of the boundary to the modes supported on the other. The surface plasma wave may be supported for all three sections, its properties being determined by the buffer/waveguide structure. The coupling regions shown in figure 1(iii) serve to couple any one mode of one section with all modes of the adjacent section, their relative coupling strengths being undefined. Thus all modes of the stripe guide section are expected to couple to the SPW of the adjacent sections. In addition, the propagation properties of the waveguide section, if

this in isolation is assumed to be infinite in extent, will also be affected by the SPW, as predicted in chapter 3.

4.2.1 Effect of thin metal films

It is known that if the metal bounding the dielectric is made sufficiently thin (typically some tens of nanometres) the SPW splits into two waves with symmetric and asymmetric field distributions (see chapter 3)-the w_- and w_+ waves respectively. These may be considered to be superpositions of the waves which would exist on the two boundaries in isolation. The antisymmetric distribution (long range SPW) was shown to have a lower loss than for the SPW existing at the bulk metal-dielectric interface, while the symmetric w_- mode (short-range SPW) has a higher loss.

In order to achieve a compact polariser with high extinction ratio it would be beneficial to excite the w_- SPW. This imposes stringent constraints on the theory which may be used and on the fabrication of the devices. The metal film must be (i) thin, (ii) uniform, ie no "islands", (iii) in the correct environment, ie the appropriate dielectric must exist on either side of the metal. The fabrication of a thin film of metal presents no problems from a practical standpoint: however, some surface roughness is inevitably incurred (ref 18), even for evaporation onto a smooth substrate. The deposition of a dielectric, identical to that of the buffer layer, on the metal would appear to ensure the correct environment for the short-range SPW. However, if the buffer is sufficiently thin, the SPW will be affected by the guide-buffer boundary. The properties of the metal and dielectric and those of the waveguide will determine the extent of coupling of the propagating modes to the SPWs. In experiments performed by other authors to demonstrate the existence of the modes (see chapter 2), it was found that the range of angles for which the relevant SPW is excited is extremely small (say 1^0). Thus we expect the manufacturing tolerances for a waveguide based device to be extremely narrow.

4.2.2 Analytical Methods

Exact solutions for the complex propagation constant are attainable only for the slab model of chapter 3. In other cases approximations are generally used to yield the desired information on the guided modes. Unfortunately these generally rely on the optical field being well confined to the core of the guide, and on the spatial variation of the optical field being a relatively simple function. For example, Goells' circular harmonic analysis (ref 13), which works well for a square core guide in an isotropic surrounding approximates the optical field by a series of Bessel functions and modified Bessel functions, each modified by a trigonometrical function of the angle around the waveguide core ("circular harmonics"). The method works well for waveguides with small relative refractive index differences and moderate aspect ratio. The effective index method implicitly ignores the optical field at the corners of the square guide. The method works well for dielectric waveguides far from cutoff. However, both methods may yield incorrect results for the TM like modes at the metal-buffer layer boundary where the field changes rapidly, and is far from the core.

A full treatment would require a finite element method (ref 15,16). This would consist of dividing the cross-section of the guide into a large number of small elements of shape consistent with the waveguide boundaries. In each element a simple (usually linear) function is fitted, the variational method being used to obtain a "best fit". For rapidly varying functions, a large number of elements is therefore needed. Unfortunately the method requires extremely large amounts of active computer memory, and in reported implementations requires large amounts of computer time for even reasonable accuracy (ref 15).

A variety of workers have condidered the problem of the graded index profile (ref 19), either using stripe guides with a range of different refractive index profiles, or in planar geometries with metal layers (with and without buffer layers).

Masuda (ref 19) predicts that for a graded index slab guide on Z-cut $LiNbO_3$ the optimum buffer thickness for SiO_2 would be 11nm. It is to be noted that no theoretical study has been published concerning stripe waveguides with metal claddings.

For lithium niobate at wavelengths longer than the limit of the visible spectrum, the imaginary component of the refractive index is negligible: thus problem (iii) will not be considered.

The variation of the optical properties of metals with deposition conditions (ref 18) presents a severe hindrance to the efficient design of metal clad devices. Using the data of Weaver (ref 18), it is possible to select data taken from metals fabricated under similar conditions to those to be used.

Suppression of outdiffusion is possible by a variety of experimental means (ref 20), using powdered lithium niobate or flowing wet gases in carefully controlled environments.

Surface roughness at waveguide edges is likely to have two deleterious effects on polariser performance. Firstly the perturbations will give rise to polarisation conversion (ref 30), and secondly to increased excess loss of the guide.

Photorefractive effects (ref 21) may be reduced by operation at successively long wavelengths. Holman (ref 22) has shown that propagation along the crystal Z axis gives a significant reduction of optical damage. However, this geometry will not necessarily be suitable for other components where the electrooptic effect is to be utilised.

4.2.1 Summary

It is seen that no exact solution for the propagation constant and the attenuation may be obtained for the stripe geometry. All approximate methods have some disadvantage in the context of this device, whether in terms of accuracy or computation time. It was therefore decided to use the information on buffer and metal layers obtained from the slab model to fabricate a device. Using this data as an initial estimate of the relevant parameter, it could then be varied to optimise the

performance of the polariser. This procedure has also been adopted by Cytroky (ref 5) and Eberhart (ref 9).

4.3 Device fabrication

4.3.1 Material selection

Since it was desired to select the TE-like modes of a titanium indiffused stripe waveguide, a set of stripe waveguides were fabricated on Z-cut $LiNbO_3$. The basic waveguides were fabricated using standard techniques: these have been described in section 2.5.2. In order to investigate any change in extinction ratio and insertion loss with waveguide width, a series of waveguides were fabricated on each substrate. Eight guides with widths from 2 to 10 microns were used. Three of these sets were fabricated on each substrate in order to check the consistency of the results, and to allow for the inevitably unsuccesful fabrication of some guides. The guides were separated by, on average, 20 waveguide widths, thus coupling between adjacent guides would not be appreciable (ref 14).

In order to obtain as high an extinction ratio as possible the slab model of chapter 3 predicts that the buffer layer material should have a high refractive index (ideally around 2.0). A large number of dielectrics are available with refractive index between 1.5 and 2.5, however the buffer should be easy to deposit in thin uniform films. Silicon dioxide having refractive index 1.46 may easily be sputtered (ref 19), or deposited in plasmas containing silane and nitrous oxide. However, silicon monoxide was known to have the required properties of a higher refractive index and rather simpler depostion requirements. An excellent paper by Hass (ref 17) discusses the optical properties of thin films of silicon monoxide prepared by thermal evaporation under a range of conditions. The variation of refractive index with wavelength is illustrated in figure 2, this being taken from ref 17. It is noted from this reference that to prepare suitable films it is necessary:

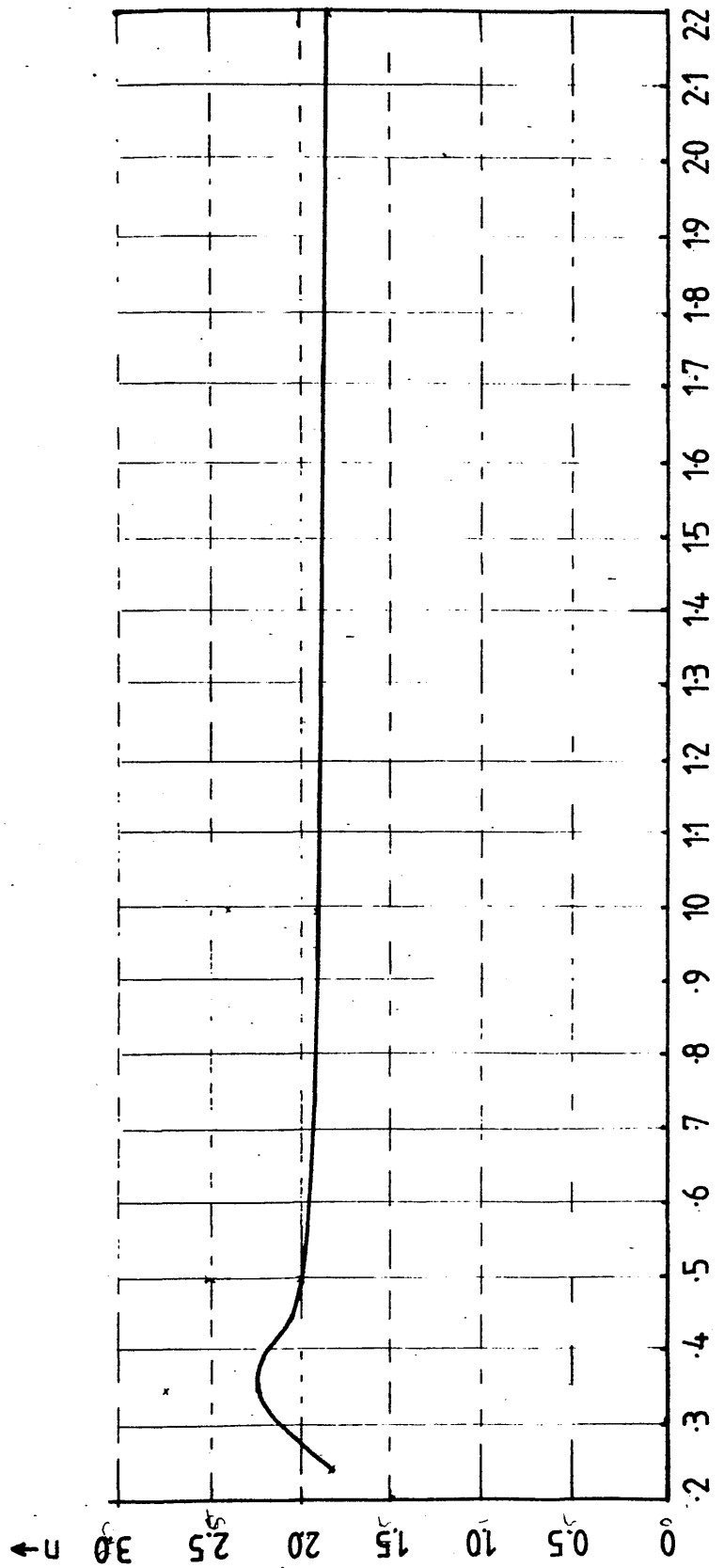

FIG 2 VARIATION OF REAL PART OF REFRACTIVE INDEX OF SILICON MONOXIDE WITH WAVELENGTH (AFTER HASS)

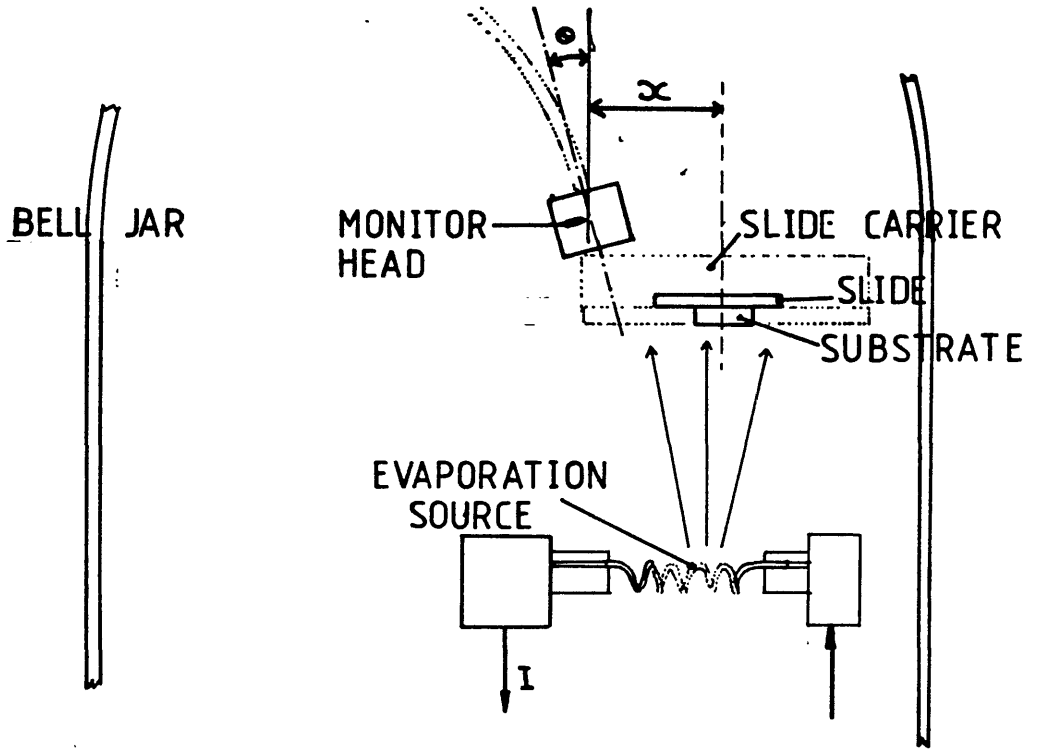

FIG 3(i) ILLUSTRATING TWO POSSIBLE SOURCES OF ERROR IN MONITORING OPTICAL THICKNESSES: (i) ANGULAR MISALIGNMENT θ AND (ii) LATERAL SEPARATION OF MONITOR HEAD AND SUBSTRATE x

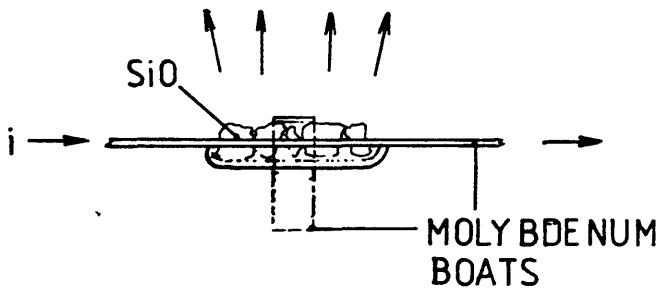

FIG 3(ii) ILLUSTRATING THE MODIFICATION OF THE SOURCE USED FOR THERMAL EVAPORATION OF SILICON MONOXIDE AVOIDING "SPITTING".

(i) to use high vacuum, approx 2x 10^{-6} mmHg
(ii) to use high evaporation rates, approximately 20Å/sec
(iii) to avoid exposing the completed films to air: at room temperature the top 20Å would oxidise to SiO_2 within a few hours (ref 17). Although data on complete oxidation are not available, the author's experiments indicate that the mechanical and physical properties of the monoxide do not change over a period of one year: thus films of SiO_2 may not be prepared by the method. It is not necessary to use heated substrates. The metal used was aluminium, as the slab model had predicted higher extinction ratios for this metal than for others considered. The optical properties of the metal were reasonably well known in the wavelength range of interest (ref 18). In addition, conditions for the evaporation of high quality films were well understood (ref 34).

4.2.2 Fabrication procedure

Titanium indiffused stripe waveguides were fabricated on Z cut lithium niobate as described in section 2.5.2 . The material was supplied by Barr and Stroud Ltd, and the propagation direction was in all cases along the crystal Y axis. The completed substrates incorporating titanium indiffused waveguides were then cleaned thoroughly as described in chapter 2 and mounted in a thermal evaporator. This machine had four separate evaporation sources available, any one of which could be selected at a given time. The bell jar of the evaporator was pumped down to a pressure of 10^{-6} mmHg. A current of 60Å was passed through the source containing the silicon monoxide granules with diameter approximately 1/2mm. The shielded source shown in figure 3.ii was used to prevent the heated granules "spitting". This phenomenon occurs when the surface of the granule is vaporised with the bulk of the substance remaining solid: the resultant force then displaces the silicon monoxide. The film thickness was monitored during deposition using a crystal film thickness monitor (Intellemetrics model IL001). Use of this monitor requires a

knowledge of the specific acoustic impedance and the density of the material. These were assumed to be 8.25×10^5 $gcm^{-2}s^{-1}$ and $2.2 g/cm^3$ respectively for silicon monoxide (ref 23) and $8.17 \times 10^5 gcm^{-2}s^{-1}$ and $2.2 g/cm^3$ for aluminium (ref 24). A film of thickness 25 nm could be evaporated in approximately thirty seconds, with thicker or thinner films taking proportionally more or less time. Having deposited the silicon monoxide, and allowed the evaporation source and sample to cool in order to avoid buiding thermal stresses into the sample and damaging the evaporation source respectively, an evaporation source containing aluminium was selected. A current of 30Å then gave an evaporation rate of approximately 10nm/sec. As thick (up to 1um) films were required, it was necessary to perform the evaporation in two stages using a further source. Only after all layers had been deposited and the substrate and deposition system allowed to cool was the system allowed to attain atmospheric pressure.

To obtain independent verification of the thickness and refractive index of the silicon monoxide, a separate evaporation was performed using identical process parameters, but on a silicon substrate. The index and thickness were then measured at 0.6328μm wavelength using ellipsometric techniques. (**note**- these measurements were performed by Dr. G. Stewart.) The thickness measured in this way gave the same result as the crystal thickness monitor to within 1% of the value recorded by the monitor. The refractive index was determined to be 1.98 ± 0.01 at 0.6328μm wavelength. This agrees well with the data of Hass shown in figure 2.

The entire process was repeated to yield further devices using different thicknesses of buffer layer. A wide range of devices was fabricated using aluminium for the metal overlay: the buffer thickness being varied from zero to 1μm, with the majority of the devices at the lower thicknesses where the slab model predicts higher extinction ratios and more rapidly varying attenuations.

Several devices were made using thin metal films, some of which were coated with silicon monoxide layers in order to attempt to make devices exhibiting coupling to the short-range SPW. The fabrication conditions in this case were indentical to those outlined above apart from the modification of the metal thickness and the addition of the extra layer.

The end-faces of the waveguides were polished normal to their length in order to measure their performance using end-fire excitation.

Mechanical considerations of the polishing process

During polishing it was noted that some samples, particularly those with thick buffer layers, exhibited a tendency for the aluminium to lift-off from the substrate when the sample was mounted on the polishing jig, this being accomplished using heated shellac: when allowed to solidify a strong bond is obtained between the glass carrier and the substrate. The arrangement is illustrated in figure 4. The sample may not be reversed on the mount as poor edge quality results. While the disintegration effect finds a ready explanation in terms of the differential coefficients of thermal expansion (ref 23), a cold mounting technique would require a prohibitively long removal time (several days) in dangerous solvents . In the few cases where the metal lifted off, the samples were re-coated. Results obtained with such devices will be presented separately from those obtained with ideal devices, as exposure to air may have adverse effects on the silicon monoxide film..

4.4 Determination of device performance

The measurement of the devices has been discussed in chapter 2. The experimental procedure used was as detailed for the proton exchanged devices described in that chapter. The waveguides were located and excited using the standard "rising sun" technique. The procedure must be optimised for metal clad guides (with or without buffer layers) in order to maximise the transmitted power for either TE- or TM- like modes. For a description of the

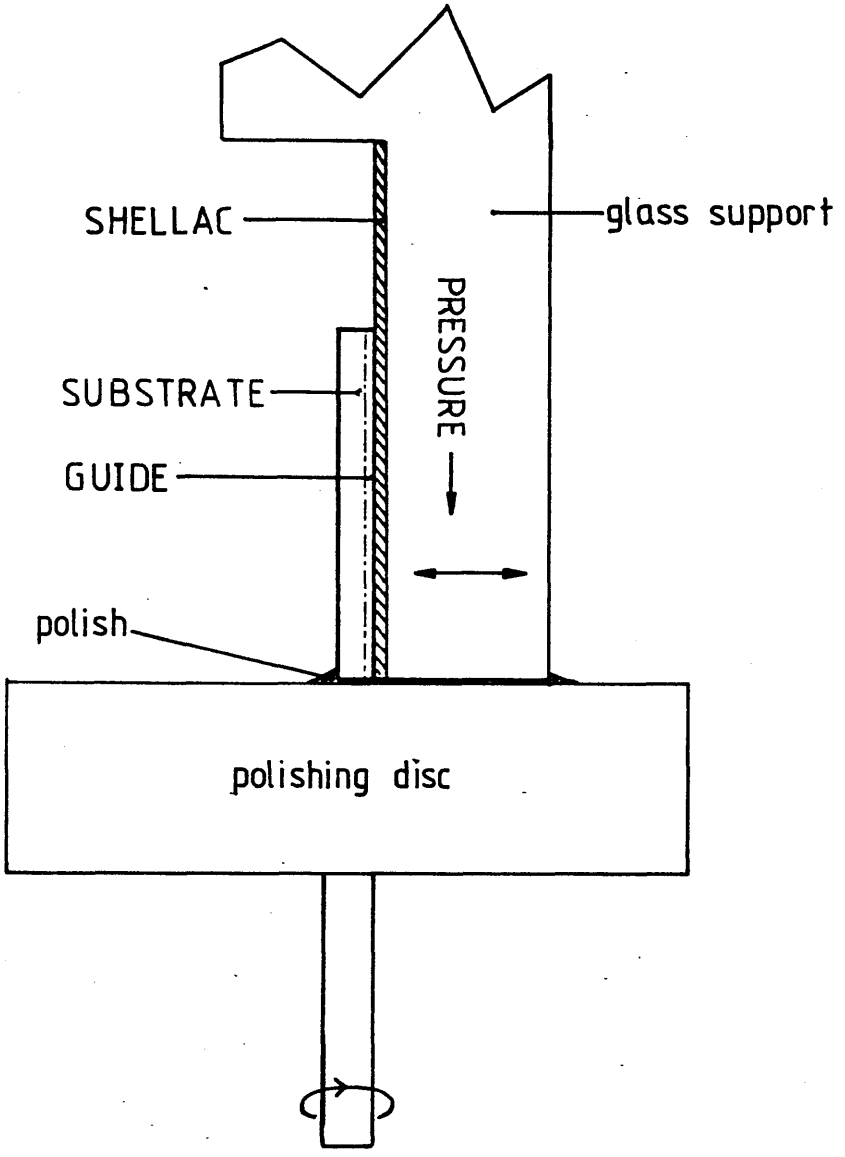

FIG 4 ILLUSTRATING THE METHOD USED FOR POLISHING LITHIUM NIOBATE FOR END-FIRE EXCITATION OF WAVEGUIDES.

conventional technique, the reader is referred to ref 25. In essence, the method consists of moving the substrate first horizontally and then vertically with respect to a focussed laser in order to excite the "rising sun" pattern. Subsequent motion, predominantly vertical, then optimises the transmitted power. For the metal-clad polarisers under investigation here however, it was noted that the transmitted power initially decreased with variation of substrate height, and then increased to a maximum value. The steps in alignment of such a polariser in end-fire coupling are shown in figure 5.

It was noted that the cross coupled field resulting from excitation of the transmitted mode resulted in a visible field profile when the gain of the **Hamamatsu** camera was suitably increased. For this reason, it was considered necessary to use a linear polariser at the output objective. However, the sensitivity of the **Photodyne** detector used was such that the off-diagonal elements of the Jones matrix could not be measured with an accuracy of greater than 10%: in practice considerations of alignment would worsen this figure.

Since some of the devices were measured to have extinction ratios greater than approximately 60dB, it was necessary to use method (iii) described in section 2.6.1, ie. to launch in with a linearly polarised laser and record the ouput in each case. To ensure consistency, the same method was then used for all measurements. The wavelength used was 1.15μm

4.5 Results

4.5.1 Errors

In presenting the results of these experiments, it is important to consider the error mechanisms involved and their effects. The errors in the thickness of the films of silicon monoxide and aluminium arise from two main sources:

(i) The horizontal distance between the crystal monitor head and the sample to be coated; the head may detect a different thickness from that deposited on the sample

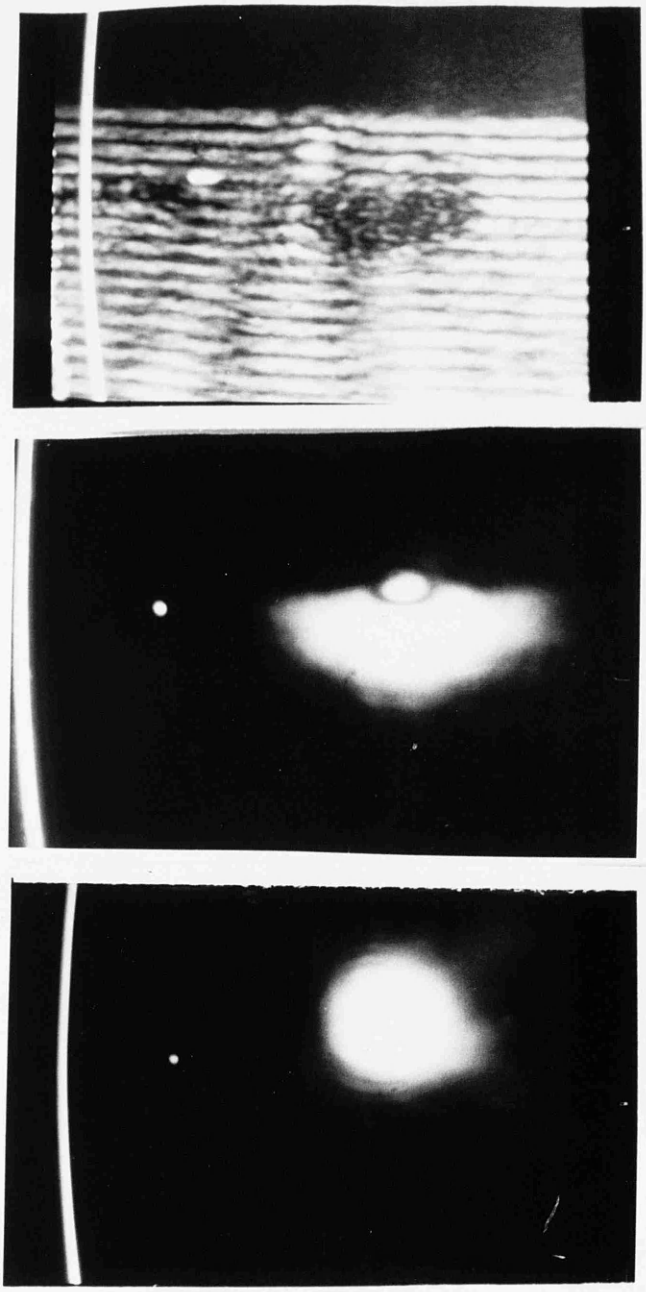

FIG 5 THREE STEPS IN END-FIRE EXCITATION OF SINGLE MODE POLARISERS: (i) "RISING SUN" PATTERN (ii) EXCITATION OF GUIDE WITH SOME ENERGY IN SUBSTRATE (iii) "CLEAN" EXCITATION

(ii) The crystal head may not be perpendicular to the line joining its centre to the centre of the source.

These error mechanisms are illustrated in figure 3.1. Allowing generous bounds for these errors, the error was approximately 1% of the recorded thickness. The recorded thickness correlates well with measurements obtained using ellipsometric techniques.

The error in the measured extinction ratio arose from several sources.

(i) The error in the **Photodyne** power meter (ref 26): for detected signals stronger than -80dBm, $\pm$1% of the reading **and** $\pm$1 in the least significant digit. For signals below this figure $\pm$1 in the least significant digit **and** 10% of the displayed power.

(ii) Correct spatial filtering of the near field profile: it is important to exclude from the measurement light guided by the substrate. Since the **positions** of the optical fields for TE- and TM like modes did not coincide, care must be taken to avoid obscuring part of either output field. The spatial filter was re-positioned between measurements.

(iii) Optimisation of the input power; Since the input polarisation was rotated by use of a half-wave plate, it is essential to ensure that the axis of this device is at 45^0 to that of the optical bench. In addition, the input beam may inadvertently be displaced laterally or vertically by the retarder. The input coupling must therefore be re-optimised between measurements. This process incurs errors, the magnitude of which was determined by successively exciting and determining the extinction ratio of a given waveguide.

For devices with high extinction ratio, where the detected power was below -80dBm, the dominant error mechanism was (i), typically $\pm$12dB-a large figure. For other measurements, consideration of the above mechanisms (ref 27), and realising that the errors apply to measurement of both modes, yields an error in the insertion loss of approximately $\pm$3dB, and in the extinction ratio of $\pm$4dB. The error bars in the presented results

are accordingly based on these estimates.

4.5.2 Qualitative results

For the TE-like mode, a clear field profile with no detectable substrate radiation was observed. The "rising sun" method with the modifications described was used to locate the waveguides.

The number of modes supported for the TE case was in all cases the same as for an unclad device. The addition of the silicon monoxide (but no aluminium) produced no detectable change in either extinction ratio or insertion loss within the bounds of experimental error ($\pm$3dB) for either TE or TM input polarisations. However, for some dielectric-metal clad devices supporting one TE-like mode the output with TM excitation displayed two main lobes, as shown in figure 6, indicating transmission of the TM_1 mode. This was not observed for the unclad device, nor for one with only aluminium cladding. Field profiles of TE and TM like modes for a device with a nominal width of 7μm are shown in figure 7. Note their relative positions-the output alignment had not been altered between photgraphs. The burn-mark on the camera tube may be used as a reference point. Figure 8 shows the field profile (TE) for a wider guide fabricated on the same substrate with identical conditions.

The input alignment for all metal clad polarisers appeared to be far more critical than for an unclad device, small adjustments giving large variations in output power.

Figure 9 illustrates the TE and TM mode profiles associated with a narrow guide- the nominal width being 3μm. Note that the camera gain was not constant throughout the experiments, considerable variation being required to display clearly the profile.

During the excitation of many guides, a "crescent" of transmitted light was observed immediately adjacent to the waveguide. This is shown in figure 10. The crescent exhibited the

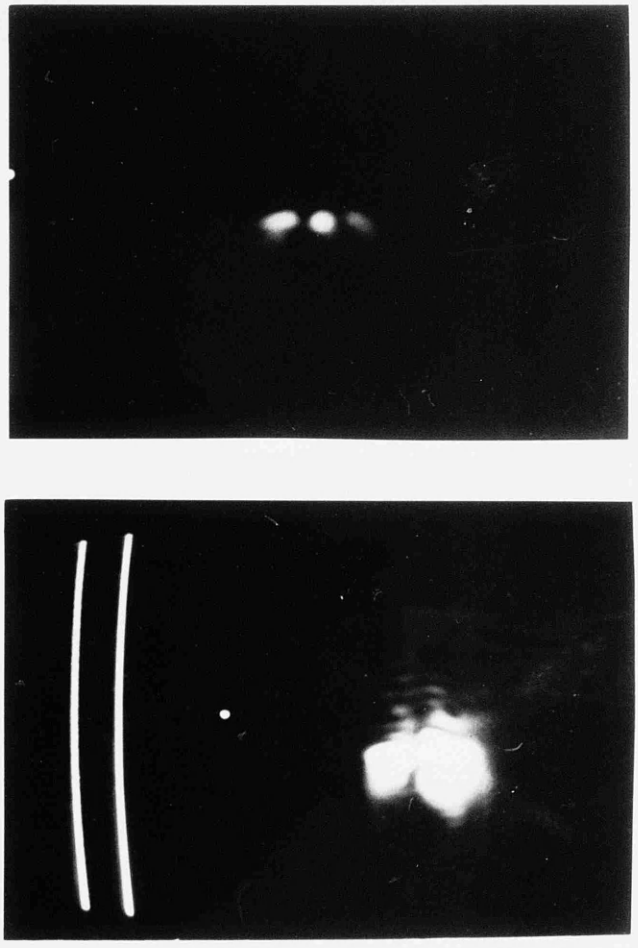

FIG 6 MULTIMODE EXCITATION OF 10μm STRIPE WAVEGUIDE POLARISERS (i) TM AND (ii) TE (NOTE: GAINS AND MAGNIFICATIONS DIFFER)

(i)

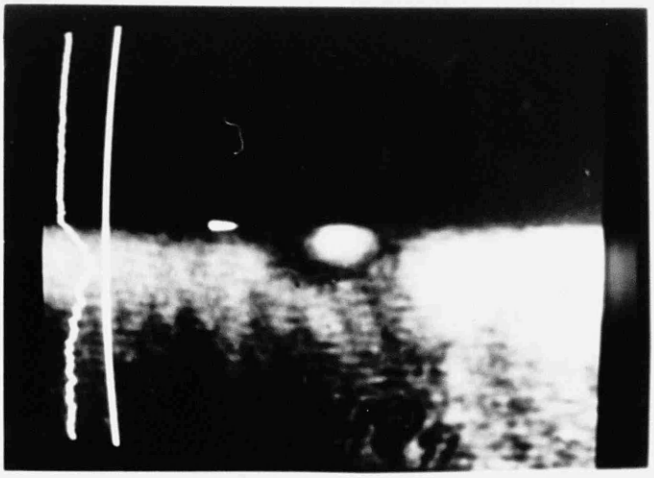

(ii)

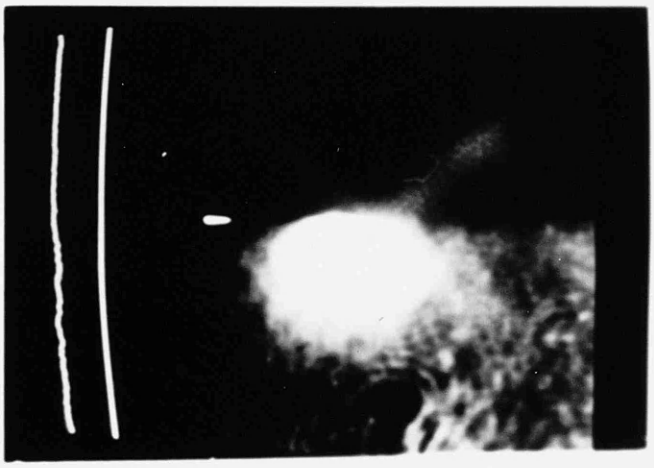

FIG 7 TYPICAL NEAR FIELD PROFILES ASSOCIATED WITH (i) TM AND (ii) TE MODES OF METAL CLAD STRIPE WAVEGUIDE POLARISERS

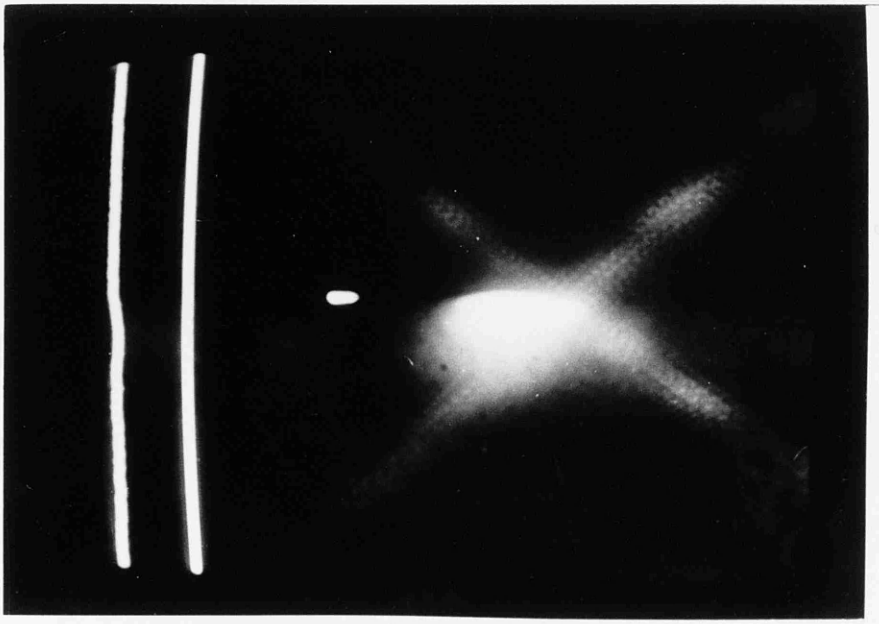

FIG 8 NEAR FIELD PROFILE FROM 9μm WIDE STRAIGHT STRIPE WAVEGUIDE POLARISERS (TE)

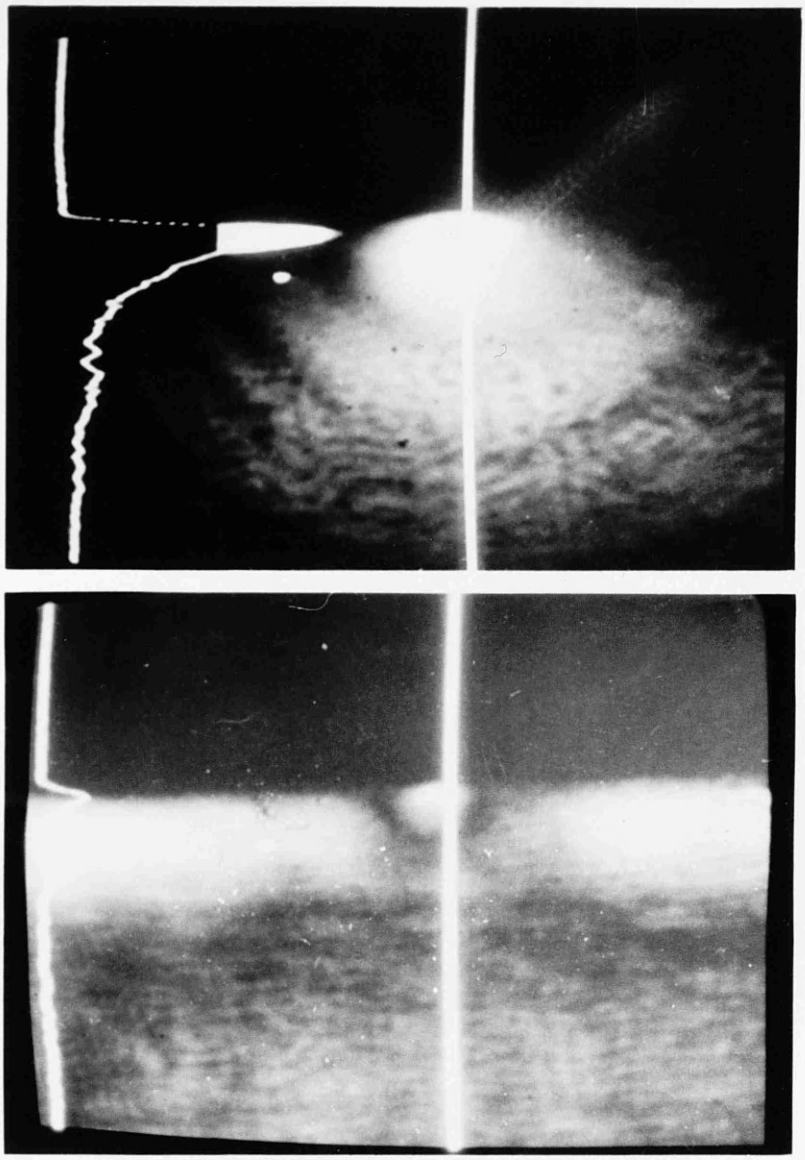

FIG 9 IMAGED NEAR FIELDS FROM 3um WIDE STRIPE WAVEGUIDE POLARISER : TOP- TE LIKE MODE AND TM-LIKE MODE (BOTTOM)

FIG 10 "CRESCENT" ASSOCIATED WITH END-FIRE EXCITATION OF 6um METAL-CLAD STRIPE WAVEGUIDE POLARISER

input coupling properties of a guided wave. Possible explanations for the effect will be considered at a later stage.

Careful input alignment ensured that in the majority of cases the crescent was not excited. However, in a few cases the crescent was inseparable. Such a situation is illustrated in figure 10, this being for a 6um guide.

Waveguides of the correct nominal width gave rise to highly symmetric mode profiles. A photograph of such a plot is shown in figure 11, this being for a 6μm guide.

The variation of experimentally determined extinction ratio and excess loss with buffer thickness for three different nominal guide widths is illustrated in figures 13 and 14. It is seen that for all three guides a principal peak of up to 85±13dB is seen at a buffer thickness of approximately 30nm, while a second peak at approximately double this thickness is also seen. The extinction ratio at the second peak is some 60±13dB down on that of the principal peak. It is to be emphasised that the results presented in this chapter refer to individual devices and are not "scaled".

The excess loss associated with two waveguide widths is shown as a function of buffer thickness in figure 14. Although the spread of results is large, it is seen that the excess loss decreases with increasing buffer thickness.

Figure 15 shows the variation in extinction ratio for three different buffer thicknesses. Two effects are noted. Firstly the position of maximum extinction ratio increases with decreasing buffer thickness, and secondly the extinction ratio at that peak increases.

4.5.3 Quantitative results

Devices were tested without cladding, and with silicon monoxide coatings (in thicknesses up to lum), again with no metal cladding. In neither case did the extinction ratio of any one guide exceed 3±4dB. The large fractional error in measurements of small extinction ratios makes deductions based on them difficult.

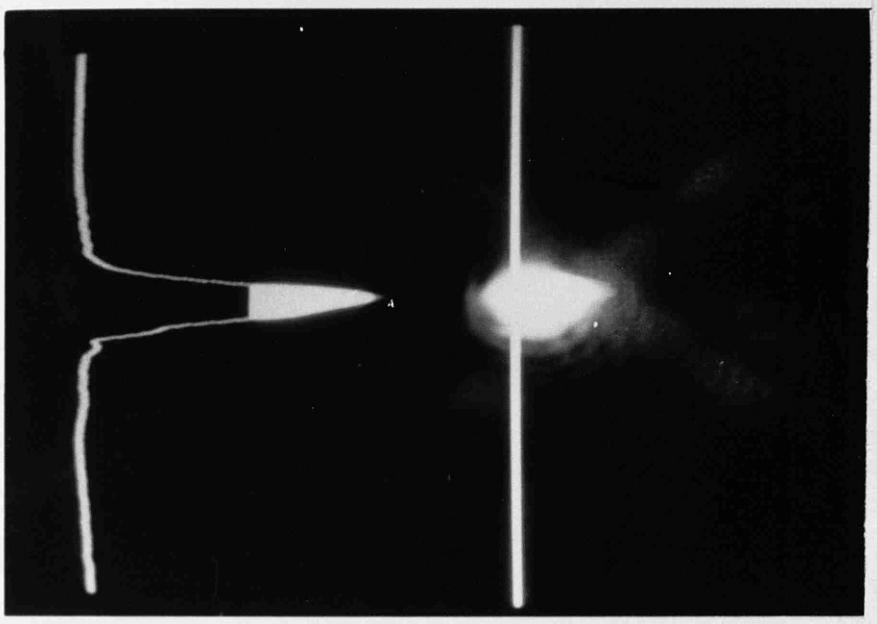

FIG 11 ILLUSTRATING AN INSEPERABLE CRESCENT ASSOCIATED WITH END-FIRE EXCITATION OF 5μm WIDE STRIPE WAVEGUIDE POLARISERS.

A graph showing the variation of extinction ratio for the best guide within each set against buffer thickness is shown in figure 16.

The extinction ratios measured ranged between 10 and 80dB, although the experimental error associated with the latter results is high. The optimum thickness of the buffer layer for the fabrication conditions used here was 28nm.

4.6 Discussion

Study of figures 13,14 and 15 shows distinct trends in all three graphs. Consideration of figure 15 shows that within each set of guides, there is one guide with a high extinction ratio, with narrower or wider guides having an inferior extinction ratio. In some cases the guide with the highest extinction ratio occurred at the start or end of the set (ie. at the 2μm or 10μm guide). In this case, the following or preceding guides exhibit decreasing extinction ratio.

Although our slab model can give no predictions concerning the effect of variations in waveguide width, qualitative predictions are possible. Each guide with different width will have a slightly different effective index, or, equivalently, propagation constant. The phase velocity of the surface plasma wave, the mechanism postulated to be responsible for the high TM-like mode loss, is determined by the (complex) permittivities of the aluminium and silicon monoxide under the given deposition conditions. Reference to chapter 3 shows that for a given buffer thickness, only one phase velocity of the light propagating in the waveguide below will give rise to optimal coupling between the modes. Phase velocities below or above this value should give reduced coupling and hence poorer extinction ratio. The existence of a peak in the extinction ratio-waveguide width indicates that the surface plasma wave is the loss mechanism. Simple absorption loss, considering the system to be a lossy dielectric, would be expected to yield a decreasing extinction ratio with waveguide width as the fraction of light present at the waveguide-metal

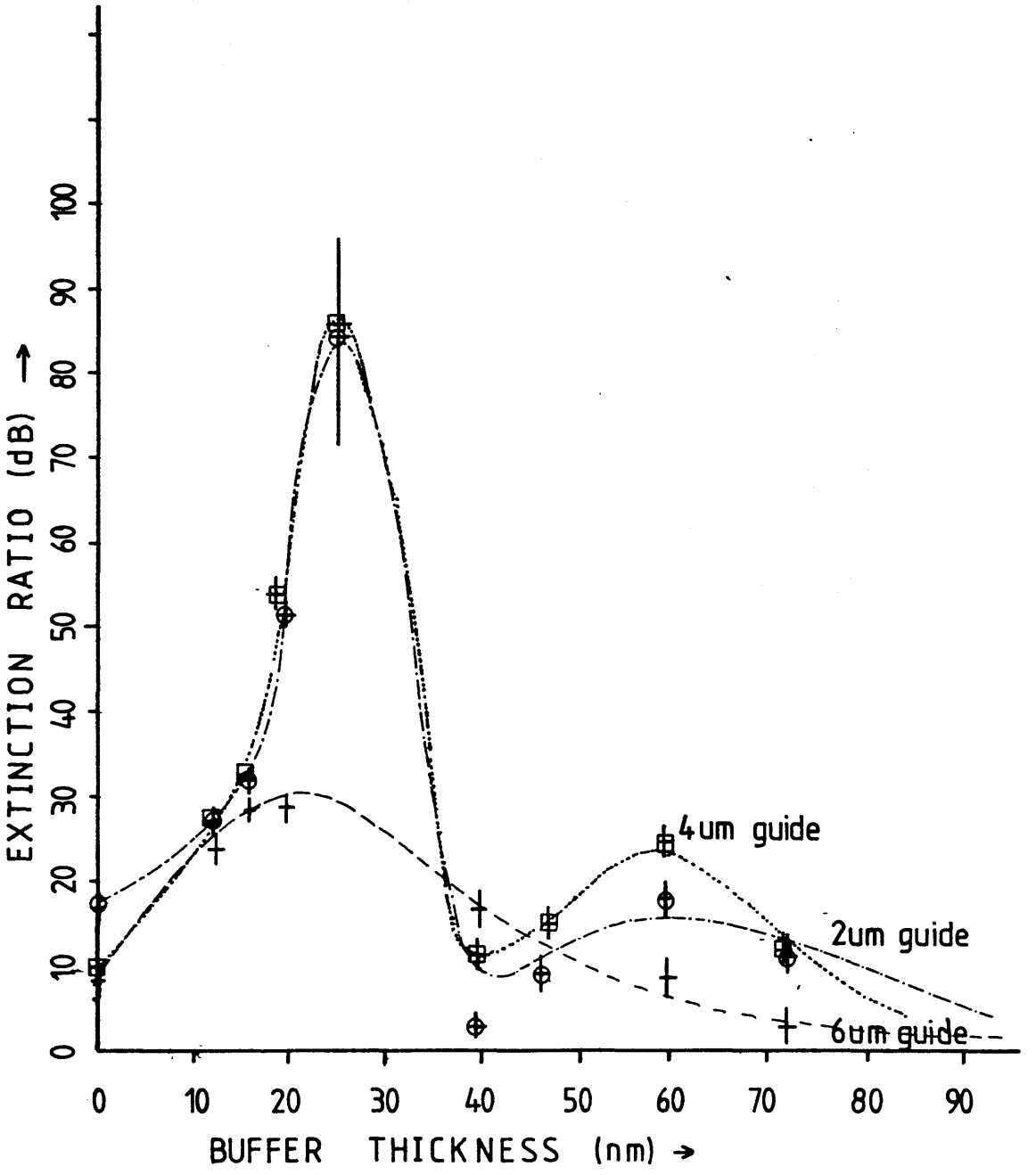

FIG 13 EXTINCTION RATIO (EXPERIMENTALLY DETERMINED) VS. THICKNESS OF SILICON MONOXIDE FOR DIELECTRIC/ALUMINIUM CLAD STRIPE WAVE-GUIDE POLARISERS. (ONLY THREE NOMINAL GUIDE WIDTHS ARE SHOWN FOR CLARITY)

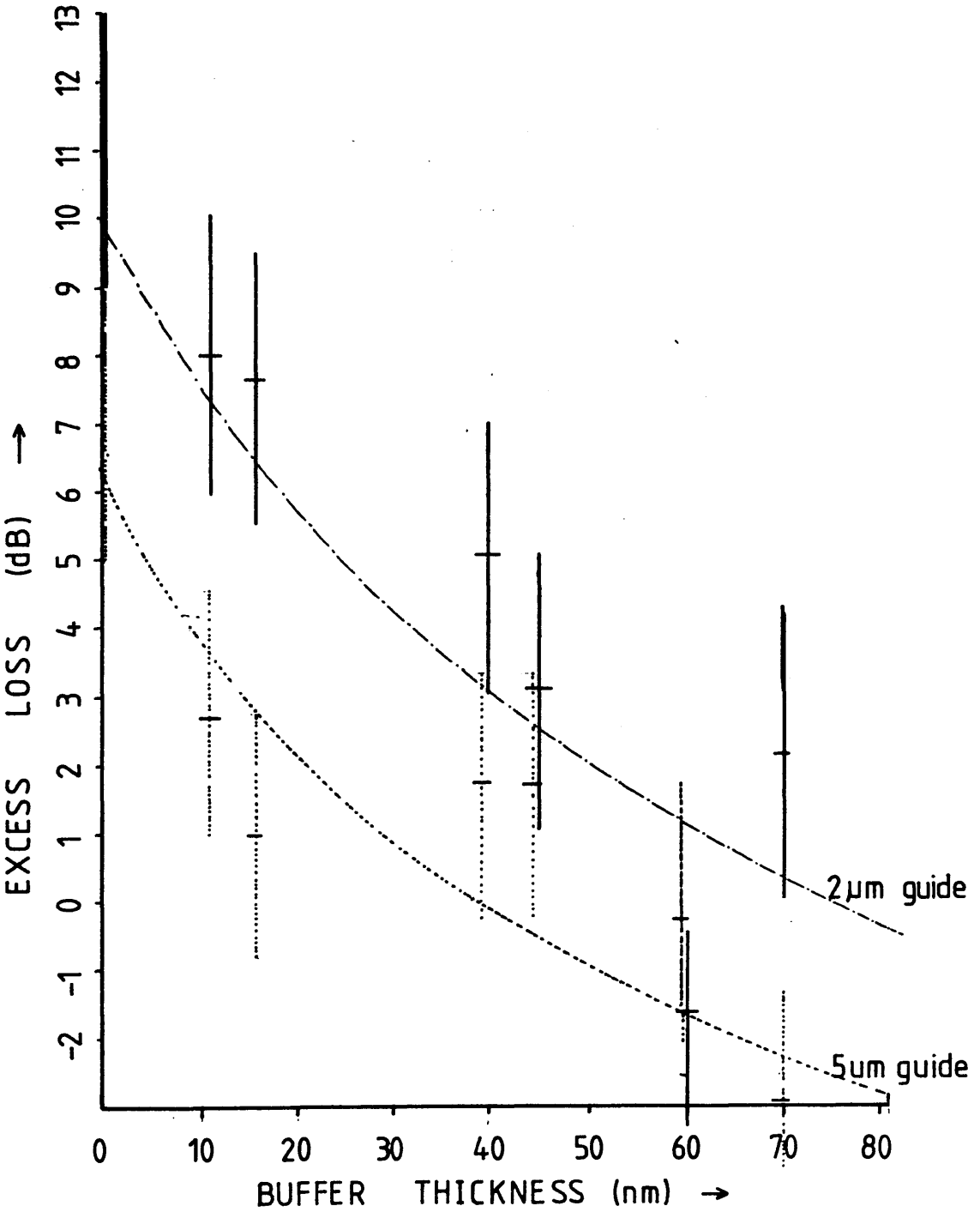

FIG 14 EXPERIMENTALLY DETERMINED EXCESS LOSS VS. THICKNESS OF SILICON MONOXIDE FOR DIELECTRIC ALUMINIUM CLAD STRIPE WAVEGUIDE POLARISER. WAVELENGTH = 1.15 MICRONS

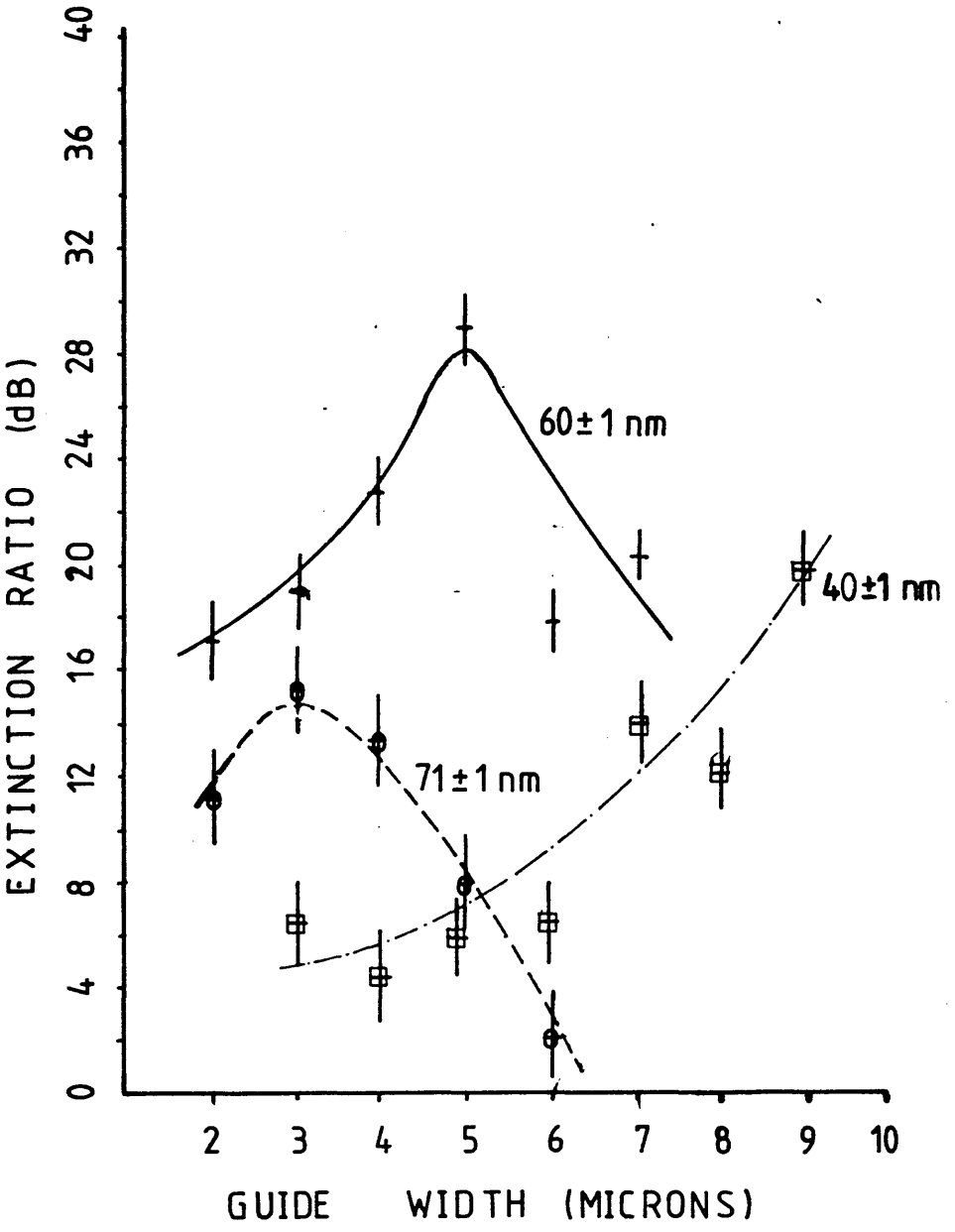

FIG 15 ILLUSTRATING THE VARIATION IN EXPERIMENTAL EXTINCTION RATIO WITH WAVEGUIDE WIDTH FOR SILICON MONOXIDE/ALUMINIUM CLAD STRIPE GUIDE POLARISERS. SEVERAL DIFFERENT BUFFER LAYER THICKNESSES ARE SHOWN, WAVELENGTH=1.15 MICRONS

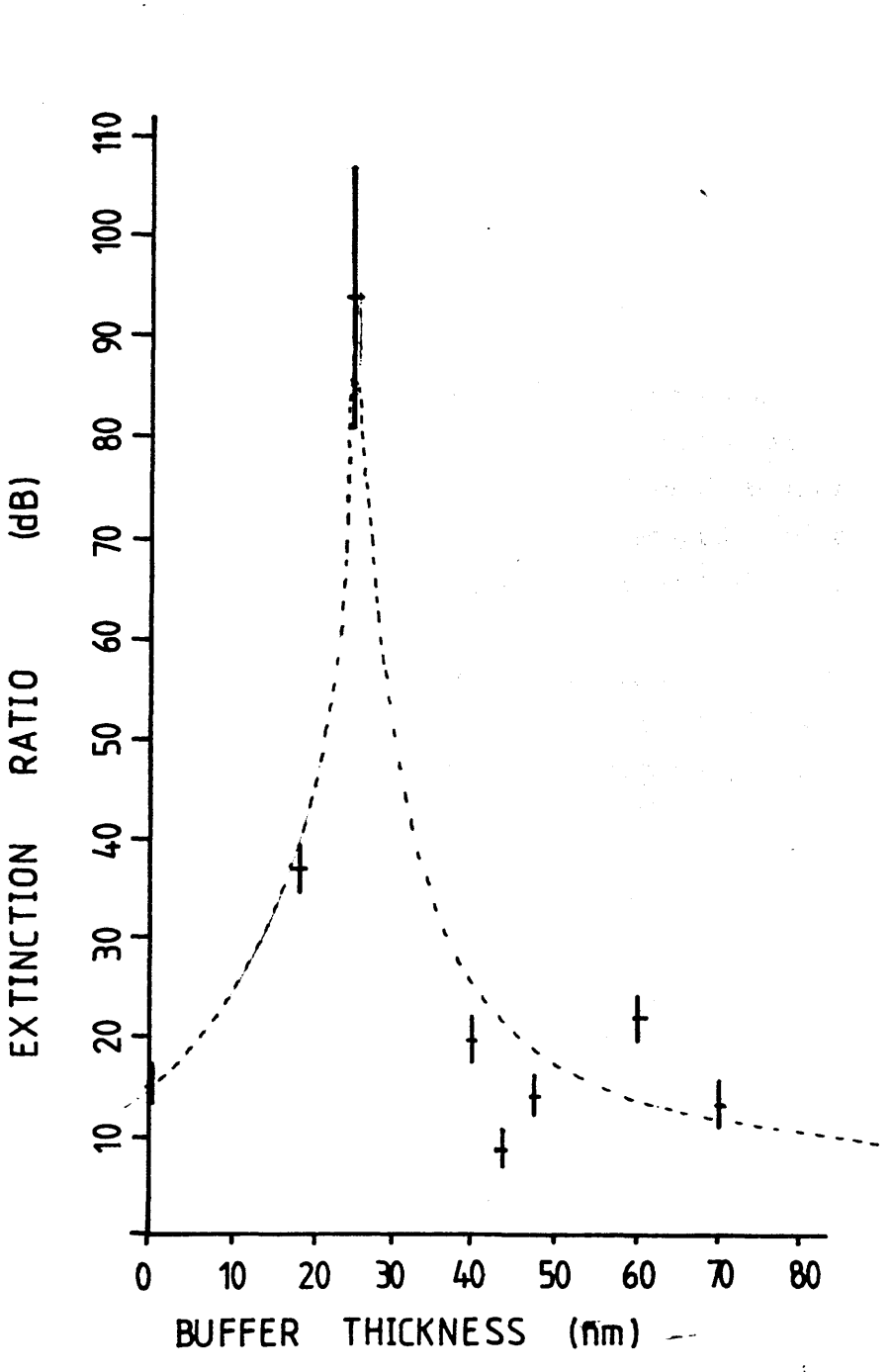

FIG 16 EXTINCTION RATIO VS. THICKNESS OF SILICON MONOXIDE BUFFER LAYER FOR DIELECTRIC/Al CLAD Ti:$LiNbO_3$ STRIPE WAVEGUIDE POLARISERS.

boundary was reduced. Indeed, no peak was observed for the pure aluminium clad devices.

Despite the large fractional error in the reported measurements of the excess loss, distinct trends are still obvious. While the experimental accuracy precludes an accurate determination of the excess loss for a given nominal guide width, it is seen that the figure decreases for increasing buffer thickness, agreeing well with the qualitative predictions of the theory.

The graph shown in figure 16 represents the "best" extinction ratio within each set, plotted against buffer thickness. One might at first expect to see no significant variation of extinction ratio with this parameter, since for a given buffer thickness and index with a particular metal there is a sufficient number of waveguides that phase matching should occur for one guide. However, it would appear that the propagation constants are too widely spaced, and only in the vicinity of 25nm buffer thickness is efficient attenuation observed.

Although the spread of results is large, it is seen that the excess loss decreases with increasing buffer thickness. With buffer thicknesses greater than approximately 30nm the experimental error precludes drawing further conclusions concerning this trend.

The highest extinction ratio obtained with any device was 80 ± 13 dB. This was measured for a device with 25nm buffer thickness and 523nm Al. This result is important as it is the highest ever reported for such a device. Although the figure of 100dB/cm reported by Eberhart and Bulow appears impressive, it is to be noted that no error estimates were given (ref 9) and that the result was obtained by multiplying by 10 the (presumed) figure of 10dB for a device of 1mm length. For reasons given in chapter 2 this may not be valid.

Study of figure 13 indicates that for a given nominal guide

width, the extinction ratio obtained is a sensitive function of buffer thickness. This is predicted from the calculations based on the slab model. Also noted is a second peak in the extinction ratio, this occurring at a greater thickness of buffer than the main peak. As the relatively large error bars are believed to represent accurately the uncertainty in the measured result, it is likely that the trend is genuine. Each sample was exposed, developed and processed separately: while variations in development time will give rise to variations in guide width the effect will be random. Thus some theoretical explanation must be sought.

One fundamental difference between the model of section 4.2 and the practical devices is the finite extent of the aluminium normal to the crystal surface in the latter case. One possible explanation may then be the excitation of a second surface plasma wave at the air-aluminium boundary, or at the aluminium-oxide boundary which will form in a device exposed to air for any length of time.

The devices fabricated with the intention of exciting either the short-range SPW or the long range SPW exhibited significantly poorer extinction ratios than devices with thick metal films. In particular, within the limits of experimental error, no difference was noted between the device with an additional layer and that without. Reference to chapter 3 shows that for the metal thickness used here, splitting of the w_1 SPW (using Ottos nomenclature (ref 31)) into w_+ and w_- should occur. Three situations are then possible:

(i) the effective index for the guide may be such that no coupling to either SPW results

(ii) the effective index may enable coupling to the w_+ mode with resultant low loss, or,

(iii) to the w_- mode with commensurate high loss.

Since both devices fabricated exhibited the same low loss, it is unlikely that the long-range SPW was excited in both cases.

Similarly, this information, along with the unexceptional extinction ratio, would imply that the long-range SPW was not excited. Thus we conclude that the fabrication conditions were not suitable for the excitation of either mode. This was observed for all devices fabricated in this manner with the aim of achieving strong coupling to the short-range (symmetric) SPW.

In view of the limited angular range over which the phenomena are observed in the case of bulk optical experiments (see chapter 3), this result is not surprising. A suitable theory is not available to describe sufficiently accurately the phenomenon. While in the case of a single metal-dielectric boundary it was possible to fabricate a large number of guides with different widths and buffer thicknesses (approximately 1,500 waveguides being fabricated), the extra degree of freedom introduced by a variable metal thickness would require approximately 75,000 guides to be fabricated in order to achieve the same resolution as was used for the buffer thickness in the previous case.

In a real integrated optical system the transition between the non-polarising and polarising sections of the waveguide will give rise to higher excess loss than would be obtained for a gradual transition (ref 32). However, for a range of thicknesses in the tapering region, the excess loss will be higher than for the final multilayer structure. Careful design will be neccessary to minimise the deleterious effect of this tradeoff.

The crescent arising from excitation of some of the metal-clad waveguides is believed to result from a strip-loading effect, possibly associated with the residual titanium oxide on the wavguide surface. Guiding either directly in this region, or via a complex strip loading effect involving the buffer and metal layers results. Since for the devices with higher extinction ratios, careful alignment avoided the effect, further work in this direction was not undertaken.

4.7 Coupling metal clad stripe waveguides to optical fibres- permissible tolerances on alignment

Since the ultimate aim of these polarisers is to fix the degree of polarisation of light entering an optical fibre, it is important to consider (i) whether the free-space measurements are valid, and (ii) how misalignment of the fibre affects the excess loss.

4.7.1 Experimental details

To investigate problem (ii) the following experimental procedure was adopted: linearly polarised light was launched into a single-mode fibre (with no particular polarisation maintaining properties). The plasic fibre coating had been removed by burning and wiping with acetone to remove the charred residue. The exposed section was coiled and immersed in methyl salicylate to act as a cladding mode stripper. The fibre ends had been prepared by the "score and break under tension method" (ref 29). Mounting on the standard Micro Controle stage permitting 5 degrees of freedom in movement (3 translational and 2 rotational) permitted the fibre to be butted to the integrated optical waveguide. Alignment was aided with a microscope with magnification of 60. Fine adjustment was then executed with the 0.1 micron resolution fine drives. With the fibre in an initially optimum position, it was moved in 0.1 micron steps horizontally. The intensity of light emerging from the chip was monitored as in the extinction ratio measurements.

Measurement of extinction ratio using polarised light from fibres

It is known that twisting the fibre rotates the polarisation of the propagating light, depending on the exact nature of the twist (ref 28). Thus, to align the input polarisation with the transmission axis of the integrated optical chip, the fibre was twisted by rolling on the optical bench with a plastic block. While the two ends of the fibre are fixed, rotation of the output polarisation from the fibre was still possible. For small twist rates, the polarisation rotates with the material of the fibre.

For larger twist rates however, this no longer holds (ref 28). Thus a combination of a long, gentle twist and a short fierce twist achieved the desired rotation of polarisation. In this manner it was possible to determine the performance of the integrated optical polariser using light from a fibre.

It is to be noted that the fibre used here was not of the polarisation maintaining variety (ref 33): the polarisers are designed to work well with standard fibre. Polarisation maintaining fibres may have differing field profiles from that used here, and the resulting polarisation mode conversion may have a deleterious effect on the measured extinction ratio. The use of standard fibre however may mean that polarisation coupling mechanisms within the fibre excite the orthogonal mode with some finite strength.

4.7.2 Results

Figure 17 shows the reduction in power with horizontal position for a device using 28nm of silicon monoxide, and approximately 500nm of aluminium. Results are presented for several waveguide widths. The vertical error bars represent the manufacturers quoted error in the displayed reading, while the horizontal error bars indicate the uncertainty in positioning the fibre to a given 0.1μm marker using the Micro Controle fine drive.

The extinction ratio was measured using this fibre method for a selection of waveguide polarisers. In practice, the output intensity fluctuated strongly, constant mechanical pressure being necessary to achieve the desired maximisation. As the effect was produced within the fibre, it was not possible to use the double-headed **photodyne** detector to compensate. The fractional error in the recorded intensity for the maximum reading was approximately 10%, giving rise to a fractional error in the extinction ratio of approximately 17%. This is significantly higher than for the free-space measurements. The measured extinction ratio by this method was within 10% of that obtained by the free space method.

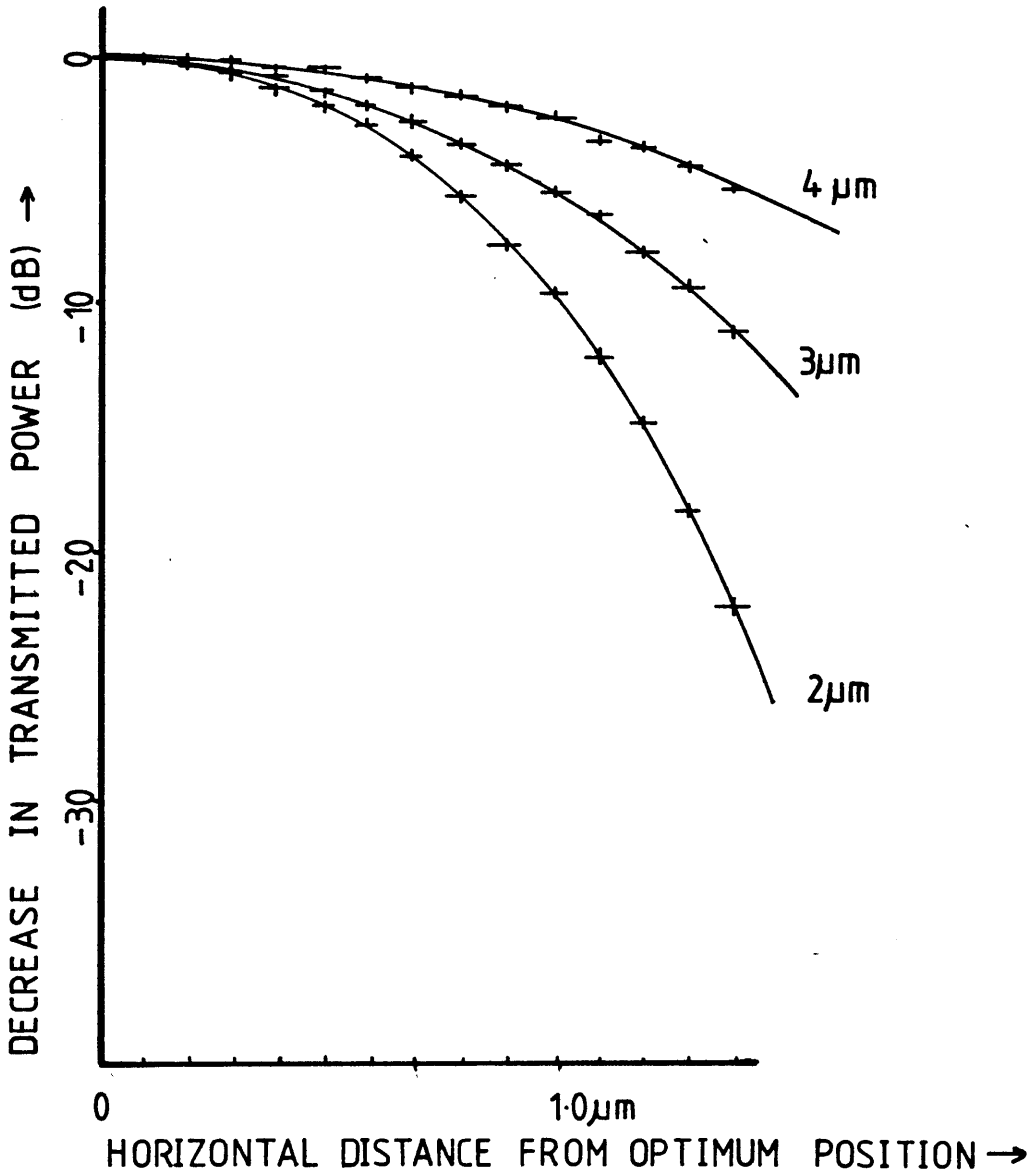

FIG 17 DECREASE IN DETECTED TRANSMITTED POWER FOR SINGLE-MODE FIBRE INITIALLY OPTIMALLY BUTTED TO INTEGRATED OPTICAL POLARISING WAVEGUIDES (OF VARYING WIDTHS) WITH HORIZONTAL DISTANCE. BUFFER-SILICON MONOXIDE, 28nm, ALUMINIUM CLADDING.

4.7.4 Discussion

It is immediately obvious that the alignment requirements are greater for the dielctric-metal-clad stripe guides than for the unclad waveguides. For a practical device, this would neccessitate a tolerance of ±0.1μm in the fibre-waveguide alignment. This is just within the limits of the ion-milled coupler described in chapter 6.

The phenomenon is readily explained in terms of the minor field components of the transmitted mode; if the fibre is displaced from the ideal position when butted to an essentially polarisation inselective waveguide, the field "bending" at the extremes of the integrated optical waveguide means that the linearly polarised light from the fibre can couple at least partially to the "wrong" mode. For the metal/dielectric clad devices, the fields are more linearly polarised, and the drop in coupling efficiency will be more pronounced.

Due to the large experimental error in the extinction ratio determined by the fibre method it is not possible to determine whether the extinction ratio in the fibre corresponds exactly to that obtained in the free-space case.

References

4.1 Riviere,L, Yi-Yan, A, Carru,H, "Properties of Single-Mode Optical Planar Waveguides with Gaussian Index Profile", Journal of Lightwave Technology, Vol lt-3, No 2, pp368-377, 1985

4.2 Wright,S, DeOlivera,A.D, Wilson,M.G.F, "Optical Waveguide Polariser with Synchronous Absorption", Electronics Letters, Vol 15, 1979, pp510-511

4.3 Bristow,J.P.G, Nutt,A.C.G, Laybourn,P.J.R, "Novel Integrated Optical Polarisers Using Ion Milled Grooves and Surface Plasma Waves", Electronics Letters, November 1984

Letters

4.4 Bristow, J.P.G. "Integrated Optical Polarisers", Presented at U.R.S.I. Colloquium, Royal Society, London, 12th July 1985

4.5 Ctyroky,J et al "Thin Film Polariser for Optical Waveguides" 10th European Conference on Optical Communications, Stuttgart Sept3-6 1984 paper 3A6

4.6 Gruchmann,D, Petermann,K, Staudigel,L, Weidel,E, "Fiber Optic Polarisers with High Extinction Ratios", 9th European Conference on Optical Communications, Geneva 23-26 October 1984

4.7 Hosaka, T. et al. "Fabrication of Single-Mode Fiber Type Polariser", Optics Letters Vol8, No.2, February 1983 pp124-126

4.8 Thyagarajan, K, "Expaerimental Demonstration of TM Mode-Attenuation Resonance in Planar Metal Clad Optical Waveguides", Optics Letters Vol 10, No.6, June 1985 pp288-290

4.9 Eberhart,D, Bulow,H, "Single Mode Channel Waveguide Polariser on $LiNbO_3$", 4th European Conference on Integrated Optics, Berlin, 1985

4.10 Griffiths,G, Esdaile,R.J, "Analysis of Titanium Indiffused Planar Optical Waveguides in Lithium Niobate", I.E.E.E. Journal of Quantum Electronics, Vol QE-20, No 2, 1984 pp149-159

4.11 Oliner,A.A, Peng,S.T, "Effects of Metal Overlays on 3-D Optical Waveguides", Applied Optics, Vol 17, No 18, pp2866-2867, 1978.

4.12 Masuda, M, "Effects of a Buffer Layer on TM Modes in a Metal Clad Optical Waveguide using Ti-diffused $LiNbO_3$ C-Plate", Applied

Optics, Vol 16, No.11 November 1977 pp2994-3000

4.13 Goell,J.E, "A Circular Harmonic Computer Analysis of Rectangular Dielectric Waveguides", The Bell System Technical Journal, pp2133-2160, 1969

4.14 Marcatili,E.A.J, "Dielectric Rectangular Waveguide and Directional Coupler for Integrated Optics", Bell System Technical Journal, pp2086, Vol 48, 1969

4.15 Yeh,C,et al, "Single Mode Optical Waveguides", Applied Optics Vol 18, No.10, May 1979 pp1490-1504

4.16 Bradley,J.C, et al "Multimode Structure of Diffused Slab Channel Waveguides in Uniaxial Crystals", Integrated Optics III, Arlington 1983

4.17 Hass, "Optical Properties of Silicon Monoxide in the Wavelength Region from 0.24 to 14.0 Microns", Journal of the Optical Society of America

4.18 Weaver,J.H, Krafka,C, Lynch,D.W, Koch,E.E, "Opitcal Properties of Metals", Physics Datea, Nr 18-12, Fach Informations Zentrum, ISSN 0344-8401, 1981

4.19 Masuda,M, Koyama,J, "Effects of a Buffer Layer on TM Modes in a Metal-Clad Optical Waveguide Using Ti-diffused $LiNbO_3$ C-Plate", Applied Optics, Vol 16, No 11, 1977 pp2994-3000

4.20 Rasch,A, Rottschalk,M, Karthe,W, "Suppression of Outdiffusion in Ti:$LiNbO_3$", Journal of Optical Communications, Vol 6, 1985 pp14-17

4.21 Becker,R.A "Characteristion of Instability in Ti-indiffused

$LiNbO_3$ Modulators Due to Photorefractive and Non-Optical Sources", 7^{th} Topical Meeting on Integrated and Guided Wave Optics, Kissimee, Florida, April 1984

4.22 See Chapter 2

4.23 Handbook of Chemistry and Physics, CRC Press

4.24 Intellemetrics Ltd -instruction manual for IL001

4.25 Andonovic, I Ph.D Thesis, University of Strathclyde,1982

4.26 Photodyne-instruction manual for meter model 22XL

4.27 Squires, "Practical Physics", McGraw-Hill, 1968

4.28 Ulrich,R, Simon,A "Polarisation Optics of Twisted Single Mode Fibres", Apllied Optics, Vol 18, No. 13, July 1979 pp2241-2251

4.29 Hsu,H.P, Milton,A.F, Burns,W.K, "Multiple Fiber End Fire Coupling With Single Mode Channel Waveguides", Applied Physice Letters, Vol 33, No 7, 1978 pp603-605

4.30 Danko,J,J, Haavisto,J.R, "Modal Conversion in a Gradient-Index Channel Waveguide Due to Boundary Perturbations", Journal of Lightwave Technology, Vol LT-3, No 1, 1985 pp176-183

4.31 Otto.A, "Excitation by Light of w_- and w_+ Surface Plasma Waves in Thin Metal Layers", Zeitshrift fur Physik, Vol 219, 1969, pp227-233

4.32 Yamamoto,Y, Kamiya,T, Yanai,H, "Characteristics of Optical Guided Modes in Multilayer Metal-Clad Planar Optical Guide with

Low Index Dielectric Buffer Layer", I.E.E.E. Journal of quantum Electronics, Vol QE-11, No 9, 1975 pp729-736

4.33 York Technology, Commercial Literature.

4.34 Hobbs,L, University of Glasgow Private Communication

Chapter 5-Optical Field Overlap Calculations- a Design Tool for Integrated Optical/Fibre Optical Systems

5.1 Introduction

A constituent loss in the transfer of power from an optical fibre to an integrated optical waveguide is due to the spatial mismatch of the two optical fields (ref 1). If all other parameters remain constant, the more closely matched the spatial distributions of the optical fields, the more power is transferred. For both titanium indiffused waveguides and proton exchanged waveguides in lithium niobate the optical field distribution may be altered by varying the fabrication conditions. Different crystal cuts, diffusion temperatures, times and conditions yield widely varying optical field distributions for titanium indiffused stripe guides (ref 2) while the fields of proton-exchanged guides may be varied by differing combinations of exchange time and anneal times (ref 3). In addition, different types of single mode fibre have differing optical field distributions (characterised by the "spot size" or 1/e width). It is therefore important to be able to determine quantitatively the loss due to the spatial mismatch of the two fields. While it would be possible to measure the coupling loss between the two waveguides in a butt-coupling arrangement (ref 1), it would not be possible to determine the component due to the field mismatch, rather than propagation loss, end-face roughness, misalignment (ref 5) etc. Several workers have used theoretical models to calculate the dependence of the coupling efficiency on various experimental parameters, generally assuming Gaussian field profiles in both fibre and integrated optical waveguide. However for some applications, for example metal-clad waveguides, this is not a valid assumption (ref 6). Indeed, the approximation is not strictly accurate even for conventional titanium indiffused guides (ref 8). A far more versatile tool would be obtained if data from experimentally determined optical field profiles could be used.

It is therefore important to be able to record quantitatively the near field distributions of optical waveguides.

5.2 Coupling coefficients- Definitions

The power transferred between two optical waveguides is generally described in the literature by the amplitude coefficient η, the squared value of which gives the power transfer between the guides in the absence of all other loss mechanisms. η is defined as (ref 14):

$$\eta = \frac{\int_{-\infty}^{\infty}\int E_1(x,y)E_2(x,y)\,dx\,dy}{\left[\int_{-\infty}^{\infty}\int |E_1|^2\,dx\,dy \int_{-\infty}^{\infty}\int |E_2|^2\,dx\,dy\right]^{1/2}} \qquad 5.1$$

Where it is assumed that the axes of the two guides are coincident. Before using this equation as the basis for designing integrated optical devices, it is important to question its validity. Marcuse (ref 7) has considered the radiation losses at the abrubt junction of two slab guides: we use his two dimensional analysis to investigate the validity of equation 5.1. By consideration of the transverse components of the fields at the boundary, the following equation is derived for TE modes, where y is the axis in the plane of the junction and parallel to the the guide-substrate boundary:

$$E_y^i + a_r E_y^r + \int_{-\infty}^{\infty} q_r(\varrho) E_y^r(\varrho)\,d\varrho = C_t E_y^t + \int_{-\infty}^{\infty} q_t(\varrho) E_y^t(\varrho)\,d\varrho \qquad 5.2$$

with an equivalent expression for TM modes. The two integral terms represent the radiated energy reflected and transmitted respectively. Subsequent elimination and manipulation (see ref 7) yields for TE modes:

$$C_t = \frac{2\beta_1\beta_2}{\beta_1+\beta_2}\,\frac{1}{\omega\mu P}\int_{-\infty}^{\infty} E_y^i E_y^{t*}\,dx \qquad 5.3$$

and for the amplitude reflection coefficient:

$$\frac{\beta_1 - \beta_2}{\beta_1 + \beta_2} \qquad 5.4$$

Where q_r, ie the reflected radiation, was neglected. Replacing

the propagation constants by effective indices yields the plane-wave amplitude reflection coefficients for normal incidence (ref 20) Similar expressions are obtained by replacing the transverse electric and magnetic field components with orthogonal components. The conditions required for q_r to be insignificant are that the reflected guided mode carries more energy than the reflected radiation mode. This will be true if guide 1 has a larger N.A. (ref 20) and/or is physically larger than the second guide. Alternatively, if the step height is small, the modes on both sides are more nearly orthogonal.

Equation 1 is then identical to 3 except for a term representing the reflection loss, and for a normalisation factor representing the total **incident** power. For this reason, the coupling coefficient will not in general be reciprocal. Depending on the position of such a junction within a system, this may have important consequences for hybrid integrated optical/ fibre optical gyroscopes.

Nemoto et al. (ref 9) have investigated a more general case, their analysis allowing for a range of different refractive indices and propagation constants in either waveguide.

Finegan (ref 10) has studied the validity of the overlap integral method in the context of such analyses, and concludes that the approximation is good if the step size is not too large (say twice the width of the smaller guide), and provided both guides only support a single mode.

With these provisions, we may therefore evaluate the power transfer for a waveguide junction as:

$$K = \frac{\left(\iint_{-\infty}^{\infty} E_1(x,y)\,E_2(x,y)\,dx\,dy\right)^2}{\iint_{-\infty}^{\infty} |E_1|^2\,dx\,dy \iint_{-\infty}^{\infty} |E_2|^2\,dx\,dy} \qquad 5.5$$

In practical terms, the calculation will then give the coupling efficiency if both fields are single-mode, and of constant phase across the field, ie the end-faces are perfectly flat across their width. The calculation assumes that the coupling is reciprocal: the validity of the assumption will decrease with increasing difference between waveguides. The method should not be used for integrated optical waveguides or optical fibres where

more than one is present.

Sampled Fields

If the two fields were to be sampled at regular, identically spaced intervals to yield a general value I_1^{ij}, the square root of which yields the modulus of the electric field E_k^{ij}, equation 1 could be re-defined as:

$$K = \frac{\left(\sum_{i,j} \sqrt{I_1^{ij}}\sqrt{I_2^{ij}}\right)^2}{\sum_{i,j} I_1^{ij} \sum_{i,j} I_2^{ij}} \qquad 5.6$$

and the calculation performed on a digital computer. The number of samples taken must be sufficient to be able to record any rapid spatial fluctuations in intensity.

5.3 Data acquisition and experimental details

5.3.1 Equipment

The optical field distributions were recorded using the experimental arrangement shown in figure 1. The waveguide under investigation was mounted on a standard crystallographic goniometer head mounted on **Micro Controle** translation and rotation stages permitting movement in three orthogonal directions, with two degrees of angular adjustment. Light from a laser of the appropriate wavelength was focussed into the waveguide using a X40 microscope objective (numerical aperture 0.85). Transverse and vertical adjustment of the integrated optical device enabled maximum input coupling efficiency to be realised. The optical output from the waveguide was then focussed onto the vidicon tube of a **Hamamatsu** camera. The infra-red sensitive tube is a non-standard item, and has a sufficiently broad response to be sensitive to both visible light and the 1.3 micron wavelength radiation used for the experiments. Two infra-red laser sources were used: firstly a semiconductor device operating at 1.3 micron wavelength driven by a constant current power supply (manufactured by MACOM). This laser provided a 5mW output which could then be collimated with a SELFOC lens. The power measured immediately after the x40 microscope objective was a few microwatts. For applications demanding higher power (for

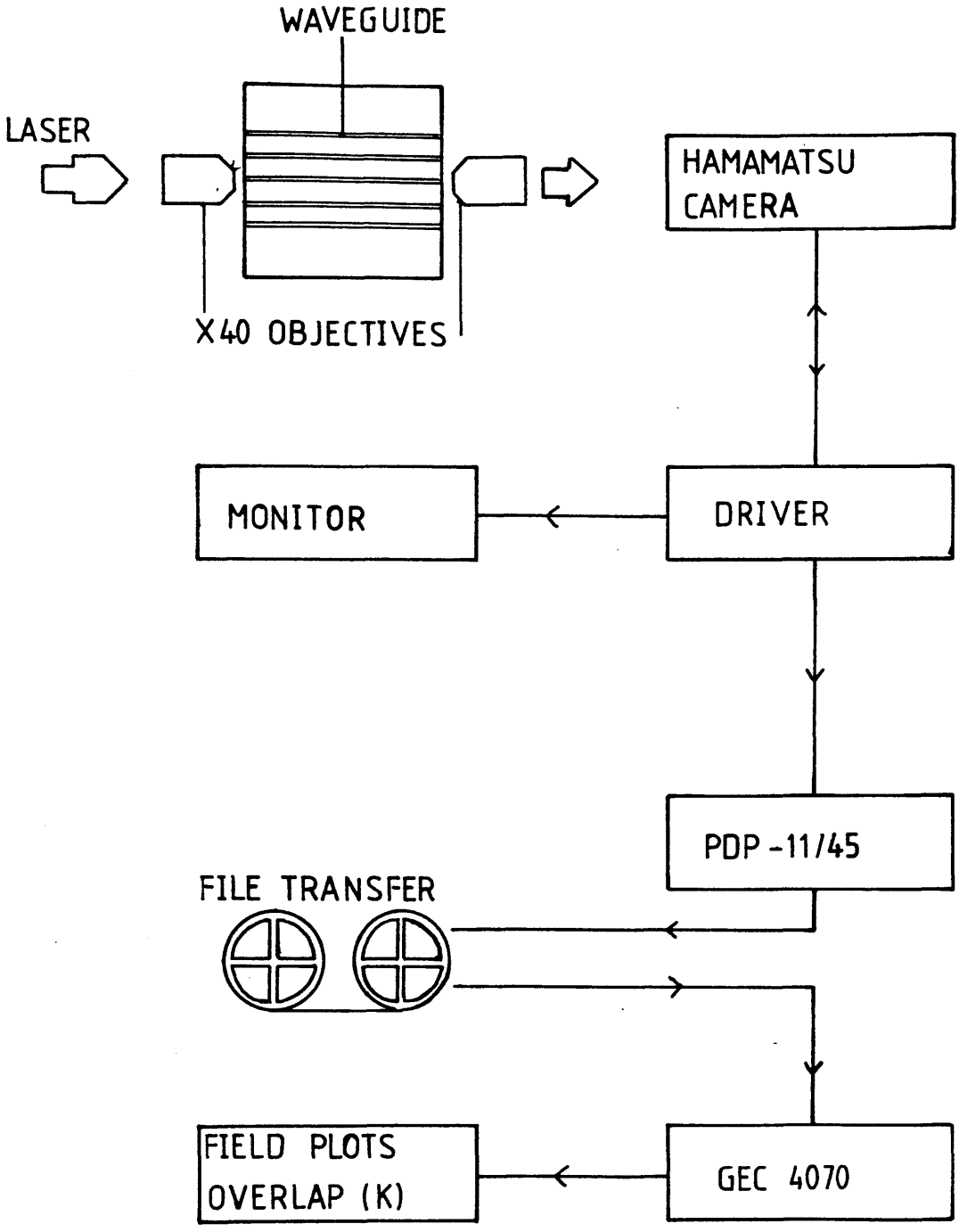

FIG 1 EXPERIMENTAL ARRANGEMENT AND DATA ACQUISITION SYSTEM FOR FIELD OVERLAP CALCULATION

example, polarising waveguides) a CVI CORPORATION Nd^{3+}:YAG laser also operating at 1.3 micron wavelength supporting continuously a single spatial mode was used. This laser uses direct water cooling on the flashlamp pumped rod, a recirculating cooler supplied by **Brunner Scientific** controlling the temperature to $\pm 1^{0}$C. This laser suffered from an intensity variation of at least 5% of the maximun value, occasionally up to 50% despite continuous alignment (ref 15) . In addition, the intensity of other wavelength output radiation was only 30dB below that of the 1.3um radiation (ref 16). A power output of 50mW was available with this laser.

5.3.2 Alignment

In order to optimise the transmitted power, the substrate was moved relative to the focussed laser, the process being monitored with the **Hamamatsu** system. The waveguides were located by the conventional "rising sun" method (ref 11). In the case of waveguides supporting more than one mode, careful adjustment of the input objective was possible to ensure that only the fundamental mode appeared to be excited. Alternatively, movement of the substrate enabled the multimode structure to be displayed. An optional polariser mounted between laser and launching objective provided input polarisation where appropriate, and a corresponding polariser at the output port transmitted linearly polarised components of the output with the appropriate field orientation.

5.3.3 Field Monitoring and Recording

The controlling electronics for the camera monitor the intensity at up to 1024x1024 points. The intensity distribution thus obtained can be displayed on a TV monitor, enabling interactive alignment of waveguides when using infra-red sources. While this qualitative examination of the waveguide is useful, and more convenient than an infra-red viewer, for the purposes of the optical overlap calculation, the field intensities must be recorded. A PDP 11-45 computer was therefore used (on a single user basis) to log the data, an integer of between 0 and 999 being recorded at each pixel. This process took approximately one minute for a 256X256 array, and approximately one third of this time for a reduced scan of 128x128 points. The data were then

formatted and transferred to a GEC 4070 computer (a process taking approximately one hour) for final data processing.

5.3.4 Data Output

A permanent record of the optical field was produced using the program "ACON". This produces from the data a plot whereby all points of equal intensity are joined, producing contouring similar to the representation of mountains on maps. If the contours are sufficiently widely spaced, the values of the intensity are also printed. The intervals between countours may be defined by the user: a default value of 20 is assumed. The contouring sub-program was provided by the "GINOSURF" routine available on the computer used.

A typical plot is shown in figure 2 this being of an optical fibre supporting a single mode at 1.3 micron wavelength. The scale is derived from a knowledge of the distance between the output objective and the waveguide. The same computer package also offers the capability to produce isometric (3-D) plots: in general the variation in intensity due to noise makes these cluttered. Quantitative deductions from such plots are also difficult.

5.4 Corruption due to Source Instabilities and Camera Defects

While the general pattern of the profile is evident, it is corrupted by a low-level background noise, and by a "ragged" appearance. The latter is due to instabilities in the Nd:YAG laser being recorded during the finite logging time for the profile. This could be reduced by using the more stable semiconductor laser should the then low detected power be acceptable, or a faster scan (by using fewer data points). Averaging a large number of data sets should yield an improvement. Figure 3 shows the contour plot of the fibre shown in figure 2, but averaged over three scans. The data transfer time becomes prohibitively long for larger numbers of data sets.

A square of maximum intensity occupying a square of side 5 pixels is seen at coordinates (63,37) for an equivalent screen length of 128 pixels. This is due to a burn on the vidicon tube which had been created by a previous user of the camera. As it was always possible to displace the useful part of the field profile away from this defect, and due to the high cost of the

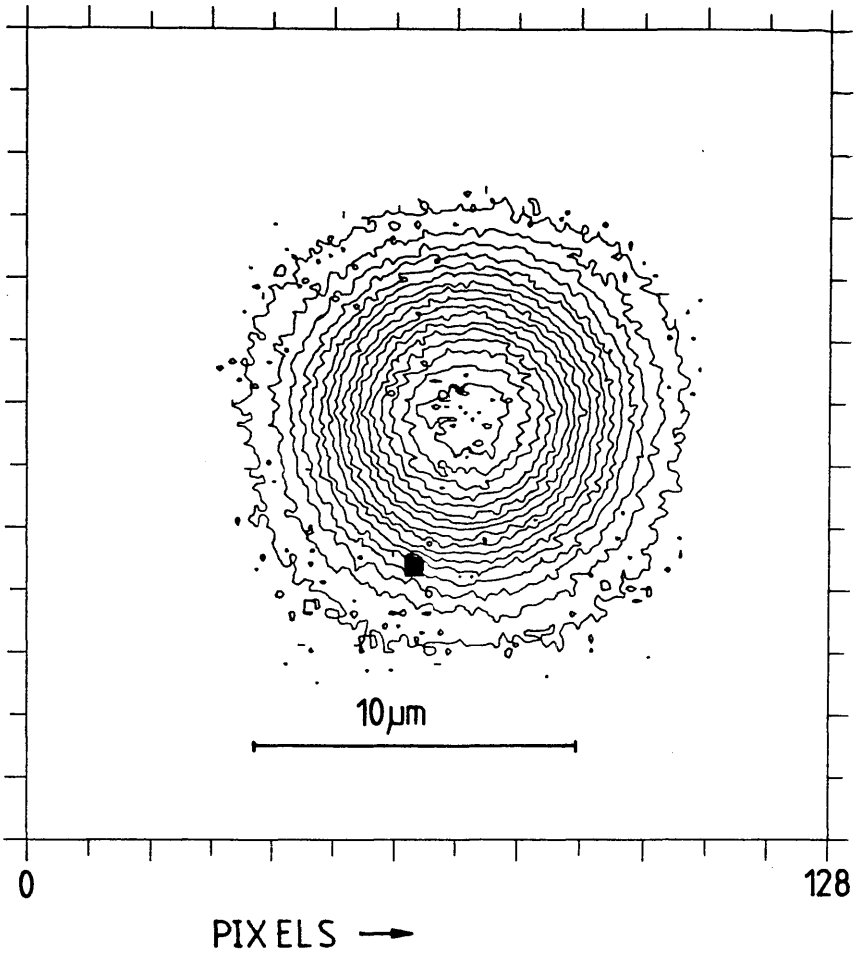

FIG 2 CONTOUR PLOT OF SINGLE-MODE OPTICAL FIBRE AT 1·3 MICRON WAVELENGTH. NOTE BURN MARK.

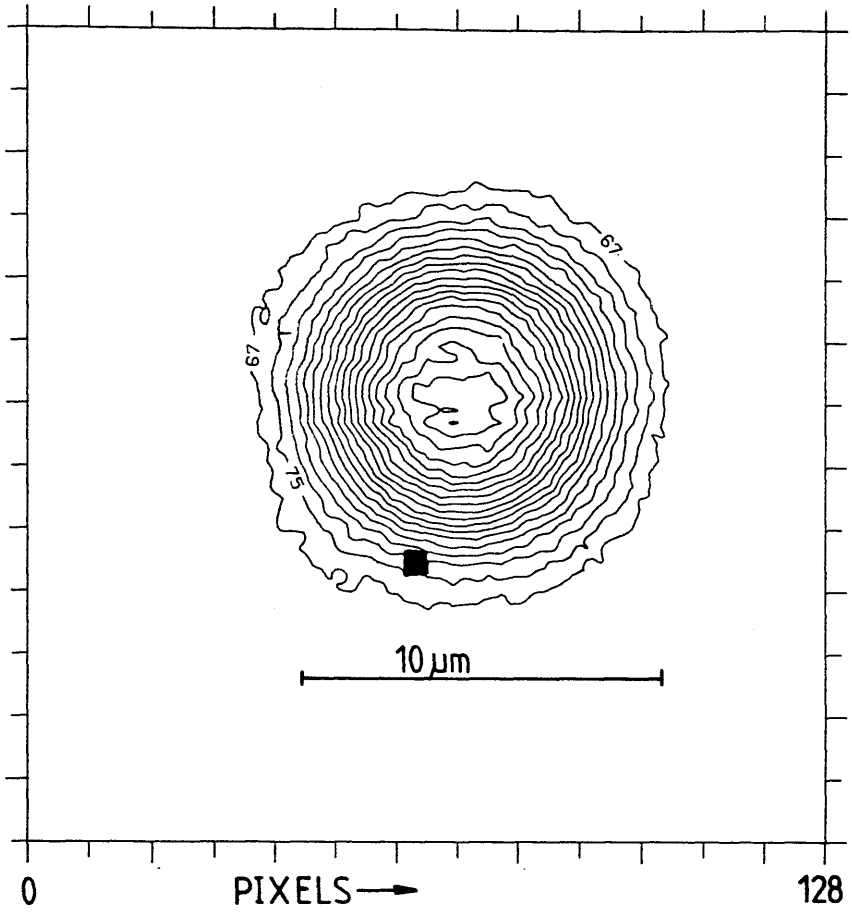

FIG 3 CONTOUR PLOT OF SINGLE MODE OPTICAL FIBRE AT 1·3 MICRON WAVELENGTH – DATA SMOOTHED OVER THREE DATA SETS.

vidicon tube, the latter was not replaced and it was not possible to eliminate the defect.

For the purposes of the overlap integral calculation, the data in this square were interpolated linearly from the intensities at surrounding points. For a given horizontal line, the intensities I(i) in the burnt region with ordinates between 61 and 65 were interpolated linearly using the following expression:

$$I(i) = I(60) + (I(66) - I(60)) \times \frac{(i-60)}{6} \quad 60 < i < 66 \qquad 5.7$$

This averaging was performed automatically

5.4 Computer overlap calculation

The program "OVER" calculates the power transfer coefficient from equation 6. An optional subroutine enables the background noise to be subtracted; this is important for situations where a low signal is present. The value to be subtracted may be input directly, being estimated from a cross-section . The latter was obtained from a visual inspection of the graphs produced by the program "CROSS", which takes a given line in either X or Y directions and plots the intensity variation across the line. The standard "GINOGRAF" routine "GRAF" was used to produce the graphs. Figure 4 illustrates the cross-section of the fibre profile shown in figure 2, taken at maximum intensity. Alternatively, one half of the profile may be assumed to be gaussian, in which case the additive constant present is calculated and then subtracted from all data values.

The overlap coefficient is then calculated to yield the value K. However, it is unlikely that the two optical fields will be centred on the same point in the array. Therefore one of the fields is shifted by 4 pixels with respect to the other, and the value of K' calculated. Should this be greater than K, the new value K' is assigned to K and the process repeated. If not, then the field is shifted in the opposite direction, again calculating K'. This sequence is repeated in the orthogonal direction, until a maximum value of K' has been found. To ensure maximum possible accuracy, the entire sequence is repeated with a shift increment of first 2,then 1, this final, maximised value of K being output.

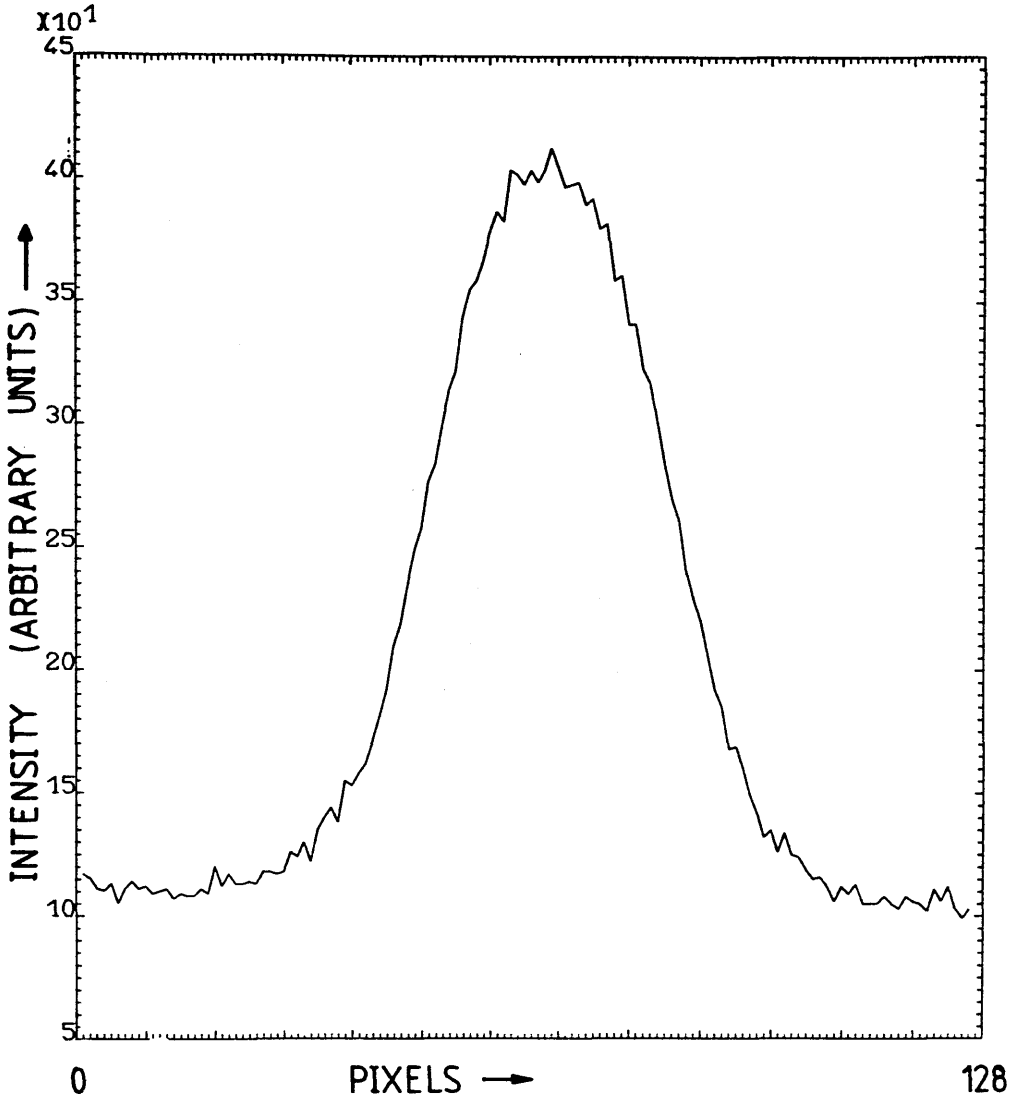

FIG 4 CROSS-SECTION OF FIELD PROFILE OF SINGLE-MODE OPTICAL FIBRE AT 1·3 MICRON WAVE-LENGTH

The program was written in Fortran 77 and run on a GEC 4090 computer at the Rutherford Appleton Laboratories, this being accessed via the GEC 4180 at Glasgow and a telephone line. No special libraries were used.

5.6 Results

In order to investigate the power transfer loss in coupling between optical fibre and integrated optical waveguide, a series of waveguides were fabricated using titanium indiffusion of lithium niobate, as described in section 2.5, except that the diffusion time used was 40 hours at 980°C, and the initial thickness of titanium was 980A. All other fabrication conditions were indentical. The initial width of the titanium stripes ranged from (nominally) 2 to 10 microns in 1 micron steps. The optical field distributions were recorded as previously described , both for this set of waveguides, and for an optical fibre which was supplied by British Telecom (single mode at 1.3 micron wavelength with the cut-off wavelength for the second mode at 1.14um wavelength, core diameter 3.88 microns).

Typical associated field plots are shown in figure 5, this being of a 5um guide, while figure 6 shows the corresponding plot for a 10um guide. The field distribution of the integrated optical waveguide shows a high degree of axial symmetry, this being characteristic of waveguides fabricated in Z-cut lithium niobate, using titanium indiffusion with particular diffusion times.

The overlap calculation was performed using the program "OVER". The results are shown in figure 7. The vertical error bars represent the uncertainty in the calculated value of K, determined by performing the calculation with two recorded profiles of the same waveguide. The horizontal error bars represent an average uncertainty in the width of the initial titanium strip, which as described in section 2.5 depends sensitively on various experimental parameters. It is evident that the transfer coefficient varies with guide width, although an exact trend is difficult to define due to the large spread of data. It is to be noted that all loss mechanisms other than modal mismatch are implicitly excluded.

5.7 Other applications of the recorded field profiles

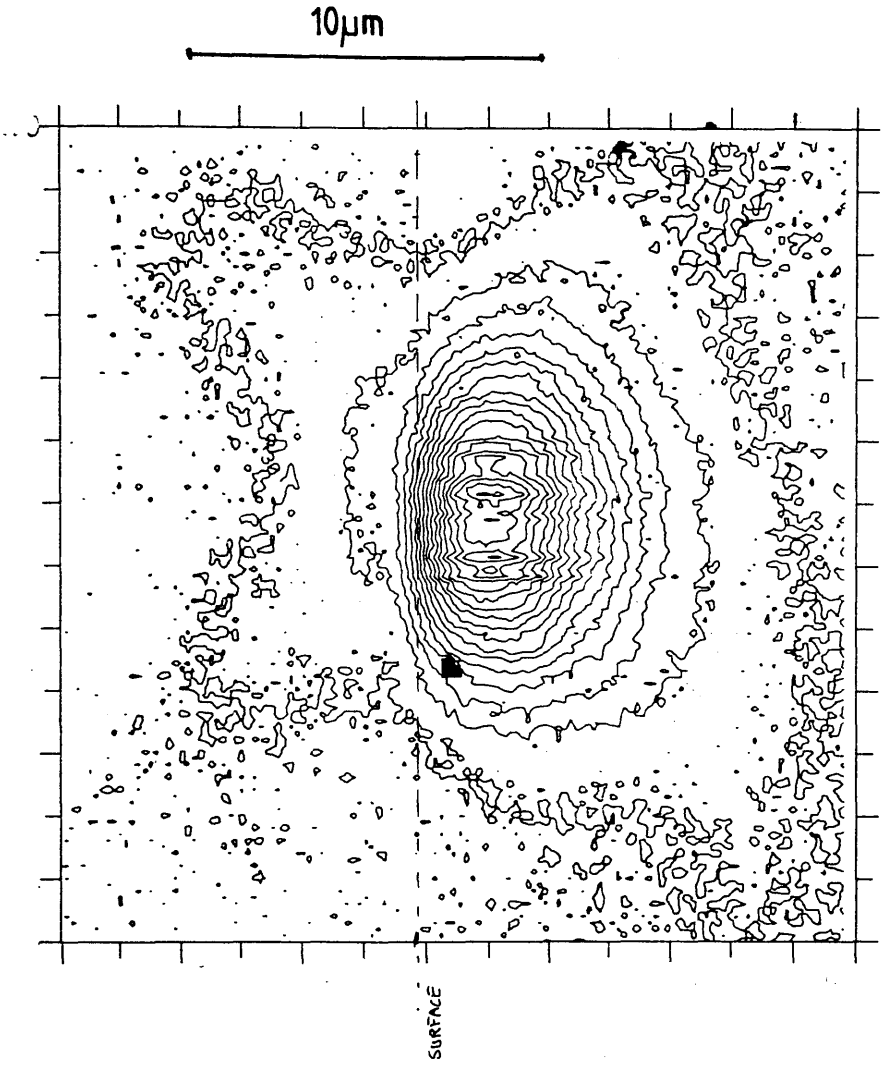

FIG 5 CONTOUR PLOT FROM 5μm Ti:$LiNbO_3$ WAVEGUIDE (LONG DIFFUSION TIME)

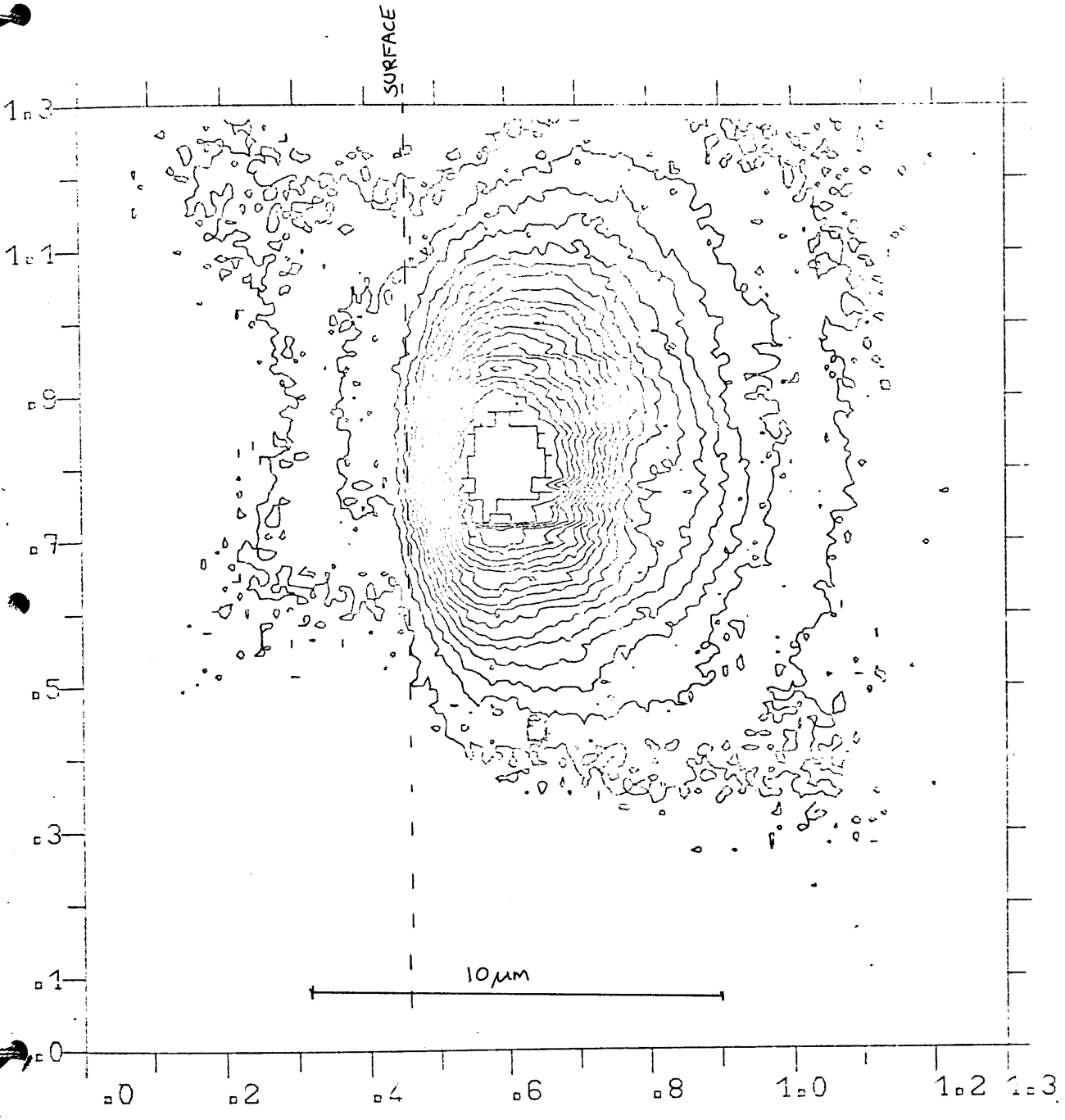

FIG 5a FIELD PROFILE FROM 5um STRIPE GUIDE USING SHORT DIFFUSION TIMES.

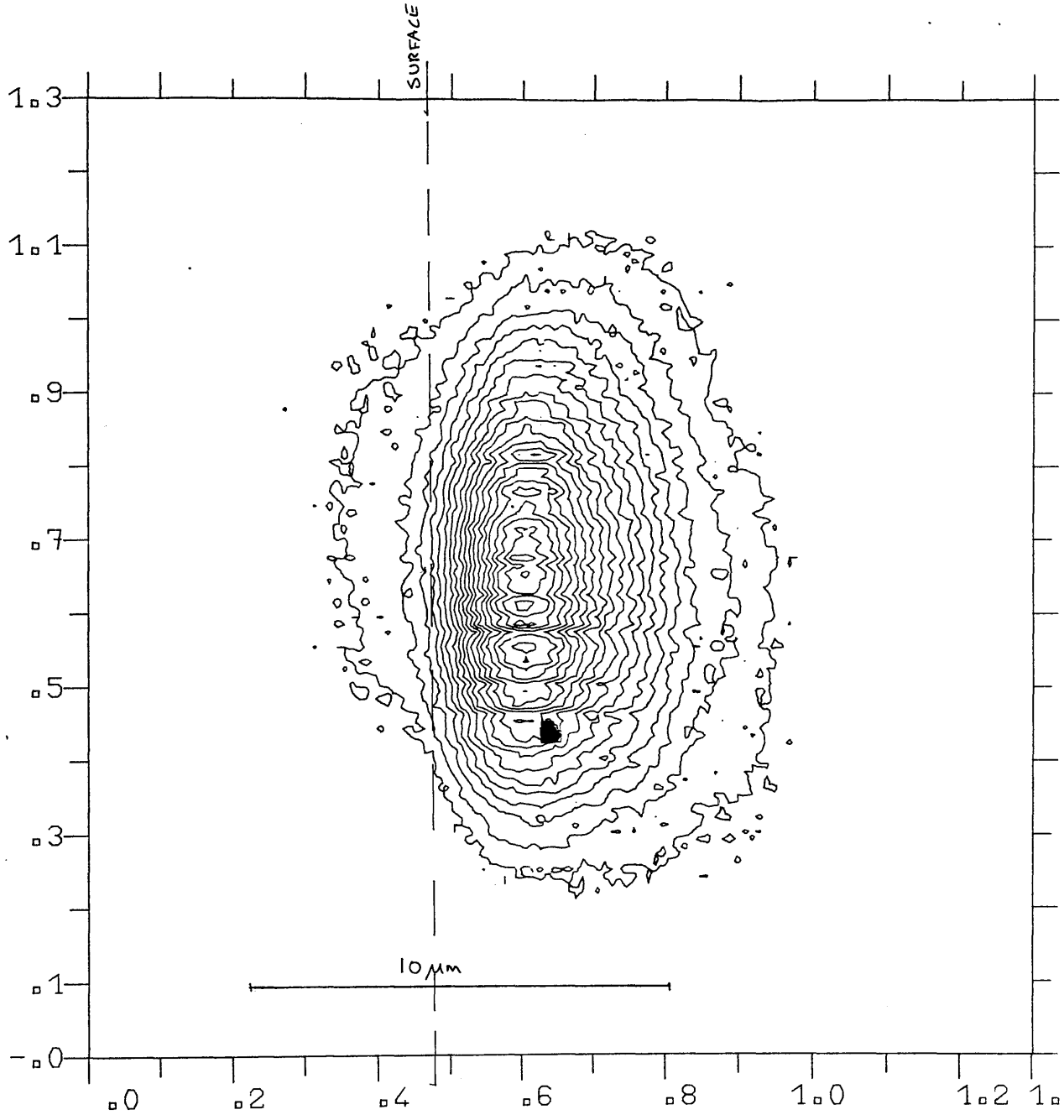

FIG 6 IMAGED NEAR FIELD PROFILE FROM 10 um STRIPE WAVEGUIDE FABRICATED WITH LONG DIFFUSION TIME. SCALE AS FIG 5

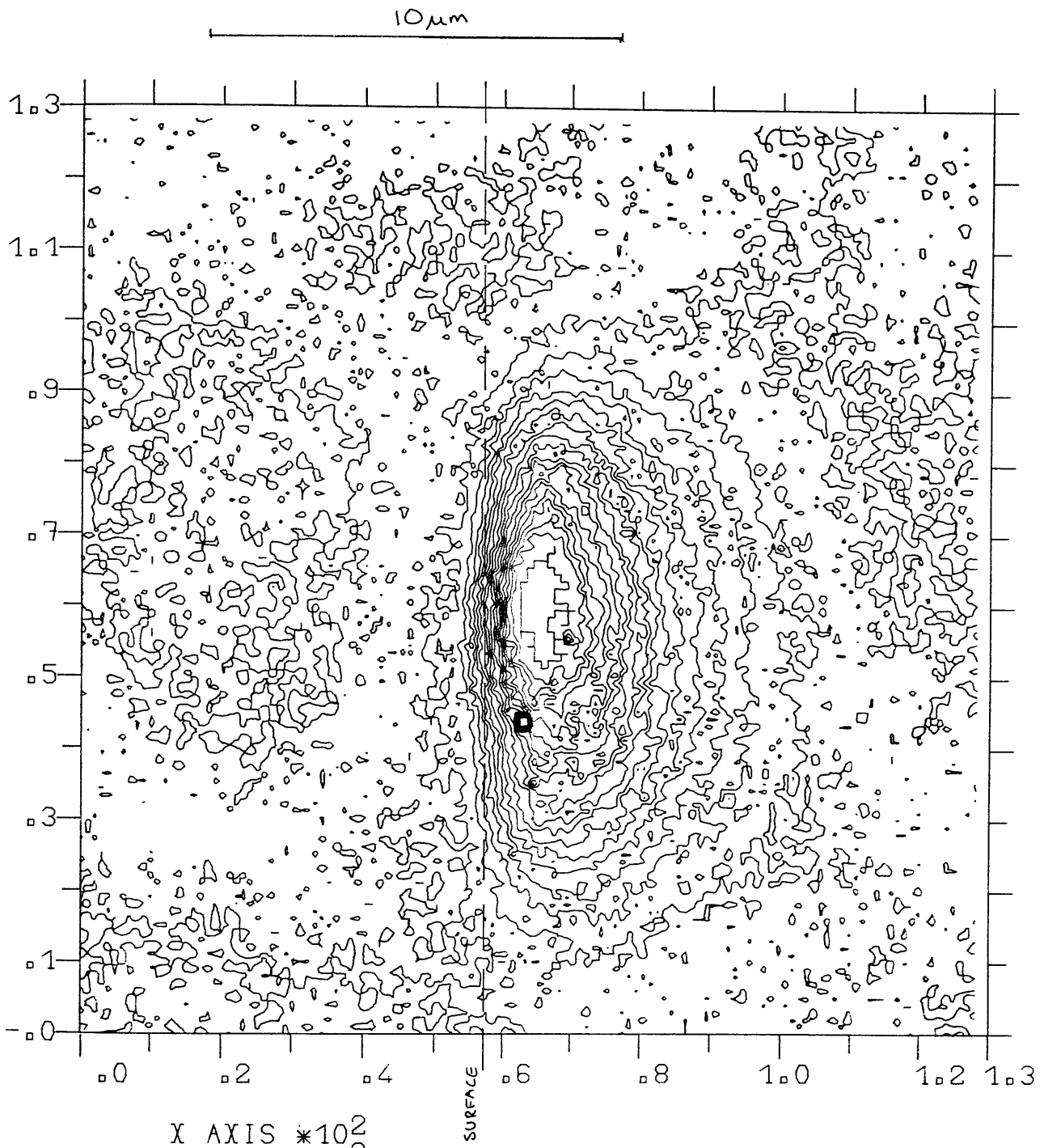

FIG 6a FIELD PROFILE FROM 10μm STRIPE GUIDE USING SHORT DIFFUSION TIMES.

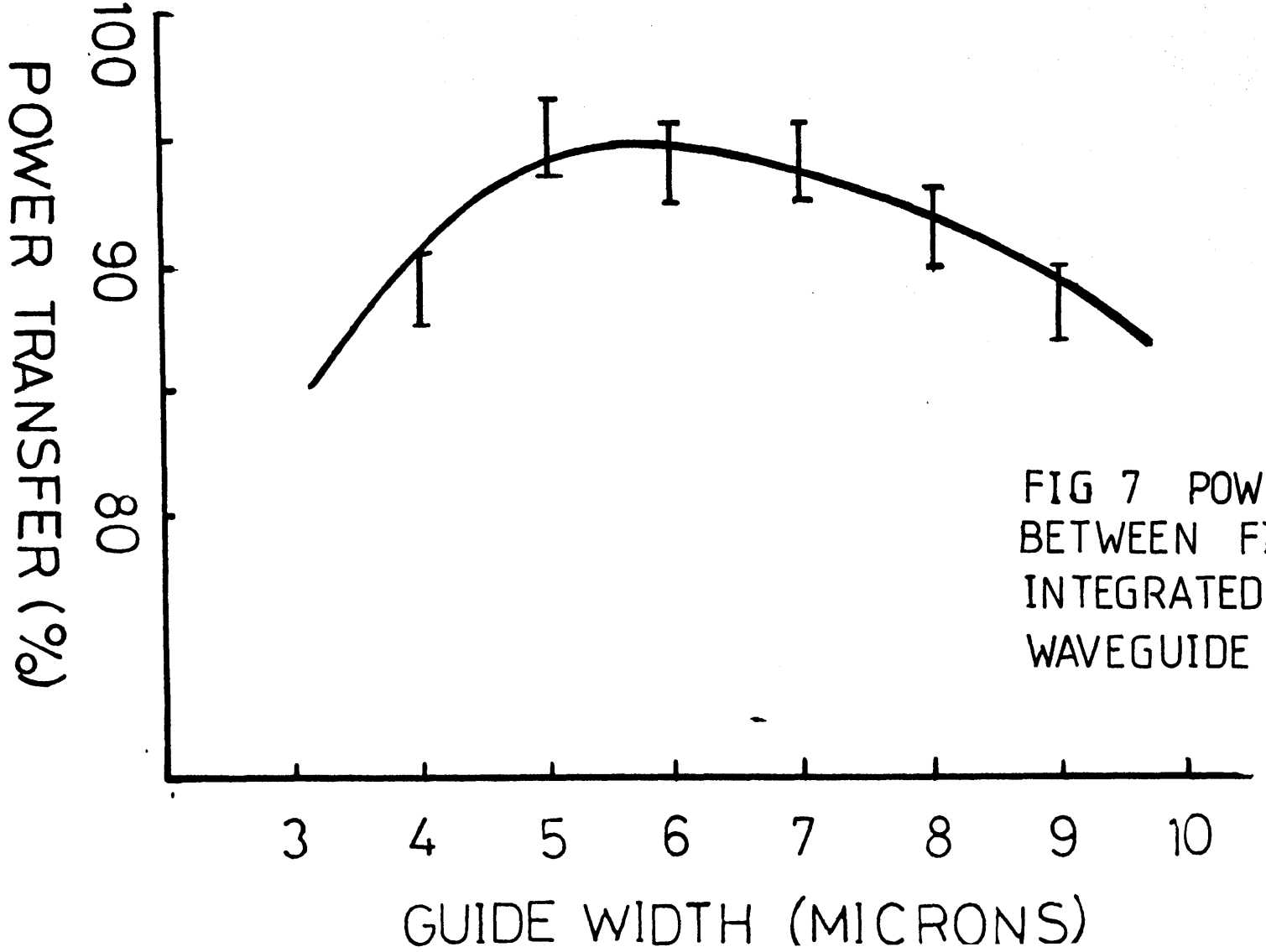

FIG 7 POWER TRANSFER. BETWEEN FIBRE AND. INTEGRATED OPTICAL WAVEGUIDE

The recorded field profiles may be used for several other purposes, notably the reconstruction of the waveguide refractive index distribution, the effect of lateral waveguide misalignment, and the optimal design of electrooptic guided wave modulators. The preceding discussion also suggests that the program could be used to evaluate the reduction in coupling efficiency associated with lateral displacement of one of the waveguides. Using a modification of the program "OVER" it was possible to evaluate this trend for the recorded field data. Having obtained the optimum value of the overlap coefficient, and noted its position, one field is shifted by one pixel and the process repeated. The power transfer coefficient is again calculated, and the process repeated. Figure 8 show the results for the junction of two guides: one with initial width 5um and the other with initial width 10um. The waveguides used here were fabricated with short (9.5 hour) high temperature (1000°C) conditions, the field profiles from which are illustrated in figure 5 and 6 respectively. The shifting is performed parallel to the substrate surface, thus the results correspond to a lateral misalignment. For all points with $i,j<1$ or $i,j>128$, no value is recorded for the optical field. It is therefore either necessary to assume it to be zero, or to make the data "cyclic", ie to repeat the data set after 128 pixels. In either case error will be introduced for appreciable intensities at the field edge: here the first option was chosen for convenience.

The effect was also investigated using the synthetically generated field profiles from the program "GAUSS". The effect of a lateral displacement can be calculated theoretically: For a gaussian field of half-width at half-maximum (HWHM)1,the amplitude overlap coefficient is proportional to:

$$\int_{-\infty}^{\infty} e^{-x^2} e^{-(x+h)^2} dx = \left(\frac{\pi}{2}\right)^{1/2} e^{-h^2/2}$$

Figure 10 shows the results of the calculation of the overlap coefficient for the synthetically generated fields, evaluated using the program "OVER".

Morishita (ref 17) has shown that for a radially symmetric fibre the refractive index distribution may easily be

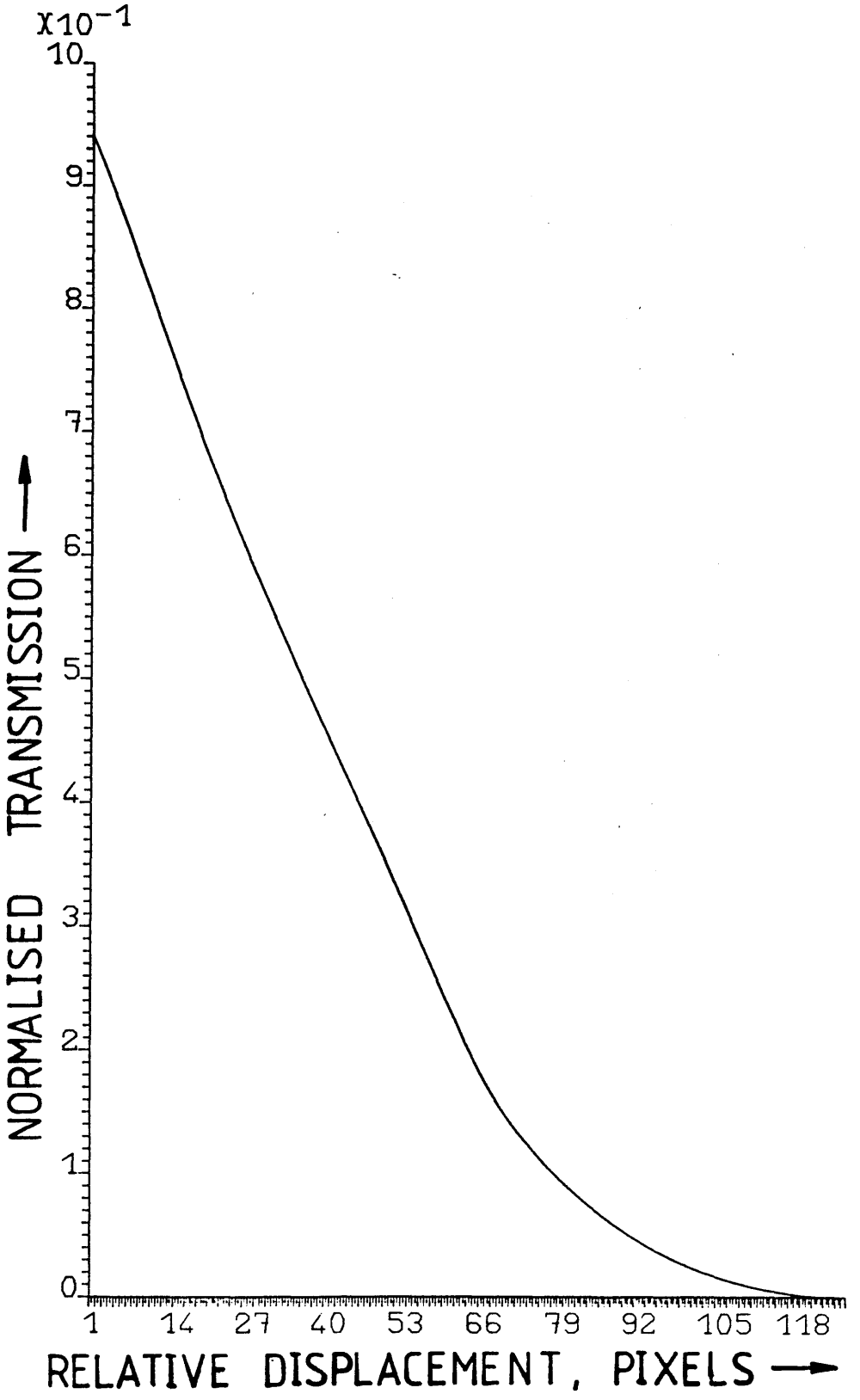

FIG 8 CALCULATED TRANSMISSION VS. GUIDE DISPLACEMENT FOR FIELD DATA FROM 5 AND 10 MICRON SHORT DIFFUSION TIME STRIPE GUIDES

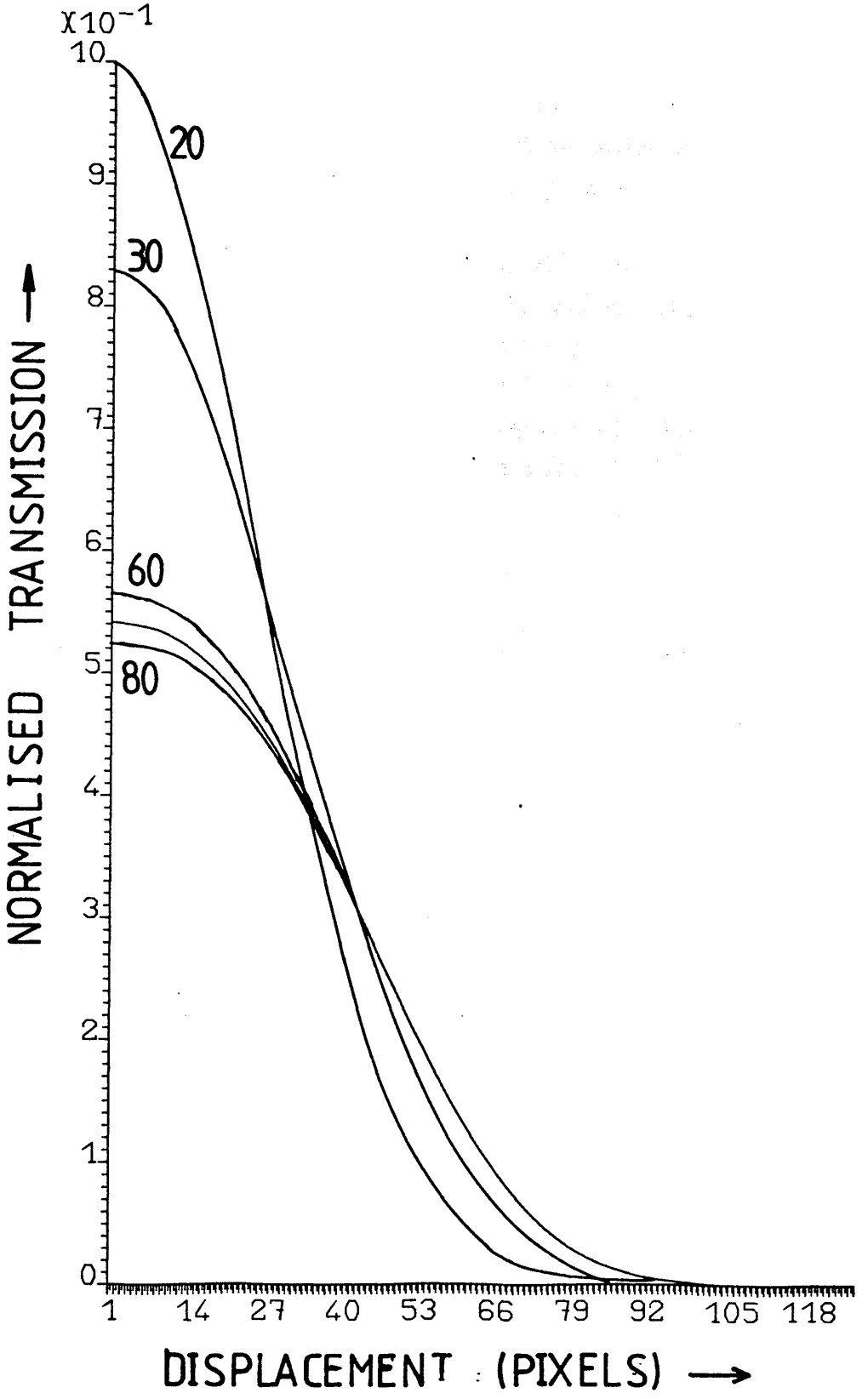

FIG 10 TRANSMISSION VS. GUIDE DISPLACEMENT. GUIDE 1 H.W.H.M 20 PIXELS, GUIDE 2- 20, 30, 60, 70, 80 PIXELS - BOTH SYNTHETICALLY GENERATED.

reconstructed by evaluation of the first and second radial derivatives of the optical power. The author reports that noise associated with the low-intensity field far from the waveguide centre gives rise to errors in the refractive index distribution. However, due to the radial symmetry, integration is possible to improve the accuracy of results.

This is not possible for the case of the titanium indiffused waveguide where radially symmetry rarely exists. Maccughan and Murphy (ref 18) using a system similar to the one reported in this chapter require a large number of field profiles to be averaged in order to yield even mediocre results. For intensity values $I_{i,j}$ recorded, the modulus of the electric field is given by $(I_{i,j})^{1/2}$. The refractive index at this point may be found from:

$$\left(\frac{2\pi}{\lambda} n_{i,j}\right)^2 - \beta^2 = -\frac{\nabla_t^2 (I_{i,j})^{1/2}}{I_{i,j}^{1/2}} \qquad 5.8$$

where

$$\frac{\nabla^2 A_{i,j}}{A_{i,j}} = \frac{A_{i,j-1} + A_{i,j+1} - 2A_{i,j}}{\Delta_x A_{i,j}} + \frac{A_{i-1,j} + A_{i+1,j} - 2A_{i,j}}{\Delta_y A_{i,j}} \qquad 5.9$$

β is the propagation constant associated with the waveguide. The quantisation of the signal represents a possible error. Suppose that a linearly quantised intensity scale is used. For large intensities the quantisation error will be relatively small. However, let us suppose that the intensity at a given point is 10.51 units, while that of the four immediate heighbours is 9.49 units. The quantisation process will assign values of 11 and 9 to the points respectively. Thus the right hand side will assume appoximately the value $0.8/\Delta_x$ assuming $\Delta_x = \Delta_y$, instead of $0.4/\Delta n$- a large fractional error. Thus results obtained at the field edge are of limited accuracy, and averaging of the optical signal is essential to reduce noise. In view of the long (1 hour) transfer time associated with the files used here, this was not possible. Using the data recorded from the optical fibre previously

described, it was attempted to reconstruct the refractive index distribution using the above process. The results are shown for a horizontal scan in figure 11- little information may be deduced from the plot.

Neither Matsushita or Maccaughan considered the effects of diffraction on the results.

Marcuse (ref 23) has shown that a knowledge of both the electric field and the optical field associated with an integrated optical modulator may be used to optimise the device. For electric fields giving rise to a local change in permittivity $\Delta\epsilon$, with optical fields E being polarised in a particular direction, the relative phase change may be written as:

$$\frac{\beta_z}{k} = \frac{\iint_{-\infty}^{\infty} dx\,dy\,\Delta\epsilon\,|E|^2}{|E|^2} \qquad 5.10$$

where $\Delta\epsilon=\epsilon_0 2n\Delta n$ and $\Delta n=(1/2)rn^3\epsilon$ where r is the appropriate electrooptic coefficient (ref 23). However, this line of research was not persued.

5.8 Validity of results - The effects of Diffraction

The above treatment has assumed that the recorded intensity is a true representation of the field at the end of the waveguide under investigation. In general this is not true, as a single point on the object plane will map to the point-spread function in the image plane (ref 21), where this includes both aberations and diffraction. If in equation 5 one replaces the spatially varying field E(x,y) by the Fourier transform of the spatial frequency spectrum $E'(f_x,f_y)$ (ref 21), and in frequency space multiplying the spectral components by the Fourier transform of the point-spread function G, one obtains for K:

$$K = \frac{\left[\iint_{-\infty}^{\infty} \mathcal{F}\left(G(x,y)\,E_1(x,y)\right)\mathcal{F}\left(G(x,y)\,E_2(x,y)\right)\right]^2}{\iint_{-\infty}^{\infty} \mathcal{F}\left(G(x,y)\,E_1(x,y)\right)\iint_{-\infty}^{\infty} \mathcal{F}\left(G(x,y)\,E_2(x,y)\right)} \qquad 5.11$$

Where $\mathcal{F}$ denotes the operation of taking the Fourier Transform.

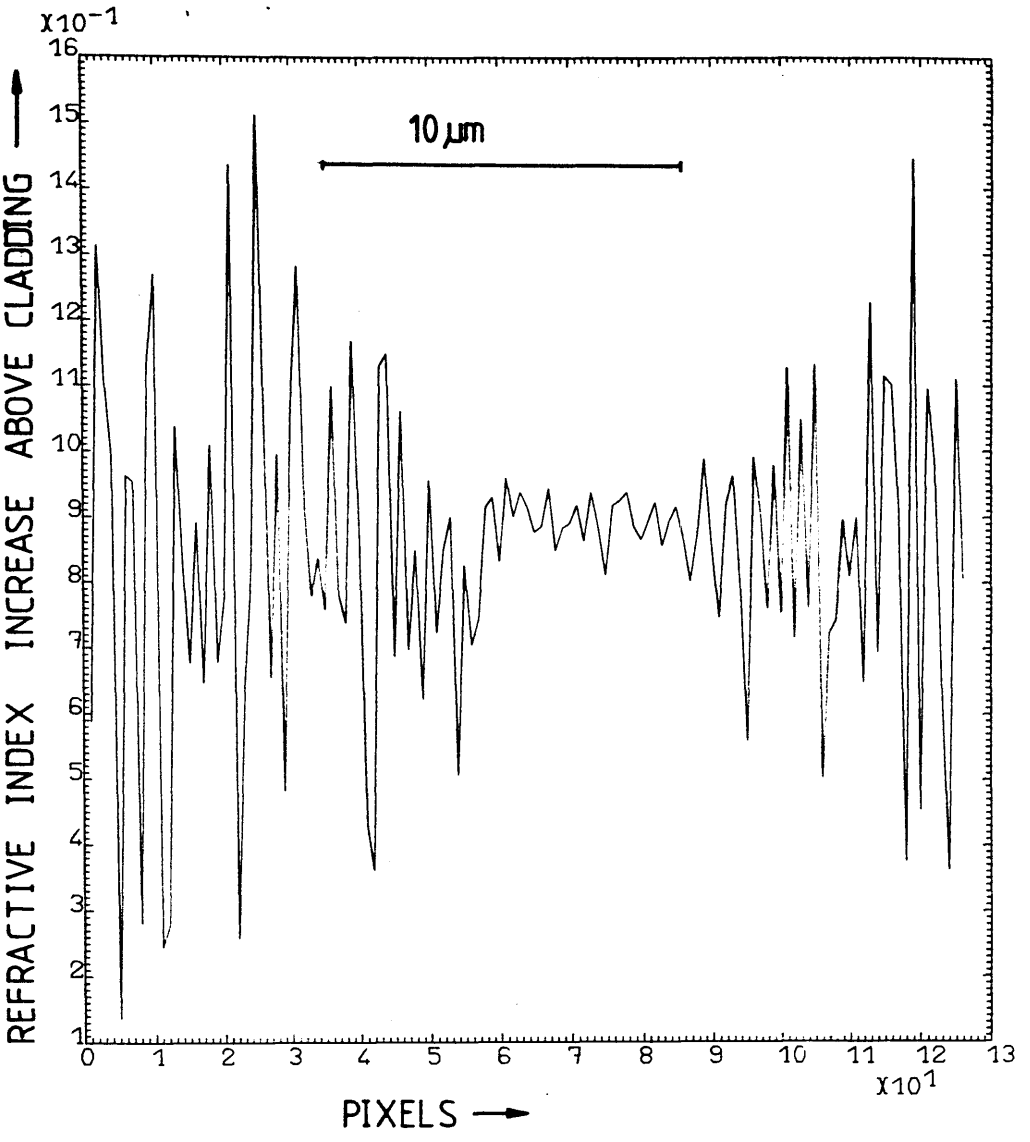

FIG 11 ATTEMPTED RECONSTRUCTION OF REFRACTIVE INDEX OF SINGLE MODE OPTICAL FIBRE FROM FIELD PROFILE AT 1·3 MICRON WAVELENGTH. (NO AVERAGING OF DATA)

It is evident that even in the case of diffraction-limited optics, the function G is inseparable as diffraction will always be present. Thus the calculated value will always be corrupted. Deconvolution (ref 19) is not possible as $G(f_x,f_y)$ may at some spatial frequency be zero . Using a theoretical model , it was possible to investigate the effect on the accuracy of the overlap calculations of diffraction in the objective. The computer programme **"GAUSS"** generates gaussian optical field distributions of variable half-width, centred on point (64,64). The program **"DIFFRACT"** then simulated diffraction and various optional defects. A flow chart for the program is illustrated in figure 12. First the spatial Fourier transform of the object field is taken (by virtue of symmetry, this need only be in one dimension), and multiplying in the spatial frequency domain by the spatial frequency response of the optical system to be modelled. A second discrete Fourier transform (DFT) gave the Fraunhofer diffraction pattern arising from the system (ref 21). Squaring the field values yielded a synthetic generation of the intensity distribution which would have been incident upon the camera vidicon tube.

For a simple transmission function as illustrated in figure 12, it was found that the general trend of power transfer coefficients followed that produced with uncorrupted Gaussian fields, provided the width of the function in frequency space was (approximately) greater than the 1/e width in frequency space for the Fourier transform of the object field for the fibre. Figure 13 illustrates a case where this criterion was satisfied the ratio being 1.1 . Also illustrated on the same graph is the curve for an uncorrupted Gaussian, and for a diffracted field where the previous criterion was not met, the value being 0.7. It is therefore believed that the trends seen in the curves describing, for example, the experimentally determined variation of power transfer with waveguide width are valid, although a small error may be present in the absolute value.

5.9 Resolution of field plots

It is important to consider the accuracy of the intensity contour plots. A thorough treatment of resolution in the case of

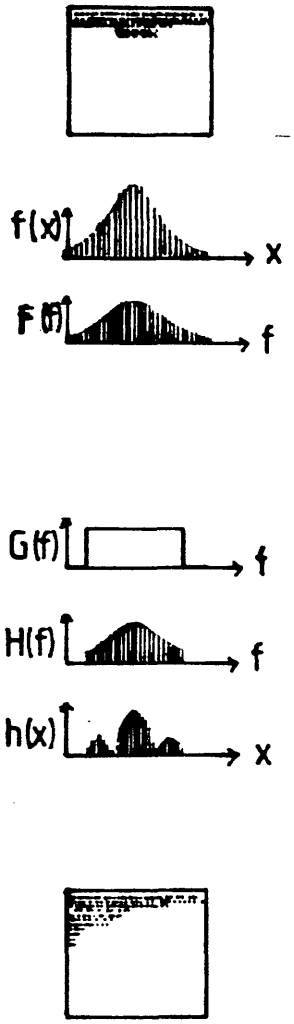

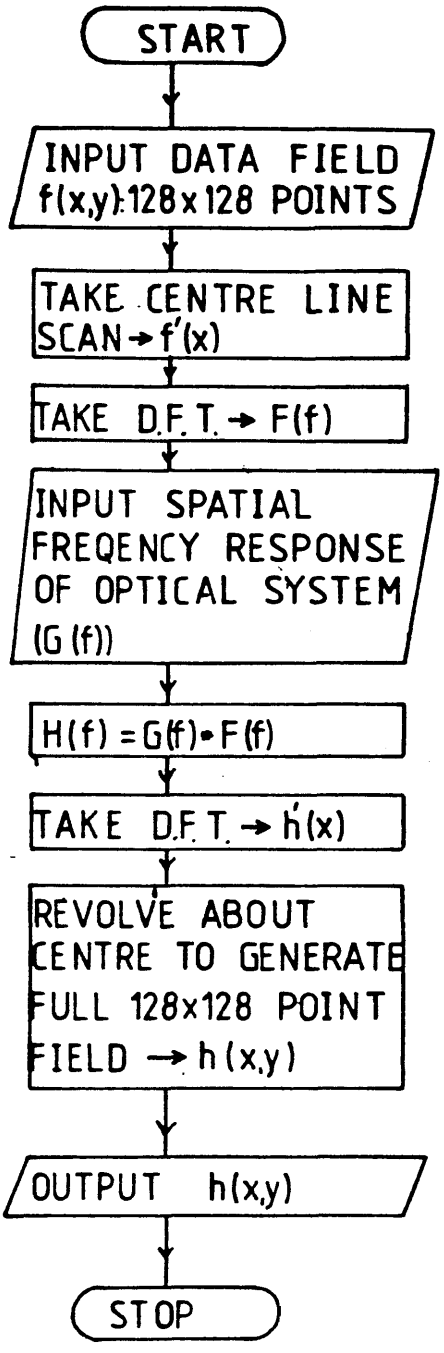

FIG 12 FLOW CHART ILLUSTRATING THE PROGRAM "DIFFRACT" TO SIMULATE THE EFFECT OF DIFFRACTION AND DEFECTS OF IMAGING SYSTEM ON SYNTHETICALLY GENERATED FIELD PROFILES

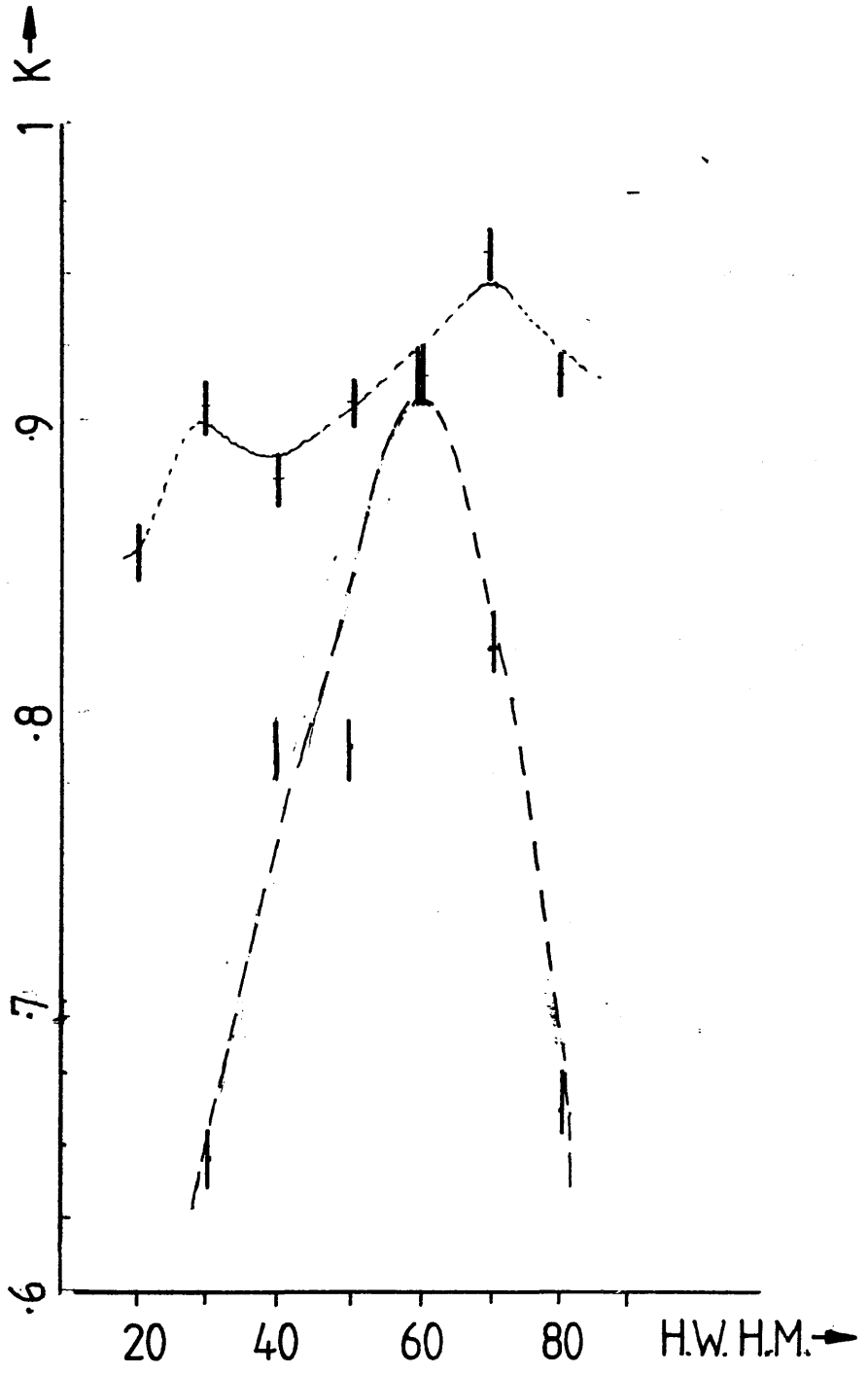

FIG 13 CALCULATED POWER TRANSFER FOR SYNTHETIC FIELD PROFILES OF VARIOUS H.W.H.M. AND H.W.H.M. 60 UNITS, ---- NARROW APERTURE --- WIDE APERTURE

coherent source illumination is given in reference 20. The minimum resolvable separation of two points in the object field will be obtained when the intensity difference between the maximum value and the local minimum between the two peaks is the minimum resolvable by the optical system. For the human eye, the figure normally quoted is 1μm. However, our detection system may resolve intensity changes far greater than the approximate figure of 3dB obtained with the human eye. Following the analysis of ref 20, using a maximum intensity resolution of .001 yields a minimum resolvable separation of 0.9μm interpolating visually the argument of the Bessel function. This represents a marginal improvement upon the figure with the unaided eye. Even with an infinite intensity resolution, the resolution does not improve significantly beyond this figure.

The plots presented are of the recorded, corrupted field. It is therefore possible to plot these to any arbitrary accuracy, although no additional information on the object field distribution may be obtained by so doing. (ref 24).

5.10 Discussion

The aim of this investigation was to set up a computer program to be used with the **Hamamatsu** camera to enable a quantitative investigation of optical field profiles at infra-red wavelengths to be underaken. It was also desired to study the effect of modal mismatching on the power transferred between two similar, but not identical, optical waveguides.

The data logging and recording of optical field data has been demonstrated. Computer programs have been developed to give both a cross-section and a contour map of the optical fields. For practical purposes, data fields of 128x128 points were used.

The validity of the overlap integral method of evaluating coupling loss has been considered: for the waveguide interfaces encountered in coupling single-mode optical fibres to single-mode integrated optical waveguides, the method is shown to be accurate. The method was then applied to data recorded from integrated optical waveguides, and a quantitative trend of variation of coupling efficiency with waveguide parameters observed.

The method was also extended to investigate the effect of

small lateral displacements of the waveguides, good agreement with theoretical predictions for Gaussian field profiles being observed.

The effect of diffraction on the accuracy of the results was also considered: for the imaging systems used in the experiments, the results are shown to be slightly corrupted, but the trends are unaffected. Care should be taken when applying the method to other waveguides or to different imaging systems.

The determination of refractive index distributions from the recorded data has been shown not to be feasible with the present experimental arrangement: other direct methods offer considerable advantages (ref 12). It is however suggested that further work would enable the data to be used to optimise the electrode configuration for any given optical profile.

Thus the technique and programs developed constitute an important design tool for any situation where two dissimilar waveguides with variable fabricational parameters are to be butt-coupled. In particular, the method is useful for some integrated optical/ fibre optical hybrid systems.

References

5.1 Hsu,H.P, Milton, A.F, "Single Mode Coupling Between Fibers and Indiffused Waveguides", I.E.E.E. Journal of Quantum Electronics, Vol QE-13 No4, April 1977.

5.2 Murphy,E.J, Rice,T.C, "Low Loss Coupling of Multiple Fibre Arrays to Single Mode Waveguides", Journal of Lightwave Technology, Vol LT-1, No 3, 1983 pp479-482

5.3 De Micheli,M, ,Botineau,J, Neveu,S, Sibillot,P, Ostrowsky,D.B, Papuchon,M, "Independent Control of Index and Profiles in Proton Exchanged Lithium Niobate Waveguides", Optics Letters, Vol 8, No 2, 1983 ppl14-115

5.4 Ramer,O.G, Nelson,C, Mohr C "Experimental Integrated Optic Circuit Losses and Fiber Pigtailing of Chips" I.E.E.E. Journal of Quantum Electronics Vol QE-17 No.6, June 1981

5.5 Hsu,H.P, Milton,A.F, "Single Mode Coupling Between Fibers and Indiffused Waveguides", I.E.E.E Journal of Quantum Electronics, Vol QE-13, No 4, 1977 pp224-233

5.6 Polky,J.N, Mitchell,G.L, "Metal Clad Planar Dielectric Waveguide for Integrated Optics", Vol 64, No 3, 1974 pp274-279

5.7 Marcuse, D. "Radiation Losses of Tapered Dielectric Slab Waveguides", Bell System Technical Journal, Vol 49, February 1970 pp273-291.

5.8 Riviere,L, Yi-Yan,A, Carru,H, "Properties of Single-Mode Optical Planar Waveguides with Gaussian Index Profile", Journal of Optical Communications, Vol 6, No 1, 1985 pp8-9

5.9 Nemoto,S, Makimoto,T, "Radiation Losses Caused by Discontinuities in a Dielectric Slab Waveguide", Wave Electronics, Vol 3, 1970 pp249

5.10 Finegan,T, "An Investigation into Approximate Techniques for Describing Planar Optical Waveguide Junctions", Optical and Quantum Electronics, Vol 17, 1985 pp109-118

5.11 Andonovic,I Ph.D thesis, University of Strathclyde, 1982

5.12 Korablev, E.M, Proklov, V.V, "Acousto-Optic Measurements of Effective Refractive indices of Guided Modes in Planar Waveguides", Electronics Letters Vol 19, No.7, 1983 pp238-239

5.13 Noda,J, Mikami,O, Minakata,M, Fukuma,M, "Single Mode Optical Waveguide Fiber Coupler", Applied Optics, Vol 17, No 13, 1978 pp2092-2096

5.14 McCaughan L, Murphy,E.J, "Fiber-Ti:LiNbO3 waveguide loss at L=1.3um" I.E.E.E. Journal of Quantum Electronics, Vol QE-19 No.2 February 1983 p132.

5.15 Wong,K.K. Marconi Research Centre, Great Baddow, Chelmsford, Essex

5.16 Barr and Stroud Ltd, Anniesland, Glasgow Private Communication

5.17 Morishita,K, "Measurement of Refractive Index Profile of Single-Mode Optical Fibers by the Propagation Mode Near-Field Method", Journal of Lightwave Technology, Vol LT-3, No 2, 1985 pp244-247

5.18 Mccaughan,L, Bergmann,E.E, "Index Distribution of Optical Waveguides from their Mode Profile", Journal of Lightwave Technology, Vol LT-1, No 1, 1983 pp241-244

5.19 Randall R.B, "Frequency Analysis", Published by Bruel and Kjaer, 1977

5.20 Born,M and Wolf,E, "Optics", Pergamon, 1954

5.21 Hecht,E, and Zajac,J "Optics", Addison Wesley, 1979

5.22 Marcuse,D, "Optimal Electrode Design", I.E.E.E Journal of Quantum Electronics, Vol QE-18, No 3, 1982

5.23 Yariv , A, "Otical and Quantum Electronics"

5.24 Bristow,J.P.G, Nutt,A.C.G, McDonach,A, Laybourn,P.J.R, "Locating and Coupling Fibres to Integrated Stripe Guides", I.E.E. Proceedings J, Special Issue, October 1985

Chapter 6 Coupling between optical Fibres and Integrated Optical Waveguide- a mechanically stable approach.

6.1 Introduction

In order to be able to couple light from an integrated optical waveguide, such as may be used to process the signal from an optical fibre sensor, to or from an optical fibre, some arrangement is necessary to ensure that the relative alignments are optimised and do not change with time. While our main concern here is with lithium niobate as a substrate, it would be advantageous to be able to use any technique developed with other substrates, for example semiconductors (ref 1)

Of the various methods reported, the butt-coupling method would appear to be the simplest. Several versions of this method have been discussed in the literature (refs 2-14). The simplest of these involves merely mounting the fibre end-face adjacent to the integrated optical waveguide (ref 2). The effects of both positional and angular misalignments in such an arrangement have been investigated using a theoretical model to describe the optical fields (ref 11,5). A mechanical manipulator may be used to optimise the relative positions and hence maximise the coupled power (ref 5). Epoxy or cyanoacrylate resins may then be used to achieve a permanent fixture (ref 8). Noda (ref 5) has obtained a fibre-integrated waveguide loss of 3dB at 1.15μm wavelength. Using index matching fluid and with careful attention to waveguide fabrication parameters, Ramaswamy (ref 12) has demonstrated a 1dB loss for fibre/chip/fibre with a 1cm guide on Z-cut lithium niobate. Campbell (ref 7) has reported experimental coupling losses of 0.5dB. However, the complexity of the mechanical manipulators used becomes prohibitive if a large number of connections are required, as would be the case for the Star couplers with many branches recently reported in the literature.

The use of an external mount for the fibres which may then be butted to the integrated optical waveguide has been investigated. Silicon was etched to leave V-shaped grooves in which optical fibres could be located (refs 8,14,). The arrangement is shown in figure 1a &1b, and is referred to in the

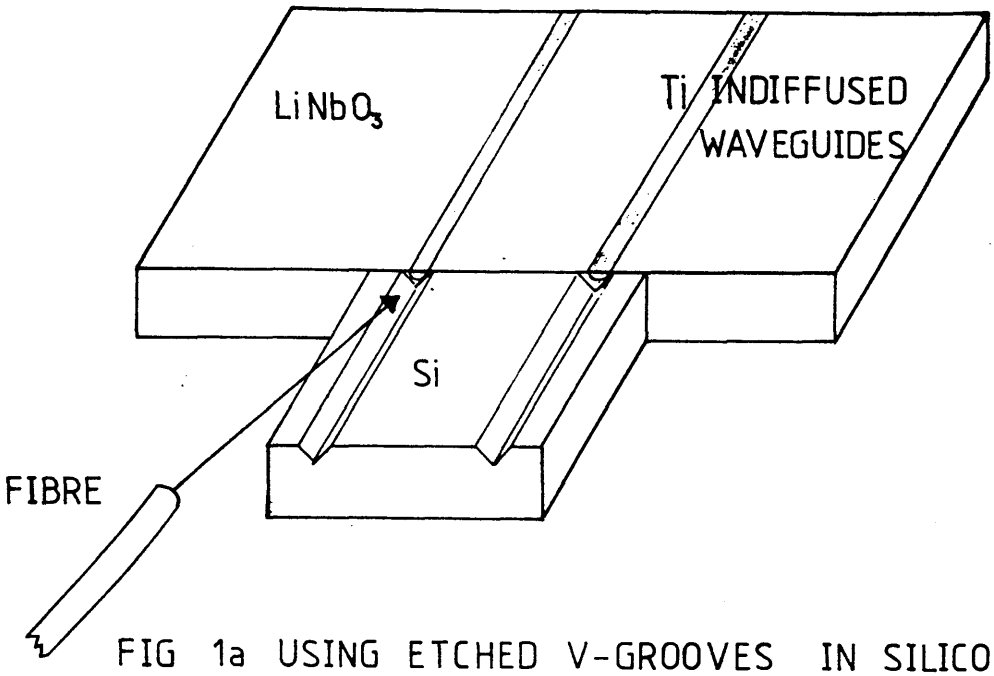

FIG 1a USING ETCHED V-GROOVES IN SILICON TO LOCATE FIBRES AGAINST INTEGRATED OPTICAL WAVEGUIDES IN A BUTT-COUPLING ARRANGEMENT

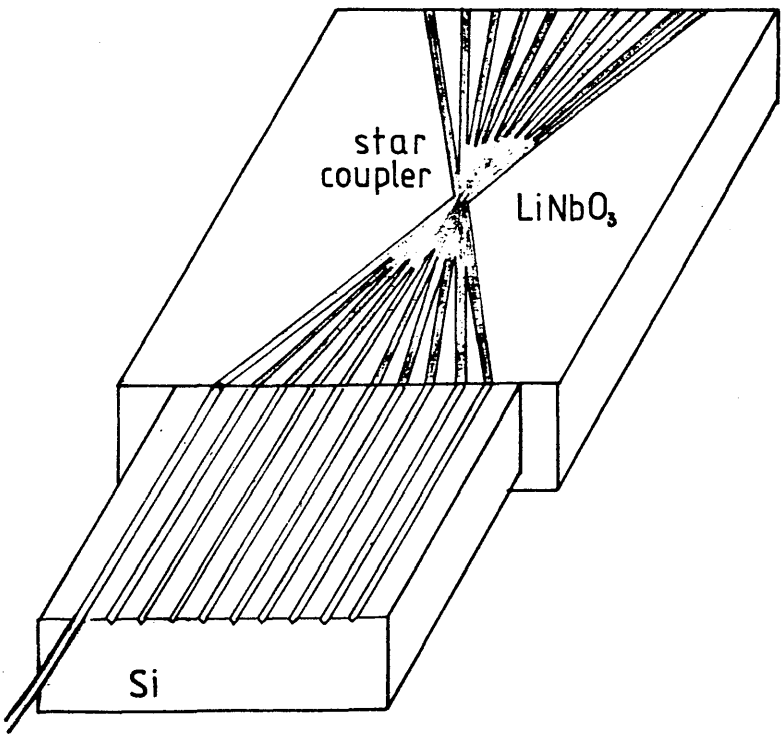

FIG 1b ILLUSTRATING THE POSSIBLE USE OF SILICON V-GROOVES IN COUPLING A LARGE NUMBER OF FIBRES TO INTEGRATED OPTICAL WAVEGUIDES

literature as "flip-chip" coupling. Bulmer (ref 8) has reported a throughput loss of 3dB fibre/chip/fibre. However, when a large number of fibre-waveguide interfaces are required, it may be harder to ensure that simultaneous optimal coupling is obtained in each case. In addition, the two crystals have differing coefficients of thermal expansion. Using for lithium niobate the data in ref **15** and for silicon the data in ref **16** the effect of temperature change on coupling efficiency may be investigated.

Consider the coupler shown in figure 1b. 10 fibres are used. Due to the width of the fibres with their protective plastic coatings, a minimum practical separation of 300μm between centres may be assumed. Thus the outer waveguide centres will be separated by 2.7mm. Allowing the temperature to change from $0^{o}C$ to $100^{o}C$ increases this separation by 0.864 microns for Silicon, while for the Z-cut lithium niobate this becomes 4.347 microns. Thus the separation of the centres of the outer fibres from the outer waveguides will be approximately 1.7μm. The effects of misalignment are documented in ref 5 for a theoretical case, yielding a reduction in transmitted power of 1dB. Alternatively, experimentally obtained data may be used with a modified version of the program **"OVER"** described in chapter 5 for a given fibre/waveguide system.

In this version of the program, having determined the relative positions of the two data sets which allow maximum power transfer, one profile is shifted, the power transfer at each incremental movement being recorded. The results of the calculation show a reduction of approximately 1.5dB for the lateral misalignment assumed here.

6.2 Asymmetric Coupling in integrated optical circuit/ fibre gyro coils: its effect on zero rotation rate offset

The repeatability and stability of the coupling process has important consequences for the use of integrated optical processing systems with optical fibre gyroscopes and other sensors. We consider the single-pass gyroscope shown in figure 2. The effect of one imperfect coupler is represented by the introduction of a reciprocal semi-silvered mirror with amplitude reflection coefficient **r**. We assume that the elements on the leading diagonal are equal, and that the off diagonal elements in

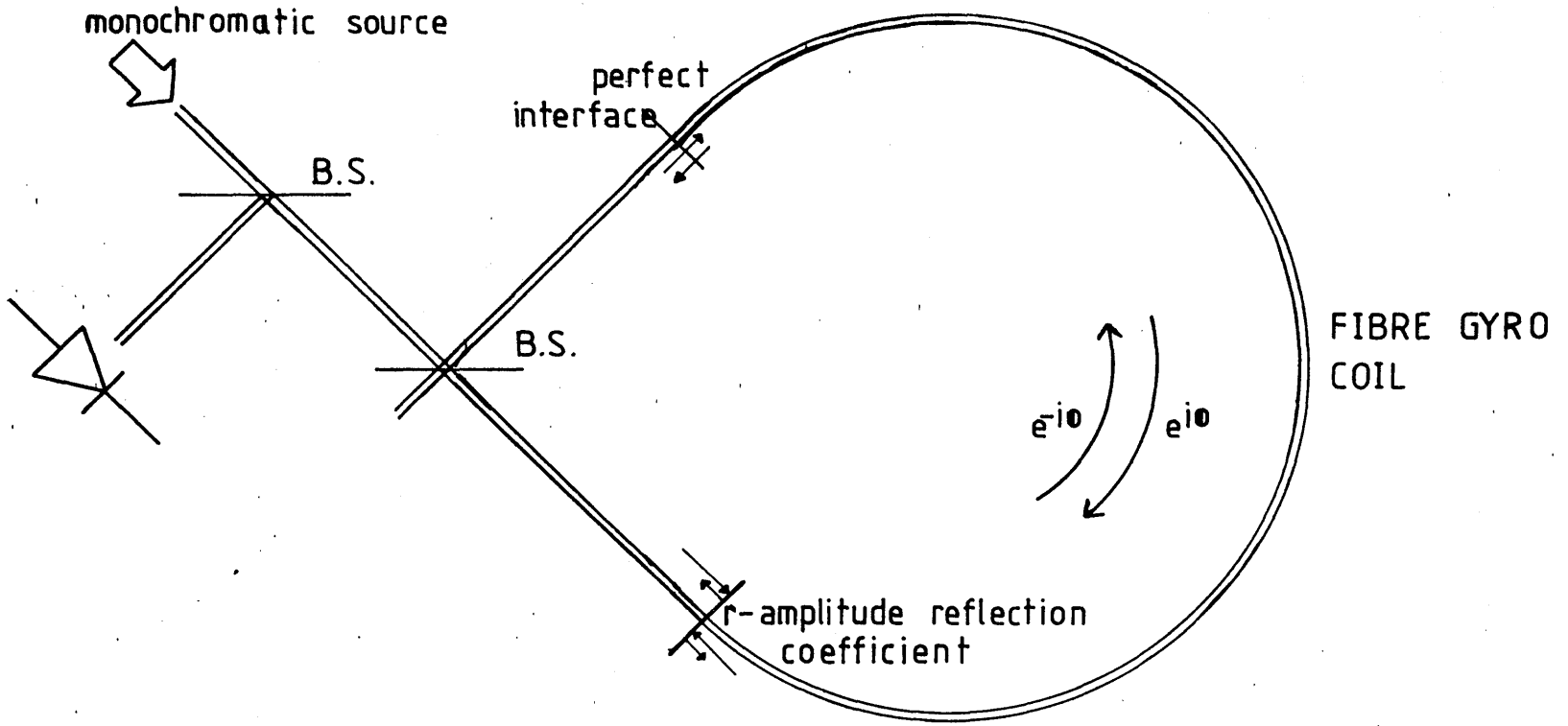

FIG 2 MODEL USED TO CALCULATE EFFECT OF IMPERFECT WAVEGUIDE ALIGNMENT ON OUTPUT OF FIBRE OPTIC GYRO.

the Jones Matrix (ref 22) are zero. Thus the reflected signal has the same state and degree of polarisation as the incoming light. The phase shift associated with the non-rotating input/output leads is φ_0. The anticlockwise propagating beam has a phase shift of $+\Omega$ where the total non-reciprocal Sagnac shift was defined in chapter 1, while the clockwise propagating beam has the same magnitude but opposite sign of shift. Due to reflections, the field apparently emanating from the clockwise beam is:

$$E_c \propto (1-r)e^{i\varphi} e^{2i\varphi_0} + re^{2i\varphi_0} \qquad 6.1$$

while for the signal apparently emenating from the counterclockwise beam is:

$$E_A \propto (1-r)e^{-i\varphi} e^{2i\varphi_0} + re^{2i\varphi_0} \qquad 6.2$$

Expanding, and taking the time-average of the signal yields an intensity proportional to $(r + 2(1-r)\cos\Omega)^2$. For perfect alignment, the signal would be simply $4\cos^2\Omega$. Thus assymmetric coupler alignment gives rise to an offset in the rotation rate. If mechanical perturbations are allowed to disurb the coupling in a time-varying manner, an apparent variation in rotation rate will result.

To consider the effect of two unequal reflections at the coupling interface, and to investigate the effect of their variation we consider a similar model shown in figure 3. Fields of unit amplitude are incident upon the two input ports. The reflection coefficients at the two interfaces are r_1 and r_2 inside the fibre, and r_1' and r_2' within the integrated optical guide. With phase delays Ω_1 and $-\Omega_2$ associated with the clockwise and counter-clockwise beams respectively, we obtain for the total fields:

$$E = r_1' + r_2' + 2\cos\varphi \sum_n (1-r_2)(1-r_1)(r_1r_2)^n \qquad 6.4$$

We now set $r_1=-r_1'$ and $r_1=r_2+\Delta$, then
The detected signal will be proportional to the square of the total field E. Differentiation with respect to Δ yields

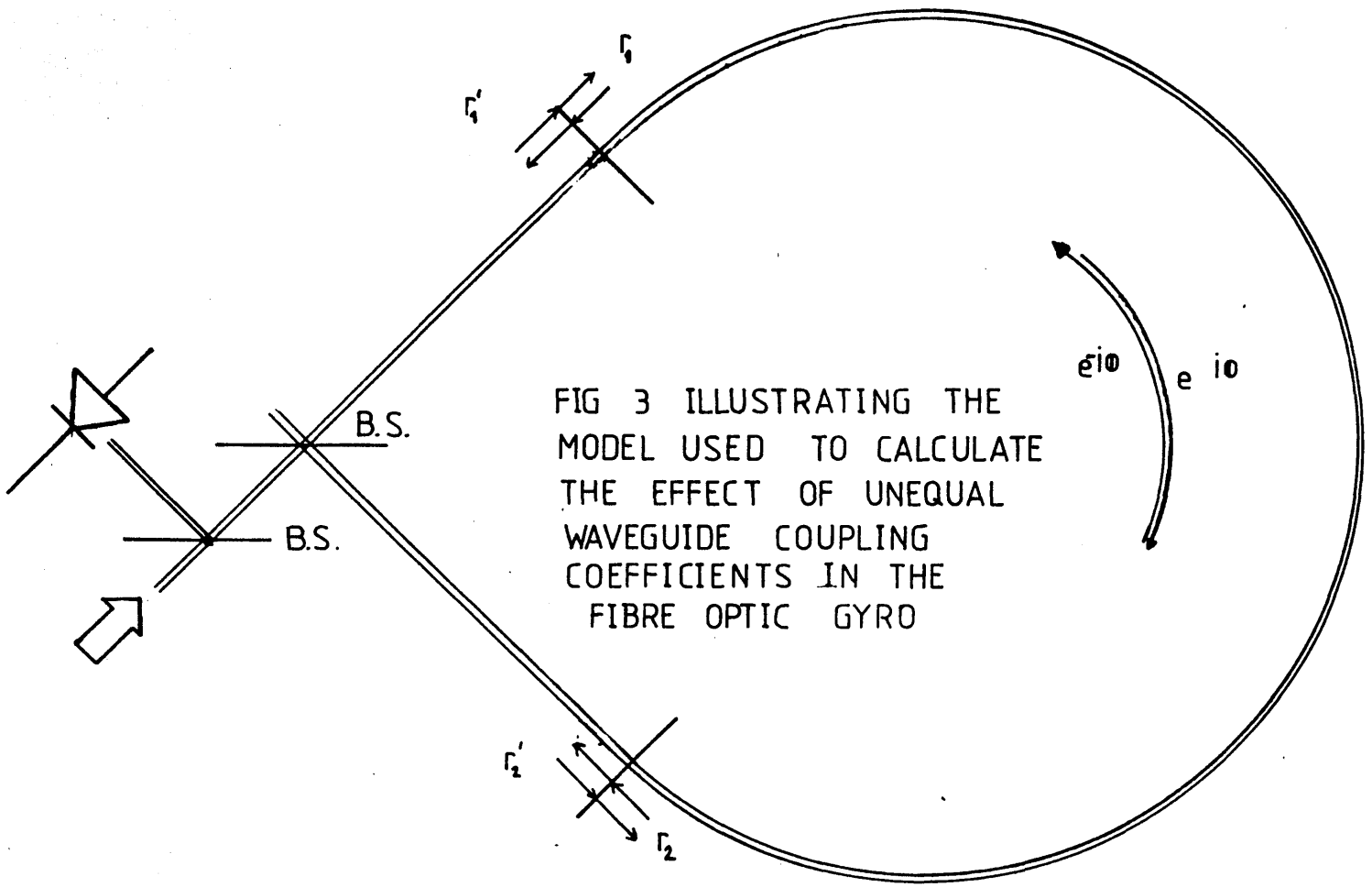

FIG 3 ILLUSTRATING THE MODEL USED TO CALCULATE THE EFFECT OF UNEQUAL WAVEGUIDE COUPLING COEFFICIENTS IN THE FIBRE OPTIC GYRO

$$E = 2r_1 - \Delta + 2\cos\varphi \sum_n r_1^n (r_1 - \Delta)^n \left[(1 - r_1)^2 + \Delta(1 - r_1)\right]$$

$$\frac{dE}{d\Delta} = -1 + 2\cos\varphi \sum_n -n r_1^n r_2^{n-1} \left[(1 - r_2)^2 + \Delta(1 - r)\right] + (1 - r_1) r_1^n (r_1 - \Delta)^n \quad 6.5$$

Thus variation in the alignment of either coupler will appear as an apparent rotation rate. Increasing the reflectivity of the mirrors and hence the finesse of the resonator would make the contribution from higher-order reflections more significant: this is the basis of the resonant ring gyroscope.

For simpler sensors, such as the Mach-Zehnder the same consideration merely gives rise to a reduction in modulation depth or, if the phenomenon varies with time, noise in the signal. It is thus apparent that the alignment grooves should be on the same substrate as the integrated optical waveguides. This would make the initial alignment a trivial affair and would render the coupling efficiency immune to changes in temperature. Such a mechanism was in fact proposed by Maclaughlin (ref 17) and is illustrated in figure 4. The method has also been used to align fibres with photochromic waveguides in organic substrates, where wet chemical etching through photolithographically defined masks is easily performed (ref 18). However, the deeper grooves required with lithium niobate, and the absence of directional etching as compared with say silicon, require an alternative fabricational method to be used.

6.3 Design Considerations

Argon ion beam milling, a non-reactive technique, has been demonstrated to yield controllable, repeatable erosion of lithium niobate substrates (refs 19,20,21). The process is characterised by a well defined beam-energy and direction. The argon ions remove material in a way analogous to sandblasting of buildings. In both cases, material with a clear path to the source is removed, at rates which will in general vary according to the materials. Metals are quickly eroded (indeed, this may be used as an alternative method to lift-off in patterning titanium prior to diffusion into lithium niobate substrates). Suitable materials are plastics having a high carbon content, yielding a minimal amount of re-sputtered material. Thick polyimide layers have been used with success, however they are eroded at a rate approximately twice that of lithiun niobate. Thus, in order to

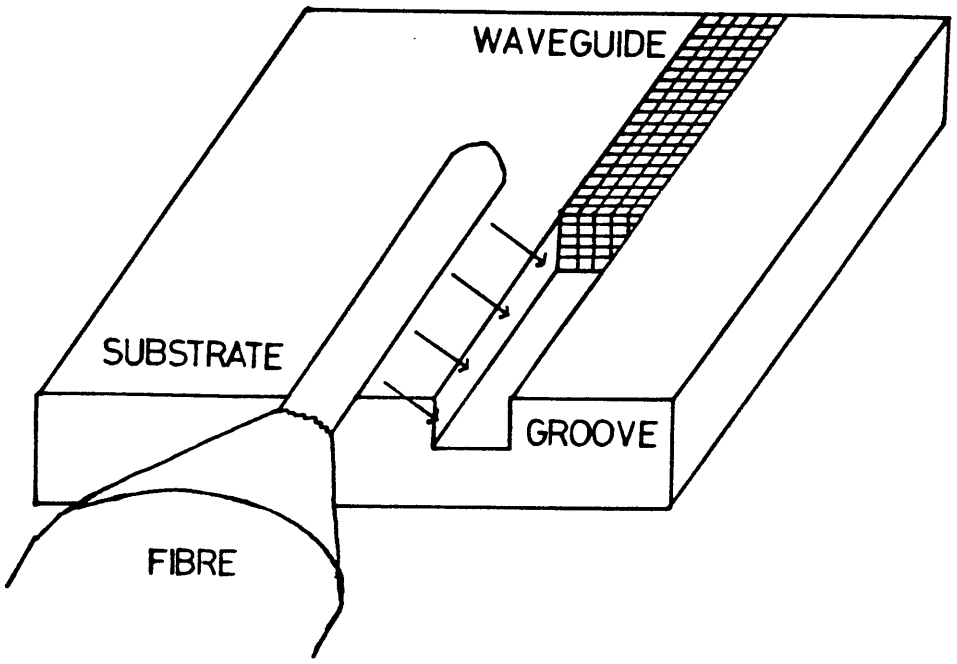

FIG 4 SCHEMATIC DIAGRAM OF ION-MILLED COUPLING ARRANGEMENT.

define grooves of say 10μm depth, approximately 20μm of masking material would be required. Any pattern delineated in the polyimide mask will be replicated exactly in the lithium niobate, including any imperfections.

Practical considerations dictate a limit of 20 microns for the final thickness of polyimide which may be produced. Since the maximum depth of groove which may then be fabricated is approximately 10μm, it will be necesary to reduce the diameter of the fibre accordingly. Most commercially available fibres have a cladding diameter of approximately 125μm, although minor vaiations with length and between sample batches are common. Thus a large fraction of the fibre must be removed.

6.4 Location groove fabrication

The experimental processes required are illustrated in figure 5. The substrate, cleaned as described in chapter 2 is coated in polyimide. This is performed by dissolving 20% polyimide by weight in a 156/100 by volume solution of acetophenone and xylene. Spinning at 2000 rpm for 1 minute yields the required final thickness. Unfortunately the solution is extremely thick, having approximately the consistency of treacle, and may not therefore be filtered to remove impurities. Heating the sample to 150^{o}C for 30 minutes , followed by 60 minutes at 250 ^{o}C drives off excess solvent to leave the polyimide. This may then be cross-linked by maintaining the sample at 350^{o}C for 90 minutes. Successful completion of the process is indicated by a lilac colour compared to the original yellow of the polyimide.

Patterning of the mask is accomplished by coating the polyimide with approximately 1μm of aluminium by standard thermal evaporation. This is then coated with photoresist as described in chapter 2. Standard exposure with dark-field masks is then used to yield a "clear" area where the final groove is required. Etching with standard aluminium etch removes the aluminium in the exposed region, after which the remaining photoresist may be removed by immersion in acetone. It is important to avoid the use of ultrasonic baths at this stage as the polyimide layer has a tendency to lift away from the substrate.

The next stage in the fabrication process is the removal of the polyimide in the region in which the final groove is desired.

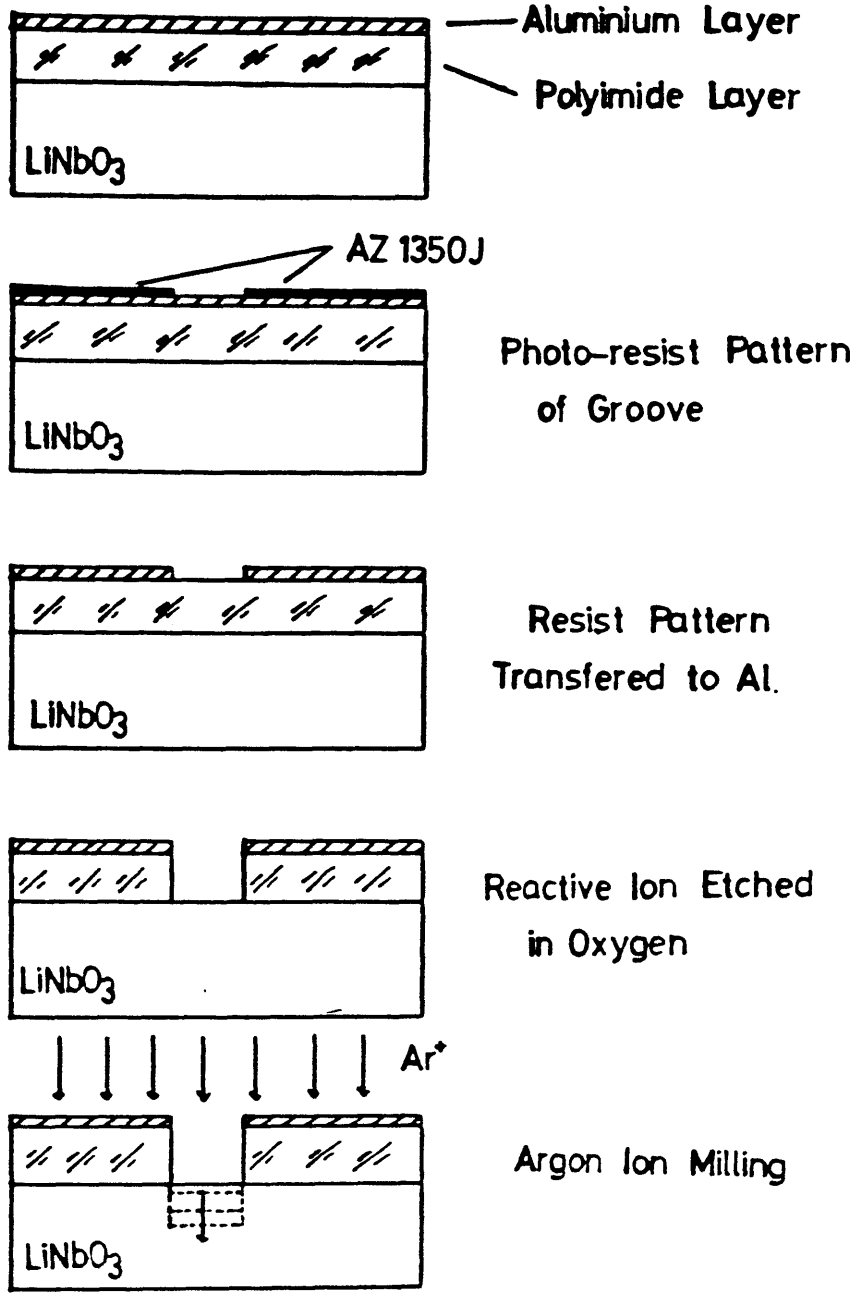

FIG 5 ILLUSTRATING THE FORMATION OF ION-MILLED GROOVES.

The polyimide forms the masking layer for the subsequent groove fabrication, thus a well-defined pattern in the former is essential. Reactive ion etching in oxygen provides vertical walls, the edge definition of which is dictated by the original photolithographic definition. A photograph of a patterned polyimide mask is shown in ref 20.

The final step in the groove fabrication is the etching of the substrate itself. A 1KeV energy beam of argon ions (Ar^+) with a beam current density ranging from 0.6 to 1.0 mA/cm^2 was incident normal to the crystal surface. The rate of etching of the substrate is a sensitive function of the beam current density; while this effect may be calibrated, to ensure repeatable results it is necessary to continuously adjust this variable during the process. Typical etch rates obtained for the process are 45nm/min. The residual aluminium at the start of the milling process is quickly removed, the selective etching being determined by the polyimide masking layer.

The final groove wall quality is determined by the definition at the initial photolithographic stage. A photograph of a completed groove is shown in ref 20. A small ridge of re-sputtered $LiNbO_3$ formed at the upper corner of the groove may be removed by scrubbing the substrate with detergent using a soft plastic sponge. In practice, it was found difficult to obtain a high quality corner in the groove plan view, thus the cross-groove seen in ref 20 was used. This would enable the fibre to be pushed to the end of the groove at a later stage.

6.5 Fibre preparation

As even with the large polyimide thickness used, the maximum groove depth was approximately 10μm, it would not be possible to locate the fibre directly in the groove. Thus it was necessary to etch the fibre to a suitably small diameter. This process was carried out by Dr A.McDonach, and the exact experimental condtions required are detailed in ref **19,20,21.** Using a variety of mixtures of nitric and hydrofluoric acids and water, repeatable etching of the initally 100 μm fibre suppied by British Telecom (core diameter= 3.88um, single mode at 1.3 micron wavelength) was demonstrated. Monitoring of the process led to a final tolerance of ±0.5μm in the diameter.

The etching process damages the end face of the fibre due to the inhomogeneity across the fibre diameter. While it may be possible to use this to advantage, eg. in the fabrication of microlenses, for the purposes of this experiment it was desired to use a flat end-face. The fibre was therefore polished as described in refs 19,20,21 by potting with soft wax in a glass capillary tube, which is then polished normal to its axis. The fibre may then be removed by immersion in trichloroethane if desired.

6.6 Integrated optical waveguide selection and fabrication

As was discussed in chapter 5, the power transferred between two optical waveguides depends on, among other parameters, the relative distributions of the two optical fields concerned. It will therefore be important in the fabrication of a low-loss coupler to minimise this constituent loss. Since the desired geometrical properties of the fibre had already been obtained via the etching properties, it was decided to optimise the integrated optical waveguide to achieve maximum power transfer from this fibre. The waveguide design may be performed using the field overlap calculation described in chapter 5.

In this case, a series of 8 stripe guides of widths between 2 and 10 μm and initial thickness 87nm were diffused in a flowing wet argon atmosphere for 40 hours with the substrate cooling in flowing wet oxygen as shown in figure 6. These guides were fabricated on a separate sample of z-cut $LiNbO_3$, using the processes described in chapter 2. The resulting guides, once polished for end-fire coupling, were excited with a semiconductor laser operating at 1.3 micron wavelength. The resulting near-field profiles were imaged onto the infra red sensitive vidicon tube in the usual way, and the data recorded. The field profiles of the fibre to be used were also recorded, both before and after etching of the cladding. The overlap calculation was performed as described in chapter 5 for both etched and unetched fibres with each titanium indiffused waveguide. The resulting values of the power transfer coefficient are shown in figure 7.

The error bars drawn represent an estimate of the effect of the error mechanisms detailed in chapter 5. While the large spread of values precludes the selection of any one waveguide as

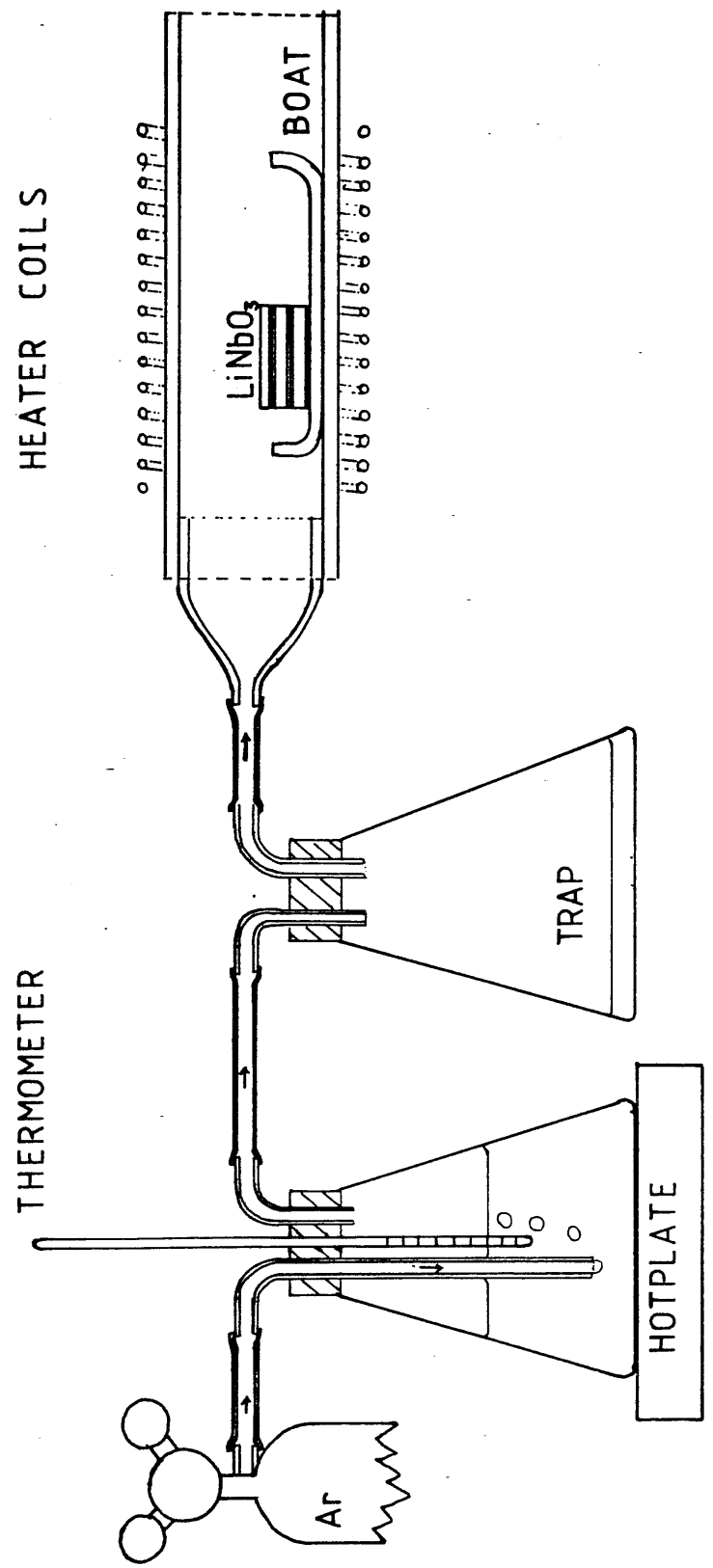

FIG 6 EXPERIMENTAL ARRANGEMENT FOR FABRICATION OF TITANIUM INDIFFUSED WAVEGUIDES IN LITHIUM NIOBATE USING FLOWING WET ARGON TO SUPPRESS Li_2O OUTDIFFUSION.

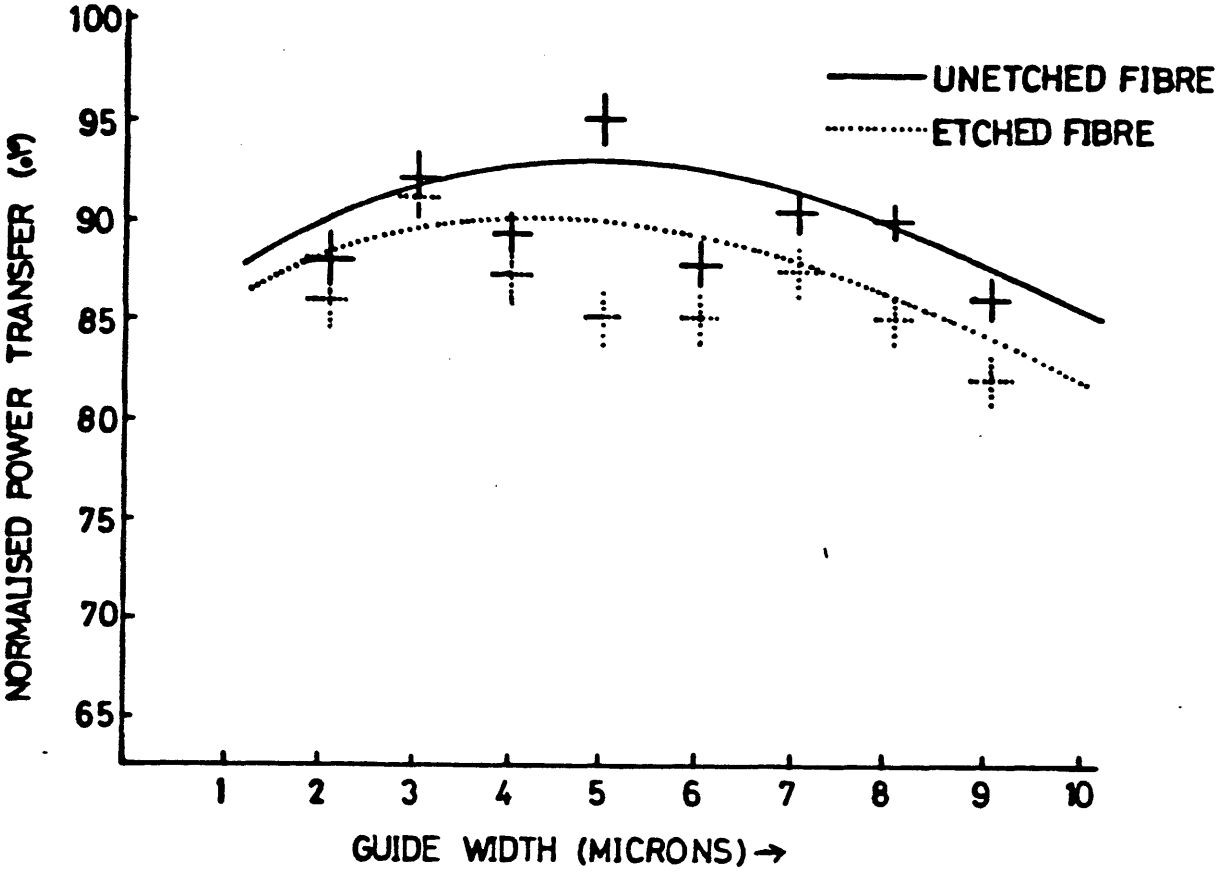

FIG 7 A COMPARISON OF THE POWER TRANSFERRED BETWEEN OPTICAL FIBRE AND INTEGRATED STRIPE GUIDE FOR BOTH ETCHED AND UNETCHED FIBRES AND A RANGE OF GUIDE WIDTHS.

the most suitable, it is evident that the width of the initial titanium strip should be between 3 and 8μm for efficient transfer. It is also seen that etching the fibre causes a drop in power transfer of approximately 5%. It is to be emphasised that selection of different diffusion times, temperatures, conditions etc. may yield differing results from those presented here.

6.7 Measurement of coupler performance

The experimental arrangement used to test the coupler is shown in figure 4. The fibre, held in a glass capillary tube, is mounted on a combination of rotation and translation stages arranged to give movement with a resolution of 0.1μm in three orthogonal axes, and rotation in the horizontal plane. The lithium niobate device was mounted on a standard crystallographic goniometer head (supplied by **Stoe and Son GmBh**). The etched fibre was placed in the groove with the polished end-face proud of the substrate and somewhat beyond the end of the groove. Having located the shank of the fibre in the groove, drawing back the fibre allowed its end-face to locate against the ion-milled groove end-face. A second fibre resting on top of the first and at 90° to its axis provided vertical pressure to ensure mechanical stability during the measurements. The alignment was facilitated by the use of a stereo microscope used at X60 magnification. For the complete device, an insertion loss of -3.1dB was determined from fibre to output face of the integrated optical waveguide. This was measured by determining the power output from the integrated optical waveguide, and comparing it with the power emerging from the fibre before inserting in the groove.

6.8 Determination of constituent loss mechanisms

In evaluating the usefulness of the coupler, and to be able to improve the coupling efficiency, it is important to determine the magnitudes of the constituent losses. From a knowledge of the Fresnel losses involved, one can calculate the coupling loss alone to be -2.6dB for fibre to integrated optical waveguide as shown in table 1. The power loss due to modal mismatch has already been discussed, a minimum value of -0.5 dB being obtained in this case. The loss due to the fibre resting in the milled groove was determined by holding the etched fibre in a separate

Table 1- Constituent Losses in Ion Milled Coupler

Calculated Fresnel reflection loss- waveguide ends, 2x 0.68dB	1.36dB
Measured groove scattering loss	0.5dB
Calculated field overlap	0.51dB
Measured taper loss	0dB
Total	2.37dB
Measured value	3.1dB
Remainder (due to end-face scattering etc)	0.73dB
Net coupler insertion loss	
Fresnel loss (i) waveguide end	0.68dB
(ii) Fibre end	0.16dB
Groove scatter	0.16dB
Field overlap	0.51dB
End face scatter, alignment	0.73dB
Reduction by index matching	0.76dB
Net loss with optimal index matching	1.82dB

open-ended groove and determining the excess loss, a value of -0.5dB being measured. No loss could be measured for the tapered section of the fibre. Thus as shown in table 1, the remaining loss, due to such mechanisms as end-face scattering, alignment, and waveguide attenuation is calculated to be 0.73dB. It is also seen that the use of an optimum index matching fluid between the fibre and the titanium indiffused waveguide would reduce the unmatched value of -2.6dB to -1.8dB.

6.9 Discussion

A rugged device has been demonstrated for coupling between titanium indiffused waveguides in lithium niobate, and optical fibres. While the losses of initial devices have been determined at 1.3μm wavelength to be -2.6dB, attention to groove quality and index matching should yield significantly improved performance. The groove quality is limited by the photolithographic exposure used in the fabrication. It is envisaged that electron beam exposure with the appropriate resists would yield smoother walls and thus improve the situation, if the shorter groove length could be tolerated. Experimentation with different waveguide fabrication parameters, such as diffusion time, initial titanium thickness etc. may reduce the 0.51dB modal mismatch loss. Adjustment of the waveguide fabrication parameters may however incur increased waveguide loss due to scattering. The excess loss of the device may vary with wavelength- this has not been investigated.

The coupler could be made mechanically rigid by the use of, for example, epoxies. However, care must be taken that capillary action does not lift the etched fibre out of the groove. The method would be applicable to other substrates, eg, semiconductors, glasses . In addition, the method would lend itself to mass production, should integrated optics reach such a stage. The coupling efficiecy of an array of fibres connected to a corresponding array of integrated optical waveguides should be immune to the otherwise adverse effects of temperature. The method would appear to be ideal for coupling the fibre sensing coils to an integrated optical implementation of the processing system of a fibre optic gyroscope.

The long-term mechanical stability of the device has not

been determined. As discussed in this chapter, unstable coupling may have an adverse effect on the performance of an integrated optical/fibre optical gyroscope using the component.

Note: Andonovic et al (Barr and Stroud Ltd) have recently demonstrated the application of the method to coupling between an integrated optical frequency shifter and a birefringent fibre obtaining comparable losses.

References

6.1 Bludau,W, Rossberg,R.H, "Low Loss Laser to Fiber Coupling with Negligible Optical Feedback", Journal of Lightwave Technology, Vol LT-3, No 2, 1985 pp294-302

6.2 Alferness, R.C., Ramaswamy, V.R., Korotky,S.M., Divino,M.D, Buhl,L.L, "Efficient Single Mode Fibre to Titanium Indiffused Waveguide Coupling for l=1.32um" IEEE Journal of Quantum Electronics, QE-18, pp.1807-1812 ,1982

6.3 McCaughan,L, Murphy,E.J, "Influence of Temperature and Initial Titanium Dimensions on Fiber-Ti:$LiNbO_3$ Waveguide Insertion Loss at l=1.3 um", I.E.E.E. Journal of Quamtum Electronics, Vol QE-19, No 2, pp131-135, 1983

6.4 Bulmer,C.H, Sheem,S.K, Moeller,R.P, Burms,W.K, "High Efficiency Flip-Chip Coupling Between Single Mode Fibers and $LiNbO_3$ Channel Waveguides", Applied Physics Letters, Vol 37, No 4, pp351-353, 1980

6.5 Noda,J, Mikami,O, Minakata,M, Fukuma,M, "Single Mode Optical Waveguide Fiber Coupler", Applied Optics Vol 17, No 13, pp2092-2096, 1978

6.6 Cameron,K.H, "Simple and Practical Technique for Attaching Single-Mode Fibres to Lithium Niobate Waveguides" Electronics Letters, Vol. 20 No. 23 pp974-976, 1984.

6.7 Campbell,J.C, "Coupling of Fibers To Ti-Diffused $LiNbO_3$

Waveguides by Butt- Joining", Applied Optics, Vol 18, No 12, pp2037-2040, 1979

6.8 Bulmer,C.H., Sheem,S.K, Moeller R.P, Burns,W.K, "Fabrication of flip-chip couplers between single-mode fibres and diffused channel waveguides", Applied Physics Letters Vol.37, pp351-355, 1980

6.9 Murphy,E.J, Rice,T.C, "Low Loss Coupling of Multiple Fiber Arrays to Single Mode Waveguides", Journal of Lightwave Technology, Vol LT-1, No 3, 1983 pp479-482

6.10 Hsu,H.P, Milton,A.F, "Single Mode Coupling Between Fibers and Indiffused Waveguides", I.E.E. Journal of Quantum Electronics, Vol QE-13, No 4, pp224-233, 1977

6.11 Fukuma,M, Noda,J, "Optical Properties of Titanium-Diffused $LiNbO_3$ Strip Waveguides and their Coupling to a Fiber Characteristics", Applied Optics, Vol 19, No 4, 1980, pp591-597

6.12 Ramaswamy,A, Alferness,R.C, Divino,M, "High Efficiency Single Mode Fibre To Ti:$LiNbO_3$ Waveguide Coupling", Electronics Letters, Vol 18, No 1, pp30-31, 1982

6.13 Ramer,C.G, Nelson,C, Mohr,C, "Experimental Integrated Optic Circuit Losses and Fiber Pigtailing of Chips", I.E.E. Journal of Quantum Electronics, Vol QE-17, No 6, 1981, pp970-974

6.14 Sheem,S.K, Giallorenzi,T.G, "Two Dimensional Silicon Grooves for Altiduninal Alignment in Fiber End Butt Coupling", Optics Letters, Vol 3, No 3, pp73-75, 1978

6.15 Rauber, Chemistry and Physics of Lithium Niobate, Current Topics in Materials Science, F.Kaldis Ed, 1978

6.16 American Institute of Physics Handbook

6.17 Maclaughlin, A, Ph.D. Thesis, University of Glasgow 1981

6.18 Bennion,I, Hallam,A.G, Stewart,W.J, "Optical Waveguide Components in Organic Photochromic Materials", The Radio and Electronic Engineer, Vol 53, No 9, 1983 pp313-317

6.19 Nutt, A.C.G., Bristow,J.P.G, McDonach,A, Laybourn P.J.R."Fibre to waveguide coupling using ion-milled grooves in Lithium Niobate at 1.3um wavelength" Optics Letters Vol.9,pp463-465, 1984

6.20 Bristow,J.P.G, Nutt,A.C.G, McDonach,A, Laybourn,P, "Coupling Fibres to Integrated Optical Waveguides", I.E.E. Proceedings J-Optoelectronics, Vol 1, No 5, October 1985

6.21 Nutt,A.C.G, Bristow,J.P.G, McDonach,A, Laybourn,P.J.R, "Efficient Fibre to Chip Coupling Using Ion Milled Alignment Grooves", 7th Topical Meeting on Integrated and Guided Wave Optics, Kissimee, Florida, April 1984

6.22 Schurcliff,W.A, "Polarised Light", Oxford, 1962

Chapter 7- Processing the Signals from the Single Fibre Polarimetric Sensor: Detection Schemes and Component Requirements

7.1 Introduction

The single fibre polarimetric sensor, described in chapter 1 offers considerable advantages in terms of improved cross-sensitivity and simplicity of construction over other configurations (ref 1,2,3). The sensors may also be manufactured in localised rather than distributed form (ref 4). In its simplest form, detection of the measurand is accomplished by exciting with equal amplitude the two degenerate eigenmodes of a highly birefringent fibre and examining the interference term between the two beams. The intensity is then a periodic function of the measurand affecting the fibre, as indeed it would be for the equivalent Mach-Zehnder interferometer. Methods of retrieving the phase term, and the effect of variation in power splitting ratio vetween the two modes were considered in chapter 1. Problems associated with even a perfect implementation of the technique are:

(i) The periodic nature of the output, and resultant ambiguity unless fringe-counting and tracking techniques are used, and

(ii) The high dynamic range: for a versatile system we require high accuracy of detection (say 0.01^0C for a temperature sensor) but with a large range of signal (say 100^0C for process applications).

Heterodyne and closed-loop detection schemes may overcome the second problem: such techniques have also been used with advantage with optical fibre gyroscopes. Kersey (ref 4) has reported immunity of input and output leads to the measurand using a particular geometry: he also reports the use of frequency switching and frequency ramping to generate pseudo-heterodyne outputs. A change in the differential polarisaton mode delay $\Delta\Phi$ is given by $\Delta\Phi=2n\Delta l\Delta\nu/c$ where $\Delta l=LB=Ll/L_p$, B is the birefringence (ref 6) and L the fibre length. L_p is the optical beat length, ie the length of fibre over which the relative modal delay changes by 2π. Switching the source by $\Delta\nu=\nu_1-\nu_2$ gives outputs of the form

$(1+\cos\Phi)$ and $(1+\sin\Phi)$, provided $L_o=l_p c/l\Delta\nu$, or any odd multiple thereof. This imposes restrictions on either the fibre length (and thus on the sensitivity) or on the two sources which must be used. Subsequent electronic processing yields an output of the form $\sin(w_c t-\Phi)$. Alternatively, the frequency of the source may be modulated, either directly or externally to drive the output over the $(1+\cos\Phi)$ fringe. However, compensation for variations in source intensity must be made in the signal processing system.

7.2 Improved system configuration

A new method of processing the signal from this type of sensor will now be described. The method makes use of integrated optical components, although an all fibre-implementation would also be possible. The sensor operates in a closed-loop configuration, giving an essentially analogue output. The sensitivity of the system will be shown to be high: the dynamic range is limited by available components and an intrinsic limitation of the technique. For an ideal arrangement, the apparent value of the measurand is independent of source intensity, although this will affect the sensitivity of the system. The method is ideal for the detection of DC measurands. Appropriate selection, and possibly coating, of the fibre will enable such measurands as pressure, strain and magnetic field to be detected.

Consider the system shown in figure 1. We assume unit field amplitudes excite with equal strength the two eigenmodes of a fibre with high intrinsic birefringence (ref 6,13). The frequencies of the two beam are made to differ, ie we have f_1 and f_2 where $f_1=f_2+\Delta f$. The phases of the light beams leaving the fibre are :

$$\varphi_1 = n_1 k_1 L \qquad 7.1$$

$$\varphi_2 = n_2 k_2 L \qquad 7.2$$

If the two beams were initially in phase, the output,

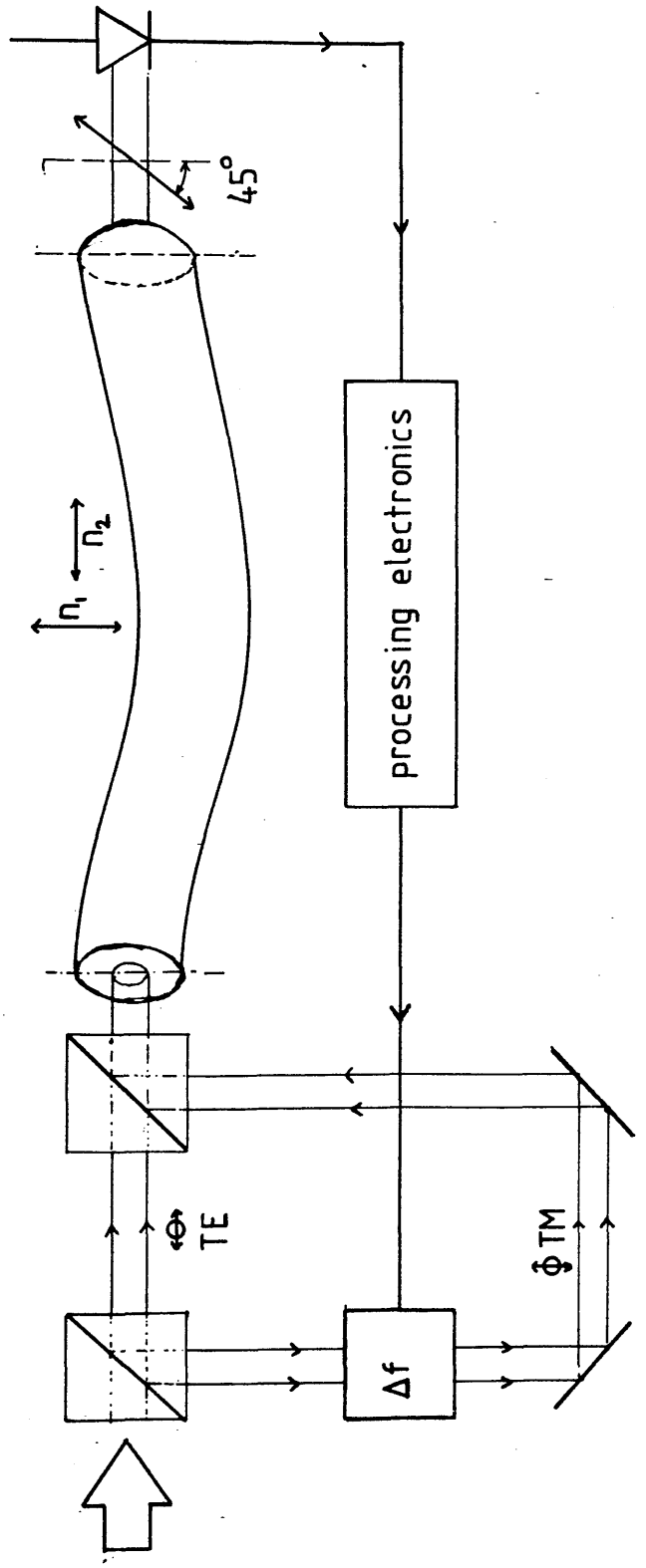

FIG 1 CLOSED LOOP DIFFERENTIAL MODAL FREQUENCY OPERATION OF THE SINGLE FIBRE POLARIMETRIC SENSOR - SCHEMATIC DIGRAM

proportional to $(1+\cos(\Phi_1-\Phi_2))$, would be such as to minimise the sensitivity of the sensor. Thus a $\pi/2$ bias is introduced for DC detection schemes. Any noise in this bias will appear as noise in the detected signal. The bias may also be accomplished by a given fixed relative frequency shift of the beams. We now consider the refractive indices to depend upon wavelength and some external influence. The choice of the latter is unimportant: we use temperature in this example, but selection of the appropriate coefficients would give a similar analysis for pressure, strain etc. The changes of phase are then:

$$\Delta\varphi_1 = \frac{2\pi f_1 L}{c}\left(\frac{\partial n_1}{\partial T}\right)\Delta T + \frac{2\pi f_1 n_1}{c}\left(\frac{\partial L}{\partial T}\right)\Delta + \frac{2\pi f_1 L}{c}\left(\frac{\partial n}{\partial \lambda}\right)\Delta\lambda \qquad 7.3$$

and

$$\Delta\varphi_2 = \frac{2\pi f_2 L}{c}\left(\frac{\partial n_2}{\partial T}\right)\Delta T + \frac{2\pi f_2 n_2}{c}\left(\frac{\partial L}{\partial T}\right)\Delta T + \frac{2\pi f_2 L}{c}\left(\frac{\partial n_2}{\partial \lambda}\right)\Delta\lambda \qquad 7.4$$

Suppose now we wish to vary the frequency f_2 to "null" the resulting phase change, ie we require $\Delta(\Phi_1-\Phi_2)=0$, expanding the above expression and gathering like terms yields:

$$0 = \frac{2\pi f_2 L}{c}\left(\frac{\partial B}{\partial T}\right)\Delta T + \frac{2\pi f_2 B}{c}\left(\frac{\partial L}{\partial T}\right)\Delta T + \Delta f\frac{2\pi}{c} L\frac{\partial n_1}{\partial T}\Delta T + L\frac{\partial n_1}{\partial \lambda}\Delta\lambda + n_1\frac{\partial L}{\partial T}\Delta T \qquad 7.5$$

Where $B=n_1-n_2$ is the modal birefringence, and the dispersion affects only the mode with changing frequency. Further, we assume that no cross-coupling exists along the fibre length. If we assume that the dispersion term is zero, and the terms describing change in birefringence are much smaller than those affecting the change in length, we obtain:

$$\Delta f = \frac{f_2 B}{n_1} = f_2\frac{(n_1-n_2)}{n_1} = f_2\left(1-\frac{n_2}{n_1}\right) \qquad 7.6$$

Thus the relative frequency difference required to maintain the null depends on the refractive index (a function of temperature),

and is independent of length. The sensitivity will of course depend on the length. A similar result is also obtained for the phase nulling fibre optic gyro (ref 9).

7.2.1 Magnitude of frequency shift required

For an optical source of wavelength 1 micron and assuming $dn/dT=1\ 0^{-6}$, with core indices approximately 1.46, the frequency shift required to null the phase difference arising from a change of temperature is given approxiamately by:

$$\Delta\phi \simeq 2\times10^{8}\,\Delta T\,(^{\circ}C) \qquad 7.7$$

7.2.2 Implementation

The large frequency shift required for high dynamic range operation imposes considerable requirements on the optical device used to perform the function. Fibre optic implementations reported to date have relied on PZT (lead zirconium titanate) (ref 5) transducers. These tend to have low bandwidth and uneven frequency responses. Bulk devices relying on either the acousto-optic or electro-optic effects (ref 7) are available with the required performance, but are inappropriate for low-cost or mass-produced systems. Integrated optics however is highly suitable. Frequency shifters have been demonstrated on lithium niobate with shifts of up to 20GHz being predicted in serrodyne arangements (ref 8). This would lead to a range of temperatures of $100^{0}C$ with which the system could cope. A possible implementation is shown in figure 2. It is noted that a considerable complexity of processing electronics is needed.

Two orthogonal modes of a titanium indiffused guide are selected on separate guides. The polarisation operation is performed as close to the fibre as possible to minimise mode mixing in the integrated optical guide (ref 11). One beam is shifted in frequency by a serrodyne frequency translator (ref 12). Upon launching into the short titanium indiffused guide, no interference between the modes will take place due to their othogonality. Thus one unshifted mode and the orthogonal, shifted

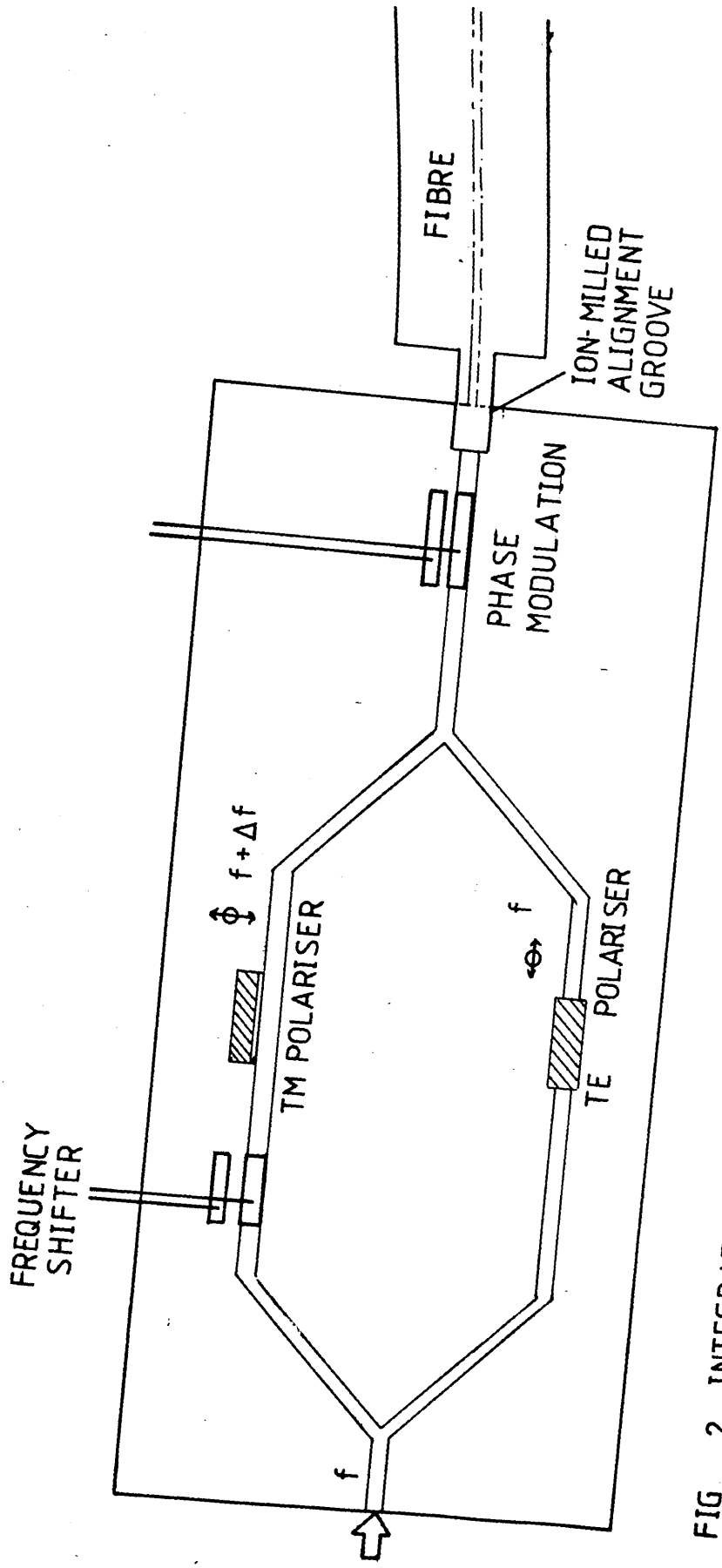

FIG 2 INTEGRATED OPTICAL IMPLEMENTATION OF CLOSED LOOP DIFFERENTIAL FREQUENCY OPERATION OF SINGLE FIBRE POLARIMETRIC SENSOR

mode are launched into the fibre. Detection is simply accomplished by coupling the return lead to the polarising receiver guide with the axis rotated by 45^0 and using a photodetector. The frequency shift is then altered to improve the null of the signal. Upon successful nulling, the frequency shift used is recorded. The phase modulator shown serves to impose a sinusoidal relative phase delay between the two modes: this will aid detection of DC measurands.

7.2.3 Adverse effects on system performance

Several effects will operate to reduce the sensitivity of the system. They are:

(i) mode-mixing in the launching section (titanium indiffused guide),

(ii) coupling between the modes along the fibre: this is minimised by the use of fibre with very high birefringence

(iii) sidebands being present in the shifted signal

7.2.4 Effect of partially non-shifted beam and unwanted frequency components

Suppose that the frequency shifter is imperfect: a fraction (1-A) of the light is shifted, while a fraction A is at some other frequency f_3. Thus f_1 in expression 7.3 is replaced by

$$(1-A)f_1 + Af_3 \qquad 7.8$$

Expansion as previously descibed yields for the required frequency shift:

$$\Delta f = \frac{f_2(n_2 - n_1(1-A))}{n_1(1-A)} \quad \frac{-Af_3}{n_1(1-A)} \qquad 7.9$$

If f_3 represents the unshifted beam, the second term on the right hand side constitutes a constant error term. Provided this is stable, for a given system this may be calibrated out, merely affecting the sensitivity. If f_3 is a harmonic of f_1, the results

will be corrupted, while for a harmonic of f_2 (say due to light propagating in the substrate at the unshifted frequency) a constant error term will be present. Due to the small magnitude of the numerator of the first expression on the right hand side of 7.9, we require A to be extremely small, ie sidebands and unshifted components must be well suppressed.

7.2.5 Effect of imperfect mode selection

To investigate the effect of imperfect mode selection via the polarisers, we consider the model shown in figure 3. Field amplitudes A and B, where B<<A, are present at the unshifted frequency f_1, while amplitudes C and D where D>>C are present at the shifted frequency f_2. A and B are aligned along one of the axes of the birefringent fibre with mode index n_1, while C and D are associated with the orthogonal modes and mode index n_2. Thus the field associated with n_1 is

$$E_{norm} = Ae^{2\pi i f_2 n_1 L} + (1-D)e^{2\pi i f_1 n_1 L} \qquad 7.10$$

$$E_{perp} = (1-A)e^{2\pi i f_2 n_2 L} + De^{2\pi i f_1 n_2 L} \qquad 7.11$$

Where we have set A+B=1 and C+D=1. If the analysing polariser is orientated at 45^0 to the fibre axes, the detected intensity I is

$$I \propto \left| E_{perp} + E_{norm} \right|^2 \qquad 7.12$$

With some algebraic manipulation, this becomes

$$\begin{aligned} I \propto\ & A^2 - D + D^2 + 1 - A \\ & + A(1-D)\cos 2\pi l (f_2 n_1 - f_1 n_1) \\ & + A(1-A)\cos 2\pi l (f_2 n_1 - f_2 n_2) \\ & + AD \cos 2\pi L (f_2 n_1 - f_1 n_2) \\ & + (1-A)(1-D)\cos 2\pi l (f_1 n_1 - f_2 n_2) \\ & + D(1-A)\cos 2\pi L (f_2 n_1 - f_1 n_2) \\ & + D(1-D)\cos 2\pi l (f_2 n_1 - f_1 n_2) \end{aligned} \qquad 7.13$$

If the polariser were perfect, this would become $\cos 2\pi l(f_2 n_1 - f_1 n_2)$ as expected. The term containing (1-A)(1-D) will be small. The effect of the (1-A)D and similar terms will in general be

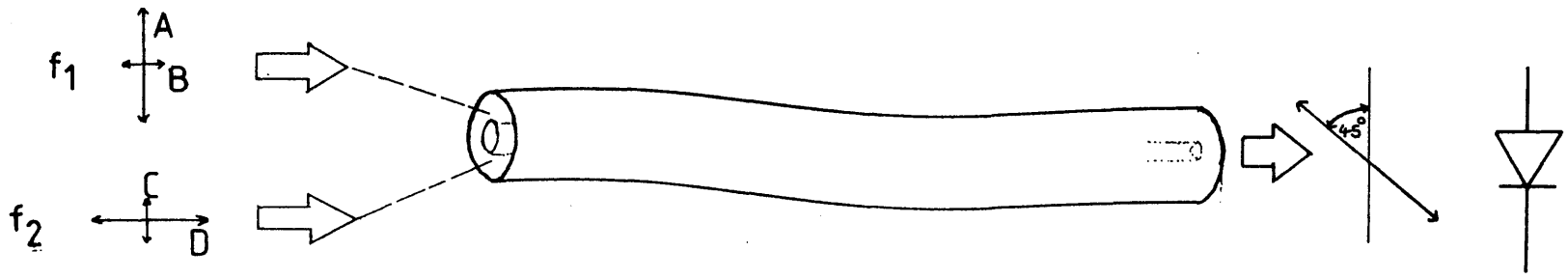

FIG 3 MODEL USED TO CALCULATE EFFECT ON PERFORMANCE OF CLOSED LOOP SINGLE FIBRE POLARIMETRIC SENSOR OF IMPERFECT POLARISERS.

corrupting, but is difficult to calculate, depending both on the extinction ratio of both polarisers and on the relative phase delay associated with the two modes.

Suppose one polariser were perfect, ie A=1, we may consider the effect on the extinction ratio of the one remaining imperfect polariser. The intensity is proportional to I where:

$$I \propto 1 - D + D^2 + (1-D)\cos 2\pi l(\beta_2 n_1 - \beta_1 n_1) + D\cos 2\pi l(\beta_2 n_1 - \beta_1 n_2) + D(1-D)\cos 2\pi l(\beta_1 n_2 - \beta_2 n_1) \quad 7.14$$

Allowing the worst case of the trigonometrical arguments gives

$$I \propto 1 - D + D^2 - (1-D) - D(1-D) - D \quad 7.15$$

This represents a deviation from the true value, the latter being given by

I = 2 -the maximum value of the argument.

thus the fractional error is $(2D^2-2)/2$. Since we may at best detect an intensity change of 10^{-6} using AC detection techniques (ref 10), the tolerable value for D is $1-10^{-6}$, or a power extinction ratio of 60dB is required. This ratio must be defined with integrated optical components and **maintained** upon launching into the fibre. It is to be emphasised that this is a worst case: however, a well-engineered system should be accurate at any value of the relative phase delay.

7.3 Integrated optical implementations: the need for selection of both TE-like and TM-like modes

In previous chapters methods have been discussed for the selection of TE-like modes of titanium-indiffused waveguides by the use of dielectric-metal overlays, and both TE and TM modes using proton exchanged waveguide sections in various configurations. It is also known that the mounting of a suitable birefringent crystal on the waveguide surface may couple a given mode out of the guide. This method is however subject to

mechanical instabilities, and would certainly not be an economic solution in a production environment. However, in processing the signal from the single fibre polarimetric sensor described above it will be necessary to define both modes on the same substrate. This may readily be accomplished by use of internal and external modification of titanium-indiffused waveguides in lithium niobate using proton exchange techniques as described in chapter 2. However, such arrangements may not be suitable due to poor coupling efficiency between the two sections, and the careful alignment required. The poor extinction ratios obtained for such devices to date preclude their incorporation into the system under consideration.

The selection of TM modes may also be desirable for systems incorporating phase modulators using Z-cut $LiNbO_3$ since the r_{33} electrooptic coefficient associated with the TM modes is significantly larger than all other elements of the matrix.

If titanium-indiffused waveguides are to be used throughout, the most promising mode selection technique would appear to be the use of dielectric and metal overlays as described in chapter 4 where extinction ratios higher than the requisite 60dB have been determined for individual devices. In this case the TM like modes were selectively absorbed by coupling to the lossy surface plasma wave excited at a dielectric-metal boundary. Using the same technique, the TE modes with respect to the crystal surface could be absorbed in the appropriate buffer layers and metals were to be deposited normal to the surface. This is likely to require more complex fabrication techniques as the surface is normally inaccessible.

7.4 Edge polishing techniques

The most obvious method of accessing the waveguide normal to the crystal surface would be to polish the edge of the sample until one had cut into the waveguide. The appropriate buffer and metal overlays could then be evaporated to yield preferential absorption of TE modes. The arrangement is shown in figure 4. Since the indiffused waveguide is extremely narrow, perhaps a few

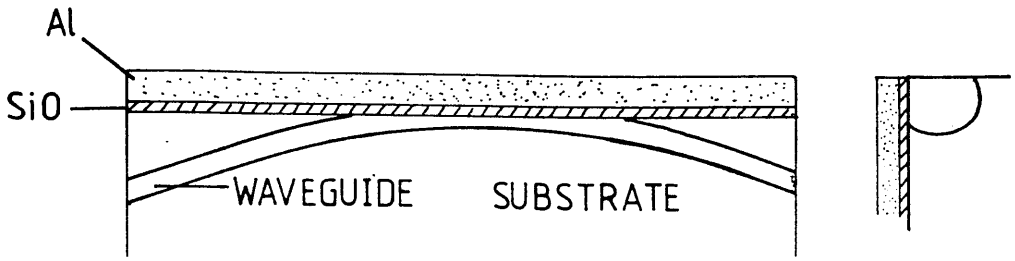

FIG 4 (a) EDGE POLISHED POLARISER USING VERTICAL DIELECTRIC BUFFER LAYER AND METAL OVERLAY (BEND RADIUS GREATLY EXAGGERATED)

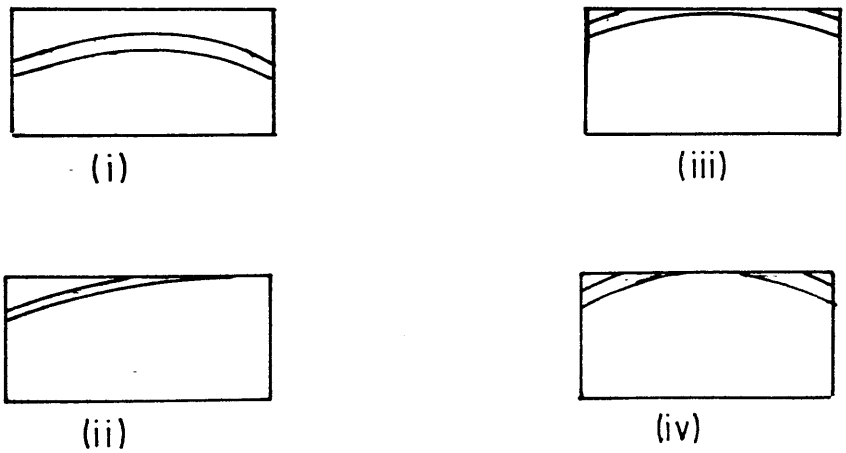

FIG 4 (b): DEFECTS ENCOUNTERED IN POLISHING OF WAVEGUIDE / SUBSTRATE BOUNDARY : (i) GUIDE TOO FAR FROM EDGE (ii) POLISHING NON-TANGENTIAL TO GUIDE (iii) MILD AND (iv) SEVERE OVER POLISHING

microns in width for a single mode guide at 1.3 micron wavelength, it would be essential to polish parallel to a straight waveguide to avoid cutting through it, as illustrated in figure 4. The requirements are made less critical by the use of curved waveguides, for any polishing angle with respect to the sample edge (within reasonable limits) , the waveguide edge will be cut at a tangent. To control the extent to which the polished edge cuts into the indiffused waveguide, it will be necessary either to monitor the polishing process, or to determine exactly the rate of removal of material. For a waveguide of 4μm width, it will be necessary to control the edge position as accurately as possible

7.4.1 Effect of variation of guide thickness on extinction ratio and insertion loss

An estimate of the variation in extinction ratio with waveguide thickness may be obtained using the computer model for the four-layer slab guide descibed in chapter 3. The program was run using the following parameters- (for a full description of the program, the reader should refer to chapter 3)

Metal-	aluminium (Weavers Data)
Buffer thickness-	0.0 to 0.2 microns
Crystal Cut-	X-cut Y-propagating
Wavelength-	1.3 microns

The results of the calculation are shown in figures 5,6,and 7, where the attenuation for TE and TM modes is shown, along with the effective index.

For TE modes, decreasing the guide thickness has the effect of increasing the attenuation, while the same decrease in attenuation with increasing buffer thickness is observed. This would be expected from consideration of the distribution of the electric field relative to the metal: surface plasmon effects are irrelevant for TE modes.

The TM modes show, with decreasing guide thickness, an

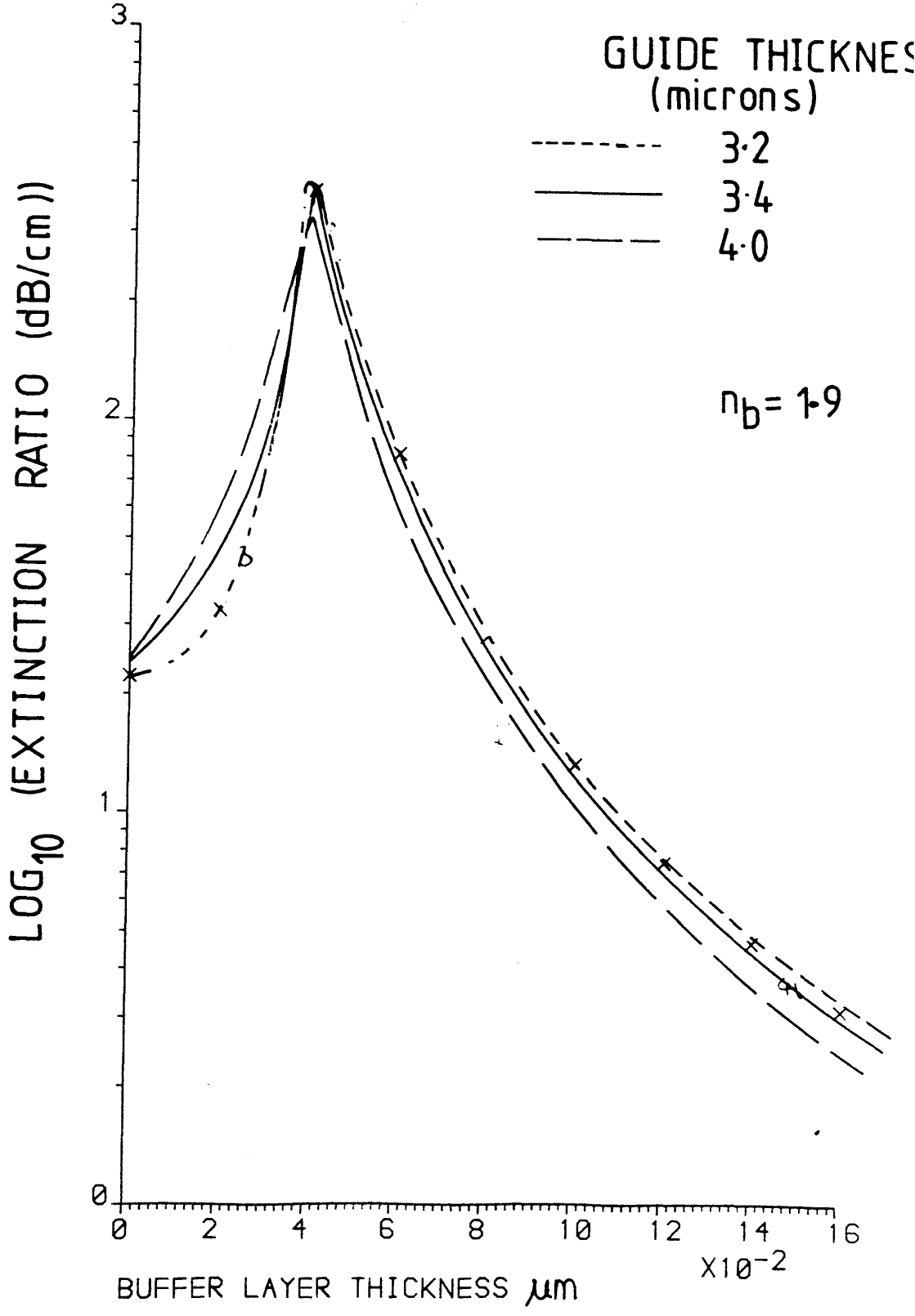

FIG 5 ATTENUATION OF TM MODES OF 4-LAYER SLAB GUIDE FOR THREE DIFFERENT WAVEGUIDE THICKNESSES.

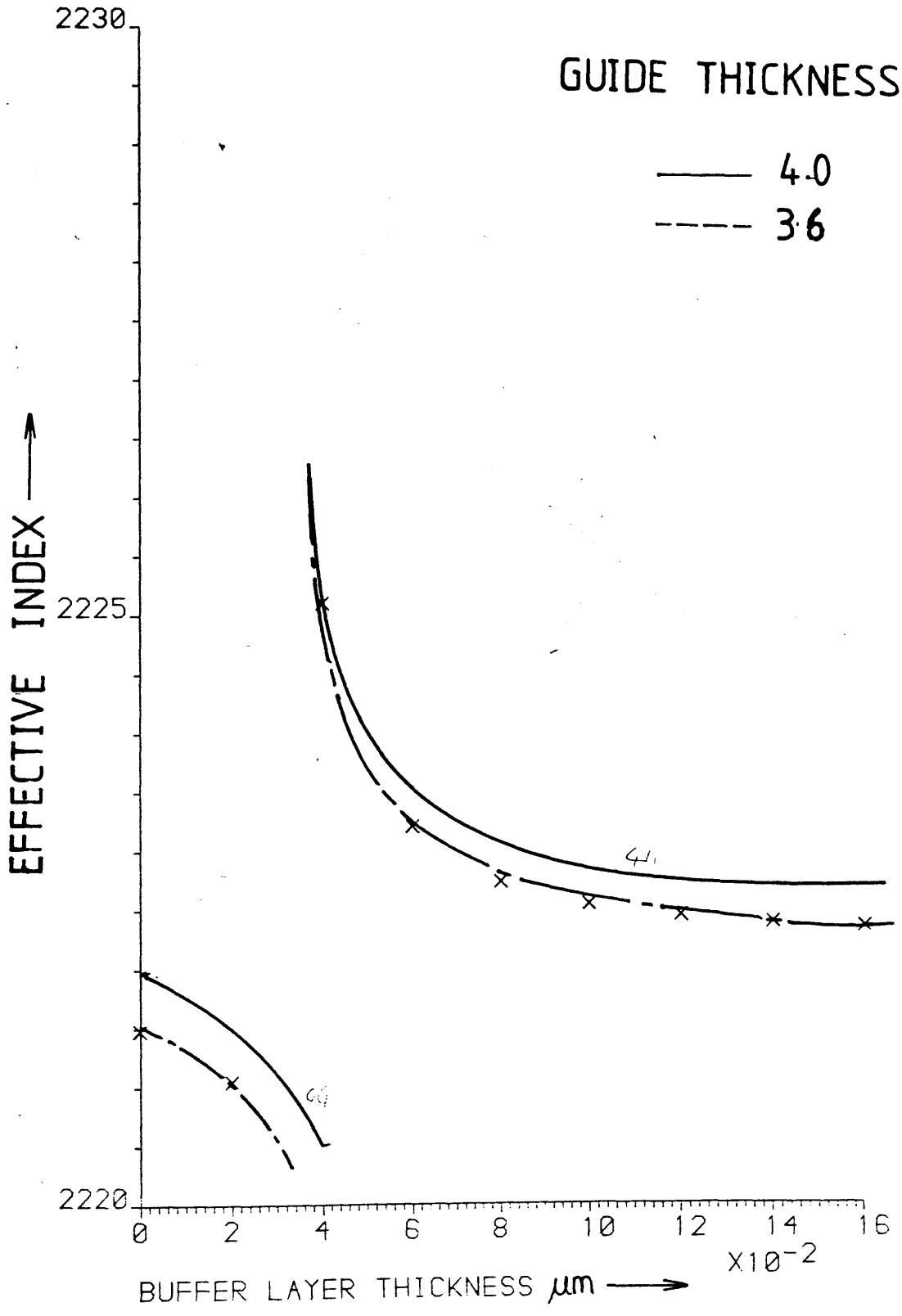

FIG 6 EFFECTIVE INDEX VS. BUFFER THICKNESS FOR TM MODES OF 4-LAYER SLAB GUIDE FOR TWO GUIDE THICKNESSES

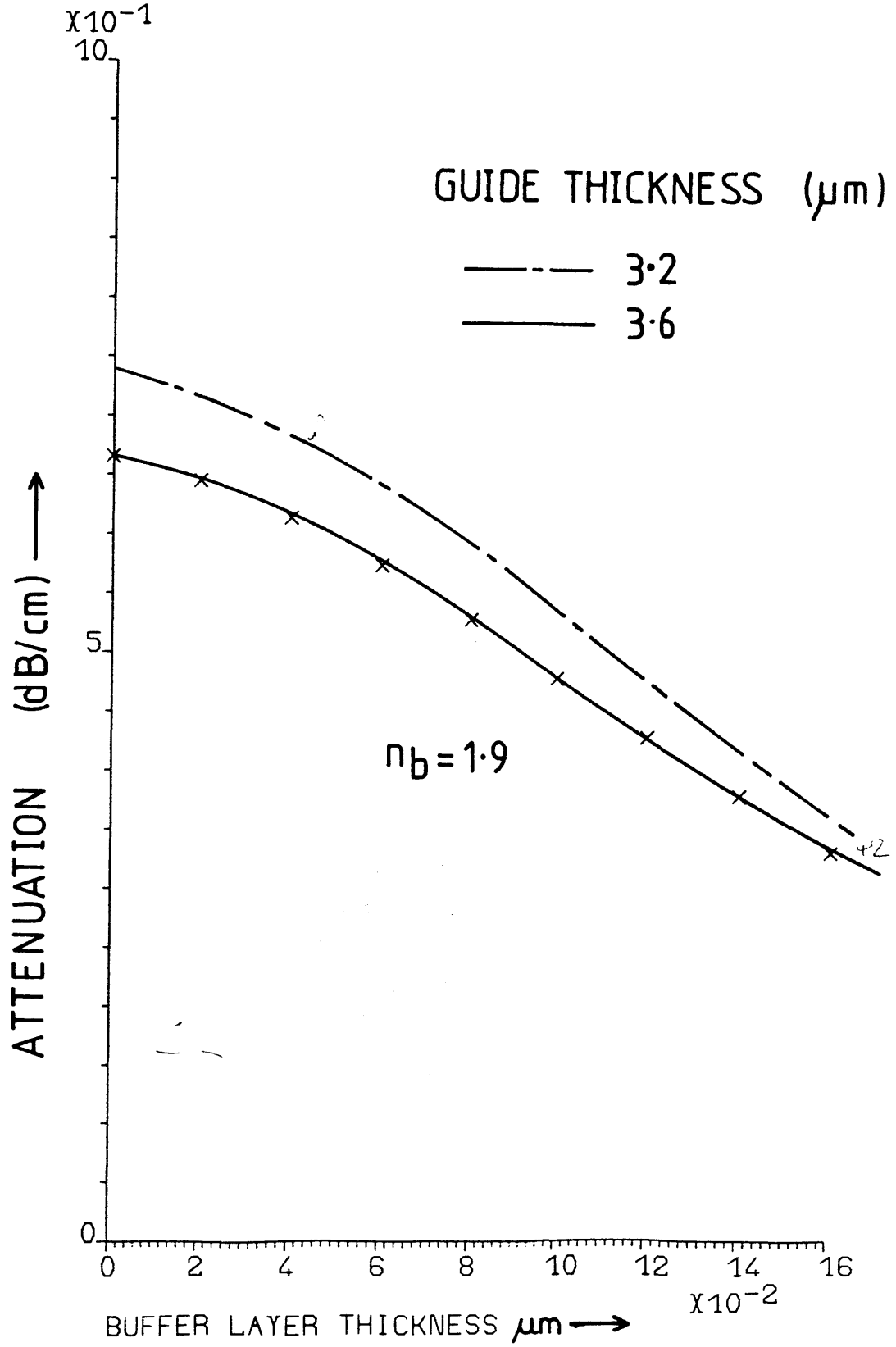

FIG 7 ATTENUATION VS. BUFFER THICKNESS FOR 4-LAYER SLAB SYSTEM - TE MODES TWO GUIDE THICKNESSES SHOWN.

increase in attenuation for all buffer thicknesses above that corresponding to the maximum attenuation, while for buffer thicknesses below this critical value, the effect is reversed. The effective index in all cases decreases with decreasing guide thickness. The qualitative trends in each case have been described in chapter 4.

It is seen that for repeatable results, and in order to be able to investigate the effect of different buffer and metal thicknesses, the polished waveguide thickness must be closely controlled.

7.5. Fabrication of edge-polished waveguides

In order to avoid large bend loss (refs 14,15), the radius of the waveguides used was chosen to be between 2cm and 4cm. A dark field chrome mask was therefore cut to these dimensions with waveguide widths of 4μm for the larger radii, increasing to 6μm for the smaller radii. The fabrication of the indiffused waveguides then proceded as described in chapter 2, a standard Z-cut substrate being used. After fabrication, the sample was polished in the normal way to leave ends approximately perpendicular to the waveguide. The samples were then remounted on the polishing rig in order to polish tangentially to the waveguides.

The polish used was **Syton W15.** It was discovered that the polishing rate was not repeatable to a sufficiently high accuracy, this depending on the previous history of the polishing bed, and the length of time for which the sample had been polished in a non-linear way. It was therefore decided to monitor the polishing process at frequent intervals. Having examined the sample to determine the amount of material to be removed, the sample was polished to within approximately 20μm of the waveguide. Examinations were performed after successive polishing times of approximately 5 minutes.

7.5.1 Experimental results

Photographs of the resulting samples are shown in figures 8

and 9. It will be seen that in no case could the desired structure be obtained. Two classes of defects are seen;
(1) The polished edge is either too far away from, or too far into, the waveguide.
(2) The polishing has taken place at too steep an angle and the waveguide has been cut as a result.

The second class of defect is a result of poor alignment of the waveguide with respect to the crystal surface. This could be rectified by the use of a mask with alignment marks parallel to the tangents to the waveguides as shown in figure 10. However, it is to be noted that no provision for fine alignment is provided on most polishing rigs, and the utmost care would therefore be required when mounting the sample. The first class however represent a more serious limitation of the technique. Using even a relatively fine polish, it was not possible to control the polishing rate to the required accuracy. In addition, the ability to repeat the alignment to the same position is questionable, thus making it difficult to investigate the variations in device performance with differing buffer and metal parameters.

Due to the limitations described above, it was not possible to fabricate a polariser using this technique.

7.5.2 Conclusions

While the edge polishing technique would yield a highly polished surface normal to the crystal plane, the process is not sufficiently controlable to enable polarisers to be constructed. In addition, the inability to repeat the alignment would make it difficult to optimise the devices with respect to fabricational parameters. Further work may however yield improved results; the polishing process was originally developed for applications where fine control of the amount of material removed is not required (eg. for end-fire coupling).

A method involving reversal of the polishing and waveguide fabrication processes, ie. aligning the waveguide to a previously polished edge, was considered. However, the induced roughness due to outdiffusion (ref 19) would have necessitated further

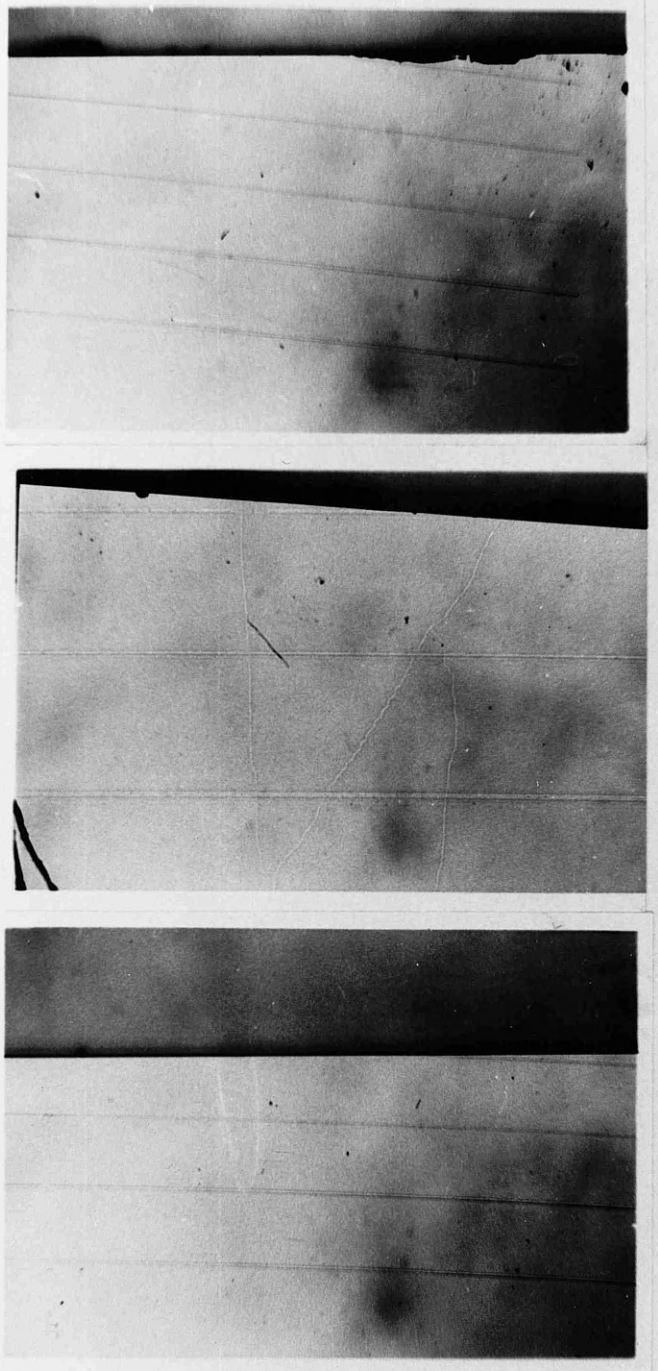

FIG 8 NON-TANGENTIAL POLISHING OF EDGE POLARISERS

FIG 9 UNDERPOLISHING OF EDGE POLARISERS
(i) DRASTIC (ii) AND (iii) MILD

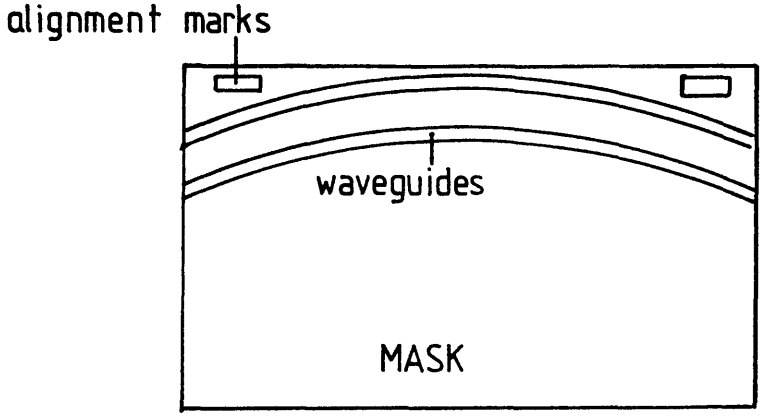

FIG 10 ALIGNMENT MARKS TO AID FABRICATION OF EDGE POLISHED TM POLARISER

polishing, which would be difficult to control as described previously. In addition, the edges are highly susceptible to mechanical damage during the waveguide fabrication process. This method was therefore not investigated experimentally.

7.6 Fabrication of vertical surface by ion milling.

The edge polishing technique to be described in chapter 7 would limit the number of waveguides which can be treated in this way to 2 per substrate. A more versatile technique is therefore required. If a vertical wall could be cut into the substrate, the buffer layer and metal overlays could be evaporated adjacent to the waveguide using selective masking. The arrangement is shown in figure 11. The quality of the surface is now determined by the groove fabrication process, rather than by polishing.

The fabrication processes for ion milling (ref 16,17,18) of grooves in lithium niobate will be described in chapter 7 in connection with fibre-waveguide coupling. The requirements here are however slightly different. The wall, in addition to being vertical, must now be smooth. The quality of the bottom of the groove is no longer critical, and the width need not be so well defined. Indeed, for the sucessful evaporation of the buffer layers on the exposed vertical surface, the groove should be much wider than that required for coupling alignment.

7.6.1 Groove fabrication

A groove of depth $10\pm0.5\mu m$ with width $50\mu m$ and length 4mm was fabricated in Z-cut lithium niobate. The process parameters were exactly as described in chapter 6. The photolithographic mask used was cut using standard techniques (see chapter 2). The resulting grooves were examined with a scanning electron microscope to investigate the wall quality. A typical photograph is shown in ref 26. It will be noted that the corner is not exactly rectangular, some rounding during milling being noted. This is due to slightly non-directional etching of the polyimide mask.

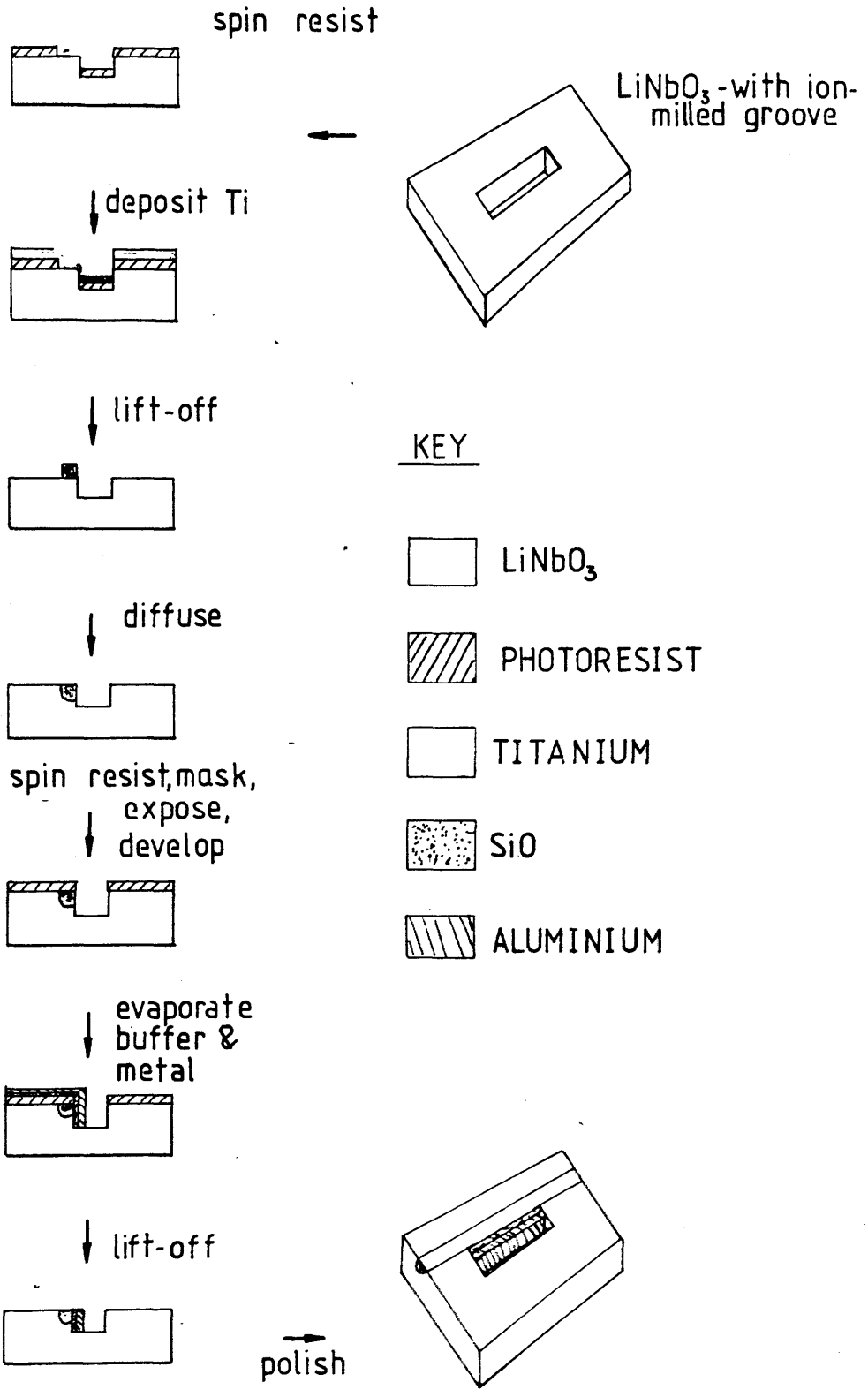

FIG 11 ILLUSTRATING THE STEPS IN THE FABRICATION OF TM POLARISERS USING VERTICAL SURFACES DEFINED BY ARGON ION-BEAM MILLING

7.6.2 Waveguide fabrication

The waveguides were fabricated using a dark field chrome photolithographic mask with stripe width 4μm. The sample was cleaned, initially by ultrasonic agitation in trichloroethylene, and then acetone and methanol as described in chapter 2. It was not necessary to use sulphuric peroxide at this stage as the sample had been de-greased prior to the ion-milling process. The sample was then coated in photoresist which was then dried and cured. The waveguide was defined as shown in figure 11 using a mask aligner (note 1). Exposure and development proceded as usual, with the subsequent evaporation of 87nm of titanium. This was diffused into the substrate as described in chapter 2 at 1000^0C for 9.5 hours (including 1 hour linear increase from ambient conditions to working temperature) in flowing wet argon followed by cooling in flowing wet oxygen.

Considerable difficulty was encountered in aligning the waveguide to the groove edge: in the case of imperfect alignment the resist was removed with acetone and the photolithographic process repeated, starting with the cleaning process.

7.6.4 Buffer and overlay fabrication

Since only a specific area of the substrate normal to the polished crystal surface is to be coated with the relevant materials, the evaporation techniques for this device required modification.

The groove area was masked using standard photolithographic techniques, to leave the groove area "clear". This is illustrated in figure 11. The SiO buffer layer was evaporated as for the horizontally orientated device, the processes used being described in chapter 4. To deposit material in the desired area it was necessary to tilt the substrate. It was therefore necessary to evaporate a larger amount of dielectric so that the resulting film thickness would be the same as for the corresponding horizontal device. Monitoring of the thickness was accomplished by tilting the head of the crystal monitor at a

corresponding angle. The aluminium was deposited as described previously, yielding a total thickness of lum. Due to the limited capacity of the evaporation sources, it was evaporated in two stages. The evaporation chamber was however kept under high vacuum (10^{-6} mmHg) throughout the experiment.

The unwanted areas of buffer and metal were removed by lift-off as shown in figure 11. It was found necessary to subject the sample to ultrasonic agitation to remove the material. At this stage a large number of samples exhibited mechanical defects: the most common fault being disintegration of the vertical aluminium layer. The one surviving sample had a buffer thickness of 25±3nm, where the error arose mainly from inaccuracies in aligning the crystal monitor head.

7.6.4. Testing

The end faces of the sample normal to the waveguide were polished for end fire excitation of the waveguides as described in chapter 2. The testing of the device followed method (ii) descibed in chapter 2, ie. linear polarisers were used at input and output ports and the four elements of the Jones matrix were determined. Due to availablity of sources, the device was operated at 1.15 micron wavelength, using a helium-neon laser. The waveguide operated with a single mode for both TE and TM plane wave excitation.

7.6.5 Obervations

It was noted that the output from the device showed a large amount of light in the substrate. Spatial filtering was thus used to avoid corrupting the measurements. Cross-polarised components were clearly visible, even without increasing the gain of the **Hamamatsu** camera system, again indicating poor performance.

7.6.6 Results

The extinction ratio of the device was 17±4 dB as reported in reference 17. The excess loss when compared to a titanium indiffused waveguide was 7±3dB. The relative magnitudes of the

cross-polarised components were high, being only about 18dB below the power transmitted in the preferred mode. However, despite these poor results, the device transmitted the desired TM-like mode with respect to the crystal surface.

7.7. Discussion

A system has been proposed for closed-loop operation of the single fibre polarimetric sensor using differential frequencies in the two orthogonal eigenmodes. While bulk or fibre-optic implementations are possible, an integrated optical version was investigated. The dependence of the system performance on component specification was analysed.

While integrated optical frequency shifters have not been demonstrated with the required high-frequency limit, Stallard (ref 8) has predicted that such devices are feasible. Provided the relative magnitude of the spectral frequency components remains stable, the non-monochromaticity is acceptable.

The proposed system would not be suitable for use in a remote sensing environment as would be the case for certain other signal processing applications (ref 4).

Integrated optical polarisers to be used in this system must have a extinction ratio of 60dB or greater to ensure accuracy over the entire operating range of measurand. This has been accomplished for the TE-like modes, but attempts to fabricate TM-like polarisers with the required high extinction ratio have failed. Devices fabricated on similar principles to those reported in chapter 4 but using a vertical, ion-milled wall, have been fabricated. Although their absolute performance was poor, the desired TM-like mode was transmitted. The extinction ratio has been found to be 17 ± 4dB but with an excess loss of 7 ± 3dB. Improvements in both parameters are needed to realise the potentially high performance of the proposed device.

The limiting factor in fabrication would appear to be the waveguide roughness. This arises from the polyimide masking layer used during the ion-milling process. Direct writing of the edge may be possible using electron-beam lithography (ref 20).

However, an ultimate limit of the polarising ability of this device may arise from the abrupt refractive index changes at the waveguide-air boundary. These were not present for the horizontal device, where the guide was surrounded almost uniformly by material of approximately equal refractive index. Thus the weakly-guiding approximation may no longer hold (ref 21) and the modes are not well represented by linear polarisations. The experimental results are however not sufficient to favour either of these theories. Further work is necessary to discriminate between the two. Modelling of the device would require a full analysis using a finite elements program (ref 22): this would be demanding both in terms of computer time and storage space. In addition, the variation of the optical properties of the metal layers with deposition conditions would render the results inaccurate.

The edge polishing technique could possibly be developed to yield a useful device. However, the problems of repeatablity and the fact that only two waveguides treated in this way could be used per substrate would indicate that the vertical milled polariser has more potential. Using the latter method, an almost unlimited number of waveguides could be used. The light initially present in the unwanted mode is absorbed, and therefore not present in the substrate to re-couple into the same, or other, waveguides. This is not the situation with proton exchanged or birefringent overlay polarisers.

A further incentive for the development of TM polarisers is given by the high efficiency of Z-Cut Ti:$LiNbO_3$ modulators using TM-like modes.

The proposed detection scheme may also be implemented using fibre, rather than integrated optical beamsplitters and combiners. Using polarisation maintaining fibre and appropriate twists, two linearly polarised states with differing frequencies could be established. Polarisation preserving couplers using the fused taper technique (ref 23) have been demonstrated (ref 24), and would eliminate problems of polarisation re-conversion found in the integrated optical version. Alternatively, the frequency

shifting could be performed by integrated optical devices, while the polarisation definition performed within the fibres. All-fibre polarisers with high extinction ratios have been reported in the literature (ref 25).

Note The fabrication steps involving the use of a mask aligner were performed at Barr and Stroud Ltd

References

7.1 Eickhoff,W, "Temperature Sensing by Mode-Mode Interference in Birefringent Optical Fibres", Electronics Letters, Vol 6, No 4, 1981 pp204-206

7.2 Rashleigh,S.C, "Polarimetric Sensors: Exploiting the Axial Stress in High Birefringence Fibres", 1st International Conference on Optical Fibre Sensors, London, 1983

7.3 Varnham,M.P, Barlow,A.J, Payne,D.N, Okamoto,K, "Polarimetric Strain Gauges using High Birefringence Fibre", Electronics Letters, Vol 19, No 17, pp699-700, 1983

7.4 Kersey,A.D, Corke,M, Jackson,D.A "Linearised Remote Sensing Using a Monomode Fibre Polarimetric Sensor", Optical Fibre Sensors, Stuttgart, 1984

7.5 Vernitron Ltd, Commercial Literature.

7.6 Kaminow,I.P, "Polarisation in Optical Fibres", I.E.E.E. Journal of Quantum Electronics", Vol QE-17, No 1, 1981 pp15-22

7.7 Hecht,E, Zajac,J, "Optics", Addison Wesley, 1979

7.8 Stallard,W.A, Daymond-John,B.E, Booth,R.C, "$LiNbO_3$ Optical Frequency Translators for Coherent Optical Fibre Systems", European Conference on Integrated Optics, Berlin, 1985

7.9 Culshaw,B, Giles,I.P, "Fibre Optic Gyroscopes", Journal of Physics E, Scientific Instruments, Vol 16, pp5-14

7.10 Jackson,D.A, Dandridge,A, Sheem,S.K, "Measurement of Small Phase Shifts using a Single Mode Optical Fibre Interferometer", Optics Letters, Vol 5, No 4, 1980 pp139-141

7.11 Cytroky,J, Janta,J, Schrofel,J, "Thin Film Polariser for Optical Waveguides", 10th European Conference on Optical Communications, Sept 3-6 1984, Stuttgart

7.12 Wong,K.K,De La Rue,R.M, Wright,S, "Electro Optic Waveguide Frequency Translator in $LiNbO_3$ Fabricated by Proton Exchange", Electronics Letters, Vol 7, No 11, 1982 pp546-548

7.13 Rashleigh,S.C, "Origins and Control of Polarisation Effects in Single-Mode Fibres", Journal of Lightwave Technology, Vol LT-1, No 2, 1983 pp312-331

7.14 Gottleib,M, Brandt,G.B, "Measurement of Temperature With Optical Fibers", Fibre Optic Communications, Chicago U.S.A, 1979

7.15 Cullen,T.J, PhD thesis, University of Glasgow, 1985

7.16 Nutt,A.C.G, Bristow,J.P.G, McDonach,A, Laybourn,P.J.R, "Fiber-to-Waveguide Coupling using Ion-Milled Grooves in Lithium Niobate at 1.3um Wavelength", Optics Letters, Vol 9, No 10, 1984 pp463-465

7.17 Bristow,J.P.G, Nutt,A.C.G, Laybourn,P.J.R. "Novel Integrated Optical Polarisers using Surface Plasma Waves and Ion-Milled Grooves in Lithium Niobate", Electronics Letters, Vol 20, No 25/26, 1984 pp1047=1048

7.18 Bristow,J.P.G, "Intergrated Optical Polarisers", Invited Paper, U.R.S.I. Colloquium, Royal Society, 12th July, 1985

7.19 Griffiths,G.J, Esdaile,R.J, "Analysis of Titanium Diffused Planar Optical Waveguides in Lithium Niobate", I.E.E.E. Journal of Quantum Electronics, Vol QE-20, No 2, February 1984 pp149-159

7.20 Patrick,W, University of Glasgow,

7.21 Yeh,C, Manshadi,F, "On Weakly Guiding Single Mode Optical Fibres", Journal of Lightwave Technology, Vol LT-3, No 1, 1985 pp199-205

7.22 Yeh,C, Ha,K, Dong,S.B, Brown,W.P, "Single Mode Optical Waveguides", Applied Optics, Vol 18, No 10, 1979 pp1490-1504

7.23 Slonecker,M "Single Mode Fused Biconical Taper Couplers", ITT Electro Optics Product Division, Confidential Publication

7.24 Villaruel,C.A, Abebe,M, Burns,W.K, "Polarisation Preserving Single Mode Fibre Coupler", Electronics Letters, Vol 19, No 1, 1983 pp17-18

7.25 Hosaka,T, Okamoto,K, Edaharo,T, "Fabrication of Single-Mode Fiber Type Polariser", Optics Letters, Vol 8, No 2, 1980 pp124-126

7.26 Bristow,J.P.G, Nutt,A.C.G, McDonach,A, Laybourn,P.J.R, "Locating and Coupling Fibres to Integrated Stripe Guides", I.E.E. Proceedings J-Optoelectronics, Vol 1, No 5 October 1985

Chapter 8- Discussion, Conclusions and Suggestions for Future Work

8.1 Introduction

The main results and achievements presented in the preceding chapters will now be summarised and discussed. The importance of the work presented will be examined, and suggestions for further work made on the basis of this examination.

8.2 Sensor Systems and Performance Requirements for Components for use with Fibre Optic Sensors

A variety of fibre optic sensor systems reported in the literature were examined. Single mode sensors, in the Mach-Zehnder configuration were found to be suitable for the measurement of a wide range of measurands, although modification of the fibre may be necessary for some applications. The sensor was shown to have poor cross-sensitivity. It was also shown that in order to realise the theoretically high sensitivity of the system, one of the eigenmodes in each of the two fibre interferometer arms must be selected with an extinction ratio of 60dB. This implied mode-selection with high extinction ratio and high birefringence fibre to minimise subsequent polarisation cross-coupling.

The optical fibre gyroscope in its single-pass form was shown to be a simple extension of the Mach-Zehnder arrangement. However, the non-reciprocal Sagnac phase shift is of such small magnitude that the requirements on optical components are even more stringent than for the Mach-Zehnder and other fibre sensors. It was shown that mode selection with extinction ratios of at least 60dB were required for a short-term device, with a figure of 90dB being required for a device with inertial stability.

Requirements of any coupler present between two waveguide sections in the gyroscope were examined for the case of asymmetric positioning of the coupler. Imperfect coupling was shown to lead to a rotation rate offset, while variation in the coupling efficiency was shown to lead to noise in the signal. Thus any coupler present must be capable of repeatable, low-loss alignment with high mechanical stability.

The single-fibre polarimetric sensor was also described, together with the various detection and signal processing schemes

reported to date. These generally had the disadvantage of periodic (and hence ambiguous) output with changing measurand, or restrictions on sensor size or other parameter. A novel system was proposed whereby the sensor was operated in a closed-loop configuration. This new arrangement required the frequency shifting of one of the two othogonal eigenmodes of the fibre. This in turn required the fabrication of mode filters for both modes with extinction ratios of 60dB, and for frequency shifters with cutoff frequencies of up to 20 GHz depending on the application of the sensor.

The sensor offered improved cross-sensitivity compared to more conventional fibre sensor systems, but with a slightly reduced sensitivity to any given measurand. The magnitude of this reduction depended on the measurand and upon the fibre selected for the sensor. The configuration offered the possibiltiy of an essentially digital readout, with high dynamic range, the latter being determined by the maximum frequency translation of the frequency shifter.

The requirements of the frequency shifter for this application were analysed. The results also apply to phase-nulling detection techniques used for the fibre optic gyro. It was found that components at undesired frequencies resulted in either corruption of the results (an effect which could be calibrated out), or a constant error term depending on the origin of the effect. It was concluded that components at the unshifted frequency are to be particularly avoided. The mode-filters were required to have an extinction ratio of at least 60dB, this being derived from a "worst case" consideration.

8.3 Integrated Optical Polarisers

The design of integrated optical polarisers using dielectric/metal claddings was investigated. It was shown that no satisfactory model for stripe guide devices exists at present. Optimisation of devices fabricated with silicon monoxide/aluminium overlays proceded on an experimental basis, approximate values for the various parameters being taken from the slab model described. Following fabrication of a large number of devices, extinction ratios as high as 80$\pm$13dB were obtained. This represents a significant improvement upon any device

reported in the literature, and would be suitable for inclusion in integrated optical systems to interface with optical fibre sensors. A second peak in the graph of attenuation vs. buffer thickness was observed at a buffer thickness approximately double that of the first peak. This is believed to be due to the finite thickness of the aluminium films used and excitation of a second surface plasma wave at the air/metal boundary. Further work is necessary to resolve the problem. The TE-like modes were shown to have unperturbed mode profiles compared to the unclad case.

The devices were tested using linearly polarised input and recording the output for orthogonal inputs. This method was used as the bulk optical polarisers used had insufficient extinction ratio. As these were the best devices available at the time of purchase, no solution to the problem is at present available. Testing using optical fibres yielded comparable results but with higher errors. Further development of a method of testing the extinction ratio of the devices when interfaced with optical fibres is regarded as essential.

It is suggested that waveguide arrays with different dielectric/metal overlays could be used in wavelength de-multiplexing, and further investigation is recommended.

A full discussion of possible methods of testing integrated optical polarisers has been given in terms of the Jones matrices for the system.

Integrated optical polarisers using proton exchanged sections were investigated. It was postulated that variation of waveguide parameters would affect the extinction ratio, and experiments were performed to verify this. However, no trend was observed for either the extinction ratio or the excess loss. This was attributed to poor waveguide end-face quality. In most integrated optical waveguides this is not important: either prism (or other transverse) coupling or polishing of the end face for end fire excitation being used. It is therefore suggested that further work be undertaken to solve the problem. The extinction ratios of approximately 20dB and the high associated excess loss make such polarisers at present unsuitable for inclusion in integrated optical systems.

It was also postulated that the poor extinction ratios

obtained with the devices were a result of the unwanted mode continuing to propagate in the substrate, and a new geometry was proposed using U-shaped bends in the proton-exchanged waveguide. Due to the reasons stated above it was not possible to investigate the performance of the device, and further work in this direction will be required. These hybrid polarisers are however far more complicated to fabricate than the dielectric/metal clad devices.

8.4 Integrated Optical Processing System for Single Fibre Polarimetric Sensor

An integrated optical implementation of the closed loop single fibre polarimetric sensor was proposed. For optimal operation, the system relied on the fabrication of components to select TE and TM like modes on the same substrate with extinction ratios exceeding 60dB. TE-like mode filters with the requisite performance were reported. Proton exchange techniques, while yielding the correct mode selection were not found to have sufficiently high extinction ratios. Two methods were therefore investigated to select TM-like modes with respect to the crystal surface. Both relied on the fabrication of vertical surfaces on the crystal. Polishing of the crystal edge was investigated, but was found to be time consuming. In addition, the process was not sufficiently controllable for the fabrication of TM-like polarisers. In fact, it was not possible using this method to fabricate a polariser. Further work on this method is not recommended. Ion milling was also investigated as a technique for the fabrication of the vertical surface. Although rough wall quality was believed to limit the polariser performance, a device was demonstrated to select TM like modes with respect to the crystal surface. Further work is recommended to improve the extinction ratio and excess loss of 17 ± 4 and 7 ± 3 dB respectively. Throughout the experiments on integrated optical polarisers, the need to express the results in an unscaled form was emphasised.

The use of birefringent crystal claddings for the mode selection is not recommended as polishing of both crystal surfaces is required. A comparison of available techniques for mode selection is presented in table 1.

CRYSTAL CUT	Z	X	X	Y	Y
PROPAGATION	X/Y	Y	Z	X	Z
METHOD					
P.E.-INTERNAL	TM	TE	(=)	TE	(=)
P.E.-EXTERNAL	TE	TM	=	TM	=
METAL WITH LOW INDEX BUFFER	TM	TM	TM	TM	TM
METAL	(TM)	(TM)	(TM)	(TM)	(TM)
BIREFRINGENT CRYSTAL	TE TM	TE TM	TE TM	TE TM	TE TM
ION-MILLING (VERTICAL)	TE	TE	TE	TE	TE

KEY: =NO PREFERENCE ( )INHERENTLY LOSSY
P.E. PROTON EXCHANGE

TABLE 1 PREFERENTIAL SELECTION OF TE- OR TM-LIKE MODES OF TITANIUM INDIFFUSED WAVEGUIDES IN VARIOUS ORIENTATIONS OF LITHIUM NIOBATE USING A SELECTION OF CONTROL METHODS.

8.5 Fibre/Waveguide coupling and field overlap calculations

A coupler to transfer energy from optical fibres to integrated optical waveguides was demonstrated. The device used ion-beam milling to fabricate a location groove for the fibre. Insertion losses of 2.6dB were determined for the device. It is suggested that the use of index matching fluid could reduce this figure to 1.8dB. While this figure is higher than that reported in the literature for butt-coupling arrangements, the device is important as it is suitable for mass production techniques. The effect of asymmetric fibre coupling distributions and mechanically unstable couplers on the performance of the fibre optic gyroscope was investigated. While both were found to have deleterious effects on system performance, measurements on the repeatability of the ion-milled coupler have not been performed to date. Further work on this problem is therefore suggested. It is to be noted that the inclusion of any interface in the fibre optic gyro will have an adverse effect on system performance, and all fibre systems offer considerable advantages in this respect. High bandwith phase and frequency modulators have yet to be demonstrated for such systems.

One loss mechanism in the coupling arrangement is due to the spatial mismatch of the optical fields of the two waveguides. A method was reported for investigation of this effect using data from real waveguides. Using a digitising camera and computer processing it was possible to present contour plots of the near field profile of any given optical waveguide at either visible or infra-red wavelengths. The data was also used to evaluate the overlap integral between the two waveguides. This method was shown to be valid for optimisation of the coupling process, but invalid for multimode guides and for waveguides with strong discontinuities. The modal mismatch for the ion-milled coupler was determined to be 0.5dB using this method. Further work is required to reduce this loss, by investigation of the effect of different diffusion times, atmospheres etc. Such alterations may however incur increased excess loss, and this too should be investigated.

It was also shown that the data recorded in the process of evaluating the overlap coefficients may also be used for other

purposes. These include reconstruction of the refractive index distribution within the waveguide. It was also shown that noise in the data due primarily to source intensity fluctuations and secondly to quantisation errors threatened the accuracy of the methods. It is recommended that hardware and software modifications to the system be implemented to reduce the time taken to record the data and also to enable averaging of several data sets to be performed. As such modifications will depend on the computer to be used, it is not possible to make more specific recommendations at this point.

8.6 Conclusion

It is recommended that an integrated optical processing system for an optical fibre gyroscope be implemented using the mode filters demonstrated here. Due to the interfaces involved, it is unlikely that such a system will ever possess the stability required for inertial appplications, however an application may lie in short-term single use systems. The system will of necessity be complicated, requiring electo-optically tuned directional couplers together with the mode filters demonstrated in this thesis, the remaining components depending upon the implementation. For a phase nulling system, which to date has shown high sensitivity, a phase modulator and either one or two frequency shifters will be required. The excess loss of such a system is likely to be extremely high, which will affect the ultimate sensitivity via the shot-noise limit.

It is also recommended that either integrated optical or fibre optical implementations of the closed-loop differential frequency single fibre polarimetric sensor be investigated, as this arrangement appears to offer acceptable sensitivity with high dynamic range and unambiguous output.

In conclusion, it is believed that the components and processing schemes discussed in this thesis represent a significant advance in the fields of optical fibre sensors and integrated optics, and will enable several new sensors and other systems to be designed and fabricated